Coding techniques for space-division multiplexed optical fiber systems

El Mehdi Amhoud

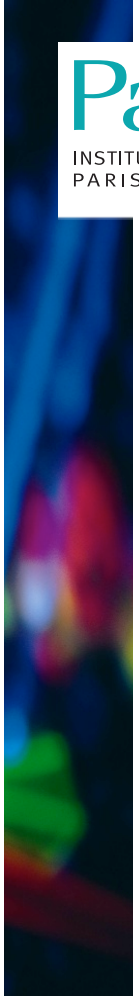

ParisTech
INSTITUT DES SCIENCES ET TECHNOLOGIES
PARIS INSTITUTE OF TECHNOLOGY

TELECOM ParisTech

2017-ENST-0067

EDITE - ED 130

Doctorat ParisTech

T H È S E

pour obtenir le grade de docteur délivré par

TELECOM ParisTech

Spécialité « Communications et Electronique »

présentée et soutenue publiquement par

El-Mehdi AMHOUD

le 11 Décembre 2017

Coding Techniques for Space-Division Multiplexed Optical Fiber Systems

Directeurs de thèse : **Ghaya REKAYA-BEN OTHMAN** & **Yves JAOUËN**

Jury

Dr. René-Jean ESSIAMBRE, Nokia Bell Labs, USA	Rapporteur
Pr. Andrew ELLIS, Aston University, United Kingdom	Rapporteur
Pr. Christophe PEUCHERET, Université de Rennes I, ENSSAT, France	Examinateur
Pr. Catherine DOUILLARD, IMT-Altantique, France	Examinateur
Pr. Mounir GHOGHO, Université Internationale de Rabat, Morocco	Examinateur
Dr. Laurent BIGOT, Université de Lille 1, IRCICA, France	Invité
Pr. Ghaya REKAYA-BEN OTHMAN, Télécom ParisTech, France	Directeur de thèse
Pr. Yves JAOUËN, Télécom ParisTech, France	Directeur de thèse

TELECOM ParisTech
École de l'Institut Mines-Télécom - membre de ParisTech
46 rue Barrault 75013 Paris - (+33) 1 45 81 77 77 - www.telecom-paristech.fr

T H È S E

Acknowledgements

This thesis is the result of three years of research work conducted at the Communications and Electronics department of Télécom ParisTech. I would like to thank all the people who made these years a great experience.

First, I would like to thank my advisors Pr. Ghaya Rekaya and Pr. Yves Jaouën for giving me such a great opportunity to carry out my Ph.D. under their supervision. I have learned a lot from you, both professionally and personally. I'm also very grateful to you for affording such an important fundings that allowed me to travel the world to present our work in conferences, make multiple research stays outside of Télécom ParisTech and also to patent our research results.

I would like to thank all the jury members for their interest in my work. I am very honored that Dr. René-Jean Essiambre and Pr. Andrew Ellis accepted to review and evaluate my thesis. I also thank Professors Christophe Peucheret, Catherine Douillard and Mounir Ghogho for accepting to be part of the jury examiners.

A special thank to Dr. Asma Mejri and Dr. Elie Awwad for all their help and transfer of knowledge during my first six month at Télécom ParisTech. I have learned from you the necessary tools and the good behaviors to carry out with confidence my Ph.D.

Many thanks to all my colleagues with whom I have spent such an exciting experience and shared lots of beautiful moments.

Abstract

Optical transmission systems are fundamental for telecommunication infrastructure. For long-haul as well as for metropolitan and access networks, this technology can carry data over long distances with low attenuation. In a very fast pace, the last two decades have known an exponential growth in the demand for more network capacity. This growth was mainly caused by the built out of the Internet and the growing traffic generated by an increasing number of users. Since frequency, time, phase, polarization have already been used to satisfy the demand for bandwidth, space-division multiplexing (SDM) remains the only available degree of freedom that can be used in optical transmission systems in order to increase the capacity. However, interactions between spatial channels in the same propagation medium is inevitable. This interactions, if not compensated, result in impairments that deteriorate the system performance. For this purpose, intensive research is being carried out in recent years in order to provide advanced signal processing capable to deal with these impairments in spatial multiplexing systems. Motivated by the potential role of few-mode fibers (FMFs) in future SDM systems, in this thesis, we present modern coding solutions to mitigate the non-unitary crosstalk known as mode-dependent loss (MDL) that affects spatial modes of FMFs resulting in degraded system performance.

Accordingly, the first part of the thesis is devoted to the study of the capacity of few-mode fibers affected by MDL. Then, we propose three different solutions to enhance this capacity. These solutions can be resumed as: Channel state information knowledge of the FMF channel to efficiently attribute power to different modes. Mode scrambling as a solution to average the non-unitary crosstalk and create strong coupling. Mode selection to use only the set of the best modes for multiplexing.

In the second part, we investigate the benefits of space-time (ST) coding in mitigating MDL. We show by simulations and explain theoretically by error probability computation the efficiency of ST codes. The obtained results are completely different from wireless communications, we derive a design criterion for ST codes construction suitable for FMF systems.

The last part is dedicated to the study of FMF systems including both polarizations. We investigate the interaction between the non-unitary crosstalk known as polarization-dependent loss (PDL) affecting polarizations and MDL. Afterwards, we conduct a transmission experiment through FMF with both polarizations in the presence of MDL. We demonstrate for the first time the robustness of full-rate ST coding against MDL.

Keywords: Multiple-Input-Multiple-Output, Optical Fiber Communications, Spatial Division Multiplexing, Mode-Dependent Loss, Space-Time Coding, Orthogonal Frequency Division Multiplexing.

Contents

Glossary

ADC Analog-to-Digital Converter

ASE Amplified Spontaneous Emission

AWGN Additive White Gaussian Noise

BER Bit Error Rate

BPSK Binary-phase Shift Keying

CAGR Compound annual growth rate

CCDF Complementary Cumulative Distribution Function

CD Chromatic Dispersion

CDF Cumulative Distribution Function

CMA Constant Modulus Algorithm

CO-OFDM Coherent-OFDM

CP Cyclic Prefix

CSI Channel State Information

CU Channel Use

DD Direct Detection

DEMUX De-multiplexer

DMGD Differential Mode Group Delay

DoF Degrees of Freedom

DPSK Differential Phase Shift Keying

DSP Digital Signal Processing

DWDM Dense Wavelength-Division Multiplexing

EAM Electro-Absorption Modulator

EDFA Erbium Doped Fiber Amplifier

FDE Frequency Domain Equalization

FEC Forward Error Correction

FMF Few-mode fiber

FFT Fast Fourier Transform

FWM Four wave Mixing

GC Golden Code

GVD Group Velocity Dispersion

HDD Hard Decision Decoding

ICI Inter Carrier Interference

IM Intensity Modulation

IP Internet Protocol

ISI Inter-symbol Interference

LD Laser Diode

LDPC Low-Density Parity Check

LMS Least Mean Squares

LO Local Oscillator

LP Linearly Polarized

MCF Multi-core Fiber

MDL Mode Dependent Loss

MDM Mode-Division Multiplexing

MIMO Multiple-Input Multiple-output

ML Maximum Likelihood

MMF Multi-mode Fiber

MMSE Minimum-Mean Square-Error

MS Mode Scrambler

MUX Multiplexer

MZM Mach-Zender Modulator

NA Numerical Aperture

NRZ Non Return To Zero

OFDM Orthogonal-Frequency Division Multiplexing

OOK On-Off Keying

OSNR Optical Signal to Noise Ratio

PAM Pulse Amplitude Modulation

PBC Polarization Beam Combiner

PC Personal-computer

PDF Probability Density Function

PDL Polarization Dependent Loss

PDM Polarization-Division Multiplexing

PMD Polarization Mode Dispersion

QAM Quadrature Amplitude Modulation

QPSK Quadrature-Phase Shift Keying

RZ Return to Zero

SD Sphere Decoder

SDD Soft Decision Decoding

SDM Space-division multiplexing

SE Spectral Efficiency

SMF Single-mode Fiber

SPM Self Phase Modulation

ST Space-Time

STBC Space Time Block Code

SVD Singular Value Decomposition

TAST Threaded Algebraic Space Time

TDE Time Domain Equalization

WDM Wavelength-Division Multiplexing

WF Waterfilling

XPM Cross Phase Modulation

ZF Zero Forcing

ZF-DFE Zero-Forcing Decision Feedback Equalization

List of Figures

List of Tables

General Introduction

The triggering of optical communication era was in 1840's when physicist Jean-Daniel Colladon showed that light could be directed along water jets for night-time fountain displays. Since that time, physicists and engineers multiplied inventions related to transmitting light in bent glass rods and first transmissions of images for television through bundle of fibers were demonstrated.

The optical communication revolution started with the invention of the laser in 1960 [4], which allowed to launch and control very small rays of light. The optical fiber was used as a medium for guiding the laser light, in the same way as electrons are guided in copper wires. The existing fibers in that time presented a huge loss ~ 1000 dB/km, but ten years later in 1970, fiber losses were reduced to ~ 20 dB/km. From this time period, the progress in optical communications has been rapid and new technologies were introduced which allowed to increase the transmission distance and throughput and compensate for the fiber loss.

The evolution of optical transmission systems from 1970 to 1990 can be grouped into three main generations mainly characterized by specific optical wavelength carriers. The first generation of optical systems was operating at a wavelength of 0.8 μm. These systems allowed a bit rate of 45 Mb/s. Additionally, distance between repeaters reached 10 km which is ten times greater than coaxial-cable systems. In the second generation, optical systems were operating at a wavelength of 1.3 μm where fiber losses were typically 0.5 dB/km. Spacing between repeaters was ~ 70 km and up to 1.7 Gb/s bit rate was achieved. The third generation of optical systems has migrated to wavelength of 1.55 μm where silica losses are minimum (~ 0.2 dB/km). Systems operating at 2.5 Gb/s with a signal regeneration distance of ~ 70km were commercially available in the early 1990s.

The development of optical fiber transmission systems between 1970 and 1990 was very impressive. The attenuation was reduced from ~ 1000 dB/km to ~ 0.2 dB/km and systems with a bit rate of 10 Gb/s were available. Nonetheless the regeneration of signal in the electrical domain each ~ 70km was a serious drawback of these systems, and the

need for more capacity was increasing year after year. To overcome these issues, two technologies were introduced: Optical amplification and wavelength-division multiplexing (WDM). Erbium-doped fiber amplifiers (EDFA) allowed to compensate for fiber loss by regenerating optically signals each ~ 100 km without electrical conversion which started the era of long-haul optical systems. At the same time, a first generation of forward error correction (FEC) codes was initially introduced to mitigate physical impairments such as the amplified spontaneous emission (ASE) of EDFAs and non-linear effects, hence lower OSNR levels requirements were enabled. On the other hand WDM allowed to increase the capacity of single mode fiber systems by using several parallel channels for transmitting the data. WDM along with EDFA allowed the transmission over thousands of kilometers of up to 80 channels separated by 50 GHz, where each channel has a bit rate of 10 to 40 Gb/s. These technologies along with the advances in electronic and optoelectronic devices have fed the growing hunger of bandwidth from 1990 to 2000.
Starting from 2000, digital communication engineering became a main concern of optical communications in order to further exploit the available bandwidth of WDM systems and to compensate for impairment by signal processing. Moreover, coherent detection allowed to access the amplitude, phase and the two orthogonal polarizations of the electromagnetic field, which permitted the use of higher order modulation formats and introduced coherent polarization divison multiplexed (PDM) systems. Hence, the differential phase shift keying (DPSK) already used with direct detection was replaced by quadrature phase shift keying (QPSK) which increased the spectral efficiency and PDM-QPSK systems reached 100 Gb/s. These high speed systems can compensate for dispersive effects thanks to DSP algorithms at the receiver.

Since wavelength, phase, polarization have already been employed in order to satisfy the demand for bandwidth, space remains the last degree of freedom that can be used in an optical transmission system to increase its capacity. Space-division multiplexing (SDM) can be realized by multi-mode fibers (MMFs) that allow the propagation of more than one mode in a single core or multi-core fibers (MCFs) where each core can be single-mode or multi-mode. MMFs with core diameter of $50/125\mu m$ can support more than 100 modes [2], however, these fibers are not suitable for spatial multiplexing because modes travel at different velocities and experience different losses. Recently a new type of fibers called few-mode fibers (FMFs) that support the propagation of a small number of modes was designed. FMFs have interesting properties [5] that make them more appropriate for spatial multiplexing over long distances.
Although SDM is a promising solution for the future of optical systems, many challenges

need to be addressed in order to maintain a reliable communication and reduce the cost per bit. For this aim, intensive research is being carried out to assess the different possible realizations of SDM, to integrate electrical and optical components to allow manipulation of many spatial paths in a single device, and also to investigate modern signal processing techniques capable of dealing with the new impairments arising from spatial multiplexing. For instance, In the European Conference on Optical Communications (ECOC) held in Gothenburg on September 17^{th}-21^{th}, 2017, 41 oral presentations were concerned with SDM transmissions, components and fibers manufacturing (Amplifiers, multiplexers, FMFs and MCFs). Also one workshop gathering 17 specialists from different companies and universities was dedicated to discus the best fiber development for SDM systems.

Motivations and thesis contributions

In this thesis, we present modern digital signal processing (DSP) techniques to mitigate the non-unitary crosstalk that affects the transmission in FMFs. In fact propagating modes in FMFs are subject to modal coupling that can be unitary, in this case multiple-input multiple-output (MIMO) techniques already known from wireless communications allow to recover signals at the receiver. Modal crosstalk can also be non-unitary, known as mode-dependent loss (MDL), causing a detriment impact on the system capacity.
In [6], the authors showed for the first time that space-time (ST) coding originally designed for wireless communications was very efficient in mitigating MDL in few-mode fiber systems. Numerical simulations were conducted on a three and six mode fibers and coding gains were observed for different amounts of modal coupling. These interesting results initiated this thesis project to further investigate the capacity of few-mode fiber systems and to extend the work on modern ST coding solutions to compensate for MDL.

This thesis began in October 2014, and was carried out at the LTCI (Laboratoire de Traitement et communication de l'information) laboratory of Télécom ParisTech. The first motivation of this work is to study the impact of mode-dependent loss on the capacity of few-mode fibers. Both the average and outage capacities were analyzed to address the capacity limits of FMF systems in the presence of MDL. We also proposed new optical and DSP solutions to increase FMF systems' capacity.

Afterwards, we investigated ST coding for FMFs analytically by deriving an upper bound for the error probability. This theoretical analysis allowed us to understand the behavior of ST coding when applied to the optical channel. From this bound we define a design criterion for ST codes specific to FMF channel impaired by MDL. Furthermore, to

enhance the coding performance, we added a forward error correction block to our system. We observed a summation of coding gains brought by ST codes and FEC and explained this behavior also through theoretical calculus.

Finally, We concluded our work by an experimental validation of ST coding for MDL mitigation for FMF systems. This experiment required a considerable amount of equipment and was conducted in collaboration with IRCICA (Institut de recherche sur les composants logiciels et matériels pour l'information et la communication avancée) laboratory of University of Lille. We showed experimentally for the first time the efficiency of full-rate ST codes in mitigating MDL in a two-mode transmission with both polarizations.

Thesis Outline

This thesis dissertation is organized in four chapters, the contributions and results of each chapter are summarized in the following:

- **Chapter 1:** We start this chapter by reviewing the evolution of data traffic and the proposed optical technologies to cope with it, we present SDM as a potential solution for future generation of optical transmission systems. Afterwards, we describe single mode fiber systems focusing on the main impairments of transmission and capacity limits. Then, we tackle the propagation in FMFs as a possible realization of SDM and we identify MDL as the main capacity limiting factor. Lastly, we review different DSP equalization techniques for MDM systems.

- **Chapter 2:** In this chapter, we study the capacity of FMF systems impaired by MDL. First, we provide a general description of different capacities used in the study of MIMO systems. Then, we define our FMF channel model impaired by MDL and study the detrimental impact of the latter on the capacity. Lastly, we propose three different optical and DSP solutions to increase the capacity of FMFs in the presence of MDL.

- **Chapter 3:** This chapter is dedicated to ST coding as a solution to enhance the reliability of the transmission over FMF systems. We start by presenting the theory of ST coding and decoding for MIMO systems. Then we study the ST coded MDM transmission impaired by MDL, we derive analytically the error probability upper bound to explain the specific behavior of ST codes in the FMF channel. Finally a study of the concatenation of ST coding and FEC is conducted, and coding gain summation is shown by simulations and proved analytically.

- **Chapter 4:** To conclude our study, we present an experimental validation of ST codes for MDL mitigation in MDM optical systems. For this aim, we start by presenting OFDM as an advanced modulation format with many benefits. Afterwards, we study by simulations FMF transmissions including both polarizations to understand the interaction between non-unitary effects arising from polarizations and modes. Lastly we present our experimental results related to ST coding for MDL mitigation in a FMF system with both polarizations.

Chapter 1

Evolution of Optical Transmission Systems

Fiber optic networks are undergoing continuous development and different technologies have been introduced to improve the performance and system reach. In this chapter, we start by reviewing the evolution of optical fiber technologies that have been following the growth of network traffic. Then, we will describe the technologies used in the actual optical systems. Afterwards we detail the propagation in single-mode fibers and focus on the main impairments of the transmission. Finally we present multi-mode fibers as a possible realization of space-division multiplexing and also describe the main propagation impairments.

1.1 The optical network: Traffic evolution and technologies to cope with it

1.1.1 Traffic evolution of optical networks

According to the Cisco visual indexing report [1], the global Internet Protocol (IP) traffic will increase nearly threefold between 2015 and 2020, which corresponds to a compound annual growth rate (CAGR) of 22%. This exponential growth is mainly due to the expansion of the Internet, the huge amount of video streams and modern technologies such as cloud services, telepresence and social networks. By the year 2020, the number of devices connected to IP networks will be three times as high as the global population of the planet and the traffic generated by smartphones will exceed personal-computers (PC) traffic. The report indicates that the IP traffic is more important in Asia-Pacific region and North America then Europe. The IP traffic in Middle East and Africa is the lowest, however it is growing very fast with a CAGR of 41% between 2015 and 2020 (see Fig. 1.1).

To feed the traffic growing hunger, future optical networks also need to be developed to provide an infrastructure capable of welcoming all these requirements and avoid a capacity crunch.

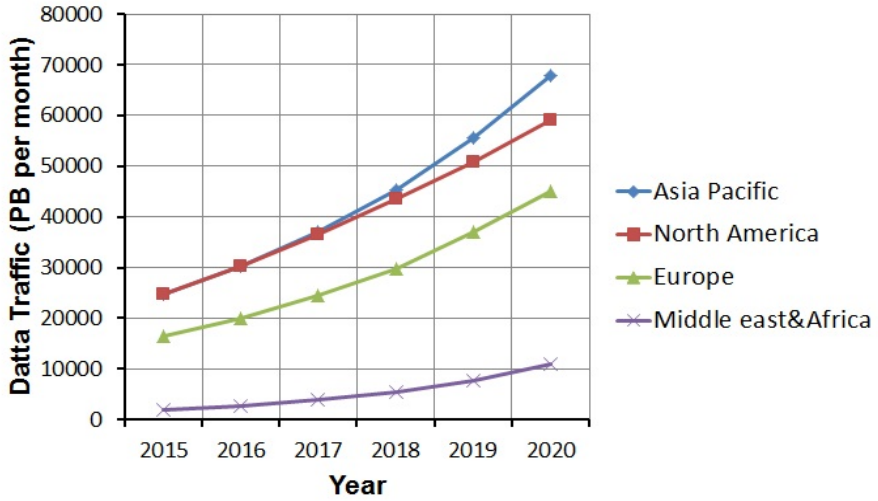

Figure 1.1: Forecast of the IP traffic evolution for different regions. Figure plotted according to the data given in [1].

1.1.2 Capacity evolution of optical fiber systems

The continuous capacity growth of optical systems since 1970 was possible thanks to the many physical dimensions that the optical fiber can afford. Five physical dimensions mostly known as degrees of freedom (DoF) allowed new multiplexing strategies and high spectral efficiency modulation formats which increased the throughput. These DoF are shown in Fig. 1.2:

1. **Amplitude:** In the first generation of optical systems, only the amplitude of the electromagnetic waves was used. The intensity modulation (IM) along with direct detection (DD) allowed to reach a capacity of 10 Gb/s. However, IM/DD systems operating at 40 Gb/s were not massively deployed because of a considerable sensitivity to propagation impairments mainly chromatic dispersion (CD) and polarization mode dispersion (PMD). Furthermore these systems also required high OSNR levels to reach the same distances as the 10 Gb/s systems.

2. **Quadrature:** The introduction of coherent detection allowed the access to the amplitude and also the phase of the electromagnetic wave. The latter was no longer a scalar but became a complex with real and imaginary parts. Consequently, the traditional On-Off keying (OOK) was replaced by more spectrally efficient modulation

formats such as the quadrature-phase shift keying (QPSK) and the quadrature-amplitude modulation (QAM). Later on, more sophisticated modulations such as probabilistic shaping of QAM [7] were proposed to increase the system throughput.

3. **Wavelength:** The optical fiber provides a huge bandwidth (nearly 4 THz in the C band). The fact of using different wavelengths for multiplexing the data and respecting a spacing between two adjacent wavelengths at least equal to the symbol rate is called wavelength-division multiplexing (WDM). This technology allowed to tremendously increase optical fiber systems capacity by transporting independent channels.

4. **Polarization:** The access to this degree of freedom was also made possible thanks to coherent detection. In fact the two orthogonal polarizations of the electromagnetic wave can carry different data, thus the capacity is increased by a factor of 2 in polarization-division multiplexed (PDM) systems. In coherent systems, polarization separation is done by MIMO signal processing at the receiver.

5. **Space:** The spatial dimension is the last degree of freedom that can be used in order to increase the capacity of optical fiber systems. The purpose of space-division multiplexing (SDM) is to increase the capacity by the number of parallel spatial paths. Two different approaches of SDM are possible, either by multi-mode fibers or multi-core fibers. In both cases, integration of optical and opto-electrical components is a must in order to maintain a reduced cost per bit.

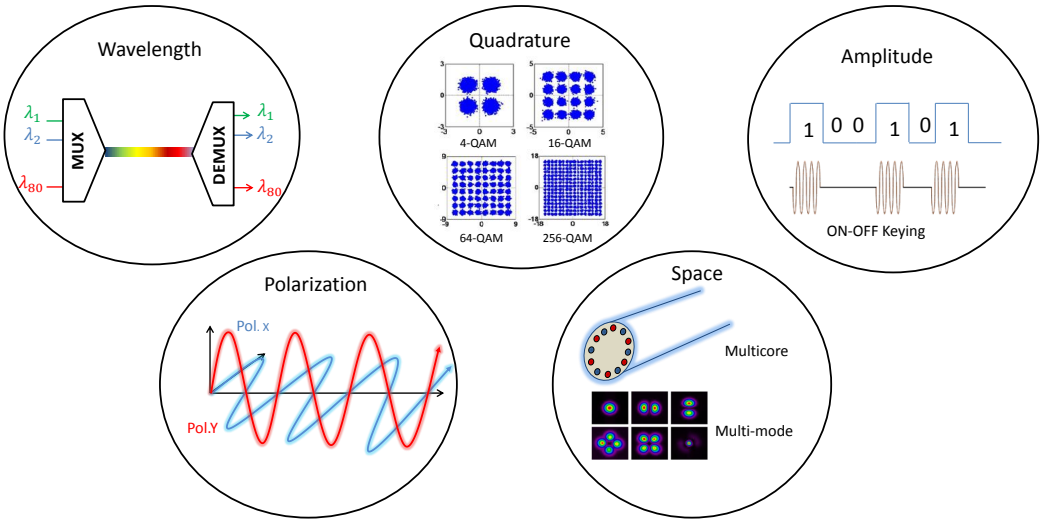

Figure 1.2: Physical dimensions for modulating and multiplexing in optical fiber systems.

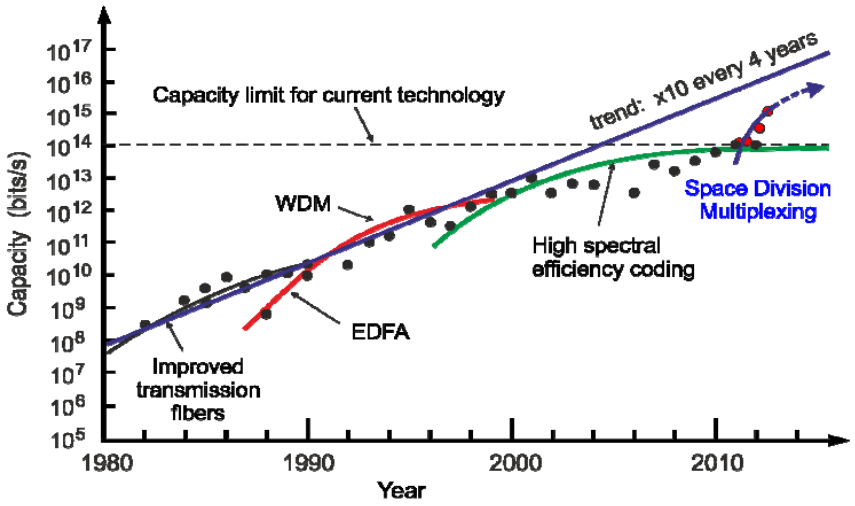

Figure 1.3: The evolution of transmission capacity of optical fibers over the years. Figure taken from [2].

The transmission capacity of optical fiber networks has made a considerable progress since the early 1970s. The first generation of optical systems had losses around ~ 3 dB/km and lasers for transmission were operating at wavelength 0.8 μm. However, the limitation of bit-rate-distance product due to intermodal dispersion [4] was behind the migration to single-mode fibers at wavelength 1.3 μm. Afterwards, wavelength 1.55 μm was adopted to minimize the fiber attenuation. In addition, the technology advancement of high-speed electronic devices enabled the manufacture of external optical modulators which allowed to reach a bit-rate of 10 Gb/s [8]

While the era between 1970 and 1990 has known a constant technology development and a moderate increase of bit-rate, starting from 1990s, optical systems have known a dramatic increase in system capacity mainly brought by wavelength-division multiplexing (WDM) and optical amplification [9] which allowed to move from few Gigabits per second to Terabits per second (see Fig.1.3). The first WDM systems were introduced in 1995 [10], they had between four and eight channels separated by 200 GHz and modulated at 2.5 Gb/s, this allowed a maximum capacity of 20 Gb/s. In 2000, dense WDM (DWDM) systems were packing more than 80 channels separated by only 50 GHz and modulated at 10 Gb/s allowed optical fiber capacity to reach nearly 1 Tb/s [10]. In the early 2010, commercially systems operating at 100 Gb/s per wavelength were available. To reach this capacity polarization-multiplexing was integrated. In fact, the coherent detection allowed to access the two orthogonal polarizations of the electromagnetic field which permitted to use them for multiplexing different data and increase capacity by a factor of 2.

As the available spectrum was nearly filled, research in optical systems was focusing in higher spectral efficiency (SE) modulation formats in order to increase the capacity. Recently a capacity record of 101 Tbps was achieved within laboratory experiment [11]. The SE that allowed this huge capacity was 11 b/s/Hz. However the high OSNR (optical signal-to-noise ratio) required by the use of 128-QAM and the sensitivity to non-linear effects has limited the transmission distance to only 3×55 km.

As we have seen, the rapid development of optical networks and the multiple technologies introduced during the last decade had enabled a system capacity that further exceeded the growing traffic. However, this situation is about to change, and the need for extra capacity is more urgent than ever. For this aim, intensive research has been carried out during the last years on space-division multiplexing (SDM) as the last degree of freedom still unused in order to increase the capacity of optical fibers [12].

In order to reduce the cost and energy per bit, future SDM optical systems will have to re-use the existing deployed WDM infrastructure and be compatible with it. Moreover, integration of optical components such as transponders, amplifiers, optical add/drop multiplexers (ROADMs), will provide a new generation of devices capable of addressing multiple spatial paths [13]. Furthermore, SDM optical systems require the development of new fibers that support the propagation of multiple spatial paths, spatial multiplexers (MUX) and demultiplexers (DEMUX), optical amplifiers capable of amplifying simultaneously all the spatial paths. Currently, two categories of optical fibers allow the realization of SDM: Few-mode fibers (FMFs) and multi-core fibers (MCFs). In both cases, coupling between spatial paths is inevitable and design of fibers that minimize the crosstalk is important. For MCFs, design of new fibers with a large separation between cores can reduce the crosstalk but this solution limits the spatial density of cores [12]. In a recent work [14], Ryf et al. demonstrated that a 4-core fiber with large effective areas shows a better tolerance to non-linearities and provides a 0.7 dB higher Q-factor than a single-mode fiber with the same core properties. For FMFs, design of fibers supporting the propagation of modes having different propagation constants is likely to reduce crosstalk. For both MCFs and FMFs, a residual crosstalk will still exist, which makes multiple-input multiple-output (MIMO) techniques important for these future systems to uncouple spatial paths.

1.2 Principle of optical transmitter and receiver

An optical system is composed of three principal blocs: The transmitter, the EDFA-based fiber line and the receiver. The role of the transmitter is to provide optically modulated signals to be sent through the optical fiber. The optical receiver extracts the information

signals at the output of the fiber. In this section we present the principle of optical transmitter and receiver.

1.2.1 Optical transmitter

The optical transmitter is composed of a laser diode (LD) that generates the optical carrier at a corresponding wavelength and a modulator that prints the information on the optical signal created by the laser.

- **Laser diode:** is a PN junction where the "P" (positive) side contains an excess of holes, while the "N" (negative) side contains an excess of electrons. the conversion of electrical signal to light is done in two main steps. A first variation in the current intensity of the PN junction leads to spontaneous emission of electrons from excited state E_2 to E_1 (see Fig.1.4). The second step consists into amplifying the output light by stimulated emission, this is done by placing the PN junction inside a resonant cavity. The laser stimulated emission starts at a certain threshold of some milliamperes and increases linearly proportional to the current intensity applied to the laser diode. An other important characteristic of laser diode is the threshold separating spontaneous and stimulated emission regimes (the point I_{th} in Fig.1.5), this point should be minimized in order to accelerate stimulated emission.

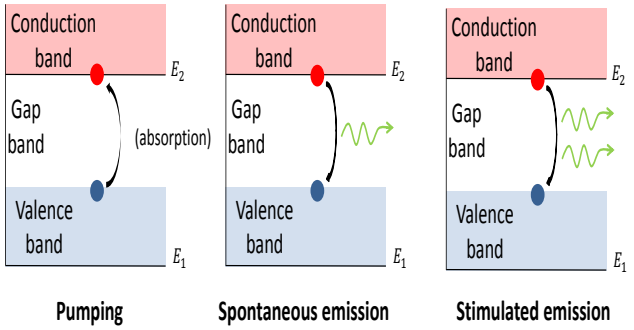

Figure 1.4: Principle of laser diode in 3 steps: pumping, spontaneous emission, stimulated emission.

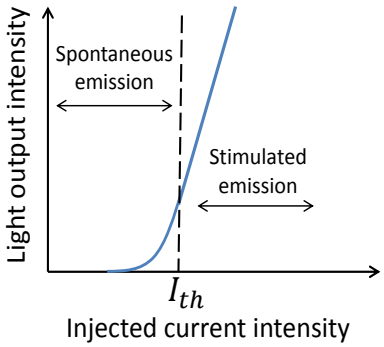

Figure 1.5: Laser intensity vs electrical input intensity.

- **Optical modulator:** is a device that allows to modify the light ray created by the laser diode into a modulated signal that can be given by:

$$E_0(t) = A_0(t).\exp(2\pi f_0 t + \phi_0(t)) \tag{1.1}$$

The output signal $E_0(t)$ varies with time t and depends on the three important parameters A_0, f_0 and ϕ_0. A_0 is the amplitude of the signal, it was used by intensity

modulation systems under the On-Off keying format where $A_0 = 0$ refers to no light emission and $A_0 = 1$ corresponds to light emission. Later on, the same physical quantity was used in pulse-amplitude modulation (PAM) in order to increase the throughput. ϕ_0 corresponds to the phase of the signal, it was used in phase shift keying (PSK) to modulate the phase of the signal. The use of both A_0 and ϕ_0 for modulation is called quadrature amplitude modulation (QAM). f_0 is the frequency of the signal and is given by $f_0 = c/\lambda_0$, where $c = 3.10^8$ m/s is the speed of light and λ_0 is the carrier wavelength.

The modulation of the optical carrier can be made following two main techniques: direct modulation and external modulation. In direct modulation, laser diode is directly powered with a modulated electrical signal. This method has a low cost since it only requires the LD, but its performance rapidly degrades due to optical frequency modulation chirp [15]. In external modulation, an external device which is the modulator modifies the optical signal issued from the laser diode according to the electrical signal (see Fig. 1.6). This strategy allows a larger bandwidth ~ 40 GHz and was widely deployed in access networks.

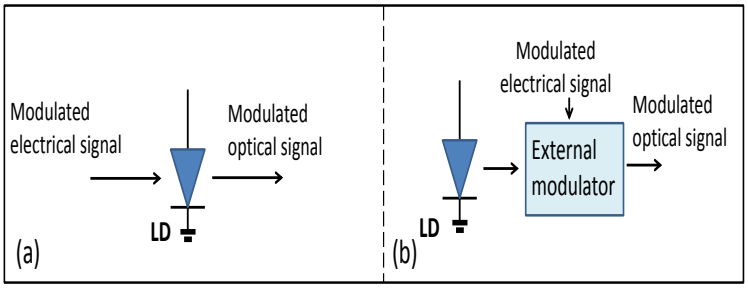

Figure 1.6: Modulation of optical carrier. (a): Direct modulation, (b): External modulation.

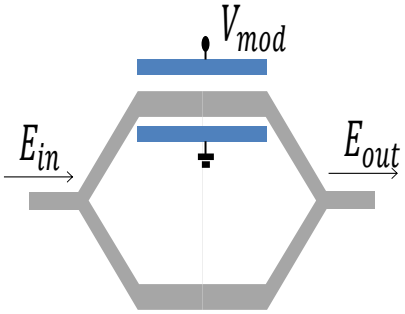

Figure 1.7: Mach-Zender modulator.

External modulators can be classified into two main families: The electro-absorption modulator (EAM) and the Mach-Zehnder modulator (MZM). The EAM is suitable for access networks of rates up to 40 Gb/s. The light is modulated according to the principle of modification of the absorption spectrum of a semiconductor inside an electric field, however, EAM generates chirped impulsions. The MZM is an electro-optical modulator composed by two 3 dB couplers. The first coupler is set as a reference while the second coupler is subject to an external phase variation. Consequently, it is possible to create constructive and destructive interference between signals at the output of the two couplers. This strategy allows to control the phase of the light at the output of the interferometer resulting in phase modulation of the

signal. Phase variation of the light at the output of the interferometer also causes an intensity variation which also allows amplitude modulation. The relation between the incident light E_{in} at the input of the MZM and the modulated optical signal E_{out} is given by:

$$E_{out} = E_{in}.\cos\left(\pi\frac{V_{mod}}{V_{\pi}}\right) \tag{1.2}$$

with E_{in} (resp. E_{out}) is the electric field at the input (resp. output) of the modulator. V_{mod} is the voltage applied to one of the arms to control phase, V_{π} is the drive tension corresponding to the phase shift from maximum to minimum interference between the two arms of the MZM.

1.2.2 Modulation formats

Capacity of optical systems can be increased either by adding more WDM channels or increasing the throughput of these channels. While the first solution is limited by the available optical bandwidth and also by the bandwidth of amplifiers, increasing the bit-rate can be done thanks to different modulation formats. The principle of modulation is to allow a propagating signal to carry useful information, this is done by modifying some characteristics of the signal according to different states called symbols. The set of all possible symbols form the alphabet of the modulation and can be binary as in the On-Off keying format and binary-phase shift keying or M-ary as in the quadrature-amplitude modulation.

1.2.2.1 On-Off keying

Non-return to zero On-Off keying (NRZ-OOK) is the basic way to create modulated signals, it was first used in intensity modulation systems. The alphabet of this modulation is binary where a '1' refers to transmission of light and '0' is the absence of light. NRZ-OOK can be realized by a single MZM by alternating from minimum to maximum power.
The simplicity and low cost of this format was not only at the transmitter but also at the receiver. In fact, a simple direct detection based on one photo-diode is enough to retrieve the signal. However, the main drawback of NRZ-OOK is a considerable sensitivity to nonlinearities originating from power fluctuations. To overcome this issue, other version of OOK were proposed such as the return-to-zero on-off keying (RZ-OOK) or the carrier-suppressed CS-OOK. Although these systems reduced considerably noise and nonlinearities sensitivity, the spectral efficiency was always limited to 1 bit/symbol

1.2.2.2 Binary phase shift keying

While OOK is an amplitude modulation, binary phase shift keying (BPSK) is a phase modulation. The phase of the optical signal is modified so that the bit '1' corresponds to a phase equal to π and the bit '0' corresponds to a null phase. Although both OOK and BPSK can be implemented by NRZ or RZ formats and have the same SE of 1 bit/symbol, BPSK has a 3 dB noise sensitivity improvement that can be intuitively understood from a higher distance between the two symbols (see Fig 1.8).

Although BPSK transmitter can also be implemented by a simple MZM, the receiver architecture is more complex. In fact, since the modulated physical dimension is phase, a simple direct detection cannot retrieve the useful information. The solution though consists in demodulating the signal optically before electrical conversion or to use a coherent reception.

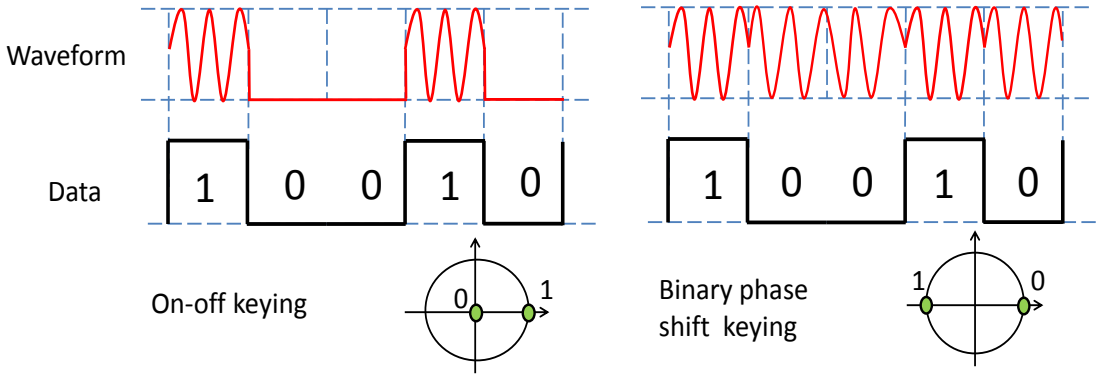

Figure 1.8: Modulated optical signal according to binary data: left OOK, right BPSK.

1.2.2.3 Quadrature phase shift keying

The two previous modulations have a limited SE of 1 bit/symbol. To overcome this limitation and allow more bits to be represented by one symbol, higher order modulation formats were investigated. Quadrature phase shift keying (QPSK), was the first modulation having four symbols in the alphabet to be introduced to optical communications, it transmits the four phase states $\{0, \frac{\pi}{2}, \pi, \frac{3\pi}{2}\}$ while conserving a constant amplitude which allows a SE of 2 bits/symbol.

Furthermore, QPSK has a half symbol rate comparing to BPSK at the same targeted bit-rate. This advantage makes QPSK occupies less spectral bandwidth and hence be less sensitive to chromatic and polarization dispersive effects. Regarding the modulation performance, QPSK and BPSK have the same tolerance to noise sensitivity. In fact the

distance between two symbols is reduced by $1/\sqrt{2}$ for the QPSK but this drawback is compensated by a double spectral efficiency.

To create QPSK symbols, two parallel MZM are needed. A $\frac{\pi}{2}$ phase shift is added after one of the modulators in order to create symbols in quadrature. To enable the detection of QPSK symbols, two BPSK receivers as described before are required.

1.2.2.4 Quadrature amplitude modulation

In order to continue the capacity growth of optical systems by increasing spectral efficiency, multi-level modulation formats were introduced to optical communications. Quadrature amplitude modulation (QAM) is one of the most efficient modulations to go beyond the spectral efficiency of 2 bits/symbol.

QAM can be considered as a generalization of QPSK. A QAM having q symbols in the alphabet is called q-QAM or 2^n-QAM where n is the number of bits per symbol. To create QAM symbols, the amplitudes of two optical carries are modulated. The first carrier contains the in-phase symbols and the second carrier is shifted by $\frac{\pi}{2}$ and contains the quadrature-phase symbols. the summation of the two carriers gives QAM symbols, the plot of all symbols of a QAM is called a constellation (some constellations are plotted in Fig. 1.9).

QAM format allowed to increase the capacity of optical systems and hence more data can be transported over the same limited bandwidth. However, this multi-level format requires a more complex system architecture both at the transmitter and the receiver.

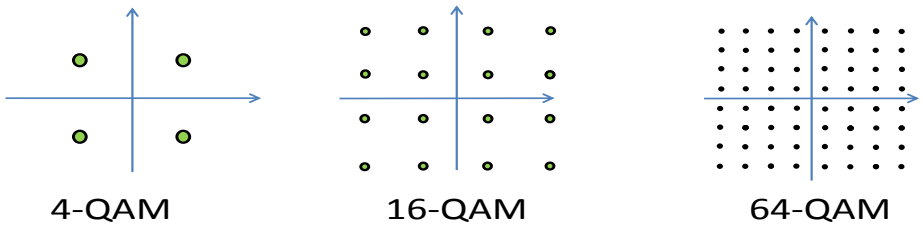

Figure 1.9: Constellations of 4-QAM, 16-QAM and 64-QAM.

1.2.3 From Direct detection to coherent detection

- **Direct detection (DD)** receivers were widely deployed with OOK and BPSK modulations allowing an optical capacity increase from 10 to 40 Gb/s. Moreover, optical amplifiers were not only used for signal regeneration but also enhanced the receivers sensitivity. In fact, optical amplifiers are placed before the receivers to provide enough power to incident signals, which ensures acceptable sensitivity for receivers.

For OOK format, the receiver detects the presence or absence of light and provides an electrical intensity proportional to the square of the intensity of the incident signal. With this simple scheme, the information contained in the phase is lost and BPSK needs a more complex implementation to be realized. The solution for this issue is to use the differential phase shift keying (DPSK) as a modulation format. The principle consists in modulating the information on the phase shifts between two consecutive symbols. At the receiver, demodulation is done in two steps (see Fig. 1.10). First, an interferometer creates a duplicate of the incident signal with one-symbol-delay. Then two photo-diodes provide an electrical current proportional to the phase shift between consecutive optical signals.

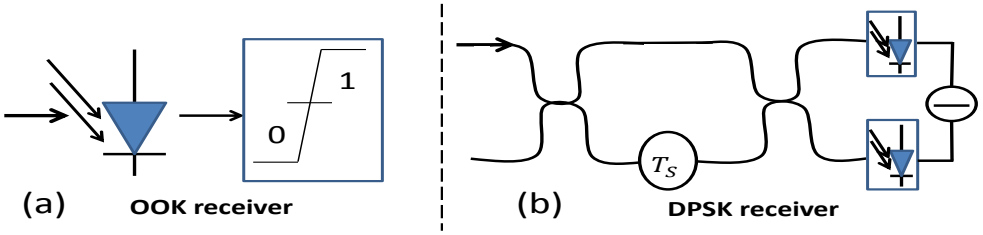

Figure 1.10: Direct detection receiver architecture : a) for NRZ-OOK format, b) for DPSK format.

- **Coherent detection** corresponds to beating the received signal with a local oscillator (LO) laser having nearly the same frequency. Coherent detection was first introduced in the 1980s [16] to improve receivers sensitivity but this technology required high complex equipment to compensate for the phase shift between the incident signal and the LO. However, optical amplification enabled DD to reach the same sensitivity with a lower complexity implementation, consequently, coherent detection was not cost-efficient comparing to DD. Later on, thanks to the advancement of high-speed integrated circuits and modern digital signal processing algorithms for estimating the carrier shift, coherent detection was revived.

  Let $E_s(t)$ (resp. $E_{LO}(t)$) be the incident signal (resp. the LO optical signal), these two signals can be represented as:

$$E_s(t) = A_s(t)\exp\left(j\omega_s t + \theta_s(t)\right),\ E_{LO}(t) = A_{LO}(t)\exp\left(j\omega_{LO} t + \theta_{LO}(t)\right) \tag{1.3}$$

  where $A_s(t)$, ω_s, $\theta_s(t)$ (resp. $A_{LO}(t)$, ω_{LO}, $\theta_{LO}(t)$) represents the amplitude, pulse frequency and phase of the signal (resp. the LO). The LO signal is split in two parts shifted by a phase of $\frac{\pi}{2}$ and then mixed with the incident signal. After that, two

photo-diodes return the intensity currents corresponding to the in-phase (I) and the quadrature-phase (Q) components of the signal that can be expressed as:

$$I_I(t) = \mathfrak{r}\sqrt{A_s(t).A_{LO}(t)}.\sin\left(\theta_s(t) - \theta_{LO}(t)\right) \tag{1.4}$$

$$I_Q(t) = \mathfrak{r}\sqrt{A_s(t).A_{LO}(t)}.\cos\left(\theta_s(t) - \theta_{LO}(t)\right) \tag{1.5}$$

where $\mathfrak{r}$ is the responsivity of the photo-diode Let $\Delta\omega = \omega_s - \omega_{LO}$ represents the carrier offset due to the LO. When $\Delta\omega = 0$, detection is said to be homodyne coherent. As given by equation (1.4) and (1.5) , coherent detection allows the access to both the amplitude and phase of the optical signal. Furthermore, the cascade of two coherent receivers gives also the access to both polarizations of the signal as shown in Fig 1.11 . In fact, the polarizations of the incident signal and the LO are extracted and set in two orthogonal axes, then two coherent receivers provides the intensity of each incident polarization. Consequently, information can be encoded in all the available degrees of freedom of PDM systems.

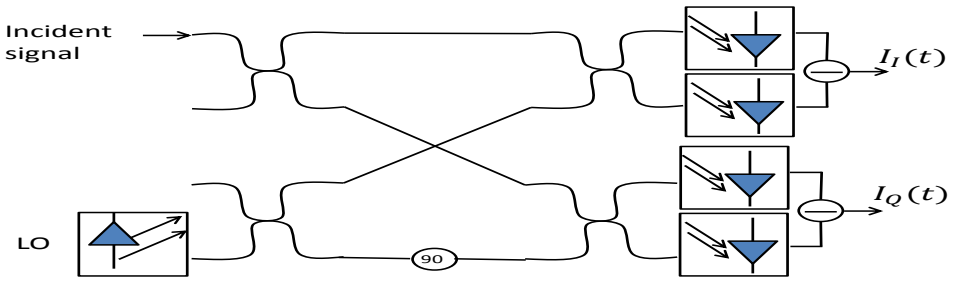

Figure 1.11: Coherent receiver architecture

1.3 Propagation in single mode fibers

Optical fiber is a cylindrical waveguide made of materials having a very low loss such as Silica. Propagation of light through the fiber consists in successive internal reflexions at the boundary between the core having a refractive index n_{co} and the cladding having a smaller reflexion index $n_{cl} < n_{co}$. Depending on the index change at the core-clading interface we distinguish two types of fibers: When the reflexion index changes abruptly between the core and the cladding, the fiber is said to be **step index**, but when the index gradually slows from the core to the cladding the fiber is said to be **gradient index** [17] (see Fig. 1.12b,c).

Another classification of optical fibers is based on the number of propagating light rays also called modes. When only one mode propagates, the fiber is said to be single-mode,

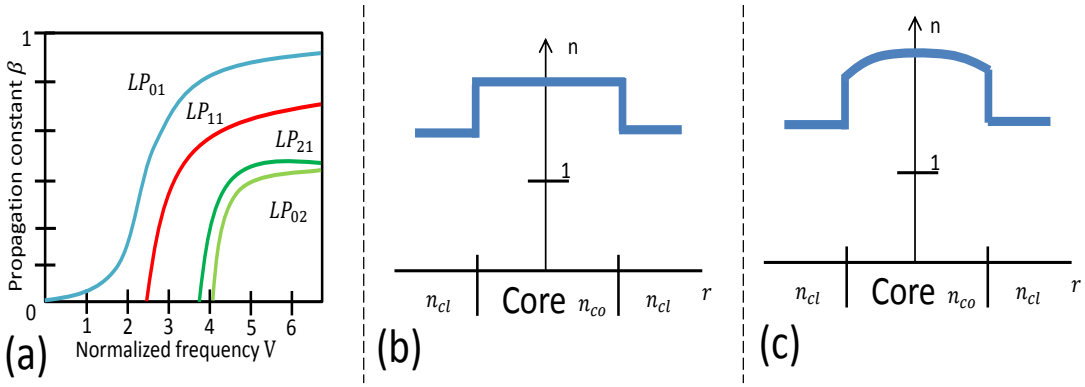

Figure 1.12: (a): Propagation constant as a function of the normalized frequency. Refractive index profile for: (b) step index single-mode fiber. (c): Gradient index single-mode fiber.

but when more than one mode propagates, the fiber is multi-mode. The number of modes allowed to propagate depends on the normalized frequency V of the fiber :

$$V = \frac{2\pi r_c}{\lambda_0}\sqrt{n_{co}^2 - n_{cl}^2} \tag{1.6}$$

where λ_0 is the wavelength corresponding to the carrier of the optical signal and r_c is the core radius. Each mode can be considered as a solution of the wave propagation equation and is characterized by its own cut-off frequency that when greater than V, the mode is allowed to propagate. In step-index fibers, the fundamental mode has a null cut-off frequency and hence is always allowed to propagate. Next modes appear at a cut-off frequency $V = 2.405$ (see the graph of Fig. 1.12a).

The electrical field of one polarization propagating along the axe z of a a single-mode fiber is given by :

$$E(x,y,z,t) = F(x,y)A(z,t)\exp(i(\beta z - \omega_0 t)) \tag{1.7}$$

where $A(z,t)$ is the complex envelope of the electrical field, $F(x,y)$ is the normalized spatial distribution of the field and β is the propagation constant that can be developed in Taylor series as a function of the angular frequency ω_0:

$$\beta_\omega = \beta_0 + \beta_1(\omega - \omega_0) + \frac{1}{2}\beta_2(\omega - \omega_0)^2 + ... \tag{1.8}$$

with β_i is the i^{th} derivative of β with respect to ω. Propagation of the electrical field of equation (1.7) obeys to the non-linear propagation equation obtained by the resolution of the four fundamental equations of electromagnetism (Maxwell equations). An approximation to the second order of the non-linear propagation equation is given by ([17],Chap 2):

$$\frac{\partial A}{\partial z} = -\frac{\alpha}{2}A - \beta_1\frac{\partial A}{\partial t} + i\frac{\beta_2}{2}\frac{\partial^2 A}{\partial t^2} - i\gamma|A|^2 A \tag{1.9}$$

with α is the attenuation of the fiber per unit length and is equal ~ 0.2 dB/km at a wavelength $\lambda_0 = 1.55\ \mu m$, α can be compensated by optical amplification but at the price of added optical noise. $\beta_1 = \frac{\partial \beta}{\partial \omega} = \frac{1}{v_g}$ is the inverse of the group velocity and represents the delay of propagation in the fiber. β_2 represents the dependence of the group velocity to the carrier frequency. γ is the non-linear coefficient and represents the dependence of the refractive index of silica to the injected power called the Kerr effect. In the next subsections we detail all these physical parameters.

1.3.1 Transmission loss

Due to propagation, traveling signals are subject to transmission loss which impacts the sensitivity of optical receivers that require a certain amount of power to detect the incident signals. Fiber losses depend on the optical wavelength λ_0 and can be divided in two categories: Rayleigh scattering and material absorption. Rayleigh scattering results from imperfections at the microscopic level that occurs during manufacturing. It causes a degradation of the signal power as $1/\lambda_0^4$ and affects mainly short wavelengths. Material absorption can be either intrinsic caused by the absorption of Silica or extrinsic originating from the impurities within Silica. Commonly used fibers called standard single-mode fibers (SSMF) have an attenuation of 0.2 dB/km when operating at wavelength $\lambda_0 = 1.55 \mu m$.

The attenuation α of an optical fiber at a distance L including all different sources of loss is given by:

$$\alpha = \frac{1}{L} 10 \log_{10} \left(\frac{P_{in}}{P_{out}} \right) \tag{1.10}$$

where P_{in} (resp. P_{out}) is the injected power at the fiber input (resp. the power at the distance L). α is commonly given in dB/km as $\alpha_{dB/km} = 10 \log_{10}(\alpha)$.

1.3.2 Chromatic dispersion

While the attenuation α affects the amplitude of the signal, chromatic dispersion (CD) causes a spectral widening of the optical signal that creates inter-symbol interference (ISI). In fact, due to the wavelength dependence of the refractive index of the fiber, spectral components of the signal travel at different velocities which causes time pulse broadening that is given by:

$$\Delta \tau = D.L.\Delta \lambda \tag{1.11}$$

where L is the fiber length and D represents the variation of the group delay per unit length. $\Delta \lambda$ is the wavelength pulse broadening. The group velocity dispersion (GVD) β_2 determines how much time the pulse has broadened when the signal has a spectral width

$\Delta\lambda$ and is given by:

$$\beta_2 = -D.\frac{\lambda_0^2}{2\pi c} \tag{1.12}$$

Neglecting fiber attenuation and non-linearities, the propagation equation (1.9) becomes:

$$\frac{\partial A}{\partial z} = i\frac{\beta_2}{2}\frac{\partial^2 A}{\partial t^2} \tag{1.13}$$

This equation has an analytical solution that represents the evolution of the envelope of the signal $A(z,t)$ at a distance z as a function of the signal envelope at the origin:

$$A(z,t) = A(0,t)\exp(-j\frac{\beta_2 z}{2}\omega^2) \tag{1.14}$$

From the last equation, it is clear that chromatic dispersion acts as filter with parabolic phase whose transfer function for a fiber of length L is given by:

$$H_{CD}(\omega) = \exp(-j\frac{\beta_2 L}{2}\omega^2) \tag{1.15}$$

To avoid ISI and hence a degradation in the performance, compensation for CD is required. One way of optically managing CD consists in inserting dispersion compensating fibers (DCF) that have a negative dispersion coefficient ($D < 0$). Moreover, coherent detection allows to compensate for CD in the electrical domain thanks to digital signal processing (DSP).

1.3.3 Polarization division multiplexing

Coherent detection has allowed the access to the amplitude, phase and the two polarizations of the optical signal. Using these three degrees of freedom with a QPSK modulation allows to reach 112 Gb/s with only 28 Gbaud sampling rates. The two polarizations represent an orthogonal decomposition of the electric field propagating in the transverse plane. the two polarizations are described by the state of polarization (SOP) given by:

$$\begin{pmatrix} E_x \\ E_y \end{pmatrix} = \begin{pmatrix} \sqrt{P_x}\exp(i\phi_x) \\ \sqrt{P_y}\exp(i\phi_y) \end{pmatrix} \tag{1.16}$$

where P_x, P_y, ϕ_x, ϕ_x are the amplitudes and phases of the polarizations E_x and E_y. The SOP also called Jones vector represents the pattern of the electrical field in the transverse plane of propagation.

Polarization division multiplexing (PDM) consists in modulating independently the two orthogonal polarizations and then recombining them with a polarization beam combiner (PBC). At the receiver, the signal from the LO is split in two to beat the two

polarizations, then two coherent receivers are required to convert light into current intensity as shown in Fig 1.13.

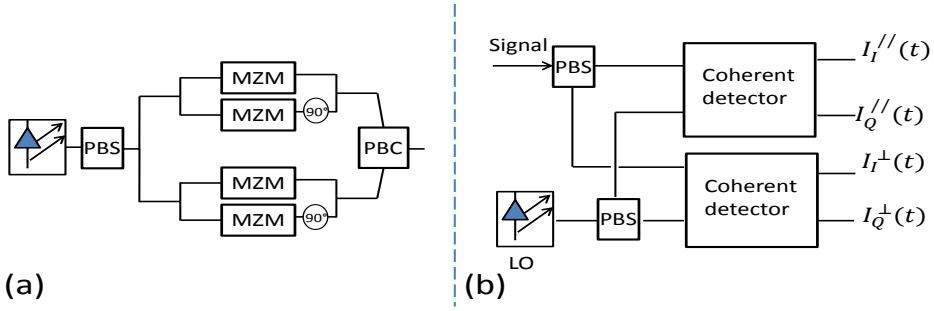

Figure 1.13: (a): PDM transmitter, (b): PDM coherent receiver

In addition to transmission loss and chromatic dispersion, PDM systems also suffer from linear impairments originating from the two polarizations. In fact polarizations are subject to different levels of attenuations, this phenomenon is known as polarizations dependent loss (PDL). Moreover, the two polarizations propagate at different velocities β_{1x}, β_{1y} due to random birefringence which creates random coupling between polarizations and a differential delay known as polarization mode dispersion (PMD). The propagation of the two polarization in the optical fiber is also governed by non-linear equations given by ([17],Chap 9):

$$\frac{\partial A_x}{\partial z} = -\frac{\alpha}{2}A_x - \beta_{1x}\frac{\partial A_x}{\partial t} - i\frac{\beta_2}{2}\frac{\partial^2 A_x}{\partial t^2} + i\frac{8}{9}\gamma\left(|A_x|^2 + |A_y|^2\right)A_x \tag{1.17}$$

$$\frac{\partial A_y}{\partial z} = -\frac{\alpha}{2}A_y - \beta_{1y}\frac{\partial A_y}{\partial t} - i\frac{\beta_2}{2}\frac{\partial^2 A_y}{\partial t^2} + i\frac{8}{9}\gamma\left(|A_y|^2 + |A_x|^2\right)A_y \tag{1.18}$$

where A_x (resp. A_y) is the complex envelope of the electrical field on the x (resp. y) direction. the term in γ represents the non-linear effects including non-linear interaction between the two polarizations.

1.3.4 Polarization mode dispersion

In a perfect circular fiber with no imperfections, the two polarizations of the electric field travel at the same velocity which creates no delay between signals modulating the two polarizations. Consequently, the fiber can be considered as a parallel 2×2 MIMO system. However in real fibers, geometric imperfections that occur during manufacturing process and thermal stresses make the fiber a birefringent waveguide. Birefringence means that the refractive index of the fiber as experienced by the orthogonal polarizations is different which result in a difference in propagation velocity that creates a time delay between the fast and the slow polarization known as polarization mode dispersion (PMD).

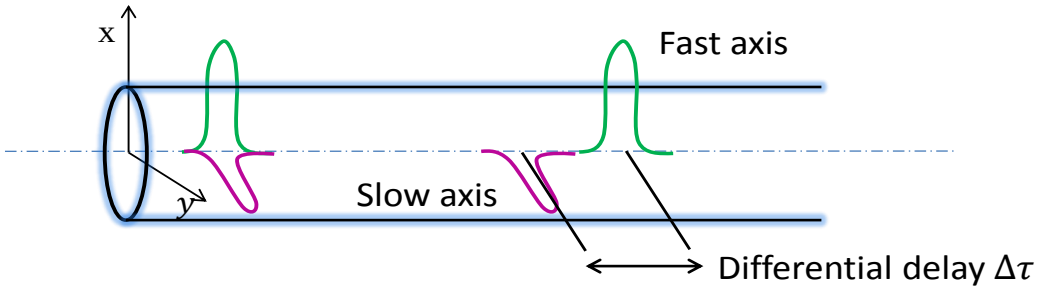

Figure 1.14: Effect of polarization mode dispersion on orthogonal polarizations.

In the presence of PMD, the received signals are subject to pulse broadening and overlapping which result in inter-symbol interference. Moreover, as delay between polarizations is not constant because thermal stress varies over time, the transfer function of PMD can be modeled as a concatenation product of N random and independent rotation matrices and birefringent matrices as follows:

$$H_{PMD} = \prod_{k=1}^{N} R_k D_k = \prod_{k=1}^{N} \begin{pmatrix} \cos(\theta_k) & -\sin(\theta_k) \\ \sin(\theta_k) & \cos(\theta_k) \end{pmatrix} \begin{pmatrix} \exp(-i\frac{\omega\tau_k+\phi_k}{2}) & 0 \\ 0 & \exp(+i\frac{\omega\tau_k+\phi_k}{2}) \end{pmatrix} \quad (1.19)$$

The rotation matrix R_k represents an orientation mismatch of angle $\theta_k \in [0, 2\pi]$ between the axes of polarizations and a birefringent element. The matrix D_k introduces a phase shift between polarizations that dependents on two elements: $\phi_k \in [0, 2\pi]$, which is caused by the birefringent element and $\omega\tau_k$ that represents the frequency dependence of the time delay τ_k between the two polarizations.

To overcome the signal distortion arising from PMD, different techniques were proposed. In [18], the authors show that a return-to-zero modulation format allows an extra 2 dB receiver sensitivity and is more robust to PMD than a non-return-to-zero format. Moreover, electronic equalizers for 40 Gb/s systems were developed [19] in order to electrically compensate for PMD which improved considerably PMD tolerance and system performance. Furthermore, with the introduction of coherent detection and the development of advanced signal processing algorithms, MIMO DSP equalization was used for chromatic dispersion and PMD compensation [20]. Later on, MIMO processing along with OFDM format allowed to completely absorb the effect of PMD in OFDM-PDM optical systems [21].

1.3.5 Polarization dependent loss

Polarization dependent loss (PDL) refers to the fact that the two polarizations experience different attenuations during propagation. PDL originates from non-ideal optical devices

such as amplifiers, connectors, couplers and filters. According to [22, 23], fiber couplers have a PDL up to 0.3 dB and optical band pass filters have a PDL in the range $0.2-0.4$ dB. The matrix representing a PDL element is given by:

$$H_{PDL} = R_\theta \begin{pmatrix} \sqrt{1+\gamma} & 0 \\ 0 & \sqrt{1-\gamma} \end{pmatrix} R_\theta^{-1} \tag{1.20}$$

R_θ is a random rotation matrix that represents a mismatch between the polarization axes and the axes of the PDL element. The diagonal matrix represents the power imbalance between the most attenuated polarization and the least attenuated. Polarization dependent loss in dB is denoted as Γ_{dB} and is defined as:

$$\Gamma_{dB} = 10\log_{10}\left(\frac{1+\gamma}{1-\gamma}\right) \tag{1.21}$$

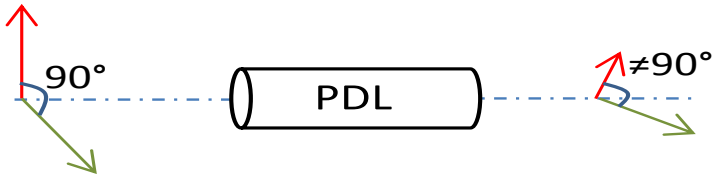

Figure 1.15: Loss of orthogonality and power imbalace due to PDL.

In optical systems containing a cascade of several PDL components, the global link PDL fluctuates which affects system performance. The link PDL is not simply the sum of the PDLs arising from all components, and in the presence of birefringence, PDL fluctuates randomly and requires to be statistically evaluated. In [24], the author showed that the standard deviation of PDL grows linearly with the number of PDL elements. In[25], the authors studied the concatenation of PDL elements and proved that the global PDL follows a Maxwellian distribution.

As mentioned previously, PDL causes a loss of orthogonality between the two polarizations which induces OSNR degradations. For PDM systems based single-mode fibers, the orientation angle θ between the polarizations of the signal and the PDL element is a key factor that impacts the OSNR performance. We distinguish two particular cases:

- $\theta \equiv 0$ [90°]: one polarization experiences the maximum loss while the other polarization is privileged (see Fig. 1.16).

- $\theta \equiv 45°$ [90°]: both polarizations observe the same attenuation but the loss of orthogonality between them is maximum [26].

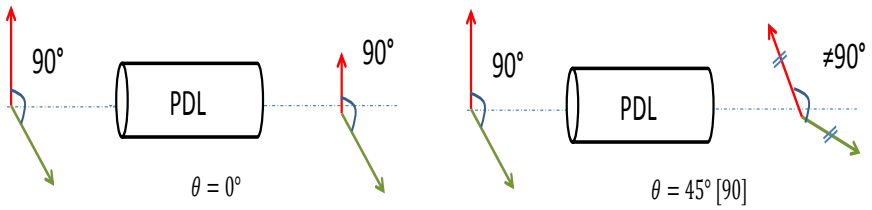

Figure 1.16: Effect of PDL as a function of the angle θ between polarizations and the PDL element.

The rapid development of high-speed electronic devices has allowed to compensate for most of physical impairments arising in single-mode fiber propagation such as CD and PMD. Consequently more tolerance to these phenomenons was allowed without reducing the performance. Moreover, different DSP solutions were proposed to mitigate PDL. In [27], the authors applied a pairwise coding on the two polarizations which brings 2 dB Q-factor improvement for a PDL of 6 dB. In [28], the authors proved the efficiency of polarization time codes to mitigate PDL in 1000 km considering distributed PDL.

1.3.6 Non-linear effects

The refractive index of optical fibers increases as the power of the electrical field gets higher, this is known as the Kerr effect. Consequently, fiber non-linearities arise from the dependence of the refractive index on the power intensity in the fiber, it is given by:

$$\tilde{n} = n + n_2 . \left(|E_s|^2 / A_{eff} \right) \tag{1.22}$$

where n is the constant linear refractive index, n_2 is the non linear refractive index and depends on the amount of power E_s present in the effective area A_{eff} of the fiber. For Silica fibers $n_2 \sim 2.6 \times 10^{-20}$ m^2/w which makes the non-linear part of the refractive index $< 10^{-12}$. However non-linearities become more severe in long distance fiber systems. In the following, we describe the three non-linear effects present in SMF transmission systems.

- **Self phase modulation:** The refractive index dependence on the power in equation (1.22) implies that the propagation constant becomes also power dependent [17]:

$$\tilde{\beta} = \beta + \frac{2\pi . n_2}{\lambda_0} . \left(|E_s|^2 / A_{eff} \right) = \beta + \gamma . |E_s|^2 \tag{1.23}$$

$\gamma = \frac{2\pi.n_2}{\lambda_0} A_{eff}$ is the non-linear coefficient also present in the non-linear propagation equation (1.9). This term induces a non-linear phase shift of the electrical field at a distance z and is given by:

$$\phi_{NL}(z) = \gamma \left| E_s(z=0) \right|^2 L_{eff} \tag{1.24}$$

$L_{eff}(z)$ represents the effective fiber length and accounts for the section of fiber where non-linear effects are considerably affecting propagation. Due to transmission loss, optical power is higher in the first part of the line and after optical amplifiers which makes these two regions more affected by non-linearities. $L_{eff}(z)$ is given by:

$$L_{eff} = \frac{1 - \exp(-\alpha L)}{\alpha} \tag{1.25}$$

where L is the fiber length and α is the transmission loss.
From equation (1.24) we notice that the non-linear change of the phase only depends on the carrier wavelength λ_0 present in the term γ. When non-linearity affecting the phase of an optical signal is self-induced, this phenomenon is called self phase modulation (SPM).

- **Cross phase modulation:** Can be seen as a generalization of self phase modulation in the presence of multiple wavelengths. Cross phase modulation (XPM) occurs in WDM systems, and the non-linear phase modulation affecting a given channel i is induced from the power of the channel itself and also other channels:

$$\phi_{i,NL} = \gamma L_{eff} \left(\left| E_{i,s}(z=0) \right|^2 + \sum_{k \neq i} \left| E_{k,s}(z=0) \right|^2 \right) \tag{1.26}$$

  In order for XPM to create a phase shift, pulses from different channels must overlap in time. For pulses widely separated XPM appears to be neglected compared to SPM. In contrast, pulses from adjacent channels interfere enough that XPM becomes more important.

- **Four-wave mixing:** is also caused in a multi-channel configuration. In fact, the propagation of three channels of carrier frequencies $\omega_1, \omega_2, \omega_3$ creates a four channel whose frequency is given by: $\omega_4 = \omega_1 \pm \omega_2 \pm \omega_3$. As four-wave mixing (FWM) includes the interaction of several channels, this non-linear effect becomes more severe when spacing between channels is reduced.

Non-linear effects represent a major limitation for optical transmission systems. To achieve the optimal bit-error rate (BER), the optical launch power must be adjusted depending

on the fiber length. Furthermore, to reduce the impact of non-linearities and increase the system reach, several compensation strategies such as digital back propagation can be used [29].

1.3.7 Optical amplification

The introduction of optical amplifiers in the earlier 1990s has started the age of long-haul optical transmission systems. Optical amplifiers are inserted typically every 40-120 km which reduces considerably the number of amplifiers in the line. Erbium doped fiber amplifier (EDFA) was deployed at the same time as WDM systems as it has a large amplification window that covers all the WDM band.

EDFA was first demonstrated by [30] and [31] and quickly became a revolution in optical communications. EDFA consists of a few meters of a SMF doped with erbium ions Er^{3+} where the optical signal propagates along with one or more signals being amplified by lasers at wavelength 0.98 μm or 1.48 μm. The pumping operation realized by semiconductor lasers makes the Er^{3+} ions absorb energy and become more excited. When these ions relax their energy level by the emission of photons signal amplification is realized.
Two categories of photon emission exist. Stimulated emission leads to the release of photons with the same physical properties as the signal (frequency, phase and polarization), this same photons generate also new photons with the same properties and so on. Another type of emission called spontaneous emission happens when photons are emitted in a disordered way in all directions. Unfortunately, a part of these noisy photons propagate along with the input signal direction which affects the signal as an additive noise. This phenomenon called amplified spontaneous emission (ASE) is the main drawback of EDFA and is commonly assumed to be additive white Gaussian noise .
Typically, EDFA gain can reach 40 dB and a maximum output power of ~ 23 dBm (0 dBm corresponds to 1mW). However an EDFA that compensates for the losses of a fiber of length L introduces extra noise having a power spectral density per polarization given by [32]:

$$N_{ASE} = (G-1)\,\bar{h} f_0 n_{sp} \tag{1.27}$$

with $\bar{h} = 6.62 \times 10^{-34}$ J.s is the Plank constant, $G = \exp(\alpha.L)$ represents the gain of the amplifier and n_{sp} is the spontaneous emission factor. The corresponding OSNR between the amplified signal and the ASE within a spectral band $B_{ref} = 0.1$ nm is given as [32]:

$$\text{OSNR} = \frac{P_s}{2.N_{ASE}.B_{ref}} \tag{1.28}$$

where P_s is the average incident optical power. The factor 2 corresponds to the ASE affecting the two polarizations of the signal.

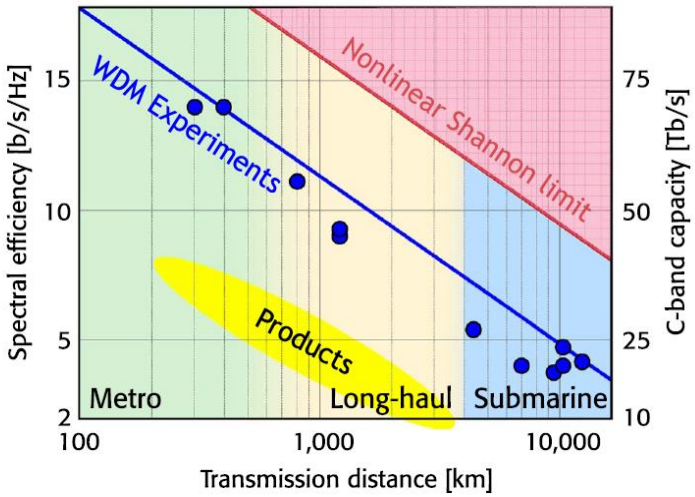

Figure 1.17: Spectral efficiency and capacity vs transmission distance for commercialized products and WDM experiments compared to the nonlinear Shannon limit. Figure taken from [3].

Optical amplification along with WDM and coherent detection have allowed to tremendously increase the capacity of SMF systems. Experimental laboratory records have demonstrated capacities up to 100 Tb/s and commercial WDM systems operate at around 10 Tb/s as shown in Fig. 1.17. However, with an annual traffic growth of 20% to 40%, commercial systems will require 100 Tb/s capacity between 2018 and 2022 [3]. The latter capacity cannot be reached by single-mode fiber systems which are restricted by the nonlinear Shannon limit [33].

1.4 Propagation in multi-mode fibers

To cope with the exponential growth in the demand for more bandwidth and to afford an optical capacity that will support future data traffic, space division multiplexing (SDM) is being intensively investigated as the last physical dimension unused in optical fiber transmission systems. In fact, optical systems based single-mode fibers have already used time, phase, frequency and polarization in order to increase network capacity. Unfortunately these single-mode transmission systems have already reached their non-linear Shannon limit [33, 34]. Hence space is the last available degree of freedom to increase optical network bandwidth and avoid a capacity crunch.

Space division multiplexing can be realized either by multi-core fibers (MCFs) which are fibers with many cores or few-mode fibers (FMFs) that support the propagation of a small number of modes. In the case of FMFs, space multiplexing is referred to as mode division multiplexing (MDM). Mode multiplexers/demultiplexers (MUX/DEMUX) are mandatory to inject and extract the set of spatial modes in and out of the FMF. Also few-mode optical amplifiers should enable the amplifications of modes simultaneously without separating them. After detection of modes by coherent receivers, digital signal processing is required in order to jointly or separately process modes according to the level of coupling.

The number of propagating modes in FMFs depends on the characteristics of the fiber through the normalized frequency V given by equation 1.6. Each exact spatial mode represents a specific solution to the wave equation taking into account the boundary limits. However these modes can be combined to form a set of M linearly polarized (LP) modes where each mode has two polarizations. For step-index fibers, the spatial distributions of LP modes can be approximated by Bessel functions. For graded-index fibers a Laguerre-Gauss representation describes better the spatial distribution of modes. By using the linearly polarized representation, a spatial mode is denoted LP_{lq} where l is the azimuthal order and q is the radial order of the mode. When $l \neq 0$, a mode has two orthogonal spatial distributions known as degenerates and denoted as $LP_{lq,a}$ and $LP_{lq,b}$.

MDM consists in modulating each mode with independent data information, hence the capacity of the optical link is increased by the number of modes. In real systems, propagation through FMFs is also affected by impairments that require either optical or DSP compensation. In addition to physical impairments such as chromatic dispersion or polarization mode dispersion also present in single-mode fiber systems, propagating modes in FMFs suffer from additional effects caused by the simultaneous propagation of modes in the same fiber. First, modes travel at different velocities which causes a differential mode group delay (DMGD) that needs to be addressed in the design of the fiber line. Moreover, modes are also subject to unitary linear coupling that can be compensated by appropriate DSP at the receiver. Linear modal coupling can also be non-unitary known as mode dependent loss (MDL), in this case, it impacts directly the capacity and performance of MDM systems. In the next sections, we focus on these different effects and their impact on the performance.

1.4.1 Linear modal coupling

In ideal MDM systems, orthogonal modes propagate in parallel paths without interfering. However, fiber manufacturing imperfections and index perturbations cause overlapping between propagating modes leading to a coupling between the transmitted signals. In

fact, modal coupling is a transfer of energy from one mode to another that can occur at discrete points such as MUX/DEMUX, splices, connectors, optical amplifiers. Also, modal coupling can originate from the propagation through the FMF itself due to micro-bends or mechanical stresses. If the coupling is unitary, which means that the set of M propagating modes remains orthogonal, then only DSP at the receiver is required to retrieve the original data multiplexed on each mode. However, coupling can also be non-unitary, in this case fluctuations in power between modes occur, resulting in OSNR penalties.

The amount of modal coupling is an important factor to take into account in the design of MDM systems. Modal coupling between two modes depends on their propagation constant difference $\Delta\beta$ and if they are degenerate or not. In fact, modes within the same mode group (modes having the same propagation constant β) are subject to strong coupling even for distances less than 1 km [35]. On the contrast, coupling remains weak between modes from different groups even after 100 km. Consequently, two regimes of modal coupling appear to be two different choices in the design of MDM transmission systems.

In the strong coupling approach, more relaxed constraints on the amount of modal coupling are permitted. In this case, less specifications are needed in the manufacturing of optical components that introduce coupling as MUX/DEMUX or few-mode amplifiers. Moreover, strong coupling alleviates the effect of mode dependent loss which increases the average capacity and avoids system outage [36]. However, this strategy brings the drawback of high DSP complexity, and requires $2M \times 2M$ MIMO processing when M modes are used with both polarizations [37], which increases tremendously processing power and receiver complexity.

In the weak coupling approach, modal crosstalk is considered as a limitation and is taken into account in the design of the MDM architecture. Hence the coupling level is reduced to the minimum to avoid using a full $2M \times 2M$ MIMO processing at the receiver. However, even in the weak coupling regime, a strong coupling occurs between pairs of degenerate modes ($\Delta\beta \approx 0$) and a common 4×4 MIMO is required to jointly process them with both polarizations. In [38], the authors demonstrated the transmission over 40 km of five data streams modulated at 100 Gb/s on five modes. The authors achieved weak mode coupling by using a high DMGD and a large effective index difference between any two modes. At the receiver, two 4×4 MIMO were used to process the $LP_{11a,b}$ and $LP_{21a,b}$ with both polarizations and a 2×2 MIMO was dedicated to the two polarizations of the LP_{01}. Hence, receiver complexity was reduced and complex 10×10 MIMO was

avoided. The transfer matrices representing weak and strong coupling are given by:

$$C_{\text{strong}} = \begin{pmatrix} c_{1,1} & \cdots & c_{1,2M} \\ \vdots & \ddots & \vdots \\ c_{2M,1} & \cdots & c_{2M,2M} \end{pmatrix} \qquad C_{\text{weak}} = \begin{pmatrix} C^{\beta_1}_{2k_1,2k_1} & 0 & \cdots \\ 0 & C^{\beta_2}_{2k_2,2k_2} & \\ \vdots & 0 & \ddots \end{pmatrix} \tag{1.29}$$

For strong coupling, C_{strong} is a full $2M \times 2M$ matrix. For weak coupling, C_{weak} is block unitary, where in each block a full matrix $C^{\beta_i}_{2k_i,2k_i}$ represents coupling between k_i modes having the same propagation constant β_i.

1.4.2 Differential mode group delay

Each mode in the FMF propagates at a different velocity due to its own propagation constant β. The difference $\Delta\beta$ between modes is differential mode group delay (DMGD). In contrast to the polarization delay in SMFs caused by fiber imperfections, DMGD in FMFs is an intrinsic property of the fiber that arises even for FMFs without imperfections. The perfect knowledge of DMGD level in a FMF is an important factor in the design of the MDM transmission system. In [39] the authors studied DMGD behavior in step index and gradient index fibers supporting a large number of modes (> 6 LP modes). The authors succeeded to manufacture gradient index fiber that allow a max|DMGD| <10 ps/km. On the other hand step index fiber was proved to authorize a high DMGD level (|DMGD| >1 ns/km). For M propagating modes with both polarizations, a modal dispersion element is represented by:

$$D = \begin{pmatrix} \exp -i\left(\phi_1 + \omega\tau_1\right) & & 0 \\ & \ddots & \\ 0 & & \exp -i\left(\phi_{2M} + \omega\tau_{2M}\right) \end{pmatrix} \tag{1.30}$$

where ϕ_i represents the phase noise of mode i and τ_i is the group delay of mode i.

Another key element directly impacting DMGD is modal coupling. In fact, in the strong coupling regime, DMGD accumulation is minimized as modes overlap during propagation. In this case the group delay spread scales with the square-root of the fiber length [40]. Modal coupling can also be intentionally increased by introducing distributed perturbations such as spinning the fiber during the pulling process [41]. In the weak coupling regime, DMGD becomes large as modes having different β travel independently at different velocities. In addition to strong and weak coupling regimes, in recent studies [42, 43] the statistics of group delay for an intermediate regime of coupling were reported which allow to design MDM transmission systems with exact amount of coupling

and DMGD.

As we have seen, modal coupling directly affects the group delay spread which in turn impacts the complexity of MIMO DSP at the receiver. When time domain equalization (TDE) is used, DMGD level is crucial to determine the temporal memory length required for the equalization, hence a large DMGD increases the complexity [37]. On the other hand, for systems using a frequency-domain equalization (FDE), DMGD is essential to fix the fast Fourier transform (FFT) block length either in single-carrier modulation format or multi-carrier format.

Realization of MDM systems can indeed take two different strategies. Strong modal coupling with very low DMGD or weakly coupled modes having very large DMGD. In both cases coupling causes a spatial interference and modal delays cause interference. The interaction of both effects results in ISI that has to be managed at the receiver. Fortunately, coherent MDM transmission systems with modern DSP techniques allow to mitigate most of the impairments arising from propagation. However, real-time systems should keep computational complexity as low as possible especially for long-haul systems where the impairments accumulate. OFDM format enables a lower complex implementation than TDE when suitable cyclic prefix is inserted to absorb all the residual DMGD. Also, only a $2M \times 2M$ single-tap frequency filter for each sub-carrier is required to uncouple modes. Unfortunately, all this compensation done by OFDM comes at the cost of extra added overhead that limits the net throughput of the transmission.

1.4.3 Mode dependent loss

Mode dependent loss (MDL) is known to be a main issue in the design of MDM transmission systems. Unlike DMGD and unitary modal coupling that can be compensated by MIMO DSP at the receiver, MDL causes power fluctuations between modes resulting in OSNR penalties. MDL can be seen as a generalization of PDL affecting polarizations in single-mode fiber systems. The effect of MDL and its detrimental impact on MDM systems capacity was reported in several studies [34, 44, 45].

In MDM systems, MDL can be either distributed through the fiber or local at the insertion of optical components. MDL arising from the fiber line is due to the manufacturing imperfections such as splices or micro-bends. Accumulated splice losses as low as 0.03 dB may lead to system outage after only a few hundred of kilometers [46]. Another source of MDL comes from the optical components such as MUX/DEMUX [47, 48] and optical amplifiers [49, 50]. When MDL arises from few-mode EDFAs, it is referred to as mode dependent gain (MDG). In fact, amplifiers increase the energy of modes with different amount of powers and manufacturing few-mode EDFAs allowing equal power gains is still

a challenge. Furthermore, it was proven that propagating noise also suffers from MDL resulting in a noise correlation at the receiver [34, 51].

As for DMGD, mode dependent loss is also highly impacted by the coupling regime of propagation. In fact strong mode coupling can be used as a solution to reduce the accumulated MDL by averaging the loss disparities over all modes [44]. In [36], the authors show for a 3×136 Gb/s transmission that the loss per mode averages for high coupling leading to high MDL tolerance compared to the weak coupling regime. Moreover, modal coupling can be intentionally added thanks to mode scramblers at local points mainly after few-mode amplifiers [52]. In order to add mode scramblers it is necessary to introduce a mechanical perturbation in the form of the fiber to allow mode mixing. Also, the authors have considered maximum-likelihood (ML) detection rather than a zero-forcing (ZF) to have the optimal performance. However, ML detection becomes very greedy in terms of computational complexity required to estimate symbols especially for high number of modes and modulation constellation size. To relax this complexity a Reduced-Search ML (RS-ML) [52] that combines the minimum-mean square error (MMSE) estimation and ML was considered.

Although the previous methods enable to alleviate the impairment caused by MDL, these strategies have several limitations. In fact, strong coupling needs a full MIMO DSP at the receiver and this constraint becomes more severe if ML decoding is considered. On the other hand adding mode scramblers in the line requires manufacturing ideal scramblers which do not introduce extra MDL, otherwise extra penalties will arise.

1.4.4 Mode multiplexers and demultiplexers

Mode multiplexers (MUX) and mode demultiplexers (DEMUX) are essential components for the realization of MDM. The role of the MUX is to combine modes from M single-mode fibers and inject them into the FMF. This is done in two steps as shown in Fig 1.18. First, the incident signals from the M single-mode fibers arrive on their fundamental mode LP_{01}, these signals are converted into the desired higher order modes. After that, all modes are combined together and injected simultaneously in the FMF. Mode DEMUX is simply a MUX operating in the inverse direction.

Mode conversion is the important part of a MUX/DEMUX, it can be realized by several techniques. A basic approach is mode stripping (MS) which consists in applying a macro bending of several turns to strip out higher order modes [48]. Another method is long period fiber grating (LPFG) mode converters [53] that consists in applying a periodic mechanical pressure on the FMF to obtain the profile of a higher order mode. LPFG converters have the advantage of a small size, low loss and easier fabrication. A more

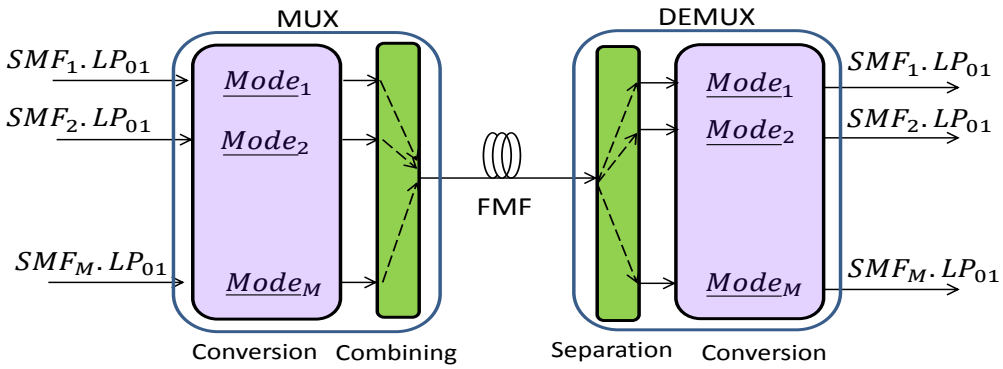

Figure 1.18: mode multiplexer and mode demultiplexer scheme

sophisticated technique for mode conversion is spatial light modulator (SLM) that can be used for any desired higher order mode [54, 55]. SLM principle is based on holograms and consists of changing the spatial intensity and phase distribution of the incident fundamental mode from the single-mode fiber to obtain the desired mode. However, this technique is very complex and limited by the pixel resolution of the SLM.

Combination and separation of modes from the input and output of the FMF can be done in a simple way by a free space mode combiner/splitter [55, 56]. The principle is to use a set of mirrors to converge the beams of already converted modes into the beam combiner, then modes are injected into the FMF. Another technique is based on fused fiber mode couplers [57, 58]. The principle is to fuse the single-mode fiber to the FMF and hence by mode coupling the FMF absorbs the desired mode. Furthermore, in recent years, a promising technique based on multi-plane light conversion (MPLC) being developed by CAILabs [59] allows to convert and multiplex modes simultaneously. The principle consists in successive reflexions on a multi-pass cavity where different phase profiles are implemented which allow to create and combine the desired higher order modes.

As discussed above, different strategies enable the realization of mode MUX/DEMUX. However, manufacturing such devices that allow the multiplexing of any number of modes is still a challenge for the integration. Furthermore, optical MUX/DEMUX are not ideal devices since they introduce modal coupling, insertion losses (IL), MDL and also a PDL between polarizations of higher order modes [48, 53].

1.5 MIMO digital signal processing for MDM systems

Current coherent PDM systems already use 2×2 DSP to compensate for CD and PMD. Increasing the number of spatial modes will result in an increased DSP complexity due to a higher dimensionality of the MIMO equalizer. In MDM systems, the group delay

(GD) spread caused by DMGD exceeds the GD spread associated with CD or PMD. Consequently, reducing the computational complexity and energy consumption of MIMO equalizers are critical assumptions in the design of MDM systems.

Linear mode coupling is directly impacting the complexity of MIMO equalizers in MDM systems. In fact the complexity of a full $2M \times 2M$ MIMO equalizer implemented for M coupled modes with both polarizations is $2 \times 2.M^2 = 4M^2$. On the other hand the equalizer complexity of MDM system where M uncoupled modes propagates is $2 \times 2.M = 4M$ [60]. In both cases signals arriving at the receiver are coherently and synchronously detected then digitalized thanks to analog-to digital converters (ADCs).

Without loss of generality, we consider that the channel matrix $H(t)$ containing symbols modulated on modes and polarizations has a dimension $M_s \times M_s$. We describe the two techniques for single-carrier channel inversion that are time-domain equalization (TDE) and frequency-domain equalization (FDE) and discuss their computational complexity.

1.5.1 Time-domain equalization

Both the in-phase (I) and quadrature (Q) components of all spatial paths are detected and digitalized to form the M_s complex signals $y(t)$. A linear equalizer estimates the channel matrix and applies its inverse $H^{-1}(t)$ to the received signal to obtain an estimation of the transmitted signal as:

$$\tilde{x}(t) = H^{-1}(t) * y(t) \tag{1.31}$$

where $\tilde{x}(t) = [\tilde{x}_1(t), ..., \tilde{x}_{M_s}(t)]$ is the vector of equalized symbols, $(*)$ denotes the element wise convolution. After this inversion operation, laser phase noise have to be estimated and compensated, this step is called carrier phase estimation (CPE) and the k^{th} signal after phase compensation is given by:

$$\tilde{x}'_k(t) = \tilde{x}_k(t).\exp(-j\hat{\phi}_k(t)) \tag{1.32}$$

where $\hat{\phi}_k(t)$ is the laser phase fluctuation estimation and can be obtained using the Viterbi-Viterbi [61] algorithm. The estimation of the coefficents h_{ij}^{-1} of the inverse channel can be done either by blind or data-aided (DA) approach. In the blind approach, information data of the signal itself is used e.g., the constant modulus algorithm (CMA). However blind approach has a slow convergence rate an weak performance for low OSNRs. For DA approach, a known training sequence is inserted at the beginning of each signal and the least-mean square (LMS) algorithm is the standard algorithm used to estimate inverse

channel coefficients iteratively as:

$$h_{ij}^{-1}(t+1) = h_{ij}^{-1}(t) + 2\mu \left[d_k(t-\Delta) - \tilde{x}'_k(t-\Delta) \right] y_k(t-\Delta) \exp(-j\hat{\phi}_k(t-\Delta)) \tag{1.33}$$

where Δ is a delay for carrier phase estimation $\exp(-j\hat{\phi}_k(t))$, μ is the convergence step size. For estimating the channel matrix, the LMS algorithm operates in the DA mode ($d_k = x_k$). after that, the algorithm switches to the decision-directed mode to estimate information symbols.

The complexity of TDE using a finite impulse response (FIR) filter adapted by the LMS algorithm is measured by the number of multiplications per symbol per mode. The number of taps in each filter is given by:

$$N_{Tap} = M_s.R_s.\Delta\tau.L.B \tag{1.34}$$

where B is the symbol rate (also called the Baud rate), R_s is the sampling rate (number of samples/symbol), $\Delta\tau.L$ represents the DMGD of the fiber of length L. From equation 1.34, updating filter coefficients requires $M_s.\Delta\tau.L.B$ multiplications. Hence the complexity of TDE is given by:

$$C_{TDE} = M_s.(R_s+1).\Delta\tau.L.B \tag{1.35}$$

From the last equation, we notice that the complexity scales linearly with the number of modes, DMGD and the symbol rate. Hence the DSP complexity of TDE for MDM systems increases according to three parameters, which makes complexity reduction a critical challenge for real implementation of TDE in future MDM system.

1.5.2 Frequency-domain equalization

In frequency-domain equalization (FDE), the complexity is reduced thanks to the use of multiplications rather than convolutions in the processing algorithm. This is done thanks to fast Fourier transforms (FFT) and inverse FFT (IFFT), which allow to estimate the filter coefficients in the frequency domain.

FDE consists in regrouping and parallelizing the received signals into blocks of length N_{FFT} to operate the FFT and IFFT operations. As for TDE, FDE also computes iteratively filter coefficients using the LMS algorithm as:

$$\bar{h}_{ij}^{-1}(f+1) = \bar{h}_{ij}^{-1}(f) + \mu E_{i,l} \otimes Y_{j,m}^{*} \tag{1.36}$$

where $\bar{h}_{ij}(f)$ is the Fourier transform of $h_{ij}(t)$, $E_{i,l}$ is the l^{th} block of the i^{th} mode, $Y_{j,m}^{*}$ is the conjugate of the signal block and $\otimes$ refers to an element-wise multiplication.

The complexity implementation of the FFT/IFFT for the M_s modes is $M_s \log(M_s/2)$, updating equalizers requires $M_s.N_{TAP}$ multiplications and the total FFT/IFFT per mode is $4+2M_s$. Hence the complexity of the FDE is given by:

$$C_{FDE} = (4+2M_s)\log(R_s.\Delta\tau.L.B) + 4M_s \tag{1.37}$$

To compare the complexities of TDE and FDE, in Fig 1.19, we plot these complexities as a function of the number of MDM spatial channels for a fiber length of $L = 2000$ km and a differential dispersion of $\Delta\tau = 50$ ps/km, a symbol rate of 25 Gbaud and $B = 1$ sample per symbol. We notice that FDE allows an important complexity reduction compared to TDE. When the number of channels is $M_s = 10$, FDE complexity is 100 times lower than the TDE complexity. Hence, FDE can be a promising candidate for long-haul MDM systems.

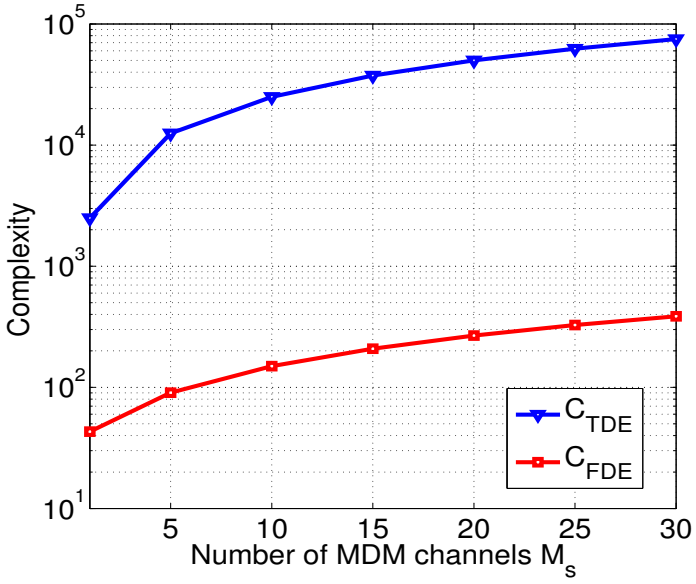

Figure 1.19: Complexity comparison of TDE and FDE as a function of the number of modes.

To further reduce the complexity, a cyclic prefix can be added at the beginning of each signal block, This allows to enhance the performance of the equalizer but at the cost of added overheads. This technique is mainly used in multi-carrier modulation format that is essentially implemented with OFDM. A study of OFDM for optical communications will be given in chapter 4.

Summary

In this chapter we have reviewed the evolution of optical fiber network traffic and the different optical technologies to cope with it. we presented the different degrees of freedom used to increase the optical fiber capacity. We presented an overview of the development of SMF systems and the importance of WDM along with optical amplification in the long-haul transmissions. Moreover, PDM with coherent detection allowed to reach a bit rate of 100 Gb/s. In the last part, we focused on MDM as a possible way to continue the capacity growth of optical transmission systems. The realization of MDM is still facing many challenges mainly an appropriate DSP to compensate for DMGD and modal coupling. Furthermore, MDL is a non-unitary effect that reduces MDM performance and capacity and cannot be mitigated with equalization at the receiver. In the next chapter, we study MDM systems impaired by MDL and we present three different solutions to mitigate this impairment and enhance the capacity.

Chapter 2

Capacity of Mode Division Multiplexed Optical Systems Impaired by MDL

We have listed in the previous chapter the main physical impairments affecting the propagation in SMF systems and MDM based MMF systems. In our thesis work, we are interested in MDM systems as a potential solution to cope with the increasing demand for capacity. Propagation through MMFs is affected by numerous impairments that require powerful DSP algorithms to be mitigated. As coherent detection allows to access the amplitude, phase and polarization of the optical signal. DSP can make benefits of these three dimensions to compensate for propagation distortions.

DMGD and modal coupling are directly related, and a trade-off between the amount of mode group delay and mode coupling is essential to determine the receiver DSP complexity. In all cases, these two effects can be compensated by time or frequency domain equalizers. In contrast, MDL cannot be compensated by MIMO DSP at the receiver. One main detrimental impact of MDL is a capacity reduction of the MDM system caused by the power fluctuations experienced by spatial modes. In the extreme level of MDL, capacity of MDM systems is reduced to the capacity of a SMF system [44].

In this chapter, we start by a capacity analysis of communication systems. After, we present the capacity of a general MIMO channel and define the average and outage capacities that allow to study the system margins. We also study the impact of channel state information (CSI) on the capacity. Afterwards, we focus on the MIMO MDM system impaired by MDL, we study the capacity and propose a statistical CSI to improve it. In the

third section, we study optical mode scrambling for MDM and its impact on the capacity, we also propose an optimal strategy to scramble modes. Lastly, we present mode selection as a strategy that allows to deploy MMFs supporting a higher number of modes while using only the less MDL affected. We also show a capacity enhancement with mode selection comparing to a MMF that allows the propagation of the same number of modes.

2.1 Capacity analysis of communication systems

Bandwidth is a limited resource in any communication system. Thus to satisfy the strongly increasing demand for higher transmission capacity, a better use of the existing frequencies and channel condition is a must. In this section, we start by reviewing the fundamentals of a single-input single-output (SISO) communication system. After that, we study how MIMO can increase the throughput in the same bandwidth and focus on different capacities used to determine MIMO systems performance.

2.1.1 Mutual information and Shannon capacity

One fundamental question in the design of any communication system is: What is the maximum possible rate of an efficient transmission? The answer to this question, was given by Claude Shannon [62], the founder of information and communication theory. To have an insight on the maximum data rates allowed to be transmitted in a communication channel with a low probability of error, we consider the general communication scheme of Fig. 2.1.

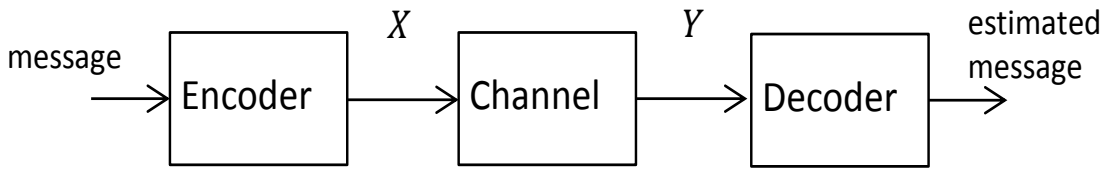

Figure 2.1: General communication channel including encoder and decoder.

A sequence of source symbols called message is mapped into channel symbols X commonly known as modulated symbols. After propagation through the channel, the received symbols Y are different from the input sequence X due to channel effect. From the output sequence Y, a decoder retrieves the initial message. If two input symbols may lead to the same output, they are said to be confusable. To overcome this issue, source messages can be encoded into widely separated symbol sequences, so we can transmit with a very low probability of error, and hence the decoder can reconstruct the initial source messages.

Shannon has defined the channel capacity as the mutual information between input X and output Y maximized over all possible distributions of input X and is given by:

$$C = \max_{f(x)} I(X;Y) = \int_{A_X A_Y} f(x,y) \log\left(\frac{f(x,y)}{f(x).f(y)}\right) \tag{2.1}$$

the integral is taken over the alphabet support A_X and A_Y of X and Y, $f(x)$ (resp. $f(y)$) represents the probability density function (PDF) of the input symbol X (resp. Y), $f(x,y)$ is the joint PDF of X and Y. For an additive white Gaussian noise channel (AWGN) with a received signal-to-noise ratio (SNR), this capacity is achieved when the input sequence distribution follows a Gaussian law, which results in the well known capacity:

$$C = \log(1 + \mathrm{SNR}) \tag{2.2}$$

The calculus to obtain the capacity given in equation 2.2 is very simple since the SISO AWGN channel is straightforward to manipulate. The Shannon capacity of equation 2.2 fixes the maximum amount of information that can be transmitted for a given channel, but is it possible to achieve this capacity ? The answer was given by the Shannon coding theorem that was proved in [63]. The theorem states that for a given channel of capacity C, if ones tries to transmit with a rate $R \leq C$, it is always possible to find an encoder such that the transmission error tends to zero when the length of the transmitted sequence tends to infinity. In contrast, if ones transmit with a rate $R > C$, there exist no encoder that allows a transmission free of error.

After we have reviewed the origin of the channel capacity and how it can be achieved, in the next section we present the capacity of MIMO channels and focus on the average and outage capacities because of their importance in defining the performance margins of communication systems.

2.1.2 Capacity of MIMO systems

The emergence of multiple-input multiple-output technique was first developed for wireless communications to make benefit of space as a degree of freedom to overcome the scarcity of wireless spectrum. MIMO systems have proven their potential in increasing wireless capacity without increasing the bandwidth, throughput and power consumption. Moreover, MIMO architecture allowed to jointly process all the spatial paths which improved the signal decoding and hence the reliability of the transmission.

A wireless MIMO system brings two advantages termed as diversity gain and multiplexing gain. Diversity gain is related to the performance enhancement brought by the

MIMO comparing to a point-to-point communication link. This gain, for example, can be achieved by placing multiple antennas at the receiver. In fact, for the same transmitted signal, different copies are received by the antennas. These copies are combined and processed together to provide a better estimate of the transmitted signal. The MIMO multiplexing gain is given by the increase of the communication rate or capacity comparing to a SISO system.

Let us consider a MIMO transmission channel where a complex vector X of symbols is sent using M transmitters and a complex vector Y is detected by M receivers. When the transmission is linearly affected by a random propagation matrix H and a white Gaussian noise with zero mean and spectral density $2\sigma^2$ per transmitter, the MIMO equation of transmission is given by:

$$Y = H.X + N \tag{2.3}$$

The channel matrix H contains the physical properties of the propagation medium. For the AWGN channel, H is equal to the identity matrix $H = I$. For the Rayleigh fading channel, the elements h_{ij} of H are random complex Gaussians with zero mean and a unit variance. In optical MDM systems, if we consider only the effect of DMGD, the channel H will be given by equation 1.30. In this study, we consider the general case when H is a random complex matrix. The maximum of the mutual information in 2.1 is obtained for Gaussian distributed inputs and the capacity is given by [64]:

$$C = \log\det\left(I + \frac{P_t}{M} H Q_x H^\dagger\right) \tag{2.4}$$

where P_t is the total power and $Q_x = \mathbb{E}\left\{X.X^\dagger\right\}$ is the covariance matrix of the input vector X. The last expression of the capacity was obtained by a maximization over all possible input distributions. However it doesn't provide any information about the choice of Q_x. The determination of the covariance matrix Q_x is essential since it represents the allocation strategy of the finite amount of power P_t available at the transmitter. This constraint is represented as:

$$\mathrm{Tr}\,(Q_x) = P_t \tag{2.5}$$

2.1.2.1 MIMO capacity without channel state information

Channel state information (CSI) refers to the properties of the channel matrix H. These properties are always known to the receiver. In fact, channel estimation based on a known training sequence inserted at the beginning of the transmitted data or blind channel estimation allow the receiver to estimate the channel. Hence, when we refer to capacity

without CSI, we conclude that it is a capacity without CSI at the transmitter.
In the absence of CSI the best choice of the covariance matrix Q_x in equation 2.4 was proven to be the identity matrix ($Q_x = I$), the capacity is then given by [65]:

$$C_{eq} = \sum_{i=1}^{r} \log\left(1 + \frac{P_t}{M} . \frac{\lambda_i}{2\sigma^2}\right) \tag{2.6}$$

where λ_i are the non zero eigenvalues of $HH^{\dagger}$ and $r \leq M$ is the rank of the channel matrix H. The last equation expresses the capacity of the MIMO channel as the sum of capacities or r independent SISO channels as shown in Fig 2.2, each channel having a gain $\frac{\lambda_i}{2\sigma^2}$. Hence, in the absence of CSI, the best power allocation strategy is to give each transmitter the same amount of power $\frac{P_t}{M}$ [64].

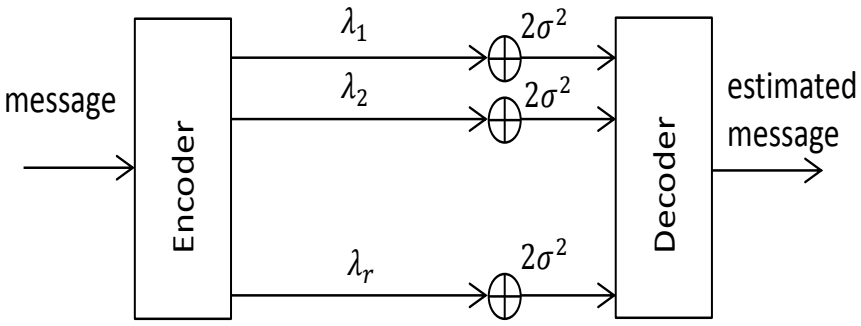

Figure 2.2: Equivalent parallel representation of a MIMO system as an r parallel SISO systems.

The equal power allocation strategy has the advantage of a low-cost implementation since no algorithm is required to distribute power among the M transmitters. However, giving the same amount of power to all paths that face different propagation attenuations is not the best power allocation strategy since it results in a loss of power on the most attenuated paths. Fortunately, this drawback can be overcome with the availability of CSI at the transmitter.

2.1.2.2 MIMO capacity with channel state information

When the knowledge of the CSI is available at the transmitter, the covariance matrix Q_x can be chosen in order to maximize the channel capacity [66, 67]. This strategy requires the receiver to send CSI in a feedback to the transmitter and also an appropriate algorithm to compute the matrix Q_x. The common algorithm used to calculate the optimal powers

is the waterfilling algorithm (WF) [65]. In this case the capacity is given by:

$$C_{CSI} = \sum_{i=1}^{L} \log\left(1 + p_i^* \frac{\lambda_i}{2\sigma^2}\right) \tag{2.7}$$

where $L \leq r$ is the number of spatial paths with a non zero power allocated by the WF algorithm. p_i^* is the optimal power allocated to the channel i and is given by:

$$p_i^* = \mu - \frac{2\sigma^2}{\lambda_i} \tag{2.8}$$

μ is a constant chosen to satisfy the power constraint of equation 2.5. From the capacity expression of 2.7, we notice that only L channels among the r available are excited, the others have a zero power. In order to determine the best channels and the corresponding optimal powers, the WF algorithm performs a singular value decomposition (SVD) of the channel matrix as $H = U.\Lambda.V^{\dagger}$. The diagonal matrix $\Lambda = \text{diag}\left[\sqrt{\lambda_1}, ..., \sqrt{\lambda_M}\right]$ is used to compute the optimal powers per channel and the matrix V is used to send correlated symbols vector $V.X$ in stead of sending the vector X. A representation of the WF power allocation is given in Fig 2.3 for an 8×8 MIMO system. More power is given to the sub-channels with highest λ_i.

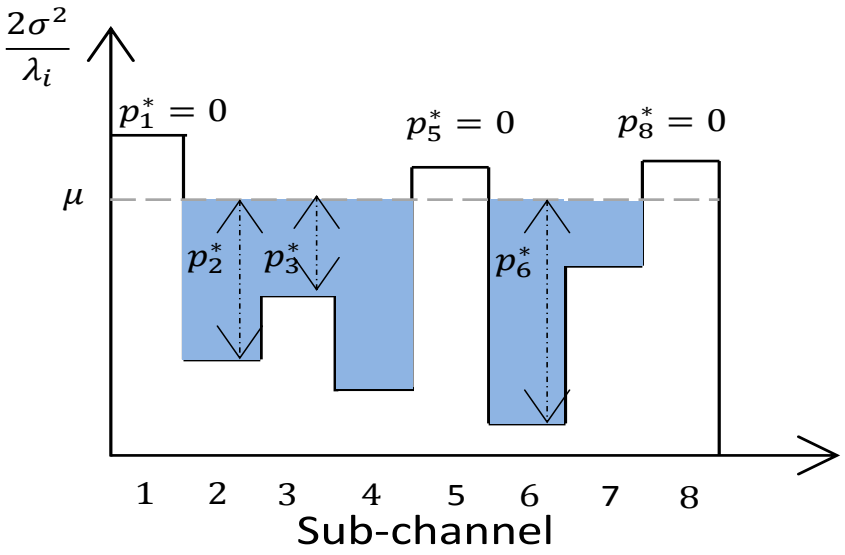

Figure 2.3: Illustration of waterfilling with power allocated to each channel.

The capacity enhancement obtained by the availability of CSI comes at the cost of a complex implementation of a sophisticated algorithm able to track channel changes and update optimal powers according to channel variations. The complexity of the WF algorithm is related to the number of iterations required for convergence. Moreover, the

accuracy of CSI sent in the feedback from the receiver to the transmitter depends on the coherence time of the channel. In fact, CSI must arrive to the transmitter before the channel impulse response changes.

Coherence time of a channel is defined as the time Δ during which channel coefficients h_{ij} remain constants. The capacities we have presented before are defined withing the coherence time of the channel. However, as the channel changes during time, the average capacity of the channel is an important parameter to predict the system performance. The average capacity also referred to as the ergodic capacity is given by:

$$C_{\text{avg}} = \mathbb{E}_H \left(C_{\text{inst}}(H) \right) \tag{2.9}$$

where $C_{\text{inst}}(H)$ refers to the instantaneous channel capacity and the average is taken over the distribution of the channel H. Hence, the computation of the average capacity requires the knowledge of the distribution of h_{ij} which is not always available. Another useful statistical measure of MIMO channel capacity is the outage capacity. Outage considerations quantify the capacity that is guaranteed with a certain level of reliability. The outage capacity C_{out} is related to an outage probability p_{out} as:

$$\Pr \left(C_{\text{inst}}(H) \leq C_{\text{out}} \right) = p_{\text{out}} \tag{2.10}$$

The outage capacity is more important than the average capacity because it defines the guaranteed capacities when H is changing and hence defines system margins. C_{out} is a measure of the spread of instantaneous capacities in term of probability. In fact, if the rate of the channel is spread over a wide range, C_{out} might be small for a certain p_{out} whereas C_{avg} can be high.

To have an insight on outage importance, we simulate 10^5 channel realizations of a 6×6 MIMO Rayleigh fading channel. We plotted the cumulative distribution function (CDF) of the channel capacity without CSI. From Fig. 2.4, we notice that the outage capacity is smaller than the average capacity, and if a random instantiation is lower than C_{out} then system is in outage. Consequently, it is very important to design systems with a very small outage capacity region to avoid system outage.

2.2 Capacity of MDM systems in the presence of MDL

In this section, we study the capacity of mode division multiplexed system based multimode fibers as a MIMO system. We are interested in the behavior of MDM channel in

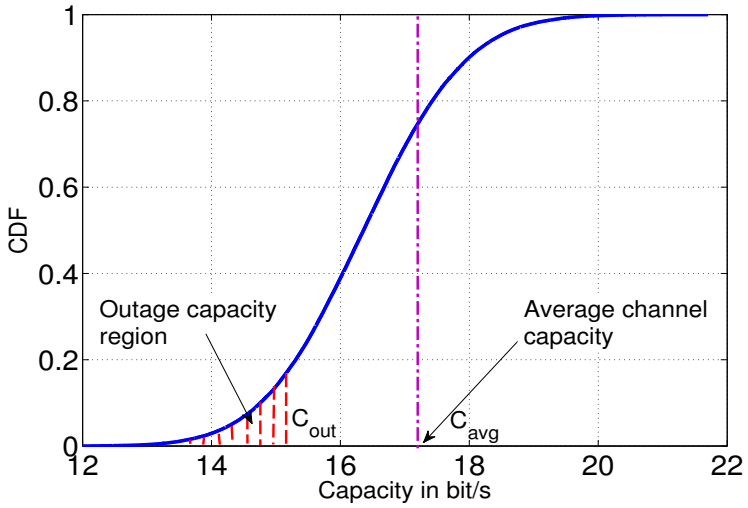

Figure 2.4: CDF of the capacity of the 6×6 Rayleigh fading channel.

the presence of MDL. The impact of MDL in MMFs is similar to PDL in SMF systems where polarizations experience different attenuations. However quantifying MDL is not straightforward since it depends on a number of modes $M \geq 2$ and it varies according to different scenarios depending on MDL sources and mode coupling levels. MDL can be distributed through the fiber, originating from fiber splices or micro-bends. In this case, the MDL generated by these physical impairments is low, nonetheless, the accumulation of MDL especially for long-haul systems gives rise to an important amount of MDL at the link end. Moreover, few-mode amplifiers also introduce a mode dependent gain (MDG) at local amplification points which also contributes to the global MDL. Manufacturing of few-mode amplifiers that have equal gains for all spatial modes is still a challenge for future MDM optical transmission systems.

In our thesis work, we study the distributed MDL arising from splices and micro-bends. In all the chapter, we consider gradient-index FMFs (GI-FMF) with core radius r_c and a numerical apperture $NA = \sqrt{n_c^2 - n_{cl}^2} = 0.205$, where n_c (resp. n_{cl}) is the refractive index of the core of the fiber (resp. of the cladding), the wavelength is set to $\lambda = 1.55\mu m$. To focus on the impact of MDL on system capacity, only one polarization is considered. The purpose of choosing GI-FMFs rather than step index FMFs is the minimization of DMGD between modes. The number of propagating modes depends on the core radius r_c, the wavelength λ and the numerical aperture NA through the normalized frequency V defined in equation 1.6. In our work we fix λ and NA and we increase r_c to allow the propagation of more modes. In Table 2.1, we report the parameters of our used GI-FMFs. The fundamental mode LP_{01} is always allowed to propagate because of its null cut-off

frequency. For a core radius of $r_c = 6\ \mu m$, the normalized frequency is $V = 3.52$ and the two degenerates LP_{11a} and LP_{11b} propagate. Increasing the core radius to $r_c = 8.6\ \mu m$ gives rise to three other modes which are the $LP_{21,a}$, $LP_{21,b}$ and the LP_{02}. To reach ten propagating modes, the core radius is set to $r_c = 11\ \mu m$.

Table 2.1: GI-FMF parameters for 3, 6 and 10 modes at $\lambda = 1.55\ \mu m$ and $NA = 0.205$

number of modes	core radius	Propagating modes
3	6 μm	$LP_{01},\ LP_{11a,b}$
6	8.7 μm	$LP_{01},\ LP_{11a,b},\ LP_{21a,b},\ LP_{02}$
10	11 μm	$LP_{01},\ LP_{11a,b},\ LP_{21a,b},\ LP_{02},\ LP_{12a,b},\ LP_{31a,b}$

In a weakly guided GI-FMF such that $(n_c - n_{cl})/n_c \ll 1$, we can express the transverse field distribution of the linearly-polarized (LP) modes with a good approximation by Laguerre-Gauss polynomials as in [68]:

$$E_{l,q}(r,\phi) = C_{l,q}\left(\frac{r}{w}\right)^{l} L_q^{(l)}\left(\frac{r^2}{w^2}\right)\exp\left(\frac{-r^2}{2w^2}\right)\begin{Bmatrix}\sin(l\phi)\\ \cos(l\phi)\end{Bmatrix} \tag{2.11}$$

The field distribution of the last equation is written in polar coordinates given by r and ϕ. l denotes the circumferential order and q is the radial order of the LP_{lq} mode. $L_q^{(l)}(x)$ is the generalized Laguerre polynomial of order l and degree q and $w = \sqrt{r_c/(k_0.NA)}$ is the spot size of the fundamental mode LP_{01} with $k_0 = 2\pi/\lambda$ is the free space wavenumber. $C_{l,q}$ is a normalization factor chosen to fulfill the orthogonal relation between spatial modes $\iint_A E_i.E_j dA = \delta_{i,j}$.

2.2.1 Spliced MDM channel model based FMF

In our capacity analysis, we consider a physical description of propagation through GI-FMF with realistic non-unitary mode coupling generated by fiber splices and connectors. This modelization is based on the electrical field distributions of spatial modes as described before rather than a mathematical modeling based on random matrices as in [34, 44]. In our work, we don't consider fiber non-linearities, the resulting linear MIMO channel is given by:

$$Y_{M\times 1} = H_{M\times M}.X_{M\times 1} + N_{M\times 1} = \sqrt{L}\prod_{k=1}^{K}(T_k C_k)\,X_{M\times 1} + N_{M\times 1} \tag{2.12}$$

where $X_{M\times 1}$ (resp. $Y_{M\times 1}$) is the vector of transmitted (resp. received) symbols, $N_{M\times 1}$ is an additive white Gaussian noise vector with zero mean and variance $2\sigma^2$ per mode.

The matrix $H_{M\times M}$ represents the spliced FMF composed of K fiber sections. The factor L represents the mode averaged propagation loss. T_k is a diagonal matrix with random phase entries $\exp(i\phi_m)$ and $\phi_m \in [0, 2\pi]$. DMGD is not considered since it does not affect the capacity of the system and can be managed using TDE filters or an OFDM format with a suitable cyclic prefix. Non-unitary modal coupling due to fiber misalignments at splice point is considered by an $M \times M$ coupling matrix C_k, with entries computed using an overlap integral of the electrical fields of propagating modes at fiber cross sections as in [46]:

$$c_{i,j} = \iint_A E_i^{(k-1)}(x,y) E_j^{(k)*}(x+\Delta x, y+\Delta y) dA \tag{2.13}$$

where $E_i^{(k-1)}(x,y)$ is the normalized complex amplitude of the of the i^{th} mode before the splice and $E_j^{(k)*}(x+\Delta x, y+\Delta y)$ is the normalized complex amplitude of the j^{th} mode after the splice. Δx and Δy are fiber misalignments assumed to be independent Gaussian distributed in x and y directions with zero mean and standard deviation (std) $\sigma_{x,y}$. At each fiber misalignment, a non-unitary coupling occurs between modes, the accumulated effect from all misalignments results in a end-to-end MDL defined as the ratio in decibels (dB) of the maximum to the minimum eigenvalues of $HH^{\dagger}$.

$$\text{MDL}(dB) = 10.\log_{10}\left(\frac{\lambda_{max}}{\lambda_{min}}\right) \tag{2.14}$$

In our simulations, we consider fibers made of $K = 300$ concatenation of misaligned fiber sections. To emulate different MDL levels, we vary $\sigma_{x,y}$ as a percentage of the fiber core radius r_c. For each of the considered fibers, MDL probability distribution function (PDF) is shown in Fig. 2.5 for 10^6 channel realizations. From the figure, we notice that MDL increases with an increasing misalignment std. Moreover, the misalignment std expressed as a percentage of the core radius becomes more important for fibers with large core that support higher order modes, hence MDL becomes very large.

2.2.2 Average and outage capacities of MDM optical channel impaired by MDL

An ideal MDM system based on MMF multiplies the available capacity of a given link by the number of propagating modes M, in this case all modes have the same attenuation. Due to MDL this capacity is reduced and for high levels of MDL the fiber supports the propagation of only one spatial mode [44]. However, the channel capacity of MDM systems impaired by MDL may be improved with the availability of the CSI at the transmitter.

Uninformed transmitter : When CSI is not available at the transmitter, the best power

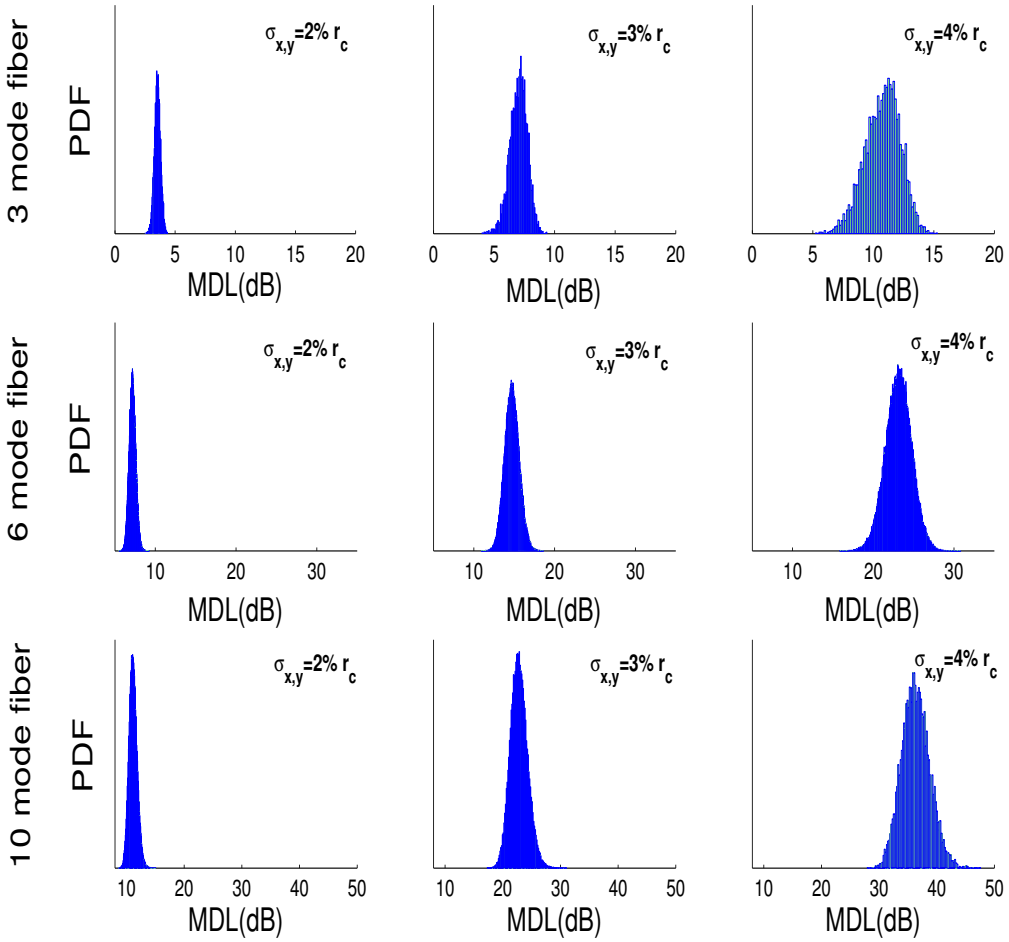

Figure 2.5: Probability distribution functions of MDL for 3, 6 and 10 mode fibers for different misalignment standard deviation $\sigma_{x,y}$.

allocation strategy is to excite all modes with equal launch power [66, 67]. In this case the capacity is given by:

$$C_{ep} = \sum_{i=1}^{M} \log(1 + \frac{\rho_t}{M} . \frac{\lambda_i}{2\sigma^2}) \tag{2.15}$$

where $(\lambda_1, ..., \lambda_M)$ are the eigenvalues of $HH^\dagger$, with $\sum_{i=1}^{M} \lambda_i = M$. In this case, each mode is given the same power $P_i = \frac{\rho_t}{M}$. Note that this is a linear capacity that increases with SNR, if non-linearities are taken into acount the capacity drops after a certain non-linear power threshold [69].

Informed transmitter : When CSI is available at the transmitter, the latter sends correlated symbols of different powers on each mode to increase the capacity. This is done through MIMO signal processing at the receiver. In fact the receiver estimates the channel

and computes its singular value decomposition as $H = U\Lambda V^{\dagger}$, where $\Lambda = \text{diag}(\sqrt{\lambda_1}, ..., \sqrt{\lambda_M})$ and U, V are unitary matrices, then sends V and Λ to the transmitter. The diagonal matrix Λ is used to compute the optimal powers per eigenmode and the matrix V is used to send the correlated symbols vector. We refer to this capacity by C_{CSI}:

$$C_{CSI} = \sum_{i=1}^{N} \log(1 + p_i^* . \frac{\lambda_i}{2\sigma^2}) \tag{2.16}$$

where p_i^* is the optimal power allocated to the eigenmode i, and N is the number of used eigenmodes for the transmission. This power allocation strategy faces two major limitations that makes it not feasible in real implementation. First, the CSI must be provided to the transmitter to send the data before the channel changes. Second, the optimal powers must be updated in the minimum as fast as the channel variations. The satisfaction of these constrains is impossible for the moment for optical fiber links. In the next part, we propose a power allocation solution to overcome these issues and increase the system capacity.

Statistical channel state information : In optical networks, CSI is available at the receiver through training sequences but unknown to the transmitter due to the long round-trip delays. We propose that the receiver computes an average of the channel that we note $\overline{H} = \overline{U}.\overline{\Lambda}.\overline{V}^{\dagger}$, with $\overline{U}, \overline{V}$ are unitary matrices, $\overline{\Lambda} = \text{diag}(\sqrt{\overline{\lambda_1}}, ..., \sqrt{\overline{\lambda_M}})$ contains the long term eigenvalues of the channel. $\overline{V}$ and $\overline{\Lambda}$ represent the statistical channel state information. The matrix $\overline{\Lambda}$ is used to compute the powers per eigenmode only once, and the matrix $\overline{V}$ will be used by the transmitter to send correlated symbols vector independently of the channel realizations. We refer to this capacity by $C_{\overline{CSI}}$:

$$C_{\overline{CSI}} = \sum_{i=1}^{N} \log_2(1 + \overline{p_i^*} . \frac{\lambda_i}{2\sigma^2}) \tag{2.17}$$

where $\overline{p_1^*}, ..., \overline{p_N^*}$ are the long term optimal powers allocated to the eigenmodes.

To have an insight on the MDM channel capacity behavior, we simulate the previous capacities for the 6-mode and 10-mode fibers. Simulations are averaged over 10^5 channel realizations. Fig. 2.6 shows the complementary cumulative distribution function (CCDF) of the capacities given by equations 2.15, 2.16 and 2.17 for the 6-mode fiber for MDL = 15 dB. We notice that both C_{CSI} and $C_{\overline{CSI}}$ are higher than C_{ep} and as the SNR increases the gain brought by CSI decreases. In Fig. 2.7 we plotted the CSI gain defined as the ratio of C_{CSI} (resp. $C_{\overline{CSI}}$) to C_{ep} as a function of the SNR for different MDL

values. We notice that the CSI gain increases with MDL and for higher SNR the CSI gain vanishes.

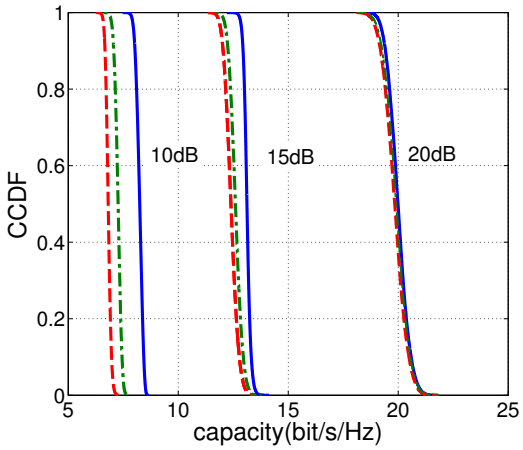

Figure 2.6: Capacity CCDF with CSI (solid), $\overline{CSI}$ (dash-dot) and *ep* (dashed) for SNR=10,15,20 dB and MDL = 15dB

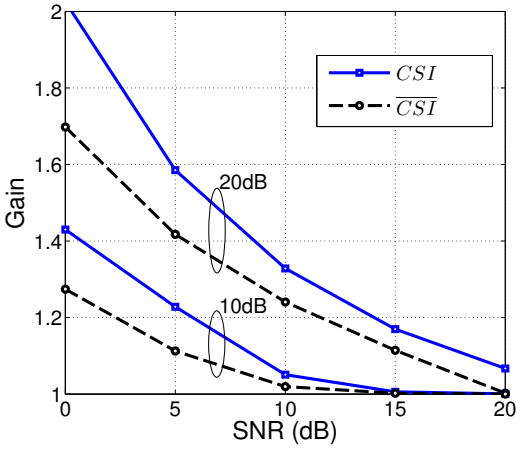

Figure 2.7: C_{CSI} gain (solid), $\overline{CSI}$ gain (dashed) as a function of SNR for MDL = 10, 20 dB for a 6-mode fiber.

To focus on the proposed statistical CSI, we compare the average capacities of equal power allocation to the long term power allocation. Fig. 2.8 shows the average capacities C_{ep} and $C_{\overline{CSI}}$ for the 6-mode and 10-mode fibers as a function of SNR for MDL = 20 dB. We notice that the proposed statistical CSI increases the capacity for both fibers.

Outage considerations are very important for the design of MDM optical systems. Since the channel changes randomly, transmitters are configured to encode for a fixed capacity that is higher than the worst case capacity to avoid system outage. In Fig. 2.9 we plotted the outage capacities for an outage probability of 10^{-3} for the 6-mode and 10-mode fibers as a function of MDL for SNR = 10 dB. We compare the capacity with equal launch power to the capacity when using the long term optimal powers based on the statistical CSI. We notice that both capacities are decreasing with MDL, however $C_{\overline{CSI}}$ is better than C_{ep}. At MDL = 20 dB we have 0.3 bit/s gain for the 6-mode fiber and 0.5 bit/s gain for the 10-mode fiber.

Consequently, since the availability of instantaneous CSI at the transmitter achieves the maximum capacity but is unfortunately unfeasible, the proposed statistical CSI can be a solution to increase the capacity rather than using equal launch power at the transmitter. This method has a low-cost complexity since it works independently of the channel variations, thus it can be feasible for real implementation.

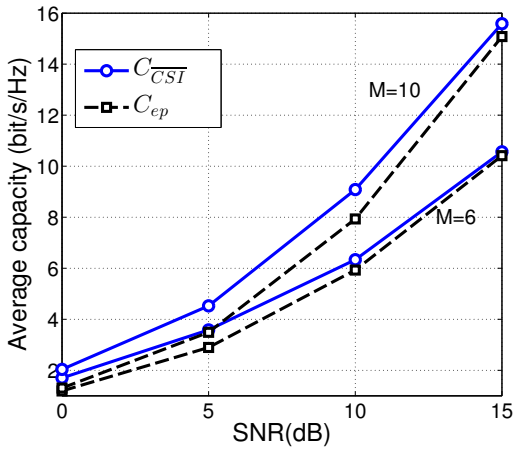

Figure 2.8: Average capacities vs SNR for $M = 6, 10$ modes. $\overline{CSI}$ (solid), and C_{ep} (dashed) for MDL = 20dB.

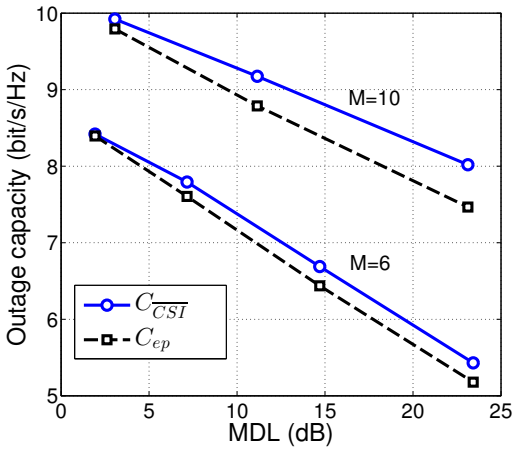

Figure 2.9: Outage capacities vs MDL for $M = 6, 10$ modes. $\overline{CSI}$ (solid) and C_{ep} (dashed) for SNR = 10dB.

2.3 Capacity enhancement of MDM optical systems using mode scrambling

2.3.1 MDM channel model including mode scramblers

As we have shown previously, MDL highly impacts the capacity of MDM systems. In this section, we study mode scrambling (MS) as another strategy that mitigates the impact of MDL and enhances the system performance.

Mode scrambling was first used to overcome the frequency dependence of MMFs on mode distribution and establish a uniform input power distribution for all modes [70]. The application of MS to reduce MDL and increase MDM system capacity was first proposed in [71], the MS principle consists in introducing a random mode permutation after K_{scr} splices. The resulting MIMO channel is given by:

$$Y_{M\times 1} = \sqrt{L} \prod_{k=1}^{K} (T_k.C_k.P_k)\, X_{M\times 1} + N_{M\times 1} \tag{2.18}$$

The last equation is similar to the equation 2.12, the only difference is the presence of the scrambling matrix P_k corresponding to a random permutation matrix if k is a multiple of the scrambling period K_{scr}, or an identity matrix otherwise. After MS, signal modulated on each mode is completely transfered into another mode. Hence, all modulated signals will experience the attenuations of all modes at the link end which effectively reduces the MDL. In [71], the authors considered ideal mode scramblers (perfect random permutation matrices) without mode dependent loss, they showed that randomly scrambling all modes after each splice ($K_{scr} = 1$) leads to a completely uncorrelated modal coupling. This

strategy can reduce the MDL of the link but a large number of scramblers is required.

2.3.2 Deterministic mode scrambling

In our scrambling approach, we propose to use a deterministic mode scrambler that permutes modes having more received power with modes having the less received power. To have an insight into this strategy, we consider the previous 6-mode and 10-mode fibers. At the transmitter we launch all modes with unit energy $E_s = 1$ and we compute the received energy per mode at the receiver side averaged over 10^5 channel realizations. Both fibers are made of $K = 300$ sections with independent random Gaussian misalignments of zero mean and std $\sigma_{x,y} = 0.26\mu m$.

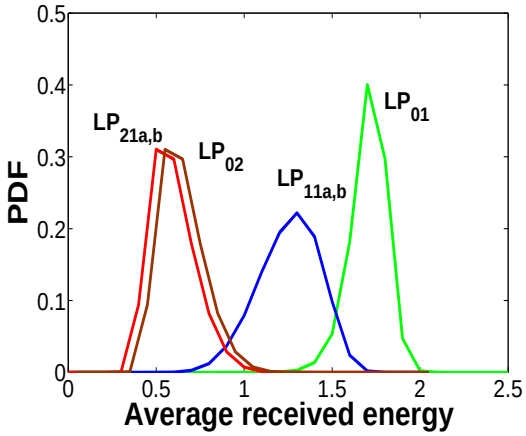

Figure 2.10: PDF of the average received energy per mode for a 6-mode fiber

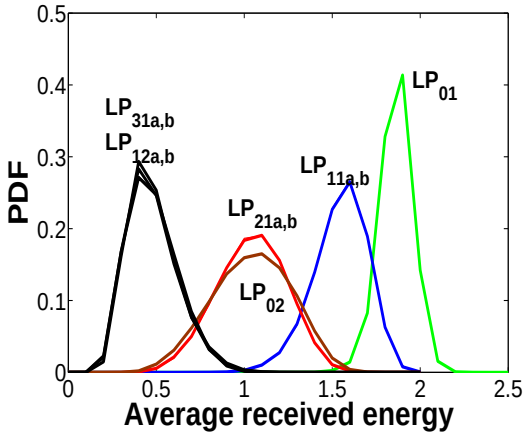

Figure 2.11: PDF of the average received energy per mode for a 10-mode fiber

From figures 2.10 and 2.11, we clearly notice that some modes arrive at the receiver with more power than the others. For the 6-mode fiber the best modes are the LP_{01} and $LP_{11a,b}$ and the weakest modes are the LP_{02} and $LP_{21a,b}$. Hence, we propose to permute the LP_{01} with the LP_{02} and the $LP_{11a,b}$ with the $LP_{21a,b}$. For the 10-mode fiber, modes arriving with more power are the LP_{01}, $LP_{11a,b}$ and $LP_{21a,b}$, these modes will be permuted respectively with modes arriving with less power which are the LP_{02}, $LP_{31a,b}$ and $LP_{12a,b}$. Our scrambling strategy, avoids permutations between modes arriving with close levels of power especially between degenerate modes that arrive with the same amount of power. However, this situations can occur if random mode scrambling is considered, which do not average power effectively between all modes.

To compare the different scrambling strategies, we add only 6 scramblers ($K_{scr} = 50$) to the previous fibers made of $K = 300$ sections. In Fig. 2.12 we plot the PDF of MDL

for 10^5 channel realizations and for different misalignment std $\sigma_{x,y}$. We can see that MS reduces the impact of MDL, and that the deterministic MS outperforms the random MS. For the 6-mode fiber, for a misalignment std of 3% the average MDL without scramblers in the line is 15 dB, with random scrambling the MDL is 9 dB and for the proposed scrambling strategy is reduced to 5 dB. For the 10-mode fiber, for a misalignment std of 3% the average MDL without scramblers in the line is 23 dB, with random scrambling the MDL is 15 dB and for the proposed scrambling strategy is reduced to 11 dB.

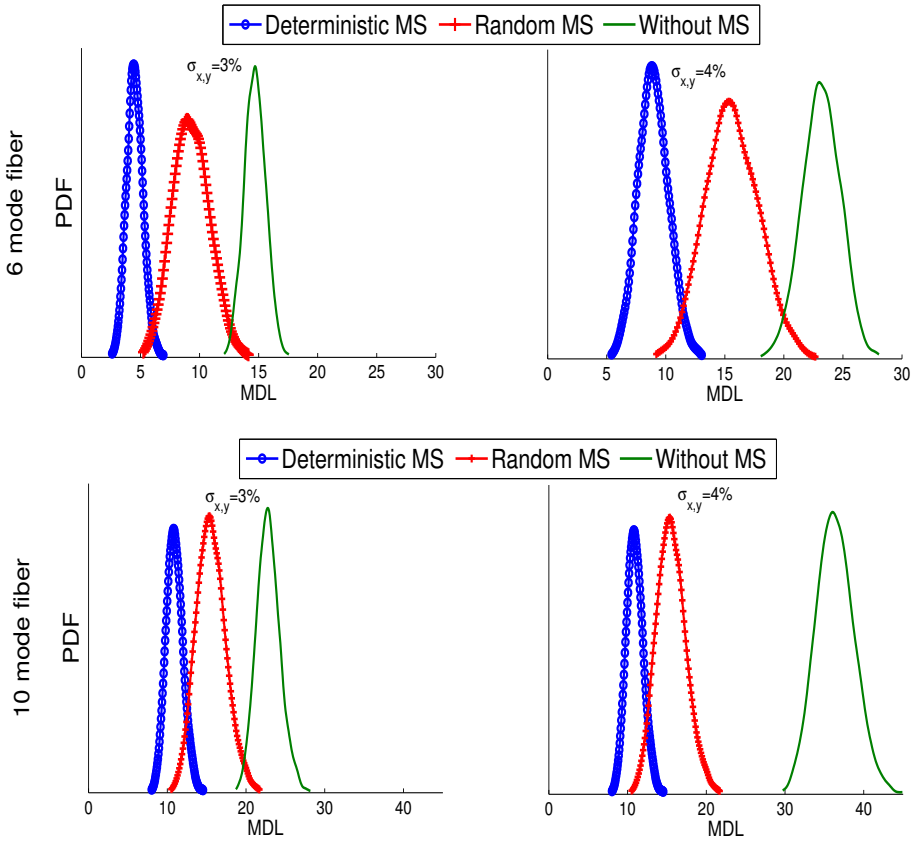

Figure 2.12: PDF of MDL for the 6 and 10 mode fibers for different scrambling strategies and misalignment standard deviation $\sigma_{x,y} = 3\%,\ 4\%$.

To have an insight on the impact of MS, we simulate the system average and outage capacities based on 10^5 channel realizations of the same previous fibers made of $K = 300$ sections and containing 6 scramblers. In Fig. 2.13, we plot the average capacities for the 6-mode and 10-mode fibers for different scrambling strategies. We notice that MS increases the system capacity and that the deterministic MS outperforms the random MS. For low SNRs, the average capacities are almost the same with or without MS. However, as the

SNR increases, the gain brought by MS becomes more important. For an SNR = 15 dB and a std $\sigma_{x,y} = 4\%$ The capacity gain brought by using deterministic MS to a strategy where no scrambler is used is 4.5 bit/s for the 6-mode fiber and 3.5 bit/s for the 10-mode fiber. Consequently, deterministic MS averages power more efficiently between all modes, which reduces significantly MDL and results in a better average capacity.

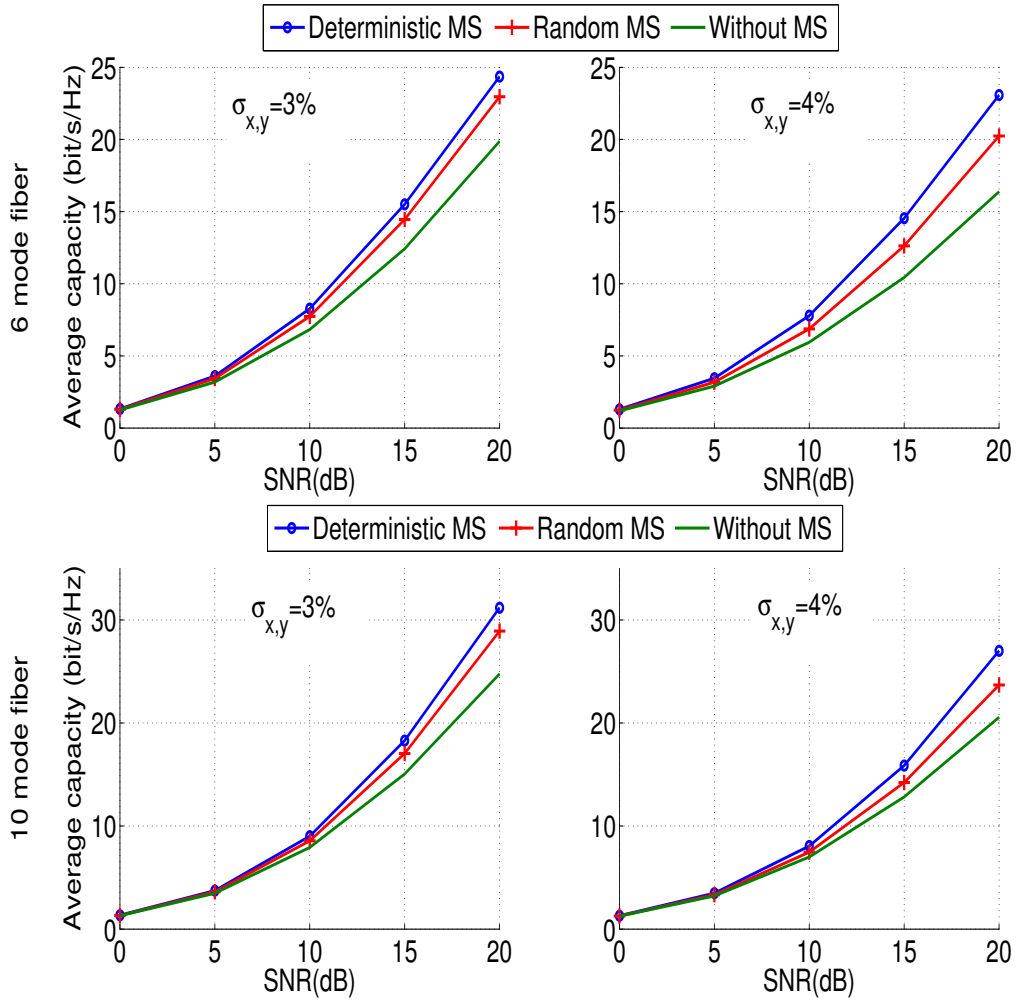

Figure 2.13: Average capacities for the 6 and 10 mode fibers for different scrambling strategies and misalignment standard deviation $\sigma_{x,y} = 3\%,\ 4\%$.

In Fig. 2.14 and 2.15, we simulate the outage capacity as a function of the std misalignment $\sigma_{x,y}$ for the different scrambling strategies and for an outage probability of 10^{-3}. We notice that as std $\sigma_{x,y}$ increases which increases also MDL, the outage capacities are decreasing. However the use of MS enhances these capacities significantly and the deterministic MS outperforms the random MS. For a std $\sigma_{x,y} = 4\%$. The capacity gain brought

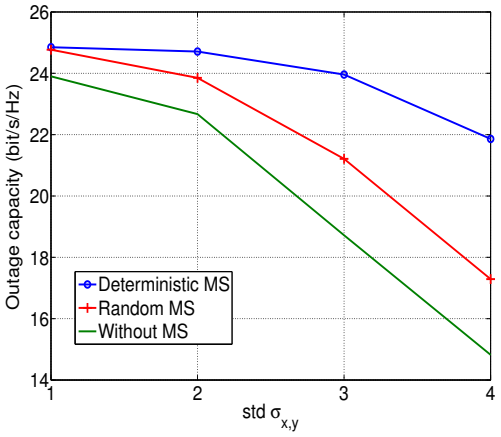

Figure 2.14: Outage capacities vs misalignment std for the 6-mode fiber for different scrambling strategies for SNR = 20 dB

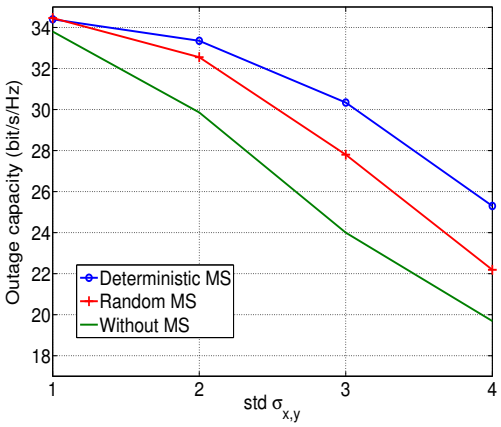

Figure 2.15: Outage capacities vs misalignment std for the 10-mode fiber for different scrambling strategies for SNR = 20 dB

by using deterministic MS to a strategy where no scrambler is used is 7.8 bit/s for the 6-mode fiber and 5.2 bit/s for the 10-mode fiber.

We have also studied the performance of the 6-mode fiber in terms of BER curves versus the SNR using the same simulation parameters as previously. At the transmitter, the modulated symbols belong to a 4-QAM constellation. At the receiver, a maximum-likelihood (ML) decoder searches for the symbol that minimizes the quadratic distance with the received symbol.

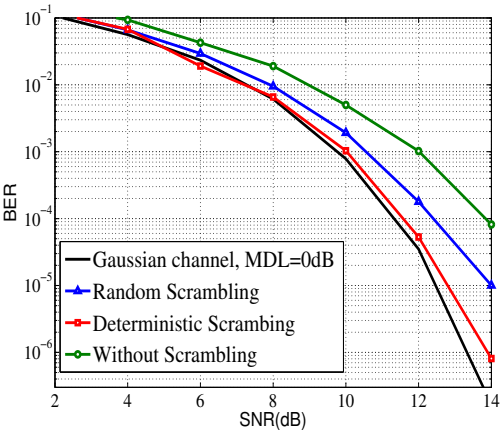

Figure 2.16: BER performance of 6-mode fiber, $\sigma_{x,y} = 3\% r_c$

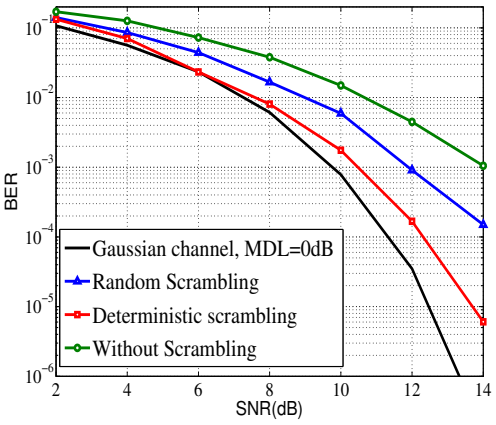

Figure 2.17: BER performance of 6-mode fiber, $\sigma_{x,y} = 4\% r_c$

From Fig. 2.16, 2.17, we can see that at BER $= 10^{-3}$ and a misalignment std $\sigma_{x,y} = 3\%$ the proposed mode scrambling has only 0.2 dB SNR penalty to the MDL-Free channel (Gaussian channel) while the random mode scrambling has 1 dB penalty. For a misalign-

ment std $\sigma_{x,y} = 4\%$ the proposed scrambling strategy has 0.4 dB penalty and the random mode scrambling has 2.2 dB loss to the Gaussian channel.

In our simulations we have considered a scrambling period of $K_{scr} = 50$ which makes only 6 scramblers in the line made of $K = 300$ misaligned fiber sections. In real transmission systems the number of scramblers to be used in the line is an important parameter in the design of MDM systems. Mode scramblers can be placed after mode-multiplexers or few-mode amplifiers [52]. In Fig. 2.18 we compute the average link MDL as a function of the number of used scramblers in the line for the two scrambling strategies. From the figure, we can conclude that to achieve an average link MDL of 4 dB only 8 deterministic mode scramblers are needed instead of 60 random mode scramblers. Consequently deterministic MS can be considered as an emerging solution that reduces very efficiently the impact of MDL and enhances both the capacity and performance of MDM optical systems.

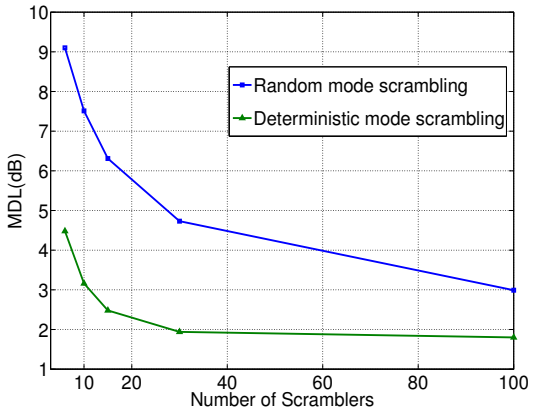

Figure 2.18: Link MDL as a function of the Number of scramblers

2.4 Capacity enhancement of MDM systems using mode selection

2.4.1 Antenna selection for MIMO wireless communications

Wireless multiple antenna systems can improve the capacity and the reliability of radio communications. Using M separate links to transmit and receive independent data increases the system capacity by M. Moreover, several antennas improve the reliability of communication through diversity. On the other hand, multiple antennas at the transmitter also improves the throughput and the diversity of the system. For instance, space-time coding can be used to send different copies of the same data on different antennas at the transmitter where these copies follow different paths before arriving at the receiver.

All these MIMO advantages, require multiple radio chains associated with different paths and also algorithms to process the data which make them costly in term of hardware, power consumption and implementation. Luckily, it is possible to alleviate this cost and keep the benefits of MIMO by using antenna selection. The principle consists in using only the set of the best antennas at the transmitter and receiver for communication. The main challenge of antenna selection is to reduce the costs while maintaining performance of the subsystem as much close as possible to the full MIMO system.

The choice of the set of best antennas is based mainly on two strategies: the maximization of the capacity or the minimization of the BER. In [72], the authors presented efficient selection algorithms for capacity maximization, they showed that the subsystem based on selected antennas achieves almost the capacity of the full MIMO system. In [73], the authors selected a subset of antennas at the receiver to reduce the hardware while keeping a reasonable high performance in terms of BER.

In all cases, antenna selection requires a good knowledge of the channel to identify the best set of antennas according to a given criterion. For this, selection algorithms must be updated regularly depending on channel variations and suitable switching between different antennas should be set. Another solution consists in using the statistical channel state information for choosing antennas but this comes at the price of suboptimal performances.

2.4.2 Mode selection for MDM optical systems

In the previous sections, we have showed that MDL causes a capacity limitations of MDM systems. Due to MDL, propagating modes observe different attenuations. The principle of mode selection consists in considering that the different attenuations experienced by modes as a useful information to select only a subset of modes for transmission. In [34], Winzer and Foschini studied the capacity of MDM channel without MDL. The authors showed that when the channel is unitary, the number of used modes for transmission has to be fully processed at the receiver in order to fully exploit the system capacity. In [74], Chen et al considered a two-mode transmission in a 3-mode fiber where only the degenerates of the LP_{11} were used, the LP_{01} was discarded to reduce DMGD. Nonetheless, all modes were detected to retrieve the power leakage in the LP_{01}.

In our work, we investigate the performance of an MDL-impaired system based MDM when an appropriate set of modes is selected for multiplexing according to an energy criterion. We consider the previous MDM spliced channel model and we select a set of $M_T < M$ modes to multiplex the data at the transmitter and we detect $M_R \leq M$ modes

at the receiver (with $M_T \leq M_R$). The resulting MIMO channel is given by:

$$Y_{M_R \times 1} = H_{M_R \times M_T}.X_{M_T \times 1} + N_{M_R \times 1} \tag{2.19}$$

where the channel matrix $H_{M_R \times M_T}$ spans a subspace of $H_{M \times M}$ given by equation 2.12. The mode selection criterion will be based on the average received power at the receiver as seen in the previous section. We excite all modes with a unit power $E_s = 1$ at the transmitter and we compute the average received power per mode at the receiver. The results for the 6-mode and 10-mode fibers were shown in Fig. 2.10 and 2.11. We notice that for the 6-mode fiber (resp. 10-mode fiber), modes with the highest received energies are $\{LP_{01}, LP_{11a}, LP_{11b}\}$ (resp. $\{LP_{01}, LP_{11a}, LP_{11b}, LP_{21a}, LP_{21b}, LP_{02}\}$).

To have an insight on the benefit of mode selection on MDM systems, we compare at the same spectral efficiency (SE) the capacity of a 3-mode fiber to a 6-mode fiber when only the three best modes are used. We also compare the capacity of a 6-mode fiber to a 10-mode fiber when only six modes are used. Since the fibers have different core radius, it it more convenient to compare the different schemes at a fixed std misalignment $\sigma_{x,y}$ rather than a std given in percentage of core radius.

In Fig. 2.19, we compare a 3-mode fiber to a 6-mode fiber with the selection of 3 modes ($M_T = M_R = 3$) according to the criterion mentioned above. We notice that the selected 3×3 subset in the 6-mode fiber has a better average capacity than the 3-mode fiber. For an SNR of 20 dB, a 0.4 bit/s gain is observed for std $\sigma_{x,y} = 0.26\mu m$ and 2 bit/s gain is observed for std $\sigma_{x,y} = 0.35\mu m$

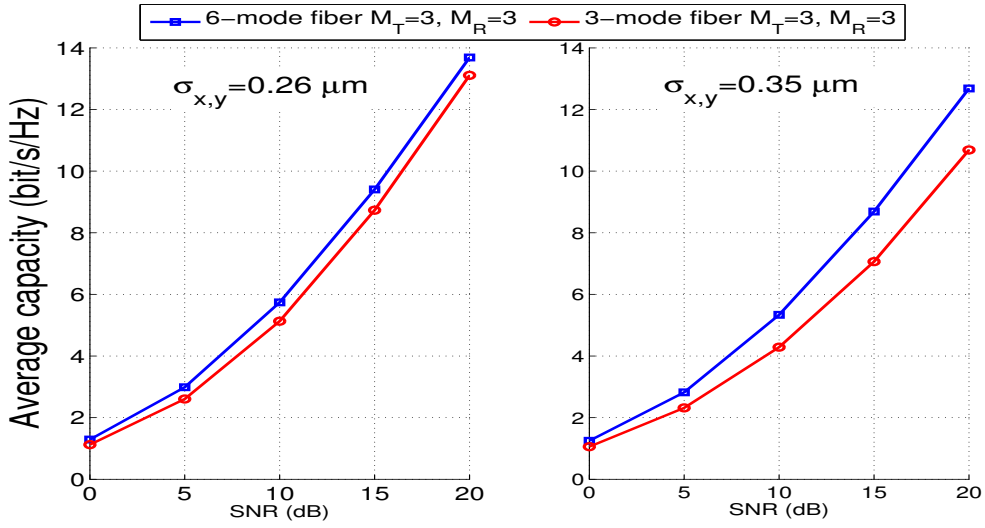

Figure 2.19: Average capacity of 3-mode fiber and 6-mode fiber using $M_T = 3$ transmit modes and $M_R = 3$ receiver side modes

In Fig. 2.20, we compare a 6-mode fiber to a 10-mode fiber with the selection of 6

modes ($M_T = M_R = 6$). We notice that the selected 6×6 subset in the 10-mode fiber has a better average capacity than the 6-mode fiber. For an SNR of 20 dB, a 1.1 bit/s gain is observed for std $\sigma_{x,y} = 0.26\mu m$ and 3.6 bit/s gain is observed for std $\sigma_{x,y} = 0.35\mu m$. These results show that mode selection in a larger core fiber provides a better capacity comparing to a small core fiber supporting the same number of modes.

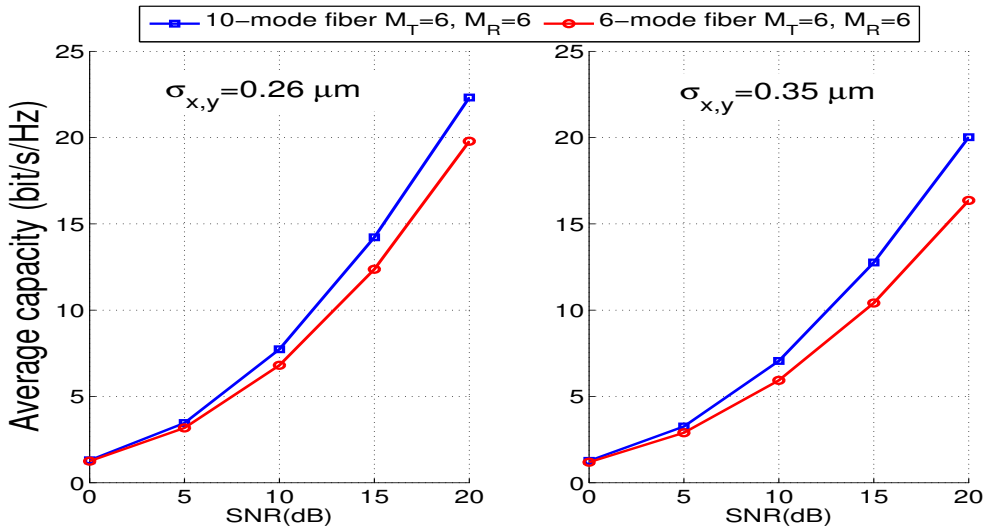

Figure 2.20: Average capacity of 6-mode fiber and 10-mode fiber using $M_T = 6$ transmit modes and $M_R = 6$ receiver side modes

Furthermore, we have also studied the performance of mode selection in term of BER. In Fig. 2.21a and 2.21b, we compare a 3-mode fiber to a 6-mode fiber with the selection of 3 modes ($M_T = 3$) according to the criterion mentioned above, at the same spectral efficiency SE = 6 bits/s and the same average received energy normalized with respect to the 3-mode system. We observe that the 3×3 channel in the 6-mode fiber performs worse than the 3×3 channel on the 3-mode fiber. This is due to important power leakage in the other three unexcited modes in the 6-mode fiber as shown in Fig. 2.10. To retrieve this power loss, we increase the number of detected modes ($M_R = 6$). From the triangle-marked curves, we notice that at BER $= 10^{-2}$, the 3×6 channel has an SNR gain of 0.5 dB (resp. 1.9 dB) compared to the 3×3 channel in the 3-mode fiber for $\sigma_{x,y} = 0.26$ μm (resp. $\sigma_{x,y} = 0.35$ μm).

In Fig. 2.22a and 2.22b, we compare a 6-mode fiber to a 10-mode fiber with the selection of 6 modes ($M_T = 6$), at the same spectral efficiency SE = 12 bits/s and the same average received energy normalized with respect to the 6-mode system . At BER $= 10^{-2}$, we notice that for $\sigma_{x,y} = 0.26$ μm, the 6×6 channel based on the 10-mode fiber is only 0.4 dB degraded compared to the 6×6 channel based on the 6-mode fiber. On the other side, for $\sigma_{x,y} = 0.35$ μm, the former channel has a gain of 0.8 dB compared to the latter.

This gain is explained by a lower power leakage in the unexcited modes that suffer further losses. When we detect all modes in the 10-mode fiber ($M_R = 10$), a gain of 1.5 dB (resp. 2.5 dB) is obtained for $\sigma_{x,y} = 0.26\mu$m (resp. $\sigma_{x,y} = 0.35\ \mu$m) compared to the 6×6 channel on the 6-mode fiber.

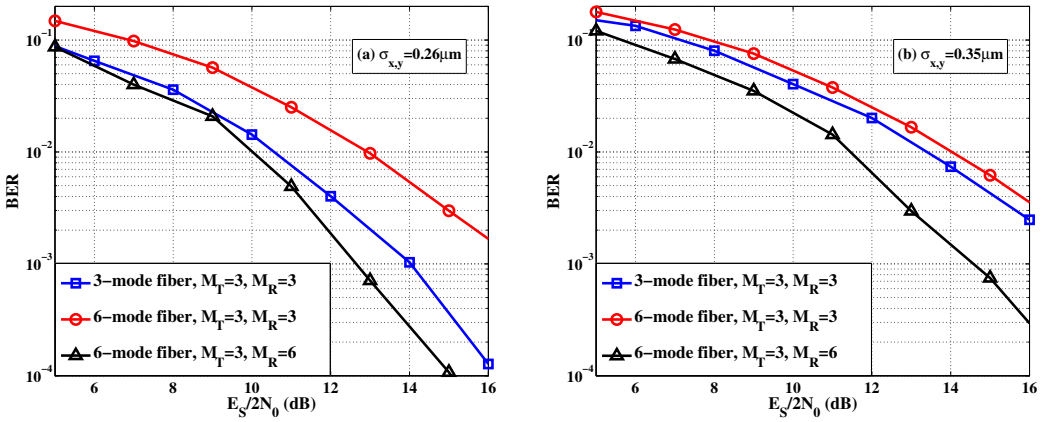

Figure 2.21: Performance of 3-mode fiber and 6-mode fiber using M_T transmit modes and M_R receiver side modes, SE = 6bits/s

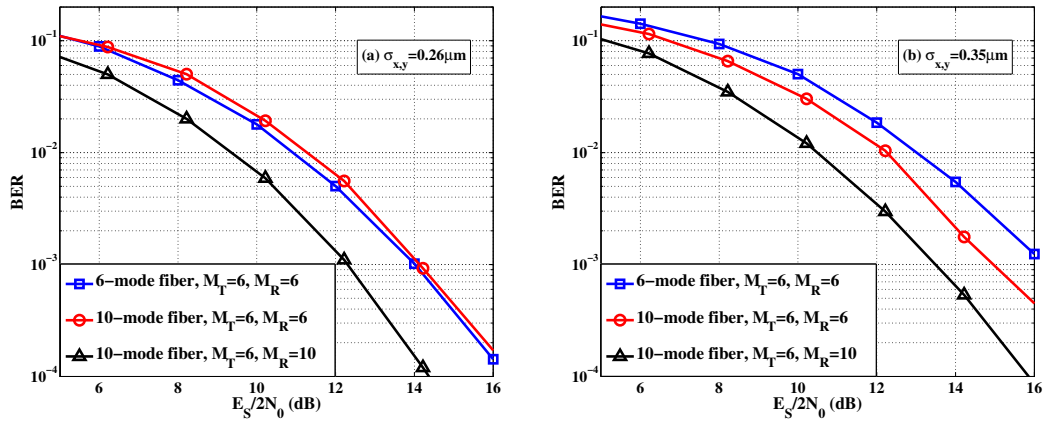

Figure 2.22: Performance of 6-mode fiber and 10-mode fiber using M_T transmit modes and M_R receiver side modes, SE = 12bits/s

The above results show that mode selection is an efficient technique that can be used in MDM systems based MMFs with a large number of modes. An additional gain can be obtained by increasing the number of detected modes at the receiver side to gain back the power leakage in unselected modes and therefore improve the performance of the system.

Summary

We have studied the capacity of MIMO MDM optical systems impaired by MDL. Both the average and outage capacities were investigated, and we showed that due to MDL, these capacities are reduced. We have proposed a statistical channel state information strategy based on long term statistics of the FMF channel to increase system capacities. This strategy has a low-cost complexity since it does not require algorithm updates with channel variations. Moreover, we have studied the benefits of inserting mode scramblers on reducing MDL, we have proposed a deterministic MS that is more efficient than the random MS. We showed through numerical simulations that only a few deterministic MS are enough to increase the system capacity and improve BER performance. Finally, we have shown that mode selection is a high-potential solution that allows the use of large-core MMFs instead of small-core MMFs and reach a better capacity in MDM systems impaired by MDL. To further enhance the performance, we have increased the number of detected modes at the receiver to gain back the power leakage in the unselected modes. Hence, it is possible to start deploying MMFs supporting a greater number of modes, and use for the moment low-complexity MIMO schemes while having an infrastructure prepared to welcome future MIMO solutions in which all modes can be used for transmission. After we have explored different strategies to achieve the maximum capacity of the MDM system, in the next chapter, we investigate the benefits of space-time (ST) coding in enhancing the performance of the system affected by MDL.

Chapter 3

Space-Time Coding for MDL Mitigation in MDM Optical Systems

In the last chapter, we have studied the capacity limits of the FMF channel and proposed some capacity improvement techniques. Once the maximum capacity of a given channel is figured out, it is important to determine the reliability of the communication. This can be done by measuring the bit-error rate (BER) of the transmission. In this chapter, we study the efficiency of space-time (ST) coding schemes to MDM optical systems in order to improve the BER performance. ST codes were already applied in a 2×2 MIMO configuration for PDM systems [28] to reduce PDL; thus OSNR gains were observed in both the linear and non-linear regimes. Moreover, benefits of ST coding in mitigating MDL have been shown in a simulation study for MDM systems based FMFs [6], the authors considered the same channel model as we have presented in the previous chapter. This channel model allows to physically simulate the FMF and generate MDL from accumulated non-unitary effects.

In this chapter, we are interested in explaining the coding gains brought by ST coding to MDM optical systems impaired by MDL through a theoretical analysis of the error probability. To derive an analytical upper bound of the error probability, a compact channel model is required. Hence, we consider a mathematical channel model that describes the effects of both MDL and coupling.
In the first section, we start by reviewing ST coding techniques and the method of computing the error probability upper bound for MIMO wireless systems. We also present design criteria that ST codes must fulfill in order to be efficient in a Rayleigh fading channel and

give examples of some ST codes. Then, we list the various decoding techniques that can be applied at the receiver to decode both ST coded and uncoded transmissions. After we have set all the required tools, in the second section, we derive an upper bound of the error probability and define a design criterion specific for the MDM optical channel affected by MDL. In the last part, we study the performance of concatenating ST coding and forward error correcting (FEC) codes in MDM optical systems. We prove through numerical simulations and also by a theoretic derivation of the error probability the summation of both coding gains.

3.1 Space-Time coding for wireless MIMO channels

The introduction of multiple antenna transmission techniques has revolutionized wireless transmission systems by the fact of linearly increasing the capacity. Moreover, to further exploit all degrees of freedom of MIMO systems, ST coding schemes have been proposed in order to create a dependence between the spatial and temporal dimensions and hence increase throughput and improve performance.
We consider a MIMO wireless channel with n_t antennas at the transmitter and n_r antennas at the receiver. The channel is supposed to be a block fading Rayleigh channel (i.e. the channel remains constant during T time-slots, that also represents the temporal length of the ST codeword). The MIMO transmission can be described by:

$$Y_{n_r \times T} = H_{n_r \times n_t} . X_{n_t \times T} + N_{n_r \times T} \tag{3.1}$$

Transmitted modulated symbols are represented by the complex codeword matrix X of dimension $n_t \times T$. The received signal on the n_r antennas is given by the codeword matrix Y of dimension $n_r \times T$. The $n_r \times n_t$ complex matrix H represents the channel transfer matrix, where each coefficient $h_{i,j}$ represents the path between the i^{th} transmit antenna and the j^{th} receive antenna. The different paths between antennas are spatially decorrelated and the $h_{i,j}$ coefficients are independent and identically distributed (i.i.d) complex Gaussian random variables with zero mean and a unit variance. N is an $n_r \times T$ matrix representing circularly symmetric white Gaussian noise with zero mean and variance $2\sigma^2$ per complex component.

The architecture of the previous MIMO system brings two major advantages comparing to single antenna systems. The first one is referred to as the multiplexing gain which increases the throughput of the system by $min(n_t, n_r)$. The second one is the diversity gain, the principle consists in sending the same copy of the information over different

antennas and use the multiple received informations at the receiver for the decoding. For example, spatial diversity at the receiver consists in receiving the same information from the i^{th} transmitter on all antennas at the receiver. Since each copy of the same information has experienced a different path before arriving at the receiver, these different copies are used to give a better estimate of the initial transmitted data.

3.1.1 Error probability upper bound of space-time coded Rayleigh fading channels

The analytical expression of an upper bound of the error probability of ST coded MIMO systems allows to derive a design criteria of efficient ST codes. In fact, the best ST code is the one that minimizes the error probability of the transmission. We derive the error probability upper bound for the Rayleigh fading channel assuming channel state information (CSI) available at the receiver. According to the channel model given by Equation 3.1, a maximum-likelihood (ML) decoder gives an estimate $\hat{X}$ of the transmitted codeword X where this estimation is computed among the set of all possible codewords C according to the following metric:

$$\hat{X} = \underset{X \in \mathrm{C}}{\operatorname{argmin}} \|Y - HX\|^2 \tag{3.2}$$

with $\|\cdot\|$ represents the Frobenius Norm. The probability that the transmitted codeword X is wrongly estimated is given by:

$$\mathrm{Pr}_{error} = \mathrm{Pr}\left\{\hat{X} \neq X\right\} \tag{3.3}$$

$$= \sum_{X \in \mathrm{C}} \mathrm{Pr}\{X\}.\mathrm{Pr}\left\{\hat{X} \neq X/X\right\}) \tag{3.4}$$

as all transmitted codewords are i.i.d., by using the union bound, the error probability can be upper bounded as in ([75], Chap.4,15)

$$\mathrm{Pr}_{error} \leq \frac{1}{\mathrm{card(C)}} \sum_{\hat{X} \neq X} \mathrm{Pr}\left\{X \to \hat{X}\right\} \tag{3.5}$$

where card(C) is the cardinality of C and $\mathrm{Pr}\left\{X \to \hat{X}\right\}$ is the pairwise error probability (PEP) of estimating $\hat{X}$ when X is transmitted. The PEP given a channel realization H

is given by ([75], Chap.15):

$$\Pr\left\{X \to \hat{X}\right\} = Q\left(\sqrt{\frac{\left\|H\left(\hat{X}-X\right)\right\|^2}{2\sigma^2}}\right) \tag{3.6}$$

with Q the tail function given by:

$$Q(x) = \frac{1}{\sqrt{2\pi}}\int_x^{\infty} \exp(\frac{-t^2}{2})dt \tag{3.7}$$

by using the Chernoff bound $Q(x) \leq \frac{1}{2}\exp(\frac{-x^2}{2})$ and averaging equation 3.5 over all channel realizations we obtain:

$$\Pr\left\{X \to \hat{X}\right\} \leq \mathbb{E}_H\left[\exp\left(\frac{-\left\|H(\hat{X}-X)\right\|^2}{8\sigma^2}\right)\right] \tag{3.8}$$

now, by averaging over the statistics of the Rayleigh fading channel matrix H we obtain the upper bound on the average PEP ([75], Chap.15):

$$\Pr\left\{X \to \hat{X}\right\} \leq \left(\prod_{k=1}^{r}\frac{1}{1+\lambda_k\frac{\mathrm{SNR}}{4}}\right)^{n_r} \tag{3.9}$$

The last equation has two important parameters. First, r is the rank of the matrix A defined as $A = \left(\hat{X}-X\right)\left(\hat{X}-X\right)^{\dagger}$ ($\dagger$ represents the complex conjugate operator). Second, λ_k are the non-zero eigenvalues of A.
At high SNR regime, the last equation yields:

$$\Pr\left\{X \to \hat{X}\right\} \leq \left(\prod_{k=1}^{r}\lambda_k\right)^{-n_r}\left(\frac{\mathrm{SNR}}{4}\right)^{-r.n_r} \tag{3.10}$$

3.1.1.1 Construction criteria of space-time codes

From Eq. 3.10, we can clearly see that the error probability depends on three parameters. The number of receive antennas n_r which allows to bring the diversity gain at the receiver. On the other hand, the parameters λ_k and r only depend on the transmitted codeword matrix X. These two parameters define the rank and determinant construction criteria [76].

- **Rank criterion**

  The error probability upper bound decreases exponentially as a function of the SNR. The diversity gain is the exponent of the SNR and is equal to $r.n_r$, it determines the

decreasing pace of the error probability and graphically it represents the asymptotic slope of the error probability versus the SNR . The diversity gain at the receiver is always achieved and is equal to n_r. In order to achieve the transmitter diversity and hence a full diversity gain of the global MIMO system, the condition to be fulfilled is $r = n_t$. Therefore the challenge is to construct the set of codewords C where all the codeword matrices satisfy this condition. The rank criterion is then given by:

Definition of the rank criterion:

In order to achieve a full diversity of $n_t n_r$, The matrix A must be full rank for all pairs of codeword matrices X and X' such that $X \neq X'$.

- **Determinant criterion**

  By rewriting equation 3.10 as:

$$\Pr\left\{X \to \hat{X}\right\} \leq \left[\left(\prod_{k=1}^{r} \lambda_k\right)^{-1/r} \left(\frac{\text{SNR}}{4}\right)\right]^{-rn_r} \tag{3.11}$$

  We clearly notice that the SNR is multiplied by the product of the eigenvalues λ_k which also represents the determinant of the matrix A. This is the coding gain of the ST coded MIMO system. Hence, to maximize the coding gain, the minimum determinant of A given by $\prod_{k=1}^{r} \lambda_k$ among all possible codewords should be maximized.

  Definition of the determinant criterion:

  To maximize the coding gain, the minimum determinant of the matrix A should be maximized for all pairs of codeword matrices X and X' such that $X \neq X'$.

We have presented two design criteria for space-time codes construction in a Rayleigh fading environment. Nonetheless, these two criteria are not the only existing ones and other criteria can be found in the literature. In ([77], Chap.9), the authors considered the worst-case pairwise error probability of channels that are not in outage which resulted in a universal coding criterion that is almost related to the determinant criterion. Another design criterion based on mutual information maximization was proposed in [78], however this criterion does not allow ST codes to achieve a maximum diversity.

3.1.2 Space-Time block codes

Space-time block codes (STBC) are a family of ST codes where the codeword matrix is of dimension $n_t \times T$, with T the number of time-slots also called channel use (cu) during which

one codeword is transmitted. Each codeword matrix contains N_s modulated symbols that are sent during T time-slots, the rate of the STBC is defined as:

$$r_{ST} = \frac{N_s}{T} \qquad \text{(symbols/cu)} \tag{3.12}$$

An element of the codeword matrix is given by $x_{i,j}$ and represents the new super-symbol transmitted from antenna i at the instant j. For example a 2×2 STBC may be given as:

$$X = \begin{bmatrix} x_{1,1} & x_{1,2} \\ x_{2,1} & x_{2,2} \end{bmatrix} \tag{3.13}$$

$$= \begin{bmatrix} f_1(s_1, ..., s_{N_s}) & f_3(s_1, ..., s_{N_s}) \\ f_2(s_1, ..., s_{N_s}) & f_4(s_1, ..., s_{N_s}) \end{bmatrix} \tag{3.14}$$

A STBC is said to be linear when the functions f_k are linear combinations of the complex modulated symbols s_k. In this case we can find a complex $n_t T \times N_s$ generator matrix $G_{\mathbb{C}}$ of the code such as:

$$\text{vec}_{\mathbb{C}}(X) = G_{\mathbb{C}} S \tag{3.15}$$

$$\begin{bmatrix} x_{1,1} \\ x_{2,1} \\ \vdots \\ x_{n_t,T} \end{bmatrix} = G_{\mathbb{C}} \begin{bmatrix} s_1 \\ s_2 \\ \vdots \\ s_{N_s} \end{bmatrix}$$

where $\text{vec}_{\mathbb{C}}(X)$ refers to the vectorization of X into a complex vector of dimension $n_t T \times 1$. A real representation of a STBC is also possible, by considering a $2n_T.T \times 2N_s$ real generator matrix $G_{\mathbb{R}}$ such as:

$$\text{vec}_{\mathbb{R}}(X) = G_{\mathbb{R}} S_{\mathbb{R}} \tag{3.16}$$

$$\begin{bmatrix} \text{Re}(x_{1,1}) \\ \text{Re}(x_{2,1}) \\ \vdots \\ \text{Im}(x_{1,1}) \\ \text{Im}(x_{2,1}) \\ \vdots \end{bmatrix} = G_{\mathbb{R}} \begin{bmatrix} \text{Re}(s_1) \\ \text{Re}(s_2) \\ \vdots \\ \text{Im}(s_1) \\ \text{Im}(s_2) \\ \vdots \end{bmatrix}$$

In the following sections, we describe some STBC that we will use later in our MDM optical channel. In order to fully exploit the MDM throughput, we will be interested in full-rate codes. Moreover, the scalability of STBC to any dimension of the MIMO system is also an important factor for the integration of such codes in future optical systems. Consequently, we start by an overview of STBC specific for the 2×2 MIMO channel then we focus on a STBC family easily scalable for any $M \times M$ MIMO system.

3.1.2.1 Alamouti code

The Alamouti code was first designed for 2×1 MIMO systems [79], it achieves a full diversity and a rate of 1 symbol/cu. The transmitted codewords are simply the two modulated symbols $[s_1, s_2]^T$. The Alamouti codeword matrix is given by:

$$X_A = \begin{bmatrix} s_1 & -s_2^* \\ s_2 & s_1^* \end{bmatrix} \tag{3.17}$$

From the last equation, we notice that the code has a straightforward construction, in fact during the first time-slot a modulated symbol is sent on each antenna and during the second time-slot the complex conjugate of these same symbols are sent again. this property makes the Alamouti code orthogonal (i.e. $X_A X_A^\dagger = (|s_1|^2 + |s_2|^2) I_2$).
The received signal from an Alamouti coded MIMO transmission can be written as:

$$[y_{1,1} \quad y_{1,2}] = [h_1 \quad h_2] \begin{bmatrix} s_1 & -s_2^* \\ s_2 & s_1^* \end{bmatrix} + [n_1 \quad n_2] \tag{3.18}$$

which can be rewritten as:

$$\begin{bmatrix} y_{1,1} \\ y_{1,2} \end{bmatrix} = \begin{bmatrix} h_1 & h_2 \\ h_2^* & -h_1^* \end{bmatrix} \begin{bmatrix} s_1 \\ s_2 \end{bmatrix} + \begin{bmatrix} n_1 \\ n_2^* \end{bmatrix} \tag{3.19}$$

From the last equation, we obtain an equivalent orthogonal transmission channel $\tilde{Y} = \tilde{H}S + \tilde{N}$ that has the same properties as the code. Since the new equivalent channel is orthogonal we can apply a channel inverse to the received signal using $\tilde{H}^\dagger$ which gives:

$$\tilde{H}^\dagger \tilde{Y} = \begin{bmatrix} \|h_1\|^2 + \|h_2\|^2 & 0 \\ 0 & \|h_1\|^2 + \|h_2\|^2 \end{bmatrix} S + \tilde{H}^\dagger \tilde{N} \tag{3.20}$$

Since the new channel in the last equation is given by a diagonal matrix, symbols can be decoded independently. Consequently the ML decoding is equivalent to a simple threshold decision (zero-forcing decoding). This low complexity decoding property has made the Alamouti code very attractive for real implementations since it also achieves a full-rate and full-diversity for 2×1 MIMO systems.
Nonetheless, for 2×2 MIMO systems, the Alamouti code does not achieve a full-rate. In fact, the code rate is the same $r_A = 1$ symbol/cu whereas the maximum achievable rate in this case is 2 symbols/cu.

3.1.2.2 Orthogonal codes

The straightforward decoding complexity of the Alamouti code has motivated many research works in order to generalize this property to any MIMO system. In [80], the authors

proved the existence of orthogonal ST codes for larger MIMO schemes. The main benefit of this code family is the low decoding complexity that is reduced to a simple channel inversion. However, a detrimental drawback related to code-rate limits the performance of orthogonal codes. In fact, for any number of transmitter antennas such as $n_t > 2$, the code rate is less than 1 symbol/cu. In general, for N_s transmitted symbols, the code-rate is given by [80]:

$$r_{\perp} = \frac{N_s}{2^{N_s-1}} \quad \text{(symbols/cu)} \tag{3.21}$$

3.1.2.3 Golden code

The Golden code (GC) was presented in [81], it has the best performance for 2×2 MIMO Rayleigh fading channels. The design of the GC is based on the Golden Number $\frac{1+\sqrt{5}}{2}$ used for the code construction. The codeword matrix is given by:

$$X_{GC} = \frac{1}{\sqrt{5}} \begin{bmatrix} \alpha(s_1+\theta s_2) & \alpha(s_3+\theta s_4) \\ i\bar{\alpha}(s_3+\bar{\theta}s_4) & \bar{\alpha}(s_1+\bar{\theta}s_2) \end{bmatrix} \tag{3.22}$$

with $\theta = \frac{1+\sqrt{5}}{2}$, $\bar{\theta} = \frac{1-\sqrt{5}}{2}$, $\alpha = 1+i-i\theta$, $\bar{\alpha} = 1+i-i\bar{\theta}$ and s_1, s_2, s_3, s_4 are QAM modulated symbols. For the GC, four different symbols are transmitted from 2 antennas during 2 time-slots. Hence the GC rate is: $r_{GC} = 2$ symbols/cu which is the maximum code rate for 2×2 MIMO systems. Furthermore, the coding gain of this code is given by its minimum determinant equal to $\frac{1}{5}$ which is the maximum possible value for a 2×2 space-time block code [81].

The real linear representation of the GC is given by :

$$G_{GC} = \begin{bmatrix} \mathrm{Re}(G_{\mathbb{C},GC}) & \mathrm{Im}(G_{\mathbb{C},GC}) \\ -\mathrm{Im}(G_{\mathbb{C},GC}) & \mathrm{Re}(G_{\mathbb{C},GC}) \end{bmatrix} \tag{3.23}$$

where $G_{\mathbb{C},GC}$ is the complex generator matrix of the code given by:

$$G_{\mathbb{C},GC} = \begin{bmatrix} \alpha & \alpha\theta & 0 & 0 \\ 0 & 0 & i\bar{\alpha} & i\bar{\alpha}\bar{\theta} \\ 0 & 0 & \alpha & \alpha\theta \\ \bar{\alpha} & \bar{\alpha}\bar{\theta} & 0 & 0 \end{bmatrix} \tag{3.24}$$

3.1.2.4 Silver code

The Silver code has also a full-rate and full-diversity for 2×2 MIMO Rayleigh fading channels. Its performance is slightly lower than the Golden code but the decoding complexity is reduced [82]. The Silver code construction is based on a layered structure composed of

two Alamouti codes.

The Silver codeword matrix is given by:

$$X_S = X_1(s_1, s_2) + TX_1(z_1, z_2) \tag{3.25}$$

$$= \begin{bmatrix} s_1 & -s_2^* \\ s_2 & s_1^* \end{bmatrix} + \begin{bmatrix} 1 & 0 \\ 0 & -1 \end{bmatrix} \begin{bmatrix} z_1 & -z_2^* \\ z_2 & z_1^* \end{bmatrix} \tag{3.26}$$

with z_1 and z_2 are given by:

$$\begin{bmatrix} z_1 \\ z_2 \end{bmatrix} = \frac{1}{\sqrt{7}} \begin{bmatrix} 1+i & -1+2i \\ 1+2i & 1-i \end{bmatrix} \begin{bmatrix} s_3 \\ s_4 \end{bmatrix}$$

The rate of the silver code is: $r_S = 2$ symbols/cu and the minimum determinant of the Silver code is equal to $\frac{1}{7}$ which explains the slightly weaker performance comparing to the Golden code.

The real linear generator matrix of the Silver code is given by:

$$G_S = \frac{1}{\sqrt{2}} \begin{bmatrix} 1 & 0 & \frac{1}{\sqrt{z}} & -\frac{1}{\sqrt{7}} & 0 & 0 & -\frac{1}{\sqrt{7}} & -\frac{2}{\sqrt{7}} \\ 0 & 1 & -\frac{1}{\sqrt{7}} & -\frac{1}{\sqrt{7}} & 0 & 0 & \frac{2}{\sqrt{7}} & -\frac{1}{\sqrt{7}} \\ 0 & -1 & -\frac{1}{\sqrt{7}} & -\frac{1}{\sqrt{7}} & 0 & 0 & \frac{2}{\sqrt{7}} & -\frac{1}{\sqrt{7}} \\ 1 & 0 & -\frac{1}{\sqrt{7}} & \frac{1}{\sqrt{7}} & 0 & 0 & \frac{1}{\sqrt{7}} & \frac{2}{\sqrt{7}} \\ 0 & 0 & \frac{1}{\sqrt{7}} & \frac{2}{\sqrt{7}} & 1 & 0 & \frac{1}{\sqrt{7}} & -\frac{1}{\sqrt{7}} \\ 0 & 0 & -\frac{2}{\sqrt{7}} & \frac{1}{\sqrt{7}} & 0 & 1 & -\frac{1}{\sqrt{7}} & -\frac{1}{\sqrt{7}} \\ 0 & 0 & \frac{2}{\sqrt{7}} & -\frac{1}{\sqrt{7}} & 0 & 1 & \frac{1}{\sqrt{7}} & \frac{1}{\sqrt{7}} \\ 0 & 0 & \frac{1}{\sqrt{7}} & \frac{2}{\sqrt{7}} & -1 & 0 & \frac{1}{\sqrt{7}} & -\frac{1}{\sqrt{7}} \end{bmatrix} \tag{3.27}$$

3.1.2.5 Threaded Algebraic Space-Time (TAST) codes

In contrast to orthogonal codes that are rate limited, Threaded Algebraic Space-Time (TAST) codes can achieve full-rate and full-diversity for any $M \times M$ MIMO scheme. TAST codes were first proposed by El-Gamal et al. in [83]. To construct a codeword, first, each thread formed by q-QAM symbols is multiplied by a rotation matrix, then all threads are scaled by a set of algebraic numbers that allow all the threads to be transparent to each others. The threaded structure is shown in Fig. 3.1 for 3×3 and 4×4 TAST codes.

An example of a 3×3 TAST code is given by [83]:

$$\mathbf{X}_{3\times3} = \frac{1}{\sqrt{3}} \begin{pmatrix} s_1 + \theta s_2 + \theta^2 s_3 & \phi^{2/3}(s_7 + j\theta s_8 + j^2\theta^2 s_9) & \phi^{1/3}(s_4 + j^2\theta s_5 + j\theta^2 s_6) \\ \phi^{1/3}(s_4 + \theta s_5 + \theta^2 s_6) & s_1 + j\theta s_2 + j^2\theta^2 s_3 & \phi^{2/3}(s_7 + j^2\theta s_8 + j\theta^2 s_9) \\ \phi^{2/3}(s_7 + \theta s_8 + \theta^2 s_9) & \phi^{1/3}(s_4 + j\theta s_5 + j^2\theta^2 s_6) & s_1 + j^2\theta s_2 + j\theta^2 s_3 \end{pmatrix} \tag{3.28}$$

where $T = 3$, $\phi = \exp(i\pi/12)$, $j = \exp(i2\pi/3)$, $\theta = \exp(i\pi/9)$ and $s_{i=1:9}$ are QAM symbols.

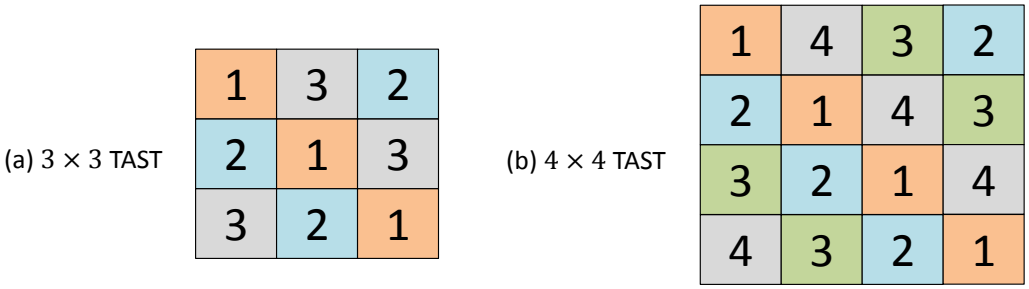

Figure 3.1: Threaded architecture of 3×3 and 4×4 TAST code.

3.1.3 Decoding of MIMO systems

We have presented in 3.1.1 the ML decoding metric for block fading MIMO Rayleigh channels. For i.i.d. transmitted codewords, the ML criterion gives the optimal BER performance over a linear MIMO channel. Moreover, we have shown that ST coded MIMO systems can achieve a diversity order of $n_t n_r$. This diversity order is achievable only when an ML decoding is implemented along with full-rank ST coding. In the case where a zero-forcing (ZF) decoding is considered the achieved diversity order is only $n_r - n_t + 1$ for $n_r \geq n_t$.

3.1.3.1 Optimal decoders

The major challenge of a MIMO decoding algorithm is to offer a good trade-off between the decoding complexity and the achievable performance. ML decoding can be realized by an exhaustive search for the transmitted codeword by minimizing the quadratic euclidean distance $\|Y - HX\|^2$ over the set of all the possible codewords. The computational complexity of this method depends on the constellation size q and the dimension of the MIMO system. For large MIMO systems using higher order modulation formats, the exhaustive search becomes unfeasible for real implementations. To have access to the modulated symbols contained in the codewords, the ML criterion can be equivalently rewritten by vectorizing the transmission equation 3.1 as follows:

$$Y'_{n_t T \times 1} = \mathrm{vec}_{\mathbb{C}}(Y) = \mathrm{vec}_{\mathbb{C}}(HX + N) \tag{3.29}$$

$$Y'_{n_t T \times 1} = \begin{bmatrix} H & 0 & 0 \\ 0 & \ddots & 0 \\ 0 & 0 & H \end{bmatrix} \mathrm{vec}_{\mathbb{C}}(X) + \mathrm{vec}_{\mathbb{C}}(N) \tag{3.30}$$

$$= H'_{n_r T \times n_t T}.G_{\mathbb{C}}.S_{n_t T,1} + N'_{n_t \times T} \tag{3.31}$$

$G_{\mathbb{C}}$ is the generator matrix of the ST code defined in Eq. 3.15, it is a unitary matrix and in the case of uncoded transmission it is equal to the identity matrix. $S_{n_t T,1} = [s_1, ..., s_{n_t T}]^{\mathrm{T}}$

is the vector of transmitted modulated symbols and by writing the equivalent channel as $H_{eq} = H'_{n_rT \times n_tT}.G_{\mathbb{C}}$, the ML decoding metric becomes:

$$\hat{S} = \underset{S_{n_tT,1} \in \text{C'}}{\operatorname{argmin}} \|Y_{n_tT \times 1} - H_{eq}.S_{n_tT,1}\|^2 \tag{3.32}$$

where C' is the set of all symbols of the used q-QAM modulation. The exhaustive search requires $q^{n_t.n_r}$ computations to decode a full-rate square ST code ($T = n_r$) that uses a q-QAM modulation. Hence, the exhaustive search strategy increases with the size of the constellation and grows exponentially with the number of antennas. Consequently, lower-complexity decoders that satisfy the ML metric are required.

Lattice decoders

A lattice Λ of $\mathbb{R}^n$ is a discrete subgroup of $\mathbb{R}^n$ that spans the real vector space of $\mathbb{R}^n$, it is given by the set:

$$\Lambda = \left\{ \sum_{i=1}^{n} a_i v_i \mid a_i \in \mathbb{Z} \right\} \tag{3.33}$$

where the vector $(v_1, ..., v_n)$ is a basis of $\mathbb{R}^n$

by applying a complex to real transformation, the equivalent channel equation 3.31 becomes:

$$Y'_{\mathbb{R}} = H_{eq,\mathbb{R}} S_{\mathbb{Z}} + N_{\mathbb{R}} \tag{3.34}$$

with

$$H_{eq,\mathbb{R}} = \begin{bmatrix} \text{Re}(H_{eq}) & \text{Im}(H_{eq}) \\ -\text{Im}(H_{eq}) & \text{Re}(H_{eq}) \end{bmatrix} \quad \text{and} \quad S_{\mathbb{Z}} = \begin{bmatrix} \text{Re}(S_{n_tT,1}) \\ \text{Im}(S_{n_tT,1}) \end{bmatrix}$$

Assuming that H_{eq} is full rank, $H_{eq,\mathbb{R}}$ forms a basis of $\mathbb{R}^n$ (with $n = 2n_tT$ is the lattice dimension) and hence it can be associated to the lattice $\Lambda_{H_{eq}}$. Consequently, the ML decoding metric can be rewritten as follows:

$$\hat{S} = \underset{S_{\mathbb{Z}} \in \mathbb{Z}^n}{\operatorname{argmin}} \left\| Y'_{\mathbb{R}} - H_{eq,\mathbb{R}} S_{\mathbb{Z}} \right\|^2 \tag{3.35}$$

From the last equation, we conclude that the ML decoding metric becomes a search problem for the closest point to $Y'_{\mathbb{R}}$ in the lattice $\Lambda_{H_{eq}}$. Reduced-search lattice decoders allow to find the closest point in a finite region of the lattice. The sphere decoder (SD) was used by Viterbo et al. [84] for uncoded and ST coded MIMO schemes, this algorithm searches for the closest point in a finite sphere centered on the received point $Y_{\mathbb{R}}$. The choice of the sphere radius is an important parameter for reducing the algorithm complexity. If for a chosen radius the sphere is empty, then the radius is increased. The appropriate sphere

radius C_{SD} is chosen as a function of the noise power and channel eigenvalues as:

$$C_{SD} = \min\left(\min\{\lambda_1, ..., \lambda_{2n}\}), 4n\sigma^2\right) \tag{3.36}$$

with $\lambda_1, ..., \lambda_{2n}$ being the eigenvalues of $H_{eq,\mathbb{R}} H_{eq,\mathbb{R}}^{\dagger}$. By using the sphere decoder, the complexity of search algorithms is tremendously reduced and becomes independent of the constellation size q. For the uncoded MIMO system is it approximated by $O(n_t^3)$ and $O(n_t^6)$ when a full-rate ST code is used [85].

3.1.3.2 Sub-optimal decoders

While the ML criterion provides the optimal performance at the cost of an important complexity, other decoding strategies give sub-optimal performances but at a lower complexity. In the next subsections we describes the most used sub-optimal decoders.

3.1.3.3 Zero-forcing

The principle of the zero-forcing (ZF) detection consists in removing the crosstalk between all MIMO channels. The received signal Y is multiplied by an equalization matrix equal to the pseudo-inverse of the channel given by:

$$H^{\ddagger} = (H^{\mathrm{T}} H)^{-1} H^{\mathrm{T}} \tag{3.37}$$

In the case of square MIMO channels the pseudo-inverse becomes simply the channel inverse H^{-1} and after the ZF filter the signal is equal to:

$$Y_{ZF} = H^{-1}(HX + N) = X + \underbrace{H^{-1}N}_{N'} \tag{3.38}$$

From the last equation, we notice that the decoded signal is the transmitted signal plus a noise vector N' that depends on the channel matrix. Hence the performance of the ZF decoder is directly related to the noise and channel conditions. The covariance matrix of the noise N' is given by:

$$\begin{aligned} R_{N'} &= \mathbb{E}[N' N'^{\mathrm{T}}] && (3.39)\\ &= \mathbb{E}[H^{-1} N N^{\mathrm{T}} H^{-\mathrm{T}}] && (3.40)\\ &= H^{-1}\mathbb{E}[N N^{\mathrm{T}}] H^{-\mathrm{T}} && (3.41)\\ &= 2\sigma^2 (H^{\mathrm{T}} H)^{-1} && (3.42) \end{aligned}$$

From the covariance matrix we conclude that if the channel matrix is unitary the noise N' remains white and the ZF gives the performance of the ML decoder.

3.1.3.4 Minimum-mean square error

The principle of the minimum-mean square error (MMSE) decoder consists in minimizing the quadratic error between the transmitted symbol and the estimated symbol. The MMSE decoder was introduced as in alternative to the ZF to overcome the noise amplification due to the channel equalization. The MMSE equalization filter minimizes the following mean square error:

$$F_{\text{MMSE}} = \underset{F}{\operatorname{argmin}} \left\{ \mathbb{E} \left\| FY - X \right\|^2 \right\} \tag{3.43}$$

The filter F_{MMSE} that achieves equation 3.43 was found to be [86]:

$$F_{\text{MMSE}} = H_{eq}^{\intercal}(H_{eq}H_{eq}^{\intercal} + \frac{1}{\text{SNR}}I)^{-1} \tag{3.44}$$

From the last equation we can distinguish two different behaviors of the MMSE filter. First, for the high SNR regime $F_{\text{MMSE}} = H_{eq}^{t}(H_{eq}H_{eq}^{t})^{-1} = H_{ZF}$, in this case the MMSE becomes a ZF decoder. For the low SNR regime, the MMSE filter is approximated by $F_{\text{MMSE}} = \text{SNR}.H_{eq}^{t}$, in this case, the MMSE filter minimizes the noise power. Hence the MMSE gives a more consistent trade-off between noise mitigation and interference cancellation which makes it better than the ZF decoder.

3.1.3.5 Zero-forcing decision feedback equalization

The two previous presented sub-optimal decoders belong to the family of linear decoders. The zero-forcing decision feedback equalizer (ZF-DFE) is a non linear decoder that takes into account the decision made on the symbol s_n to estimate recursively the previous symbols $s_{n-1}, ..., s_1$. The ZF-DFE algorithm start by a QR decomposition of the channel matrix as $H = QR$ and the transmission equation 3.1 becomes:

$$Y = QRX + N \tag{3.45}$$

where R is an upper triangular matrix and Q is a unitary matrix. Hence to obtain an equivalent system, the received vector is multiplied by the unitary matrix Q^{-1} to obtain:

$$Y' = Q^{-1}Y = RX + \underbrace{Q^{-1}N}_{N'} \tag{3.46}$$

The noise N' is additive white Gaussian because Q is unitary. From Eq 3.46, the ZF-DFE algorithm estimates the symbol s_n first, then the other symbols are recursively estimated as follows:

$$\tilde{s_i} = \left\lfloor \frac{y_i - \sum_{k=0}^{i-1} r_{i,n-k}\tilde{s}_{n-k}}{r_{i,i}} \right\rceil \tag{3.47}$$

The ZF-DFE decoder gives better performance than the traditional ZF [87], however an estimation error on a symbol is directly affecting the estimation of next symbols leading to error propagation.

To compare the performance of the reviewed ST codes and decoders, we consider a 2×2 Rayleigh fading channel. In Fig. 3.2, we compare the performance of all the reviewed decoders for an uncoded transmission using a 4-QAM constellation. From the figure, we notice that the ML decoder gives the optimal performance with a diversity equal to 3. The MMSE decoder outperforms the ZF and ZF-DFE, however all the sub-optimal decoders have poor performances comparing to the ML decoder. When a ST coded transmission is considered with an ML decoding, we notice that the Golden code outperforms the Silver and TAST code.

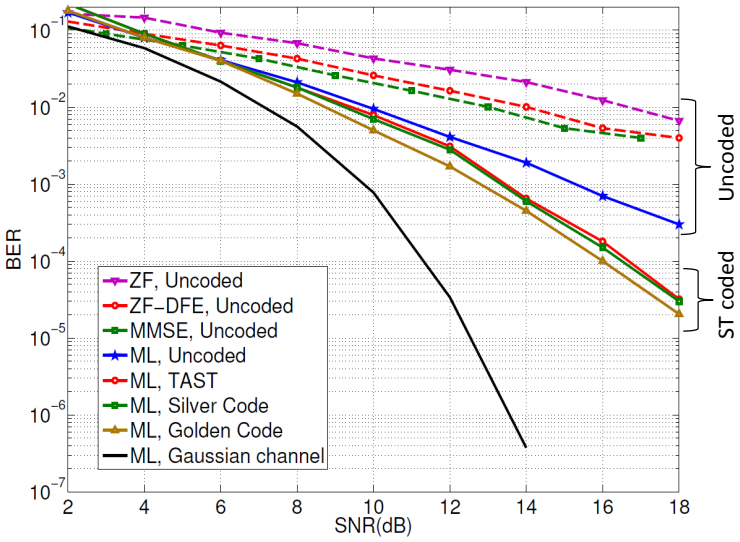

Figure 3.2: BER performance for different decoders for an uncoded and ST coded 2×2 Rayleigh fading channel.

3.2 Space-Time coding for MDM optical systems impaired by MDL

In the previous section, we have reviewed the state of the art of ST coding for wireless MIMO systems. We derived the error probability upper bound for the Rayleigh fading channel and showed that ST coding brings diversity and coding gains. The purpose of the last section is to introduce all the work elements and mathematical tools required for our study of the multi-mode optical channel. In this section, we will study the benefits of ST coding for MDM optical systems in the presence of MDL. A first investigation of ST coding for FMF systems was conducted in our research lab at Télécom ParisTech by Elie Awwad et al. [6], ST coding gains were observed for a 3-mode and 6-mode fibers. In this study, the authors considered the same optical channel as defined in Chapter 2. This channel model is based on physical properties of the fiber that allow to simulate propagation of modes taking into account real magnitudes such as propagation constants, number of spans, electrical field distributions, etc.

To extend the research work in [6], we are interested to explain the coding gains brought by ST codes when applied to the optical channel. Therefore, we are more concerned to provide mathematical evidences for the performance of ST coded MDM optical systems. For that, we consider a mathematical channel model that describes the effects of MDL and coupling. Then, we compute an upper bound for the error probability which will provide a design criterion for ST codes to fully absorb MDL.

Later on, we extend our study to a system where ST codes are implemented along with FEC, we investigate the gains brought by each coding scheme alone and then we prove the summation of coding gains when both codes are implemented together.

3.2.1 Error probability upper bound of ST coded MDM optical systems

3.2.1.1 MDM optical channel with MDL

The effect of mode dependent loss on propagation has been investigated in many studies [34–36]. The accumulated MDL depends on the modal coupling and the number of concatenated fiber spans. In order to study the benefits of coding independently of link statistics in a spirit of a back-to-back emulation measurement, we consider a simplified channel model made of a single lumped MDL element. This model was used in [88] to study the performance of the optical channel affected by MDL for different constellation sizes, also the same model allowed to study the secrecy capacity of MIMO MDM systems

in [89]. The MIMO transmission system may be described by:

$$Y_{M\times T} = H.X_{M\times T} + N_{M\times T} \tag{3.48}$$

where $X_{M\times T}$ (resp. $Y_{M\times T}$) is the transmitted space-time codeword (resp. the received codeword). $N_{M\times T}$ is the noise assumed to be additive white Gaussian with zero mean and a variance $2\sigma^2$ per mode. The channel matrix is given by:

$$H = \sqrt{\alpha}\sqrt{D}U. \tag{3.49}$$

with D is a diagonal matrix, its entries are uniformly drawn in $[\lambda_{min}, \lambda_{max}]$ and represent different losses experienced by each mode. In the absence of MDL the matrix D is equal to the identity matrix ($D = I_M$). U is a random unitary matrix, it represents coupling between modes. $\alpha = \frac{M}{\sum_{i=1}^{M}\lambda_i}$ factors out the mode average propagation loss such that $\mathrm{Tr}(HH^\dagger) = M$ (with Tr(.) represents the trace of a matrix operator). Mode dependent loss is defined as the ratio of the maximum to the minimum eigenvalues of the channel matrix: $\mathrm{MDL}_{(dB)} = 10.\log(\mathrm{MDL}) = 10.\log(\frac{\lambda_{max}}{\lambda_{min}})$.

3.2.1.2 Derivation of the error probability upper bound

For the derivation of the error probability upper bound, we start from the average PEP of Eq. 3.8. Let $X_\Delta = \hat{X} - X$ be the the difference of two codewords and by replacing the matrix H by the corresponding optical channel we obtain:

$$\Pr\left\{X \to \hat{X}\right\} \leqslant \mathbb{E}_H\left[\exp\left(-\frac{\left\|\sqrt{\frac{M}{\sum_{i=1}^{M}\lambda_i}}\sqrt{D}UX_\Delta\right\|^2}{8\sigma^2}\right)\right] \tag{3.50}$$

$$\leqslant \mathbb{E}_H\left[\exp\left(-\frac{M}{\sum_{i=1}^{M}\lambda_i}\frac{\mathrm{Tr}(DUX_\Delta X_\Delta^\dagger U^\dagger)}{8\sigma^2}\right)\right] \tag{3.51}$$

In the following, we derive the error probability upper bound for orthogonal space-time codes, afterwards we deal with the general case of space-time codes.

A. Orthogonal space-time codes

The construction of orthogonal ST codes makes the codeword difference matrix X_Δ inherits the orthogonality property of the code [90], i.e. $X_\Delta X_\Delta^\dagger = \sum_k |x_{k,i} - x_{k,j}|^2 . I_M$ for all possible codeword differences, with $x_{k,i}$ (resp. $x_{k,j}$) the emitted (resp. estimated) symbols.

Applying this property to Eq 3.51 we obtain:

$$\Pr\left\{X \to \hat{X}\right\} \leqslant \exp(-\frac{\|X_\Delta\|^2}{8\sigma^2}) \tag{3.52}$$

Reporting this in Eq 3.5, the error probability upper bound becomes:

$$\Pr_{error} \leq \sum_{X \in C} \frac{1}{\text{card}(C)} \sum_{X \neq \hat{X}} \exp(-\frac{\|X_\Delta\|^2}{8\sigma^2}) \tag{3.53}$$

The minimum euclidean distance of the ST code is defined as: $d^2_{min,ST} = \underset{X \neq \hat{X},\ X,\hat{X} \in C}{min} \left\|X - \hat{X}\right\|^2$. Hence, the number of nearest neighbors $N_{min,X}$ of X is defined as the number of codewords that are at distance $d^2_{min,ST}$ of X. By using the number of nearest neighbors $N_{min,X}$ of X we obtain:

$$\Pr_{error} \leq (\frac{1}{\text{card}(C)} \sum_{X \in C} N_{min,X}) \cdot \exp(-\frac{d^2_{min,ST}}{8\sigma^2}) \tag{3.54}$$

We denote $\overline{N}_{min} = \frac{1}{\text{card}(C)} \sum_{X \in C} N_{min,X}$ the average number of closest neighbors of X, Eq. 3.54 becomes:

$$\Pr_{error} \leq \overline{N}_{min} \cdot \exp\left(-\frac{d^2_{min,ST}}{8\sigma^2}\right) \tag{3.55}$$

From equation 3.55, we notice that orthogonal space-time codes give an error probability upper bound completely independent of MDL. Hence, we conclude that orthogonal ST codes completely mitigate MDL.

B. General case of space-time codes

In this section, we derive an upper bound of the error probability in the general case of space-time codes. We rewrite the error probability given by inequality 3.5 as a summation of two terms where the first one contains the orthogonal codeword differences and the second term contains the non orthogonal codeword differences.

$$\Pr_{error} \leq \sum_{X \in C} \frac{1}{\text{card}(C)} \underbrace{\sum_{\substack{X \neq \hat{X} \\ X_\Delta \text{orthogonal}}} \Pr\left\{X \to \hat{X}\right\}}_{} + \sum_{X \in C} \frac{1}{\text{card}(C)} \underbrace{\sum_{\substack{X \neq \hat{X} \\ X_\Delta \text{ non orthogonal}}} \Pr\left\{X \to \hat{X}\right\}}_{} \tag{3.56}$$

The first term of equation 3.56 was computed in the previous section and is equal to $\overline{N}_{min,1} \cdot \exp(-\frac{d^2_{min,ST}}{8\sigma^2})$, where $\overline{N}_{min,1}$ is the average number of nearest neighbors of X such that X_Δ is orthogonal. Let us now focus on the second term starting from the

average PEP of equation 3.51 and since $\sum_{i=1}^{M} \lambda_i \leqslant M\lambda_{max}$ we get:

$$\Pr\left\{X \to \hat{X}\right\} \leqslant \mathbb{E}_{D,U}\left[\exp(-\frac{\mathrm{Tr}(DUX_{\Delta}X_{\Delta}^{\dagger}U^{\dagger})}{8\sigma^2\lambda_{max}})\right] \tag{3.57}$$

Here, we average over the diagonal and unitary matrices D and U. $X_{\Delta}X_{\Delta}^{\dagger}$ is a square hermitian matrix, so there exists a unitary matrix V and a diagonal matrix $\Sigma = \mathrm{diag}(\sigma_1, ..., \sigma_M)$ such that: $X_{\Delta}X_{\Delta}^{\dagger} = V\Sigma V^{\dagger}$. We obtain:

$$\Pr\left\{X \to \hat{X}\right\} \leqslant \mathbb{E}_{D,U}\left[\exp(-\frac{\mathrm{Tr}(DUV\Sigma V^{\dagger}U^{\dagger})}{8\sigma^2\lambda_{max}})\right] \tag{3.58}$$

The matrix U is randomly drawn from the unitary matrix ensemble, it induces that the product UV follows the same distribution as U [91], We obtain:

$$\Pr\left\{X \to \hat{X}\right\} \leqslant \mathbb{E}_{D,U}\left[\exp(-\frac{\mathrm{Tr}(DU\Sigma U^{\dagger})}{8\sigma^2\lambda_{max}})\right] \tag{3.59}$$

by developing the term $DU\Sigma U^{\star}$ we obtain:

$$\Pr\left\{X \to \hat{X}\right\} \leq \mathbb{E}_{D,U}\left[\exp(-\frac{\sum_{i,j=1}^{M}\lambda_i\sigma_j\left|u_{ij}\right|^2}{8\sigma^2\lambda_{max}})\right] \tag{3.60}$$

$$\leq \mathbb{E}_{D,U}\left[\prod_{i=1}^{M}\exp(-\lambda_i\frac{\sum_{j=1}^{M}\sigma_j\left|u_{ij}\right|^2}{8\sigma^2\lambda_{max}})\right] \tag{3.61}$$

since the random variables λ_i's are independent, the expectation of the product is equal to the product of expectations and we obtain:

$$\Pr\left\{X \to \hat{X}\right\} \leq \prod_{i=1}^{M}\mathbb{E}_{D,U}\left[\exp(-\lambda_i\frac{\sum_{j=1}^{M}\sigma_j\left|u_{ij}\right|^2}{8\sigma^2\lambda_{max}})\right] \tag{3.62}$$

now, we average over λ_i's that are independently and uniformly drawn in $[\lambda_{min}, \lambda_{max}]$ to obtain:

$$\Pr\left\{X \to \hat{X}\right\} \leq \prod_{i=1}^{M}\mathbb{E}_{U}\left[\int_{\lambda_{min}}^{\lambda_{max}}\exp(-\lambda_i\frac{\sum_{j=1}^{M}\sigma_j\left|u_{ij}\right|^2}{8\sigma^2\lambda_{max}}) \times P(\lambda_i)d\lambda_i\right] \tag{3.63}$$

$$= \prod_{i=1}^{M}\mathbb{E}_{U}\left[\frac{\exp(-\frac{\sum_{j=1}^{M}\sigma_j|u_{ij}|^2}{8\sigma^2} - \exp(-\frac{\lambda_{min}}{\lambda_{max}}\frac{\sum_{j=1}^{M}\sigma_j|u_{ij}|^2}{8\sigma^2})}{\frac{(\lambda_{max}-\lambda_{min})\sum_{j=1}^{M}\sigma_j|u_{ij}|^2}{8\sigma^2\lambda_{max}}}\right] \tag{3.64}$$

$$= \prod_{i=1}^{M} \mathbb{E}_U \left[\exp\left(-\frac{1}{2}(1+\frac{\lambda_{min}}{\lambda_{max}}) \frac{\sum_{j=1}^{M} \sigma_j |u_{ij}|^2}{8\sigma^2} \right) \times 2\sinh\left(\frac{1}{2}(1-\frac{\lambda_{min}}{\lambda_{max}}) \frac{\sum_{j=1}^{M} \sigma_j |u_{ij}|^2}{8\sigma^2} \right) \right] \tag{3.65}$$

In equation 3.63 $P(\lambda_i)$ represents the probability distribution function of λ_i and it is given by:

$$P(\lambda_i) = \begin{cases} \frac{1}{\lambda_{max}-\lambda_{min}} & if\ \lambda_{min} \leqslant \lambda_i \leq \lambda_{max} \\ 0 & \text{elsewhere} \end{cases}$$

We use the approximation of the hyperbolic sine at high SNR: $\sinh(x) \underset{x\to\infty}{\to} \exp(x)/2$ so we obtain:

$$\Pr\left\{X \to \hat{X}\right\} \leq \prod_{i=1}^{M} \mathbb{E}_U \left[\exp(-(\frac{\lambda_{min}}{\lambda_{max}}) \frac{\sum_{i=1}^{M} \sigma_j |u_{ij}|^2}{8\sigma^2}) \right] \tag{3.66}$$

$$= \mathbb{E}_U \left[\exp(-\frac{\lambda_{min}}{\lambda_{max}} \frac{\sum_{j=1}^{M} \sum_{i=1}^{M} \sigma_j |u_{ij}|^2}{8\sigma^2}) \right] \tag{3.67}$$

$$= \mathbb{E}_U \left[\exp(-\frac{\lambda_{min}}{\lambda_{max}} \frac{\sum_{j=1}^{M} \sigma_j}{8\sigma^2}) \right] \tag{3.68}$$

$$= \mathbb{E}_U \left[\exp(-\frac{\|X_\Delta\|^2}{8\sigma^2 \mathrm{MDL}}) \right] \tag{3.69}$$

Equation 3.69 is independent of the unitary matrix U so we get:

$$\Pr\left\{X \to \hat{X}\right\} \leq \exp\left(-\frac{\|X_\Delta\|^2}{8\sigma^2 \mathrm{MDL}} \right) \tag{3.70}$$

Substituting 3.70 in the second term of equation 3.56 gives:

$$\Pr_{error} \leq \overline{N}_{min,1} \cdot \exp\left(-\frac{d^2_{min,ST}}{8\sigma^2} \right) + \sum_{X \in C} \frac{1}{\mathrm{card}(C)} \sum_{\substack{X \neq \hat{X} \\ X_\Delta \text{ non orthogonal}}} \exp\left(-\frac{\|X_\Delta\|^2}{8\sigma^2 \mathrm{MDL}} \right) \tag{3.71}$$

Let $N_{min,2,X}$ be the number of nearest neighbors of X such that X_Δ is non orthogonal, we obtain:

$$\Pr_{error} \leq \overline{N}_{min,1} \cdot \exp\left(-\frac{d^2_{min,ST}}{8\sigma^2} \right) + \sum_{X \in C} \frac{1}{\mathrm{card}(C)} N_{min,2,X} . \exp\left(-\frac{d^2_{min,ST}}{8\sigma^2 \mathrm{MDL}} \right) \tag{3.72}$$

by denoting $\overline{N}_{min,2} = \sum_{X_i \in C} \frac{1}{\mathrm{card}(C)} N_{min,2,X}$ we arrive at:

$$\Pr_{error} \leq \overline{N}_{min,1} \cdot \exp\left(-\frac{d^2_{min,ST}}{8\sigma^2} \right) + \overline{N}_{min,2} \cdot \exp\left(-\frac{d^2_{min,ST}}{8\sigma^2 \mathrm{MDL}} \right) \tag{3.73}$$

From the last equation, we notice that the error probability upper bound is a sum of two terms that decay exponentially as a function of the SNR as in the case of the additive white Gaussian (AWGN) channel. This behavior is completely different from the Rayleigh fading channel where the error probability decays as a function of SNR^{-rn_r} as shown in Eq 3.11. Hence, ST coding for the optical channel affected by MDL does not bring a diversity gain but only a coding gain that is discussed in the following.

3.2.2 Design criterion and performance analysis

From equation 3.73, the error probability upper bound is composed of two terms. The first one comes from the orthogonal codeword differences and is completely independent of MDL. The second term is affected by MDL and comes from the non orthogonal difference codewords. In order to minimize the error probability upper bound the first term should be the dominant term of the upper bound.

Proposition: In order to minimize the error probability, the average number of nearest neighbors $\overline{N}_{min,1}$ of a space-time code such that X_Δ is orthogonal should be maximized.

The obtained design criterion is directly related to the orthogonality of codeword differences. In Table 3.1, we have computed the average number of orthogonal and non-orthogonal closest neighbors of X for different 2×2 ST codes using a 4-QAM constellation. We notice that the Alamouti code has $\overline{N}_{min,2}=0$, this is due to its orthogonal structure. The codewords of the Silver code have more orthogonal nearest neighbors (6.5 neighbors) than the codewords of the TAST code (4 neighbors). Codewords of the Golden code have no nearest orthogonal neighbors. These observations allow us to deduce that the Silver code gives the best performance followed by the TAST then the Golden code.

Table 3.1: Average number of orthogonal and non-orthogonal neighbors of a codeword X for different 2×2 ST codes.

	$\overline{N}_{min,1}$	$\overline{N}_{min,2}$	$\overline{N}_{min,Total}$
Silver Code	6.5	1.5	8
TAST Code	4	4	8
Golden Code	0	8	8
Alamouti Code	8	0	8

To validate the obtained theoretical results, we compute by simulations the performance of different ST codes for 2×2 and 3×3 MIMO-MDM optical systems. We compare the performance in terms of BER curves versus the SNR. At the receiver a ML decoder is implemented.

A. Two-modes fiber optical channel

To study the impact of the orthogonality of the codeword difference matrices on the error probability, we consider four different space-time codes: The Silver, Golden, Alamouti and TAST code. In order to compare the performances at the same spectral efficiency, we use 4-QAM symbols to construct codewords of the Silver, Golden and TAST code (which are full-rate codes with 2 symbols/cu), and 16-QAM symbols to construct codewords for the Alamouti code (which is a half rate code with 1 symbol/cu).

In Fig. 3.3 we report the performance of the Alamouti code. We notice that this code gives the same performance for different MDL values which confirms the obtained upper bound of equation 3.55. Hence, we can conclude that orthogonal ST codes allow to completely mitigate MDL but unfortunately these codes are penalized by their rate that reduces the transmission throughput.

In Fig. 3.4 we compare the performance of the Silver, TAST and Golden code for MDL= 10dB. We notice that the Silver code outperforms the two other codes, this can be explained by the higher number of orthogonal codeword differences of the Silver code. The Golden code is the less performing one due to the absence of orthogonal neighbors at $d^2_{min,ST}$. The performance of the TAST code comes between the Silver and the Golden with an average number of orthogonal neighbors equal to 4.

These results are completely different from the wireless Rayleigh channel where the Golden code is the best code. In fact for the wireless channel, these codes were constructed in order to satisfy the rank and determinant criteria, however these criteria are not relevant for the optical channel affected by MDL.

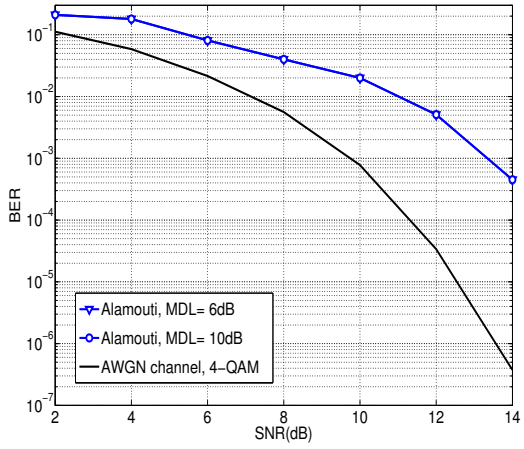

Figure 3.3: 2-modes fiber. BER versus SNR for the 2×2 Alamouti code (constructed with 16 QAM) for MDL = 6, 10 dB.

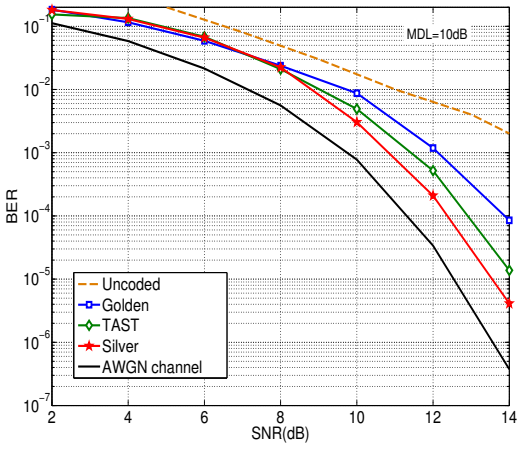

Figure 3.4: 2-modes fiber. BER versus SNR for the 2×2 {Silver, Golden, TAST} codes, for MDL = 10 dB.

B. Three-modes fiber optical channel

In this part, we consider a 3-mode fiber and study the impact of MDL on the error probability. We use a 3×3 TAST code which is a full-rate code. In Fig. 3.5 we report the performance of this code for MDL = 6 and 10 dB. We notice that for MDL = 6 dB the TAST code allows to completely mitigate all the MDL. However, for MDL = 10 dB and at BER = 10^{-4}, the SNR penalty of the MDM optical channel to the Gaussian channel is 1.2 dB. This behavior can also be explained by the equation 3.73. In fact, by increasing MDL, this leads to increase the impact of the second term of the upper bound and hence induces a loss in the performance.

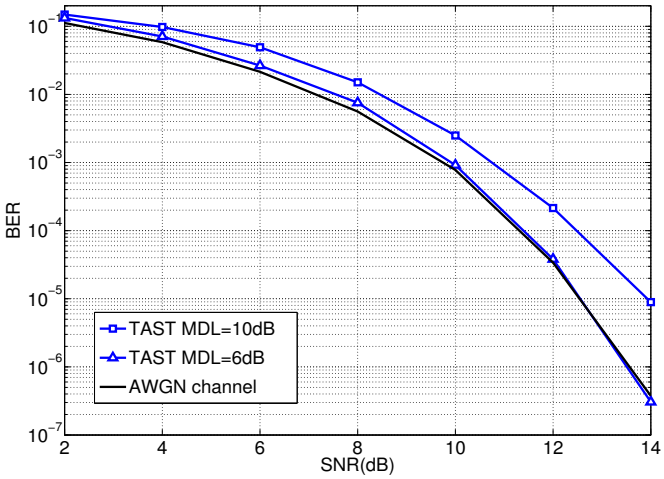

Figure 3.5: 3-modes fiber. BER as a function of SNR for the 3×3 TAST code, for MDL = 6,10 dB.

3.3 FEC and ST coding concatenation for MDM optical systems impaired by MDL

For a long time FEC was ignored for optical transmissions because these systems can achieve BER of the order $10^{-9} - 10^{-15}$. However, transmission impairments such as the degradation caused by the optical amplifiers in long-haul optical systems lead to the integration of FEC codes into optical transmission systems [92]. Since that time, several FEC codes were studied. The first generation of FEC was based on linear block codes such as the Reed-Solomon (RS) implemented along with hard decision decoding (HDD). The second generation of FEC codes was based on concatenated codes, the principle consists in using two FECs that have different properties, e.g. the RS code is implemented along with the Boss-Chaudhuri-Hocquenghem (BCH) code. The third generation of FECs has emerged

to more powerful schemes that allowed to reach important coding gains. Low-Density Parity Check codes (LDPC) [93] along with soft decision decoding (SDD) allowed to reach new coding gains for both coherent single-carrier and multi-carrier optical systems.

3.3.1 Preliminaries on FEC

The principle of a FEC code is to introduce redundancy bits to the transmitted data in order to protect the information from errors. The coding rule is known at both the transmitter and the receiver, this coding rule is used by the transmitter to encode the data and by the receiver for the decoding. The redundancy bits bring a coding gain in the SNR comparing to an uncoded scheme, however this redundancy reduces the bit-rate of the transmission. Hence a trade-off between the coding gain and the throughput limitation has to be considered.

Linear block codes are a family of FEC in which the transmitted bits are encoded by blocks of k bits, to these bits are added $n-k$ redundancy bits. Hence n bits are transmitted which corresponds to a FEC rate of:

$$r_{\text{FEC}} = \frac{k}{n} \text{ bits/s} \tag{3.74}$$

Let m be the original message of length k, the FEC encoding corresponds to the linear multiplication by the generator code matrix G, the resulting coded message c of length n is then given by:

$$c = m.G \tag{3.75}$$

The matrix G represents a basis of the subspace formed by the set of all possible codewords of length n. To the matrix G corresponds a matrix H_{FEC} called the parity check matrix of the code, it is a basis of the dual subspace and it satisfies for all codewords c the following property:

$$c.H_{\text{FEC}}^{t} = 0 \tag{3.76}$$

Due to different propagation effects such as the channel properties and noise addition, the received sequence r of length n is no longer the initial transmitted sequence c. The receiver checks first if the received sequence is still a codeword, this is done thanks to the syndrome computation. In fact, the received sequence r is actually the initial sequence c

affected by an error vector as: $r = c + e$. The syndrome s is computed as:

$$s = r.H_{\text{FEC}}^{t} \tag{3.77}$$

$$= c.H_{\text{FEC}}^{t} + eH_{\text{FEC}}^{t} \tag{3.78}$$

$$= eH_{\text{FEC}}^{t} \tag{3.79}$$

Hence, if the syndrome s is null, then the received sequence is a valid codeword but no necessarily the transmitted one.

The minimal distance $d^2_{min,FEC}$ of a FEC code is an important characteristic that determines the detection and correction capabilities of the code. It is defined as the minimal number of distinct bits between any pair of codewords. Hence, the FEC decoder can detect the presence of eventual errors in the received sequence only if the number of error bits is strictly less than $d^2_{min,FEC}$. After error detection is successfully operated, the decoder can proceed to error correction which consists to find the most likely codeword that corresponds to the transmitted sequence. The maximum number of errors t that a FEC decoder is able to correct is:

$$t = \left\lfloor \frac{d^2_{min,FEC} - 1}{2} \right\rfloor \tag{3.80}$$

3.3.2 Concatenation of ST codes and FEC for MDL mitigation in MDM systems

In section 3.2, we have studied theoretically the error probability upper bound of ST coded MDM optical system. In this section we extend the previous study by combining ST codes with FEC. We follow the same method to compute the upper bound and then we validate the obtained result by numerical simulations.

3.3.2.1 Derivation of the error probability upper bound

We consider the transmission system given in Fig. 3.6. A binary information sequence of length k is mapped into a binary sequence of length n $(n > k)$. To avoid burst error, a bit interleaver is added after the FEC encoder, the principle of the interleaver is to mix bits before being modulated. After that, bits are modulated to create symbols and the ST coder maps symbols to create codewords.

Considering the same channel model of Eq. 3.49, the probability of having m errors in a block of n bits is:

$$P_{m,n} = \binom{n}{m} p^m (1-p)^{n-m} \tag{3.81}$$

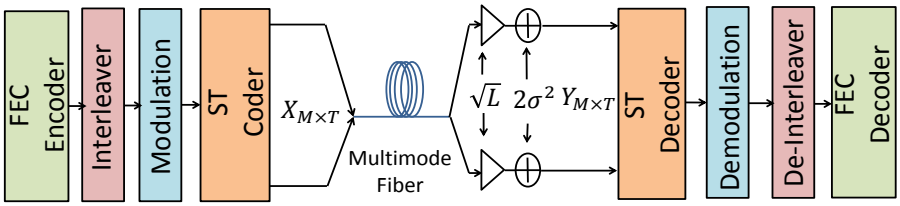

Figure 3.6: MDM transmission system including ST coding and FEC.

Where $\binom{n}{m}$ denotes m combinations among n, and p is the crossover probability of the equivalent binary-symetric channel (BSC). When the number of errors exceeds t an error is declared at the receiver. The bit error probability after hard decision decoding is upper bounded by ([75], Chap.7):

$$P_e \leq \sum_{m=t+1}^{n} \binom{n}{m} p^m (1-p)^{n-m} \tag{3.82}$$

In the high SNR regime p tends to zero and the upper bound is dominated by its first term:

$$P_e \leq \binom{n}{t+1} p^{t+1} \tag{3.83}$$

replacing $t+1$ by its value we get:

$$P_e \leq \binom{n}{d_{FEC}^2} p^{d_{FEC}^2} \tag{3.84}$$

where we denoted $d_{FEC}^2 = \left\lfloor \frac{d_{min,FEC}}{2} \right\rfloor$.
A ST codeword error results when at least one bit is in error, hence:

$$p \leq \Pr\left\{X \to \hat{X}\right\} \tag{3.85}$$

At high SNR, the PEP of the closest neighbors predominates the other terms in the union bound given by Eq 3.5, and p can be upper bounded by:

$$p \leq N_1 \cdot \exp(-\frac{d_{min,ST}^2}{8\sigma^2}) + N_2 \cdot \exp(-\frac{d_{min,ST}^2}{8\sigma^2 \mathrm{MDL}}) \tag{3.86}$$

$$\approx N_2 \cdot \exp(-\frac{d_{min,ST}^2}{8\sigma^2 \mathrm{MDL}}) \tag{3.87}$$

Where N_1 (resp. N_2) is the probability that the codeword difference matrix X_Δ is orthogonal (resp. non orthogonal). The second term in Eq. 3.86 is dominant because of the presence of MDL inside the exponential, this allows to make the approximation of equation 3.87.

Injecting 3.87 in 3.84 we obtain:

$$P_e \leq \binom{n}{d_{FEC}^2} N_2^{d_{FEC}^2} \exp\left(-\frac{d_{min,ST}^2.d_{FEC}^2}{8\sigma^2 \mathrm{MDL}}\right) \tag{3.88}$$

Substituting the average bit energy E_b by the average symbol energy using $E_s = 1 = E_b.r_{\mathrm{FEC}}.r_{ST}.\log_2(q)$, we obtain:

$$P_e \leq \binom{n}{d_{FEC}^2} N_2^{d_{FEC}^2} \cdot \exp\left(-\frac{r_{ST}.d_{min,ST}^2.r_{\mathrm{FEC}}.d_{FEC}^2.E_b.\log_2(q)}{8\sigma^2 \mathrm{MDL}}\right) \tag{3.89}$$

For an uncoded system without FEC ($r_{\mathrm{FEC}} = 1$ and $d_{FEC} = 1$) and without ST coding and a minimal distance $d_{min,NC}^2$ the error probability is upper bounded by:

$$P_{e,NC} \leq \binom{n}{1} N_2 \cdot \exp\left(-\frac{d_{min,NC}^2.E_b.\log_2(q)}{8\sigma^2 \mathrm{MDL}}\right) \tag{3.90}$$

where $d_{min,NC}^2$ is the minimum distance of the uncoded transmission. The coding gain is defined as the reduction in SNR for the coded system to obtain the same error probability as an uncoded system. It is the difference in logarithm of the two signal-to-noise ratios at the same error probability:

$$\Delta G_{dB} = \left(\frac{r_{ST}.d_{min,ST}^2.r_{\mathrm{FEC}}.d_{FEC}^2.E_b.\log_2(q)}{d_{min,NC}^2 E_b \log_2(q)}\right)_{dB} \tag{3.91}$$

$$= \left(r_{\mathrm{FEC}}.d_{FEC}^2\right)_{dB} + \left(\frac{r_{ST}.d_{minST}^2}{d_{min,NC}^2}\right)_{dB} \tag{3.92}$$

$$= G_{dB,FEC} + G_{dB,ST} \tag{3.93}$$

From the last equation, it is clearly shown that the total coding gain brought by the concatenation of ST coding and FEC is the sum of the gain of each code. For the optical channel, the pairwise error probability decays exponentially as a function of the SNR, this allows to the gain of the FEC code present in the exponent of equation 3.84 to be added to the ST code gain.

If we had considered soft decision decoding (SDD), the error probability of Eq. 3.82 would have become ([75], Chap.7):

$$P_e \leq (2^k - 1)p^{d_{\min,\mathrm{FEC}}} \tag{3.94}$$

and hence the rest of the calculus gives exactly the same result on the coding gain summation.

3.3.2.2 Performance analysis

To verify the obtained theoretical result, we present the system performance through numerical simulations, we consider hard-decision decoding for computational complexity simplification. We evaluate the performance of the concatenation of FEC code and ST code and compare to the configuration where each code is implemented alone. We simulate a 3-mode fiber system and compare the performance in term of BER curves versus SNR. At the transmitter a binary information sequence of length k is mapped into a binary sequence of length n using an LDPC encoder of code rate $r_{\text{FEC}} = \frac{3}{4}$ bits/s. After that, bits are interleaved and modulated using a 4-QAM constellation. The ST coder maps modulated symbols to create codewords, in our simulations we consider the full-rate 3×3 TAST code [83].

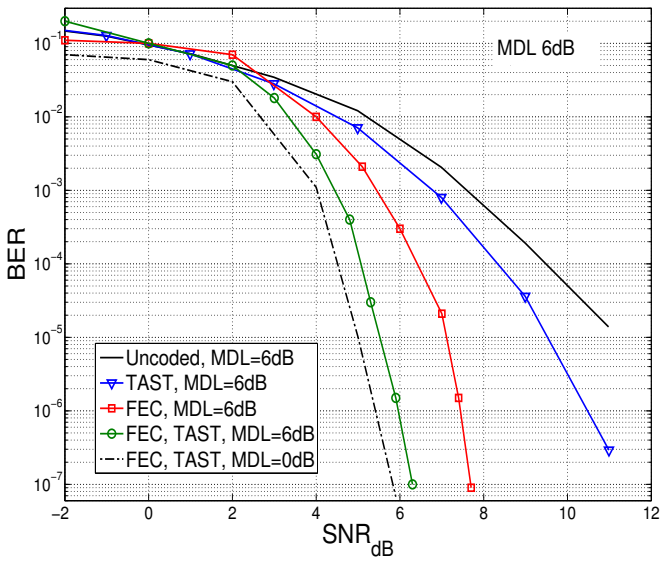

Figure 3.7: Performance of a 3-mode fiber in term of BER for the uncoded scheme and with TAST code, LDPC code, and the concatenation of both codes for MDL = 6 dB.

From Fig. 3.7, at BER $= 10^{-4}$ and for MDL = 6dB we notice that the gain (i.e. the SNR gap to the uncoded scheme) provided by the ST code alone is 1.1 dB, the gain provided by the LDPC code alone is 3.2 dB and the gain obtained by the concatenation of both codes is 4.6 dB, approximately equal to the sum of the separate coding gains $1.1 + 3.2 = 4.3$ predicted by the theoretical calculus.

In Fig. 3.8, for an MDL = 10dB, the gain obtained by the ST code alone is 2.3 dB, the gain provided by the LDPC code alone is 2.6 dB, and the gain provided by the concatenation of both codes is 5.1 dB almost equal to $2.3 + 2.6 = 4.9$.

The total gain provided analytically is a bit less than the gain observed by simulations, this is due to the approximation used in equation 3.87.

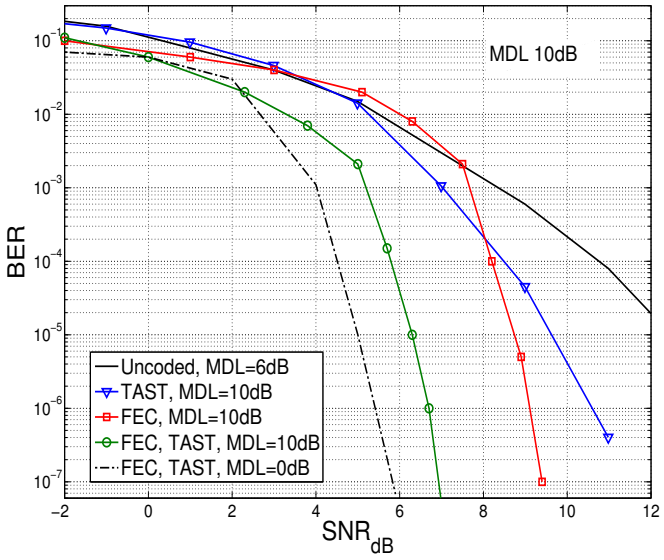

Figure 3.8: Performance of a 3-mode fiber in term of BER for the uncoded scheme and with TAST code, LDPC code, and the concatenation of both codes for MDL = 10 dB.

Conclusion

In this chapter, we have conducted a mathematical study of the benefits of two coding schemes to MDM optical systems impaired by MDL. First, we have derived an upper bound for the error probability of ST coded MDM systems affected by MDL. This expression allows to compare the performance of different existing space-time codes. Moreover, the upper bound expression also yields a design criterion for new codes construction. This criterion is different from the rank and determinant criteria known for a Rayleigh fading channel. According to this criterion, the number of orthogonal codeword differences should be maximized in order to minimize the error probability.

Furthermore, we have proven that when ST codes are implemented along with FEC, the summation of coding gains is possible which is not the case of the Rayleigh channel. FEC protects the data from errors at the bit level but is not effective in the presence of MDL. ST coding brings gain by coding information at the symbol level which is very important to average the MDL penalty over all modes.

In this study, we have focused only on MDL and modal coupling as the two characteristics of our channel model and we have omitted all other effects. This allowed us to frame MDL as it is the main concern of this research work. However in real transmission systems, other

physical impairments must be considered. In order to investigate ST coding behavior in real circumstances of propagation and to have a complete study, theoretical, by simulations and experimental, in the next chapter, we lead an experimental study of ST coding for MDM systems impaired by MDL.

Chapter 4

Realization of a ST coded MDM transmission in Experiment

The investigation of space-time (ST) coding schemes for coherent optical communications was initiated at Télécom ParisTech in 2011 through the PhD thesis of Sami Mumtaz. A first experimental study in [94] has demonstrated the potential of ST codes in mitigating polarization dependent loss (PDL) for PDM systems. In this study Orthogonal frequency division multiplexing (OFDM) format was used to manage the dispersive effects of the propagation. Later on, in 2013, Elie Awwad pursued the work and a design criterion of ST codes for PDL mitigation in PDM systems was demonstrated in [95]. Afterwards, the application of ST coding was extended to MDM systems. The first study was done by Awwad et al. in [96]. The potential of ST coding in mitigation MDL in FMFs was demonstrated through numerical simulations, however only one polarization was considered.

In the previous chapter, we have theoretically derived an upper bound for the error probability for ST coded MDM optical channel and defined a design criterion for ST codes to completely absorb MDL. In this chapter, we experimentally demonstrate for the first time the mitigation of MDL using full-rate ST codes.

Accordingly, this chapter is organized as follows: The first section, is dedicated to OFDM modulation format as it is essential to manage the dispersion effects of the channel. We review the principles of OFDM for optical communications, then we go over the properties of the OFDM transmitter and receiver and we detail each block.

In the second section, we propose a transmission channel model for FMFs with both polarizations. We extend the already existing model with only one polarization and perform simulations for ST coded transmission where MDL arises between modes and also PDL exists between polarizations of higher order modes.

Lastly, we conduct a MDM transmission experiment in which we use OFDM for dispersion management and ST coding for MDL mitigation. For an $M \times M$ MDM transmission, M dual-polarization coherent receivers are required and each receiver is coupled to the output of the DEMUX. The research lab at Télécom ParisTech is oriented to single-mode fiber transmissions, more specifically the study of non-linearities for long-haul single mode fiber systems. To overcome the equipment issue, we conduct our experiment in collaboration with the IRCICA (Institut de recherche sur les composants logiciels et matériels pour l'information et la communication avancée) laboratory of University of Lille. The IRCICA has a well developed transmission platform dedicated to space division multiplexing systems. We prove for the first time, the efficiency of full-rate ST coding in mitigating MDL. In the last section, we describe the experimental setup and show the obtained ST coding gains.

4.1 OFDM for optical communications

OFDM belongs to the class of multi-carrier modulation format in which information is carried over many lower rate subcarriers. OFDM converts a frequency-selective channel into a parallel collection of frequency flat sub-channels. The subcarriers have the minimum frequency separation required to maintain orthogonality of their corresponding time domain waveforms. The two fundamental advantages of OFDM are its robustness against channel dispersion and its easy phase and channel estimation in a time-varying environment. OFDM has been widely integrated to many wireless standards such as digital audio broadcasting (DAB) and the Wi-Fi (IEEE 802.11) [97] to combat multi-paths interference. In OFDM format, data is transmitted in parallel on a number of adjacent frequencies, this makes the symbol period much longer than for a serial system with the same total data rate. Because the symbol period is longer, inter-symbol interferences (ISI) affects at most one symbol, and equalization is simplified. Practically, in most OFDM implementations ISI is removed by using a guard interval called a cyclic prefix (CP).

Although OFDM has been studied in wireless communications for more than four decades, the research on OFDM in optical communication began only in the late 1990s [98]. OFDM was proposed as an attractive modulation format for long-haul transmissions either in both direct detection [99] and coherent detection [100] to manage dispersion and to lower the equalization complexity in optical communications [101]. Coherent OFDM (CO-OFDM) was first proposed to combat chromatic dispersion [100], later on, it was extended to PDM systems to manage PMD [102]. The first CO-OFDM transmission experiment

was reported for 1000 km of SSMF transmission at 8 Gb/s by Shieh et al. [103], right after, another CO-OFDM transmission experiment over 4160 km of SSMF at 20 Gb/s [104] was reported.

For MDM transmission systems, due to DMGD, the equalization complexity is much higher than in SMF systems. Hence, the integration of $M \times M$ MIMO equalizers is a major concern for scaling future MDM systems. In [105], a TDE requiring 400 taps was used for the equalization of a 6×6 transmission on a 3-mode fiber over 120 Km. In a recent work [106], Ryf et al. used a hybrid 20×20 FDE/TDE for the transmission on a 10-mode fiber. First a FDE with 1000 symbol-spaced taps operating with the data-aided least-mean-square (LMS) algorithm initially forced the convergence of the equalizer, then the constant-modulus algorithm (CMA) was used afterwards. In [107], the authors showed that training symbol based equalizers can be more appropriate for MDM systems compared to blind approaches. Moreover, OFDM was shown to have the lowest equalization computational complexity among all equalizers. For the next generation of high bit rate long-haul MDM optical transmission systems, CO-OFDM may be considered as an attractive competitor to the DP-QPSK single-carrier format.

4.1.1 Optical OFDM transmitter

OFDM modulation/demodulation can be implemented by using inverse Fast Fourier transform (IFFT)/ Fast Fourier transform (FFT). A block of N_{sc} modulated symbols $s = [s_1, ..., s_{N_{sc}}]^{\mathrm{T}}$ is converted to the time domain thanks to an IFFT to give the new symbol $x = [x_1, ..., x_{N_{sc}}]^{\mathrm{T}}$ which is transmitted during T_s. Each element x_k is modulated by a sub-carrier f_k and is given by:

$$x_k = \frac{1}{\sqrt{N_{sc}}} \sum_{j=1}^{N_{sc}} s_j . e^{i2\pi f_k \frac{jT_s}{N_{sc}}} \tag{4.1}$$

After creating the time domain OFDM symbol, a CP of length Δ_G is appended by repeating the last components of x to its beginning as shown in Fig. 4.1. The CP is placed as a guard interval between two OFDM symbols. The role of the CP is to maintain the orthogonality between frequencies and avoid inter-carrier interference (ICI), also the CP avoids ISI by absorbing all the dispersion effects of the channel. For PDM systems, the CP length must satisfy [108]:

$$\Delta_G \geq \frac{c}{f_0^2} . |D_{CD}| . N_{sc} . \Delta_{f_s} + DGD_{max} \tag{4.2}$$

where f_0 is the optical carrier frequency, c is the velocity of light, D_{CD} is the total accumulated chromatic dispersion, Δ_{f_s} is the spacing between two OFDM subcarriers, DGD_{max} is the maximum differential group delay of the fiber. In MDM systems, DGD_{max} is more importantly due to the delay spread from DMGD than the delay spread from PMD [107].

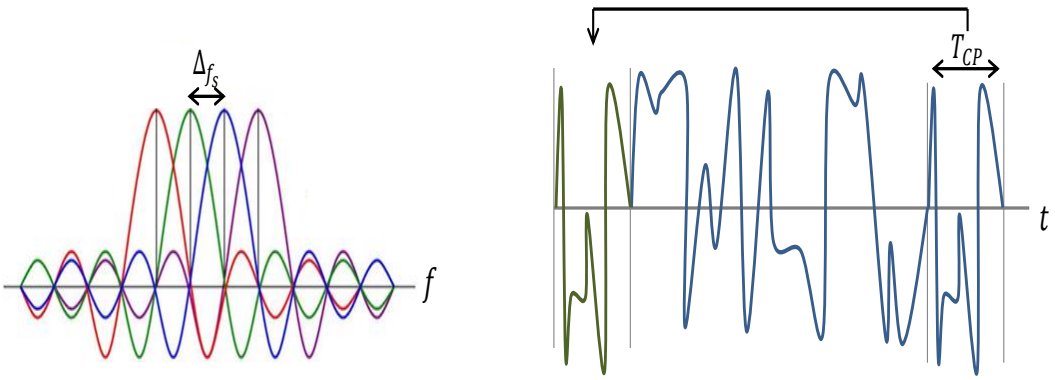

Figure 4.1: OFDM signal: On the left, the frequency-domain OFDM signal; on the right, a time-domain OFDM symbol with a cyclic prefix.

In OFDM modulation format, the N_{sc} subcarriers are not completely dedicated to modulate useful data symbols. Rather instead, a percentage of the subcarriers carry sequences that are used for synchronization, channel estimation and carrier phase recovery. All these operations are done at the receiver thanks to appropriate algorithms that will be discussed in the next section. In the design of the OFDM frame, it is very important to account for all these extra overheads to not reduce the system throughput.
Figure 4.2 shows a PDM OFDM transmitter where each OFDM block generates the signal of one polarization. The data symbols may be represented by a $2 \times N_{sc}$ matrix given by:

$$S = \begin{bmatrix} s_1^{(X)} & \cdots & s_{N_{sc}}^{(X)} \\ s_1^{(Y)} & \cdots & s_{N_{sc}}^{(Y)} \end{bmatrix} \tag{4.3}$$

where $s_i^{(X)}$ (resp. $s_i^{(Y)}$) is the data symbol transmitted by the i^{th} subcarrier on polarization X (resp. on polarization Y). After the IFFT block, a CP is inserted and digital signals are converted to analog ones thank to the DACs, then a low-pass filter is added to get rid of the aliasing replicas arising from the baseband OFDM spectrum. Finally, signals are converted to the optical domain using an IQ MZM modulator.

4.1.2 Optical OFDM receiver

CO-OFDM along with digital signal processing bring many advantages. First, phase estimation is realized in the digital domain without the need for optical phase-locked

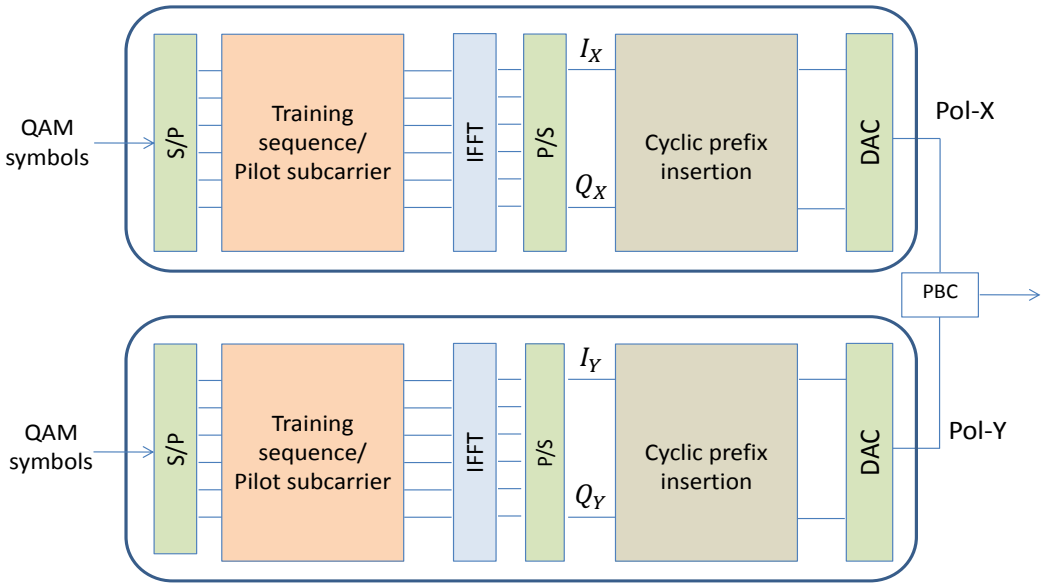

Figure 4.2: Pol-MuX OFDM transmitter

loop. Moreover, OFDM modulation and demodulation are realized by the well-established computation-efficient FFT and IFFT. Furthermore, adaptive data rates can be supported as different QAM constellations are software-defined, which do not require to change the hardware neither at the transmitter nor at the receiver.

Coherent detection enables the detection of the amplitude and phase of an optical signal thanks to a local oscillator (LO). In fact the incident signal is multiplied by the optical carrier from the LO and the product of the two signals is then detected. However, CO-OFDM systems are sensitives to frequency offset and laser phase noise. Hence, compensation of these perturbations is a must. At the CO-OFDM receiver, the two polarizations of the signal are first separated and projected into two orthogonal polarization states by a polarization beam splitter. After that signals are converted to the digital domain by ADCs. The processing of the received samples starts by the compensation for the frequency offset between the LO and the optical carrier. Then time synchronization is established in order to determine the beginning of the OFDM frame. Once the OFDM blocks are retrieved, the CP is removed and the original data symbols are extracted using an FFT. Since the CP maintains the subcarriers orthogonality and compensates for dispersion effects, a linear dependence between the received symbols y_k and the transmitted symbols s_k is preserved. The received symbols are given by:

$$y_k = e^{i\phi_0}.H_k.s_k + n_k \tag{4.4}$$

where H_k represents the frequency-domain channel matrix for the k^{th} subcarrier. The matrix H_k generally varies from one subcarrier to another because the chromatic dispersion and the PMD are frequency-dependent effects. However channel variations in optical communications are very slow and may be considered as constant for the duration of the OFDM frame. $e^{i\phi_0}$ is the phase mismatch between the LO and the signal . To compensate for this phase shift, some subcarrier frequencies also called pilot subcarriers are used. The phase shift estimation is done by averaging over all pilots, then the phase term is canceled and we obtain:

$$y_k = H_k.s_k + n_k \tag{4.5}$$

In order to have a more accurate estimation of the phase, all sources of phase noise must be taken into account in the design of the OFDM symbol. To minimize the random phase fluctuations, lasers at both transmitter and receiver with 100 kHz linewidth or lower are required. If the lasers linewidth is large, then phase estimation and correction is not correctly realized.

In order for CO-OFDM systems to be fully integrated in the next generation of MDM systems, the total bitrate should not be reduced. A longer OFDM symbol is obviously desirable as it reduces the overhead introduced by the CP. The overhead length is calculated as $\Delta_G/(N_{sc}+\Delta_G)$. However a longer OFDM symbol is less tolerant to the random fluctuations of phase noise [109]. In fact, as the OFDM symbol duration is longer, the phase has more time to change more randomly, thus phase estimation becomes impossible.

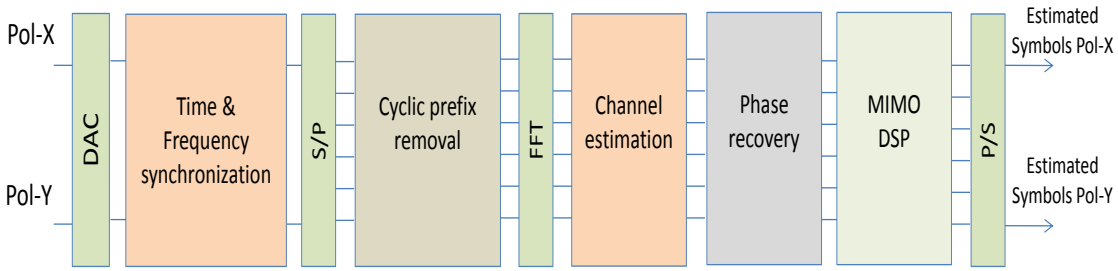

Figure 4.3: PDM OFDM receiver architecture

4.1.2.1 Time synchronization

In order for the DSP at the receiver to be properly done, an accurate temporal location of the beginning of the OFDM frame is necessary. This is the first processing operation done at the receiver and it is essential to avoid any loss of orthogonality between subcarriers which can cause ISI and ICI. Several algorithms allow time synchronization of the OFDM frame. The principle consists in adding special training symbols to the OFDM frame

that can be recognized by the synchronization algorithm at the receiver. For example, the training OFDM symbol can have identical halves in the time domain or it can be constructed by simply repeating N-times the same pattern. At the receiver, the synchronization symbols are detected using an autocorrelation operation over a sliding window followed by a search for the peak of the autocorrelation metric.
Schmidl and Cox proposed in[110] a well known synchronization algorithm in which two training symbols with identical halves are used for time synchronization. However, this algorithm does not detect a precise peak but a plateau instead.
It is also worth to mention that time synchronization algorithm can be also used for the carrier frequency offset (CFO) compensation.

4.1.2.2 Channel estimation

In order to estimate the channel matrix H_k training symbols $\mathcal{S}_k$ are used. Assuming that the matrix H_k is of dimension $M \times M$, then the training sequence must be sent on all M entries of H_k and during M time-slots at least in order to properly estimate all channel coefficients. In [21], a simple implementation of training sequence for PDM OFDM was proposed. The principle consists in sending a training symbol on X-polarization and a zero on Y-polarization and alternatively changing the process for polarizations on the next time-slot. For MDM systems, the generalization of this technique is straightforward and the training sequence matrix is given by:

$$\mathcal{S}_k = \begin{bmatrix} s_1^k(t_1) & 0 & 0 & 0 \\ 0 & s_2^k(t_2) & 0 & 0 \\ 0 & 0 & s_3^k(t_3) & 0 \\ \vdots & \vdots & \vdots & \vdots \\ 0 & 0 & 0 & s_M^k(t_M) \end{bmatrix} \tag{4.6}$$

where at each time-slot i only one symbol $s_i^k(t_i)$ is send on mode i and all other modes are excited with zeros. In order to estimate the channel matrix H_k several algorithms exist, the most popular one is the least square estimator (LSE) [21] that is very simple in real implementation. The estimated channel matrix is given by:

$$\hat{H}_k = Y_k \left(\mathcal{S}_k^\dagger \left(\mathcal{S}_k \mathcal{S}_k^\dagger \right)^{-1} \right) \tag{4.7}$$

To have a better estimation of the channel and to reduce the noise effect, several training matrices can be concatenated instead of using only one. Hence, The estimated channel is obtained by time averaging over all channel estimates.

4.2 Mode division multiplexed system with both polarizations

The first investigation of ST codes for MDM systems carried in our lab was done by Awwad et al. based on numerical simulations [96]. In this study, polarizations were discarded in order to only focus on spatial modes. This first analysis has proved the potential of ST coding in mitigating MDL, which allowed to initiate this thesis to push forward the investigations on this topic.

In real MDM transmission systems, spatial modes propagate with their two polarizations . Due to random birefringence in the fiber, both polarizations are subject to fluctuations during propagation and in the presence of polarization dependent loss (PDL) the orthogonality between polarizations is broken. Hence, before conducting our MDM transmission experiment, we were interested in proving the efficiency of ST codes in a MDM channel with both polarizations through numerical simulations. In this section, we propose a channel model of few-mode fibers supporting the propagation of modes and their polarizations. This model describes the physical propagation of the electrical fields through the fiber. Since polarizations are considered, then not only MDL will be taken into account but also PDL between polarizations of the same mode is also addressed.

4.2.1 Channel model

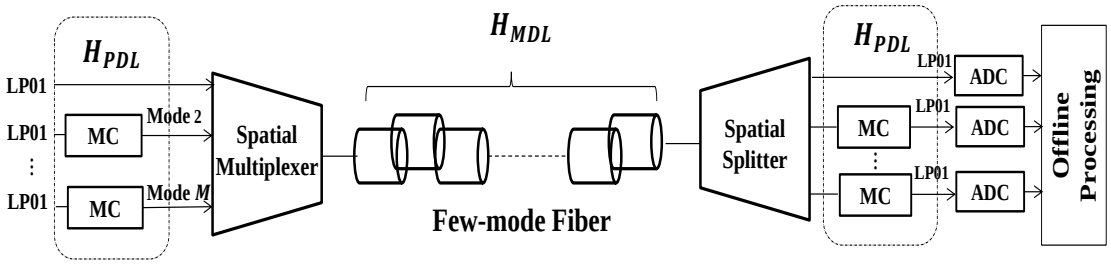

Figure 4.4: Mode division multiplexed transmission system based FMF. MC: mode converter, ADC: analog-to-digital converter.

The impact of MDL on MDM systems was reported in many studies [34, 44, 46], nevertheless, only the different attenuations affecting spatial modes were considered regardless of the effect of PDL on each mode. In [48, 53], the authors proved that one main source of PDL in MDM systems arises from spatial mode converters (MC) present in multiplexers and de-multiplexers (MUX DEMUX). The role of these devices is to convert optical signals from the fundamental mode LP_{01} in a SMF to one of the guided modes in the FMF as

detailed in subsection 1.4.4. However, these devices can add extra PDL to higher order modes resulting in OSNR difference between polarizations of spatial modes [35, 48].
In [111], the authors proposed a channel model for MDM systems supporting modes and polarizations. In this model, only unitary coupling was considered and non-unitary effects arising from PDL and MDL were discarded. In our work, we adopt the same channel model construction as in [111] and additionally we introduce the PDL and MDL effects. we consider a MDM system based FMF as shown in Fig 4.4 where M modes propagate with both polarizations on each mode. We neglect all dispersive effects since they do not reduce the system capacity and can be managed using OFDM format with suitable cyclic prefix. We consider that PDL is affecting higher order modes due to spatial MCs present before the multiplexer and after the spatial splitter, and MDL arises from propagation due to fiber misalignments. The resulting MIMO channel model is given by:

$$Y = H \cdot X + N = H_{PDL}.H_{MDL}.H_{PDL} \cdot X + N \tag{4.8}$$

where $X = [x_1, ..., x_{2M}]^{\mathtt{T}}$ (resp. $Y = [y_1, ..., y_{2M}]^{\mathtt{T}}$) is the emitted (resp. received) symbol vector. N is an additive white Gaussian noise vector of zero mean and spectral density $2\sigma^2$ per complex dimension. MDL is represented by a $2M \times 2M$ matrix that consists of a concatenation of K fiber sections and is given by:

$$H_{\mathrm{MDL}} = \prod_{k=1}^{K} T_k \cdot R_k \cdot C_k \tag{4.9}$$

H_{MDL} can be seen as a generalization of the channel matrix used in 2.12 where only one polarization was considered. T_k is a diagonal matrix that accounts for modal noise with random phase entries $\exp(i\phi_m)$ and $\phi_m \in [0 : 2\pi]$. R_k accounts for polarization coupling due to axis rotation at the intersection between sections k and $k+1$. C_k is a two-blocks diagonal matrix that represents the non-unitary modal coupling at a splice point. R_k and C_k are given by:

$$C_k = \begin{pmatrix} C_k^{(X)} & 0 \\ 0 & C_k^{(Y)} \end{pmatrix} \qquad R_k = \begin{pmatrix} \cos(\delta_k)\, I_M & -\sin(\delta_k)\, I_M \\ \sin(\delta_k)\, I_M & \cos(\delta_k)\, I_M \end{pmatrix} \tag{4.10}$$

where δ_k is the rotation angle between sections k and $k+1$ (I_M is the M square identity matrix). $C_k^{(X)}$ (resp. $C_k^{(Y)}$) is an $M \times M$ matrix that accounts for non-unitary coupling affecting the `X`-polarizations (resp. `Y`-polarizations) of the spatial modes. These matrices are computed with an overlap integral of the electric fields before and after a section k exactly as in 2.13.

Writing the singular value decomposition of H_{MDL} as $H_{\text{MDL}} = U.\Lambda.U^{\dagger}$, with U a random unitary matrix and $\Lambda = \text{diag}(\lambda_{min}, ..., \lambda_{max})$ a diagonal matrix, MDL is defined as the ratio in decibels (dB) of the maximum to the minimum of the singular values of H_{MDL}:

$$\text{MDL}(dB) = 20.\log_{10}(\frac{\lambda_{max}}{\lambda_{min}}) \tag{4.11}$$

Moreover, the PDL caused by a MC will result in a power imbalance between polarizations of the converted mode and a change in the angle orientation between its two polarizations. These two effects will be described by the matrix $H_{\text{PDL}} = R_\theta \cdot \Gamma \cdot R_\theta^{-1}$.

$$\Gamma = \begin{pmatrix} 1 & 0 & & \\ 0 & \sqrt{(1+\gamma)}I_{M-1} & 0_M & \\ & & 1 & 0 \\ & 0_M & 0 & \sqrt{(1-\gamma)}I_{M-1} \end{pmatrix} \qquad R_\theta = \begin{pmatrix} \cos(\theta)\, I_M & -\sin(\theta)\, I_M \\ \sin(\theta)\, I_M & \cos(\theta)\, I_M \end{pmatrix} \tag{4.12}$$

where R_θ is a rotation matrix that represents a random mismatch of axis between the polarization states of a spatial mode and the PDL component. The diagonal matrix Γ represents the power imbalance between polarizations of spatial modes. 0_M is the M square zeros matrix. In this representation, we have generalized the PDL matrix used for PDM systems given by Eq. 1.20 and we considered that the same PDL affects all polarizations. For a more realistic representation and based on the results in [48, 53], we assume that PDL does not affect the first mode in the absence of MC. PDL in dB is given by:

$$\text{PDL}(dB) = 10.\log_{10}\left(\frac{1+\gamma}{1-\gamma}\right) \tag{4.13}$$

The contribution of both PDL and MDL will result in a global loss given by the ratio in dB of the maximum to minimum of singular values of the channel matrix H, that we name Fiber-Dependent Loss (FDL) and is defined by:

$$\text{FDL}(dB) = 20.\log_{10}\left(\frac{\varphi_{max}}{\varphi_{min}}\right) \tag{4.14}$$

with $\{\varphi_{min}, ..., \varphi_{max}\}$ being the singular values of the global channel matrix H

4.2.2 Performance analyses of combined effects of PDL and MDL

4.2.2.1 Combined effect of PDL and MDL

In this section we analyze the contribution of both PDL and MDL on the global non-unitary effect that we named FDL. To have an insight on the impact of PDL and MDL on system performance we consider graded index FMFs supporting $M = \{3,\ 6\}$ modes with both polarizations, core radius are $r_c = \{6\mu m,\ 8.7\mu m\}$. The numerical aperture is

$NA = 0.205$, the wavelength is fixed to $\lambda = 1550\mu m$. $K = 300$ fiber sections are concatenated with random Gaussian misalignments Δx, Δy of zero mean and a standard deviation (std) $\sigma_{x,y}$.

In Fig. 4.5a, and Fig. 4.6a we plot the FDL as a function of misalignment std $\sigma_{x,y}$ for both fibers for different PDL values. We notice that FDL increases not only by the amount of MDL induced by fiber misalignments but also with an increasing PDL affecting polarizations of spatial modes. For the 3-mode fiber (Fig. 4.5a), for $\sigma_{x,y} = 2\%r_c$ and without PDL, FDL= 3.5 dB, but with PDL= 6dB, FDL increases to 10 dB.
In Fig. 4.5b and Fig. 4.6b we plot the BER as a function of SNR, we notice that for a fixed amount of MDL, the contribution of PDL degraded the performance for both fibers. At BER $= 10^{-3}$, a PDL of 4 dB induces 1.6 dB of SNR penalty for the 3-mode fiber and 2.2 dB of SNR penalty for the 6-mode fiber.
From this analysis, we can conclude that the global non-unitary effect given by FDL is approximately equal to the sum of both PDL and MDL.

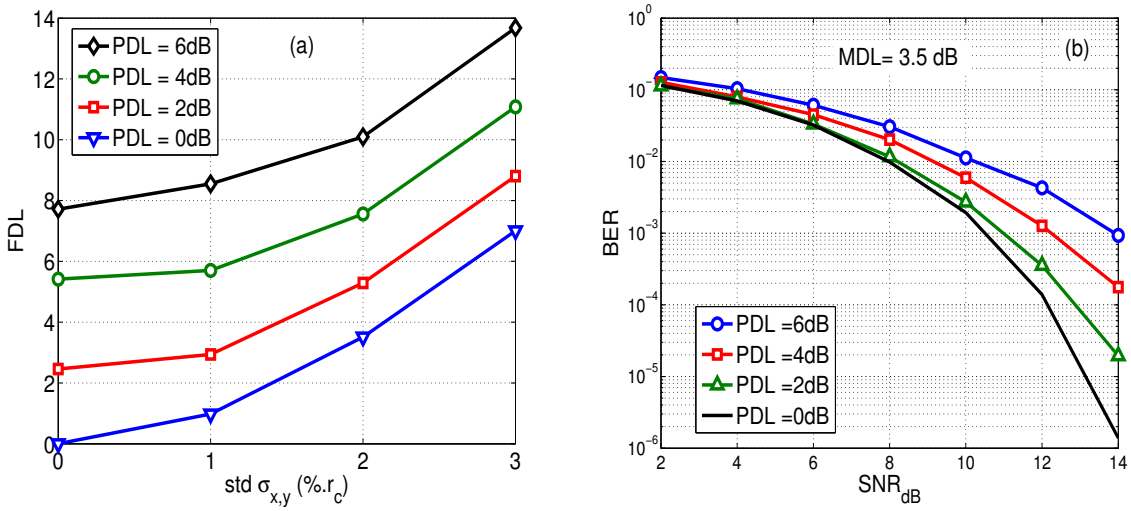

Figure 4.5: 3-mode fiber: (a) contribution of PDL and MDL to FDL, (b) BER vs SNR for different PDLs at MDL $= 3.5dB$

4.2.2.2 Effect of the orientation between axis of polarizations and PDL

For PDM systems based single mode fibers we have studied in section 1.3.5 the interaction between polarization rotation and the PDL element. In fact, the orientation angle θ between polarizations of the signal and the PDL element is a key factor that impacts the OSNR performance. When $\theta \equiv 0$ [90°] one polarization experiences the maximum loss while the other polarization is privileged. When $\theta \equiv 45°$ [90°], both polarizations observe

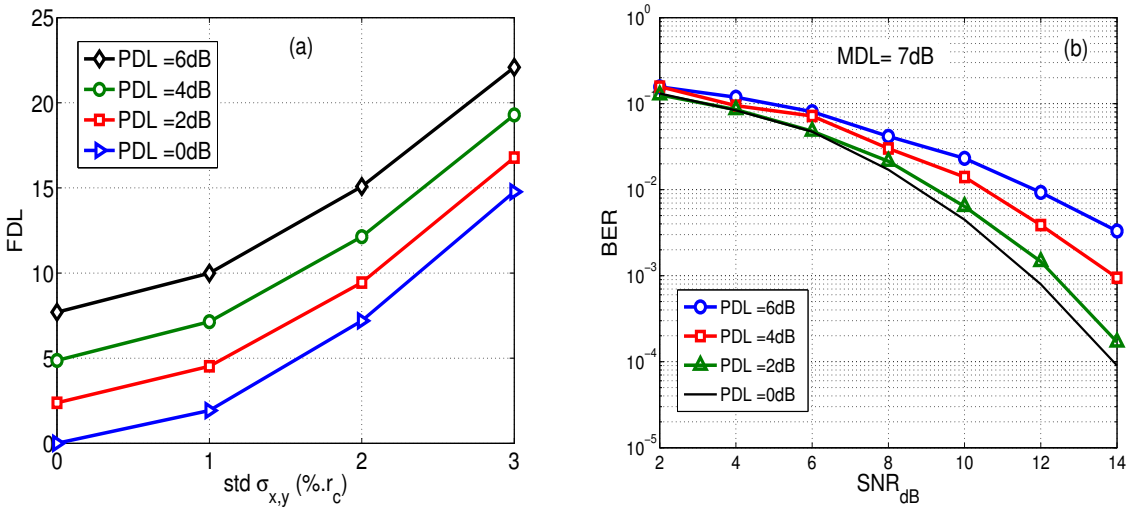

Figure 4.6: 6-mode fiber: (a) contribution of PDL and MDL to FDL, (b) BER vs SNR for different PDLs at MDL = $7dB$

the same attenuation but the loss of orthogonality between them is maximum [26].

In this subsection, we propose to study the impact of the orientation angle between PDL and polarizations of spatial modes for MDM systems. As a first step, we consider that MDL = 0dB ($H_{\text{MDL}} = I_{2M}$, with I_{2M} being the identity matrix) and only PDL is affecting polarizations of spatial modes. In Fig. 4.7a and 4.8a we plot the BER as a function of the angle θ for an SNR= 10 dB for both the 3- and 6-mode fibers. From the figures, we notice the same periodic behavior of the BER as for PDM systems, and the minimum BER is reached for $\theta \equiv 45°$ [90°].

However, when both PDL and MDL are considered, the previous behavior is no longer the same, and the interaction of both PDL and MDL affects differently the BER. From Fig. 4.7b, 4.7c and 4.8b, 4.8c we notice that the BER does not depend on the angle orientation between axis of polarizations and PDL. This is explained by the random unitary matrix U present in the SVD of H_{MDL} that changes the rotation matrix R_θ randomly This result shows that in the presence of MDL, PDL impacts the performance of MDM systems due to power imbalance between polarizations independently of the orientation angle θ.

4.2.3 ST coding for MDM systems with both polarizations

In this subsection, we investigate through numerical simulations the benefit of ST coding in mitigating MDL for MDM systems. We extend the results in [96] where only one polarization was considered to a MDM system where modes propagate with their both polarizations.

We consider a graded index 3-mode fiber of core radius are $r_c = 6\mu m$. The numerical

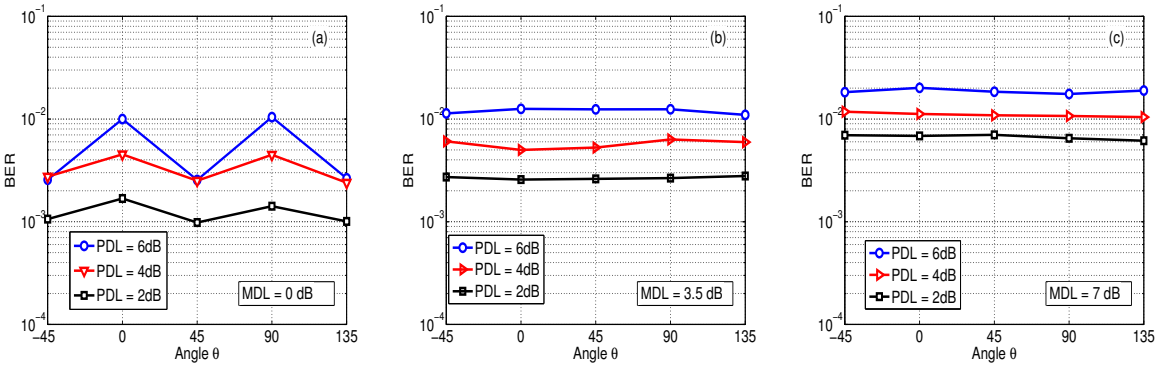

Figure 4.7: BER as a function of the angle θ at SNR= 10dB for a 3-mode fiber for different values of PDL and MDL

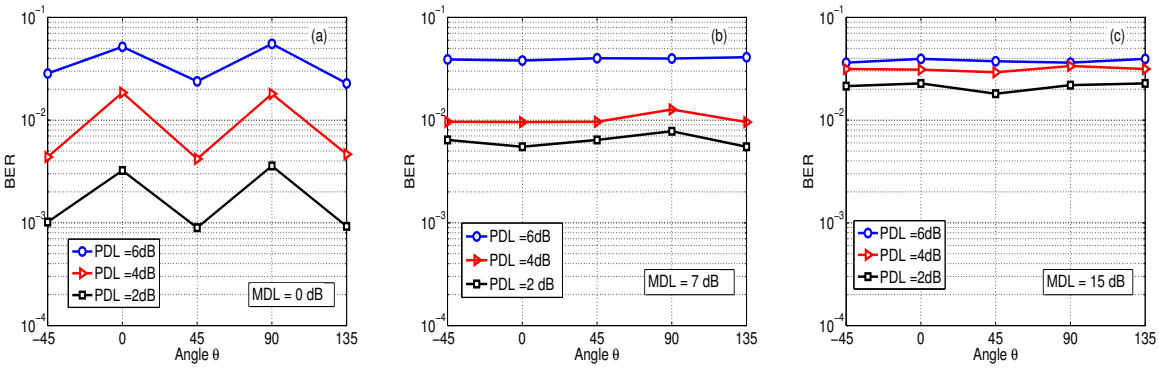

Figure 4.8: BER as a function of the angle θ at SNR= 10dB for a 6-mode fiber for different values of PDL and MDL

aperture is $NA = 0.205$, the wavelength is fixed to $\lambda = 1550\mu m$. $K = 300$ fiber sections are concatenated with random Gaussian misalignments Δx, Δy of zero mean and a standard deviation (std) $\sigma_{x,y}$. The transmission over a 3-mode fiber with both polarizations can be considered as a 6×6 MIMO system, hence an appropriate 6×6 full-rate TAST code is implemented. At the transmitter, QPSK symbols are used to construct a 6×6 codeword matrix $X_{6\times 6}$ given by:

$$X_{6\times 6} = \frac{1}{\sqrt{6}} \begin{bmatrix} f_1(\mathbf{s}_1) & \phi^{\frac{5}{6}} f_2(\mathbf{s}_6) & \phi^{\frac{4}{6}} f_3(\mathbf{s}_5) & \phi^{\frac{3}{6}} f_4(\mathbf{s}_4) & \phi^{\frac{2}{6}} f_5(\mathbf{s}_3) & \phi^{\frac{1}{6}} f_6(\mathbf{s}_2) \\ \phi^{\frac{1}{6}} f_1(\mathbf{s}_2) & f_2(\mathbf{s}_1) & \phi^{\frac{5}{6}} f_3(\mathbf{s}_6) & \phi^{\frac{4}{6}} f_4(\mathbf{s}_5) & \phi^{\frac{3}{6}} f_5(\mathbf{s}_4) & \phi^{\frac{2}{6}} f_6(\mathbf{s}_3) \\ \phi^{\frac{2}{6}} f_1(\mathbf{s}_3) & \phi^{\frac{1}{6}} f_2(\mathbf{s}_2) & f_3(\mathbf{s}_1) & \phi^{\frac{5}{6}} f_4(\mathbf{s}_6) & \phi^{\frac{4}{6}} f_5(\mathbf{s}_5) & \phi^{\frac{3}{6}} f_6(\mathbf{s}_4) \\ \phi^{\frac{3}{6}} f_1(\mathbf{s}_4) & \phi^{\frac{2}{6}} f_2(\mathbf{s}_3) & \phi^{\frac{1}{6}} f_3(\mathbf{s}_2) & f_4(\mathbf{s}_1) & \phi^{\frac{5}{6}} f_5(\mathbf{s}_6) & \phi^{\frac{4}{6}} f_6(\mathbf{s}_5) \\ \phi^{\frac{4}{6}} f_1(\mathbf{s}_5) & \phi^{\frac{3}{6}} f_2(\mathbf{s}_4) & \phi^{\frac{2}{6}} f_3(\mathbf{s}_3) & \phi^{\frac{1}{6}} f_4(\mathbf{s}_2) & f_5(\mathbf{s}_1) & \phi^{\frac{5}{6}} f_6(\mathbf{s}_6) \\ \phi^{\frac{5}{6}} f_1(\mathbf{s}_6) & \phi^{\frac{4}{6}} f_2(\mathbf{s}_5) & \phi^{\frac{3}{6}} f_3(\mathbf{s}_4) & \phi^{\frac{2}{6}} f_4(\mathbf{s}_3) & \phi^{\frac{1}{6}} f_5(\mathbf{s}_2) & f_6(\mathbf{s}_1) \end{bmatrix} \quad (4.15)$$

where $\phi = \exp(i\pi/12)$, $\mathbf{s}_{1:6}$ are vectors of 6 data symbols, $f_n(\mathbf{x}) = \sum_{k=1:6} x_k (j^{n-1}\theta)^{k-1}$

and $j = \exp(i2\pi/6)$, $\theta = \exp(i\pi/18)$. With this configuration, 36 symbols are sent on 6 time-slots in each codeword, achieving a full-rate of 6 symbols/cu.

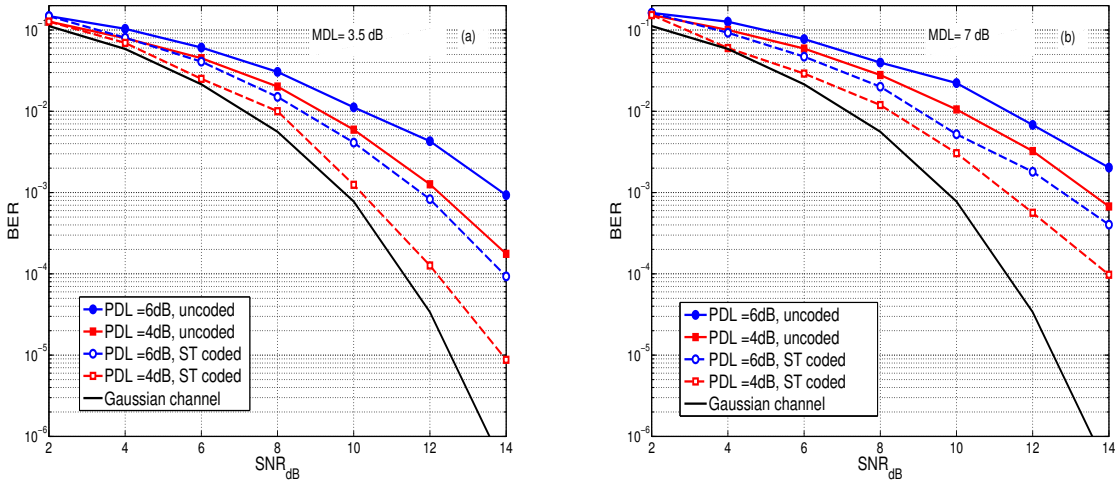

Figure 4.9: BER performance for uncoded an ST coded schemes for a 3-mode fiber for PDL = 4, 6 dB, (a) MDL = 3.5 dB (b) MDL = 7 dB

From Fig. 4.9a,b, we clearly notice that the ST coded transmission outperforms the uncoded scheme. At BER$= 10^{-3}$, for an MDL = 3.5 dB and a PDL = 4 dB, the ST coded scheme brings 2.2 dB gain comparing to the uncoded transmission. When MDL = 7 dB and PDL = 4 dB, the gain obtained by the ST code is 2.3 dB.

4.3 Experimental demonstration of ST coding for MDL mitigation

In this thesis work, we have presented three main contributions related to ST coding for mitigating MDL in MDM optical systems. First of all, we have explained theoretically the ST coding gains by deriving an error probability upper bound for ST coded MDM optical channel affected by MDL. Secondly, we have extended numerical simulations done by Awwad et al. [96] where only one polarization was considered to a MDM system where modes propagate with both polarizations. In our numerical simulations and the theoretical study, we have only focused on non-unitary effects and we have omitted all dispersive effects because we considered that it can be managed by OFDM. This simplification is very important in order to isolate and study MDL independently from all other effects. However in real MDM transmissions, considerable impairments mainly DMGD and modal coupling must be considered in the design of the system.

In this context, we have conducted an experimental study to prove the efficiency of ST

coding for MDL mitigation. In this experiment, modes propagate with both polarizations. To manage DMGD, a well designed OFDM format was implemented. OFDM along with a suitable cyclic prefix absorb dispersive effects and allow a very low complexity equalization [112]. In this section, we discuss our experimental study taking into account the interaction between all channel effects and we detail the DSP solutions to overcome all impairments.

4.3.1 Experimental setup

The experiment was conducted at the IRCICA laboratory in the frame of a collaboration between Télécom ParisTech and University of Lille 1. In a MDM transmission, each spatial mode requires one dual polarization coherent receiver and four-ports oscilloscope to detect the in-phase (real) and quadrature (imaginary) components of the complex transmitted constellations for each of the two polarizations. From the foregoing, realization of multi-mode experiments involving many spatial modes become very greedy in terms of very costly equipment. Having only two transmitters and two coherent receivers, the experimental demonstration consists in a 4×4 MIMO system based on the propagation of two spatial modes with both polarizations. MDL was emulated at the transmitter by adjusting different attenuations on modes.

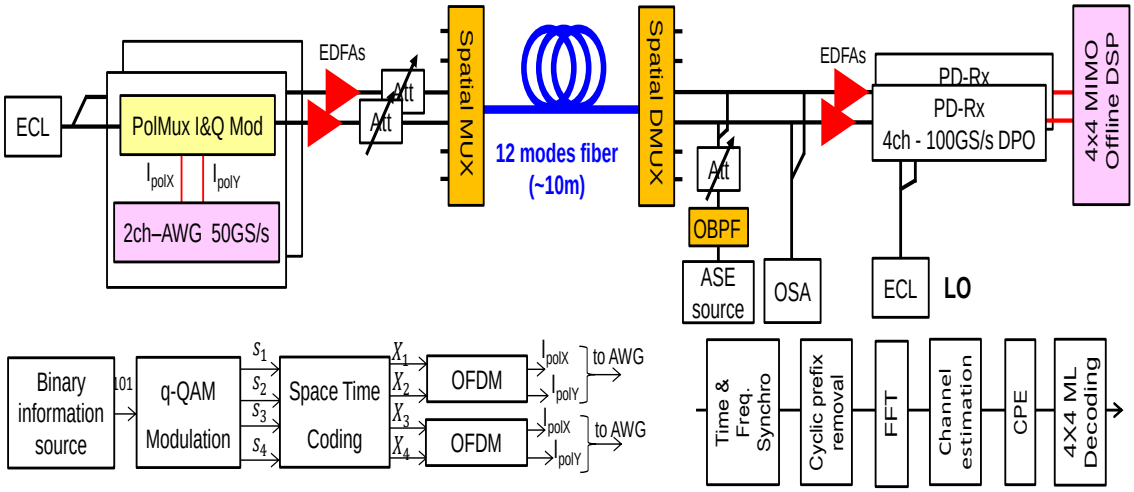

Figure 4.10: Mode division multiplexed transmission system. MC: mode converter, ADC: analog-to-digital converter.

4.3.2 Transmitter overview

Two PDM OFDM transmitters are used to send independent signals. As a light source, we use an external cavity laser (ECL) with ∼100 kHz linewidth operating at 1531 nm. To

reduce the sensitivity to the laser phase noise, the OFDM signal consists of 128 subcarriers including 90 QPSK modulated data subcarriers and 10 pilot subcarriers for common phase estimation (CPE). An 18-sample cyclic prefix is appended to each OFDM symbol to absorb the DMGD and avoid inter-symbol interference. A 22-symbols training sequence is inserted each 100 OFDM symbols for time synchronization, frequency offset compensation and channel estimation. Two 50 Gsamples/s Tektronix arbitrary waveform generators (AWGs) are used to create the OFDM symbols of polarizations `X` and `Y` whose spectra satisfy the Hermitian symmetry property so that the time domain signal is composed of real samples. This strategy does not affect our analysis knowing that the complex conjugate of the subcarriers are treated independently of the original subcarriers at the receiver. By this means, we use only four AWGs instead of eight to generate the complex dual-polarization signals. PDM signals have a 10 GHz bandwidth resulting in a 40 Gb/s raw bit rate.

For the uncoded transmission, we realize mode multiplexing by sending at each time-slot i a vector $S_i = [s_1^i, s_2^i, s_3^i, s_4^i]^{\mathrm{T}}$ of independent QPSK symbols on the two modes with both polarizations. For the ST coded transmission, we use a 4×4 full-rate TAST code. Instead of sending different symbols $\{s_1^i, s_2^i, s_3^i, s_4^i\}$ at each time-slot, we send different codeword matrices by blocks of 4 time-slots. The codeword matrix $X_{4\times4}$ is given by:

$$X_{4\times4} = \begin{bmatrix} f_1(S_1) & \phi^{\frac{3}{4}} f_2(S_4) & \phi^{\frac{2}{4}} f_3(S_3) & \phi^{\frac{1}{4}} f_4(S_2) \\ \phi^{\frac{1}{4}} f_1(S_2) & f_2(S_1) & \phi^{\frac{3}{4}} f_3(S_4) & \phi^{\frac{2}{4}} f_4(S_3) \\ \phi^{\frac{2}{4}} f_1(S_3) & \phi^{\frac{1}{4}} f_2(S_2) & f_3(S_1) & \phi^{\frac{3}{4}} f_4(S_4) \end{bmatrix} \tag{4.16}$$

where $f_n(S_i) = \sum_{k=1:4} s_k^i (j^{n-1}\theta)^{k-1}$ is a coded linear combination of the symbols $\{s_1^i, s_2^i, s_3^i, s_4^i\}$, $\phi = \exp(\frac{i\pi}{6})$, $\theta = \exp(\frac{i\pi}{8})$. In a recent work [113], Okonkwo showed that delay-diversity ST coding brings significant OSNR gains in a 3-mode transmission, but due to time-redundant transmitted symbols, the system capacity was reduced and at best achieves the SMF capacity. In our ST coded scheme, 16 different QPSK symbols are sent on 4 time-slots on each codeword matrix, achieving a full-rate of 4 symbols/time-slot. Furthermore, sending coded combination of symbols on both modes and polarizations makes ST coding suitable for mitigating also the PDL affecting different modes. However, having two PDM IQ modulators that deliver polarization multiplexed signals, we only emulate MDL by creating different attenuations between the two modes.

In Fig. 4.11, we show the OFDM signals transmitted on polarizations of each mode. Training symbols respect the architecture given by equation 4.6 where at each time-slot one training symbol is sent on each signal.

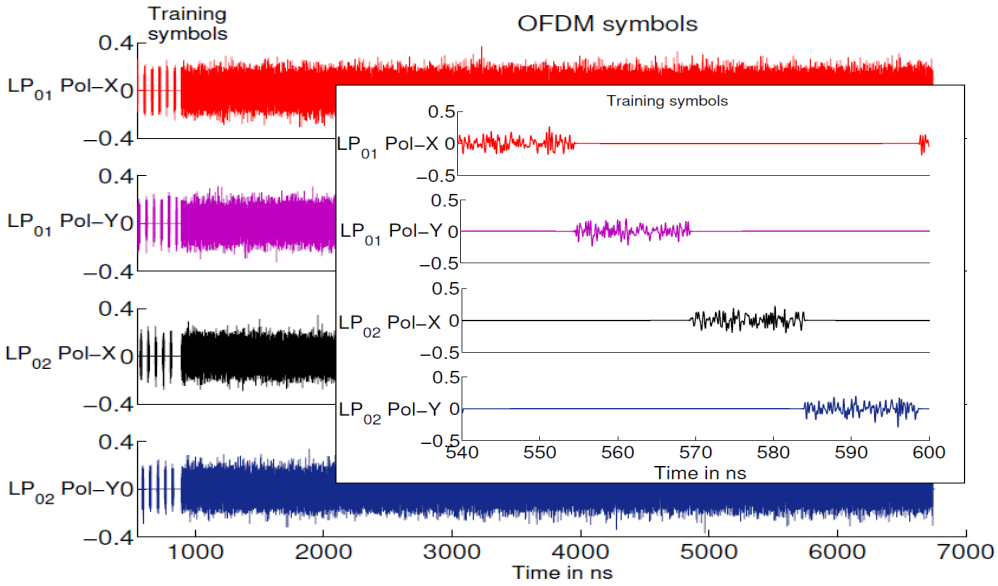

Figure 4.11: Transmitted OFDM signals showing training and data OFDM symbols

4.3.3 Optical link and receiver overview

The transmission-measurement setup is shown in Fig. 4.10. ∼10m of step index FMF that supports the propagation of 12 spatial modes is used. Two non-degenerate linearly polarized (LP) modes $\{LP_{01}, LP_{02}\}$ and five degenerate $\{LP_{11a,b}, LP_{21a,b}, LP_{31a,b}, LP_{12a,b}, LP_{41a,b}\}$. Effective index difference between any two LP modes is larger than 9×10^{-4} to minimize mode coupling, only degenerate modes within one LP mode are strongly coupled [114]. Such fiber presents large DMGD (∼14 ps/m between LP_{01} and LP_{02}). Therefore the LP_{01} and LP_{02} can be used as independent transmission channels. To inject signals from SMFs onto the spatial modes at the input end of the FMF and to extract signals from the spatial modes into SMFs at the output end of the FMF we use 10-modes MUX and DEMUX based on multi-plane light conversion[59]. To characterize the performance of the MUX/DEMUX and FMF, we measured the insertion loss (IL) and crosstalk (XT) between modes as in[59], results are averaged by group of degenerate modes and are reported in Table 4.1. The average IL (resp. average XT) was measured to be -6.8 dB (resp. -19 dB). Since we are limited with only two coherent receivers, we choose to use the LP_{01} and LP_{02} for multiplexing the data. This set of modes allows us to maintain a deterministic amount of MDL in the transmission, rather than the strongly coupled degenerated modes, where a statistical study with more channel acquisitions is required. To emulate MDL arising from few-mode amplifiers, two variable attenuators are inserted before the ∼10m of the

FMF to adjust the power imbalance between spatial modes. With this strategy we were able to emulate different levels of MDL.

Table 4.1: Insertion Loss (diagonal values), crosstalk (non diagonal values) for the MUX/DEMUX and FMF system.

Unit: dB	Output LP_{01}	Output $LP_{11a,b}$	Output $LP_{21a,b}$	Output LP_{02}	Output $LP_{12a,b}$	Output $LP_{31a,b}$
Input LP_{01}	-6.01	-16	-19	-17	-23	-30
Input $LP_{11a,b}$	-16	-6.80	-18	-22	-20	-22
Input $LP_{21a,b}$	-18	-19	-7.22	-15	-20	-20
Input LP_{02}	-17	-21	-17	-6.11	-19	-28
Input $LP_{12a,b}$	-23	-18	-19	-18	-7.96	-15
Input $LP_{31a,b}$	-25	-21	-18	-21	-14	-7.27

After additional noise loading at the receiver, signals are detected by polarization/phase diversity coherent receivers and then sampled at 100 GSamples/s using Tektronix oscilloscopes. For each value of MDL and OSNR, 5.10^6 samples are recorded and offline processing is carried to measure the BERs and the corresponding Q-factors.

First of all, Schmidl and Cox algorithm process the received OFDM signals shown in Fig. 4.12 for a time synchronization and compensate for the carrier frequency offset. Then the phase error correction is made by using the 10 pilot subcarriers. After that, the channel is estimated using the training sequence and the LSE estimator as explained in subsection 4.1.2.2. Finally, a maximum likelihood decoding is performed followed by a demodulation and error counting. In Fig. 4.12 we show the four receiver OFDM signals, from the figure, we clearly see the effect of polarization coupling resulting in mixing signals between polarizations of the same mode, however, there is no coupling between the two modes.

4.3.4 Experimental results

Before transmitting ST coded OFDM signals, we conduct preliminary measurements of the BER by transmitting uncoded independent QPSK symbols. We evaluate the performance for different MDL levels. In Fig. 4.13, we plot the BER performance as a function of the OSNR. From the figure, we can clearly notice the degradation caused by MDL on the system performance. At BER= 10^{-3}, when the MDL is 3 dB the degradation to the MDL-free channel is 2 dB and when the MDL level reaches 10 dB the degradation increases to 6 dB.

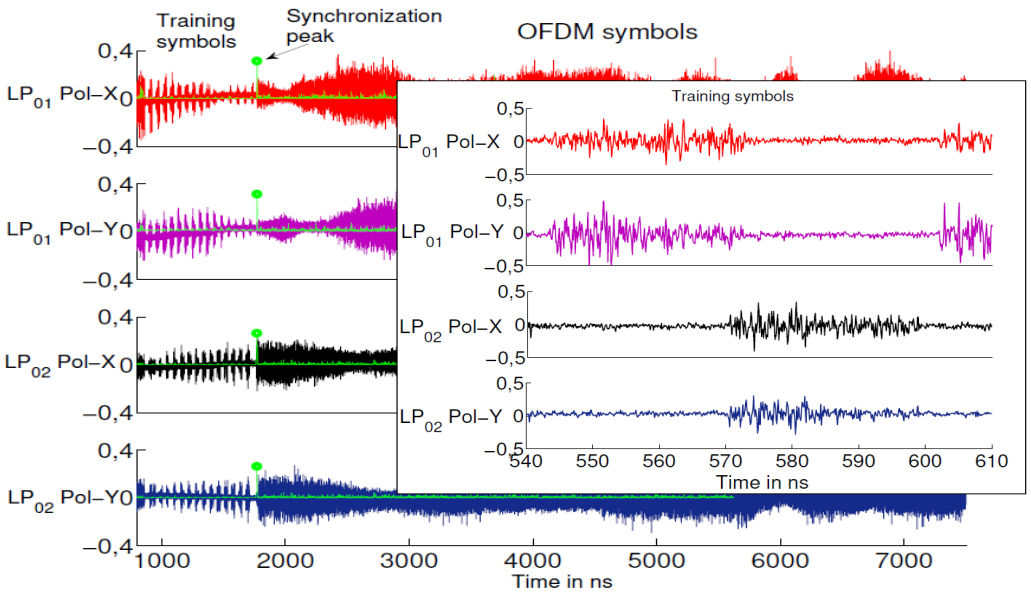

Figure 4.12: Received OFDM signals showing training symbols, synchronization peak and OFDM symbols

After these preliminary measurements, we proceed to a ST coded OFDM transmission. To show the obtained ST coding gains, in Fig. 4.14, we compare the performance of a ST coded system vs. an uncoded transmission. From the figure we notice an important gain obtained by ST coding comparing to the uncoded scheme. At BER$= 10^{-3}$, a 1.4 dB gain (resp. 2 dB) is observed for MDL = 6 dB (resp. MDL = 10 dB).

The gains brought by ST coding are explained by the fact that the same signal is transmitted on both modes that are affected by different attenuations. This allows the signal to experience different channel conditions. At the receiver, the ML detector estimates the data from different copies attenuated differently and hence gives a better estimate.

Furthermore, we have computed for an MDL ranging from 0 to 10 dB the Q-factor penalties obtained for the uncoded and ST coded schemes with regard to the MDL-free transmission at an OSNR of 14 dB. Results are reported in Fig. 4.15. From the figure, we notice that the ST coded transmission outperforms the uncoded transmission. The Q-penalty is reduced by 1.1 dB when MDL is 6 dB and by 3.4 dB when MDL is 10 dB.

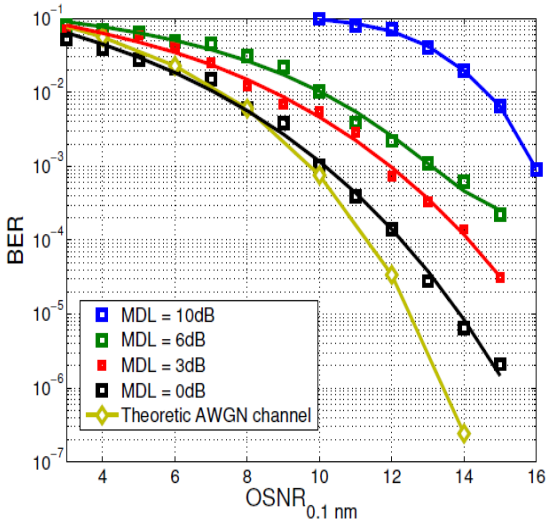

Figure 4.13: BER vs OSNR for different MDL levels for uncoded transmission

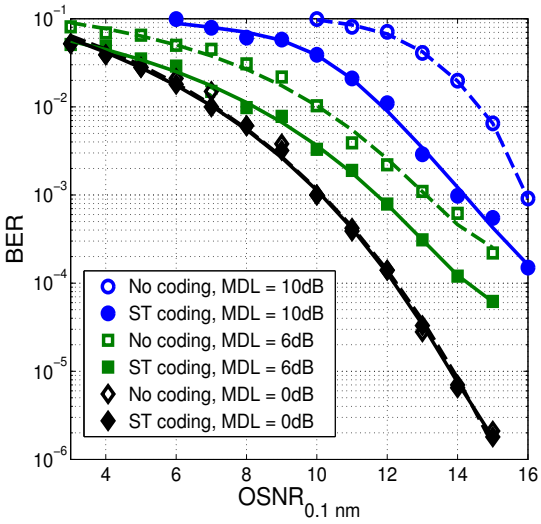

Figure 4.14: BER vs OSNR for ST coded and uncoded systems, MDL= 0, 6, 10 dB

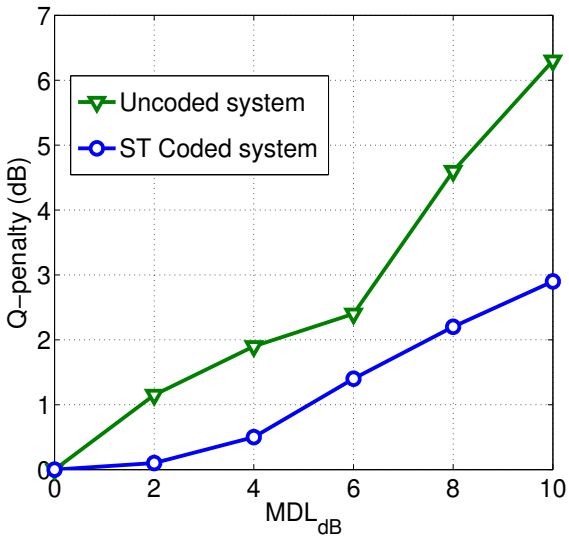

Figure 4.15: Q-penalty vs MDL at OSNR = 14 dB with regards to the MDL-free transmission

Summary

In this chapter we have demonstrated an experimental validation of the efficiency of ST coding in mitigating mode dependent loss in MDM transmission systems. Before diving into the experiment, first of all, we have built a channel model for the few-mode fiber where modes propagates with both polarizations. This channel model allowed us to study the effects of MDL and also PDL arising from MUX/DEMUX on the performance of the system. We showed that both impairments affect the global performance of the system. Moreover, we have validated the efficiency of ST coding in mitigating the non-unitary

effects arising from PDL and MDL by numerical simulations.
Lastly, an experimental transmission of two spatial modes with both polarizations was conducted. We have used a 4×4 full-rate TAST code and we showed that the ST coded transmission outperforms the uncoded transmission.

Conclusions & Perspectives

Conclusions

The continuous growth in the demand for more bandwidth will probably result in a major change in the optical network architecture and the introduction of new technologies to avoid a capacity crunch is becoming more urgent than ever. For the past decade, commercial coherent PDM systems operating at 100 Gb/s were sufficient to carry the data traffic in the optical network. However, with the exponential traffic growth generated by the built-out of the Internet and an increasing number of users and machines, the situation is about to change. Increasing spectral efficiency by higher order modulation formats and reducing the traditional channel spacing less than 50 GHz by techniques as Nyquist-WDM where the carrier bandwidth is rectangular and equal to the symbol rate have allowed to demonstrate systems operating at around 100 Tb/s. Furthermore, space division multiplexing is the last degree of freedom being intensively investigated in the optical fiber that will allow to go further beyond the Terabit capacity. In this thesis, we were interested in MDM based few-mode fibers as a possible realization of space division multiplexing. The best implementation of MDM is not yet an agreement point of all research labs. In fact, while some research teams consider that low coupling modes having high DMGD is very simple logistically, others propose strong coupling modes with low DMGD as an attractive solution with promising features. In both cases, MDL, a non-unitary effect, detrimentally impacts the capacity and quality of MDM optical transmission systems and DSP equalization techniques cannot mitigate. Consequently, to reduce the impact of MDL, the main contributions consist in improving the manufactured components to introduce low MDL. However, even with sophisticated optical components for MDM, accumulated MDL can reach important levels.

In this research work, we propose modern DSP coding techniques to improve the capacity and reliability of MDM systems. These DSP solutions can be complementary to the advancement in optical components to reduce MDL. Moreover, implemented DSP techniques can be scalable when the number of modes increases which make them a high potential

solution for the actual and future optical systems.
MDM allows to increase the optical system capacity by the number of modes. However, in the presence of MDL, this capacity is reduced and outage considerations need to be properly addressed. In this work, we have studied the average and outage capacities of MDM optical systems and we have proposed three techniques to improve them. First, we showed that channel state information (CSI) gives relevant knowledge about the optical channel and can be used at the transmitter to increase the capacity. Moreover, we have proposed a statistical CSI for capacity improvement with a reduced implementation complexity. Secondly, we have proposed a deterministic scrambling strategy to permute modes having more power with the ones having less. This scrambling strategy allows to reduce the effect of MDL by averaging power more efficiently between modes and hence increases the average and outage capacities. Lastly, we have shown that mode selection that consists in using large-core fibers instead of small-core fibers is a high potential solution to start deploying fibers supporting a high number of modes while achieving a better performance. For a further performance improvement, the three previous techniques can be combined to have a large MIMO infrastructure where only low-complexity MIMO schemes are used along with mode scrambling and CSI to increase the capacity.

Afterwards, we have investigated the benefits of ST coding to mitigate MDL in MDM optical systems. We have conducted a complete study, theoretical, by simulations and experimental to validate the efficiency of ST coding. We started by a derivation of the error probability upper bound of the MDM channel impaired by MDL. This upper bound allowed us to explain the coding gain obtained by ST coding and we could define a design criterion for ST codes construction to fully mitigate MDL. We showed that the orthogonality of codeword differences is the important parameter that allows to absorb MDL. Furthermore, we have studied the concatenation of ST coding and FEC and proved by a derivation of the error probability upper bound and verified by numerical simulations the coding gains summation.
After that, we have built a channel model for MDM systems where modes propagates with both polarizations. We showed that not only MDL but also PDL affecting higher order modes due to mode converters contributes to the global non-unitary effect that impacts the performance. Moreover, we proved by numerical simulations the efficiency of ST codes against these non-unitary effects.
Lastly, to complete our study, we validated the previous obtained results by conducting an experimental demonstration of ST coded MDM optical transmission. In this study, we have used OFDM format to manage the DMGD of the fiber and reduce the ML decoding

complexity. We have considered a 4×4 MIMO system by transmiting over two modes with both polarizations. The obtained experimental results show that ST coding brings significant BER improvement in the presence of MDL.

Perspectives

The previous conclusions pave the way to further research studies on MDM optical systems. Investigations of modern ST coding schemes to mitigate MDL can be extended as follows:

- Construction of space-time codes dedicated to mitigate MDL based on the orthogonality design criterion we have obtained. Orthogonal ST codes are rate deficient, however, the obtained criterion, only requires the orthogonality of codeword differences which makes less constraint on the construction. Moreover, we can conduct a theoretical study for polarization-multiplexed MDM systems where both PDL and MDL are taken into account. In this study, PDL and MDL can be in-line distributed, and a compact channel model that statistically describes these effects is needed.

- Investigation of the performance of ST coding in a long-haul transmission experiment taken into account the non-linear effects. Several amplification stages can be added to the line to introduce mode dependent gain. In this study, the interaction between modal coupling, MDL and non-linear effects must be taken into account in the design of an appropriate ST coded MIMO system.

- Extension of our study to few-mode MCFs (FM-MCFs) to fully exploit the spatial degree of freedom dof SDM systems. FM-MCF systems will provide unprecedented capacities that cannot be achieved by neither FMFs nor MCFs alone. Many new impairments must be taken into account for FM-MCF systems especially inter-core crosstalk (IC-XT) and inter-core DMGD (IC-DMGD). Design and manufacturing of a new generation of optical components that completely integrate with the actual deployed WDM systems is a must for a future deployment of FM-MCFs. Moreover, these dense systems will definitely require the design of new massive MIMO DSP to be able to operate. In our future research work, we look forward to implement a channel model for FM-MCFs to study the different unitary and non-unitary impairments. Afterwards, a low-complexity multi-block ST coding/decoding can be applied to modes and/or cores depending on the channel characteristics to enhance the performance.

Appendix A

Condensed French Version

Techniques de Codage pour le Multiplexage Spatial sur les Systèmes Fibres Optiques

A.1 Introduction générale

Selon le rapport Visual Indexation de Cisco [1], le trafic IP (Internet Protocol) mondial va presque tripler entre 2015 et 2020, ce qui correspond à un taux de croissance annuel de 22%. Cette croissance exponentielle est principalement due à l'expansion d'Internet, à l'énorme quantité du flux vidéo et aux technologies modernes telles que les services cloud et les réseaux sociaux. D'ici 2020, le nombre d'appareils connectés aux réseaux IP sera trois fois plus élevé que la population mondiale de la planète et le trafic généré par les smartphones dépassera le trafic des ordinateurs personnels. Le rapport indique que le trafic IP est plus important dans la région Asie-Pacifique et en Amérique du Nord puis en Europe. Le trafic IP au Moyen-Orient et en Afrique est le plus faible, mais il croît très rapidement avec un taux de 41% entre 2015 et 2020 (voir la figure E.1). Pour faire face à ce trafic croissant, les futurs réseaux optiques doivent également être développés pour fournir une infrastructure capable d'accueillir toutes ces exigences et d'éviter une pénurie de capacité.

A.1.1 Évolution de la capacité des réseaux optiques

La croissance continue de la capacité des systèmes optiques depuis 1970 a été possible grâce aux nombreuses dimensions physiques que la fibre optique peut offrir. Cinq dimensions physiques principalement connues sous le nom de degrés de liberté (DoF) ont permis de nouvelles stratégies de multiplexage et des formats de modulation, d'efficacité spectrale élevés, qui ont augmenté le débit. Ces DoF sont montrés dans la figure E.2.

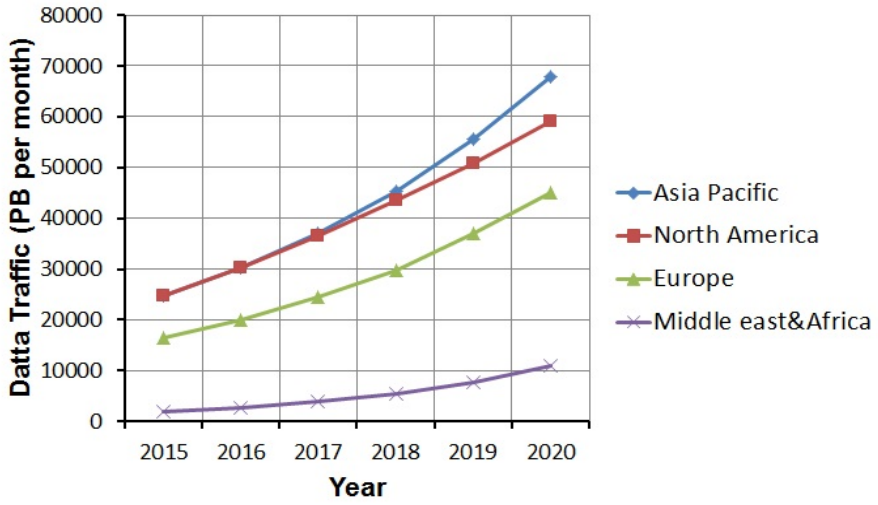

Figure E.1: Prévision de l'évolution du trafic IP pour différentes régions. Figure tracée en fonction des données fournies dans [1].

1. **Amplitude:** : Dans la première génération de systèmes optiques, seule l'amplitude des ondes électromagnétiques était utilisée. La modulation d'intensité (IM) ainsi que la détection directe (DD) ont permis d'atteindre une capacité de 10 Gb/s. Cependant, les systèmes IM/DD fonctionnant à 40 Gb/s n'ont pas été déployés massivement en raison d'une sensibilité considérable aux dégradations de propagation, principalement la dispersion chromatique (CD) et la dispersion en mode de polarisation (PMD). De plus, ces systèmes nécessitaient également des niveaux de rapport signal sur bruit optique (OSNR) élevés pour atteindre les mêmes distances que les systèmes à 10 Gb/s.

2. **Quadrature:** L'introduction de la détection cohérente a permis l'accès à l'amplitude et aussi à la phase du champ électromagnétique reçu. Ce dernier n'était plus un scalaire mais devenait un complexe avec des parties réelles et imaginaires. Par conséquent, la modulation On-Off keying (OOK) a été remplacée par des formats de modulation plus efficaces, tels que la modulation par déplacement de phase en quadrature (QPSK) et la modulation d'amplitude en quadrature (QAM). Plus tard, des modulations plus sophistiquées telles que la mise en forme probabiliste de la QAM [7] ont été proposées pour augmenter le débit du système.

3. • **Longueur d'onde:** La fibre optique fournit une bande passante énorme (près de 4 THz dans la bande C). Le fait d'utiliser différentes longueurs d'onde pour multiplexer les données tout en respectant un espacement entre deux longueurs d'onde adjacentes au moins égales au débit du symbole transmis est appelé multiplexage en

longueur d'onde (WDM). Cette technologie a permis d'augmenter considérablement la capacité des systèmes à fibres optiques en transportant des canaux indépendants.

4. **Polarization:** L'accès à ce degré de liberté a également été rendu possible grâce à la détection cohérente. En effet les deux polarisations orthogonales de l'onde électromagnétique peuvent transmettre des données différentes, donc la capacité est multipliée par deux dans les systèmes à multiplexage en polarisation (PDM). Dans les systèmes cohérents, la séparation de polarisation est effectuée par le traitement du signal à entrés et sorties multiples (MIMO) au niveau du récepteur.

5. **Espace:** La dimension spatiale est le dernier degré de liberté qui peut être utilisé pour augmenter la capacité des systèmes à fibres optiques. Le multiplexage spatiale (SDM) a pour but d'augmenter la capacité par le nombre de trajets spatiaux parallèles. Deux approches différentes de SDM sont possibles, que ce soit par des fibres multimodes ou des fibres multi-cœurs. Dans les deux cas, l'intégration de composants optiques et opto-électriques est indispensable pour maintenir un coût par bit réduit.

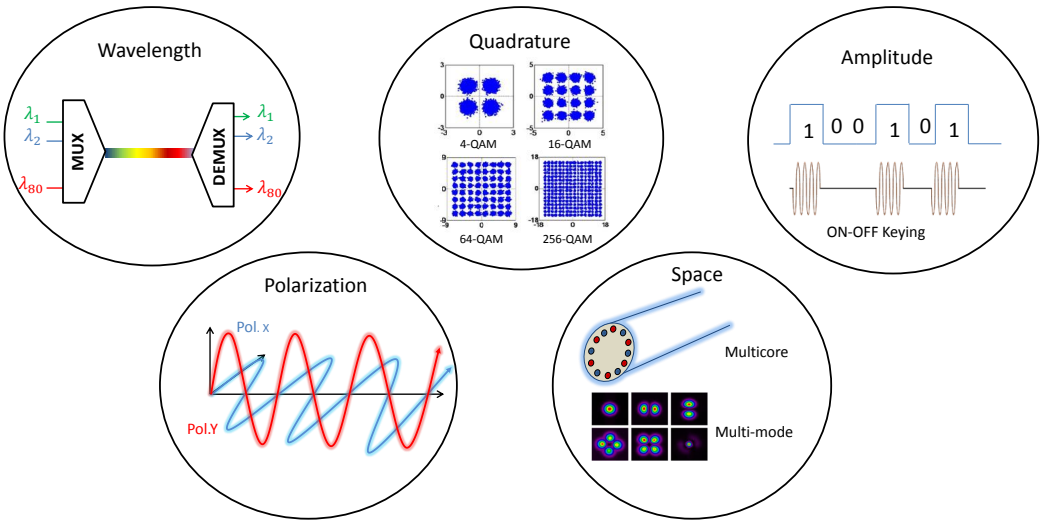

Figure E.2: Dimensions physiques pour la modulation et le multiplexage dans les systèmes de transmission optiques.

La capacité de transmission des réseaux de fibres optiques a considérablement progressé depuis le début des années 1970. La première génération de systèmes optiques avait des pertes de l'ordre de ~ 3 dB/km et les lasers de transmission fonctionnaient à une longueur d'onde de 0.8 μm. Cependant, la limitation du produit distance $\times$ débit binaire due à la dispersion intermodale [4] était à l'origine de la migration vers les fibres monomodes à la longueur d'onde de 1.3 μm. Par la suite, une longueur d'onde de 1.55 μm a été adoptée

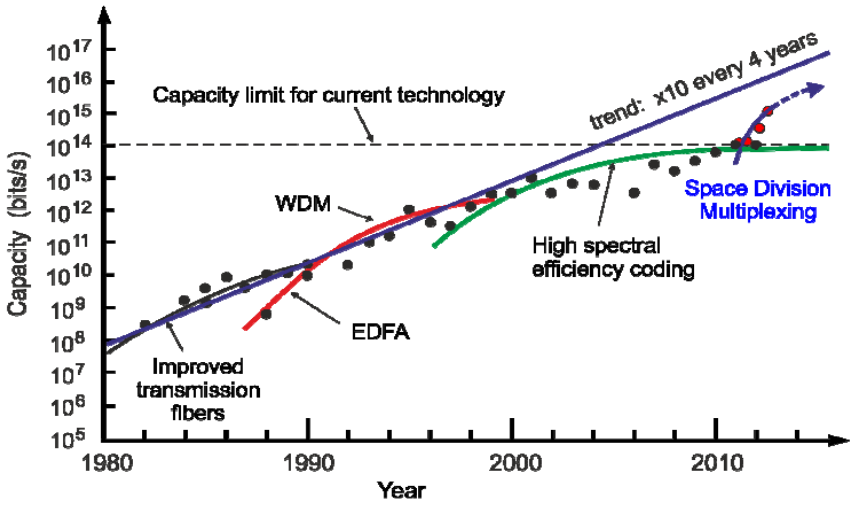

Figure E.3: L'évolution de la capacité des systèmes de transmission par fibre optique au fil des années. Figure tirée de [2].

pour minimiser l'atténuation des fibres. En outre, l'avancée technologique des dispositifs électroniques à grande vitesse a permis la fabrication de modulateurs optiques externes qui ont permis d'atteindre un débit de 10 Gb/s [8].

Alors que la période entre 1970 et 1990 a connu un développement technologique constant et une augmentation modérée du débit, à partir des années 1990, les systèmes optiques ont connu une augmentation spectaculaire de la capacité principalement apportée par le multiplexage en longueur d'onde et l'amplification optique [9] ce qui a permit de passer de quelques Gigabits par seconde à des Térabits par seconde (voir la figure E.3). Les premiers systèmes WDM ont été introduits en 1995 [10], ils avaient entre quatre et huit canaux séparés par 200 GHz et modulés à 2.5 Gb/s, ce qui permettait une capacité maximale de 20 Gb/s. En 2000, les systèmes WDM denses (DWDM) comprimaient plus de 80 canaux séparés de seulement 50 GHz et modulés à 10 Gb/s, ce qui a permit d'atteindre près de 1 Tb/s [10]. Au début de 2010, des systèmes commerciaux fonctionnant à 100 Gb/s par longueur d'onde étaient disponibles. Pour atteindre cette capacité, le multiplexage par polarisation a été intégré. En effet, la détection cohérente permet d'accéder aux deux polarisations orthogonales du champ électromagnétique ce qui permettait de les utiliser pour multiplexer différentes données et augmenter la capacité d'un facteur de 2.

Comme le spectre disponible était presque rempli, la recherche dans le domaine des systèmes optiques s'est concentrait sur des formats de modulation à efficacité spectrale (SE) plus élevée afin d'augmenter la capacité. Récemment, un enregistrement de capacité de 101 Tb/s a été réalisé dans une expérience laboratoire [11]. La SE qui a permis cette énorme capacité était de 11 b/s/Hz. Cependant, le rapport OSNR élevé requis par

l'utilisation de la modulation 128-QAM et la sensibilité aux effets non-linéaires ont limité la distance de transmission à seulement 3×55 km.

Comme nous l'avons vu précédemment, le développement rapide des réseaux optiques et les multiples technologies introduites au cours de la dernière décennie ont permis d'avoir une capacité qui a toujours dépassé le trafic croissant. Cependant, cette situation est sur le point de changer et le besoin de capacités supplémentaires est plus urgent que jamais. A cet effet, des recherches intensives ont été menées ces dernières années sur le multiplexage spatial (SDM) en tant que dernier degré de liberté encore inutilisé afin d'augmenter la capacité des fibres optiques [12].

Afin de réduire le coût et l'énergie par bit transmit, les futurs systèmes optiques SDM devront réutiliser l'infrastructure WDM existante. De plus, l'intégration de composants optiques tels que les transpondeurs, amplificateurs, add-drop multiplexeurs (ROADMs), fournira une nouvelle génération de dispositifs capables d'adresser plusieurs chemins spatiaux [13]. De plus, les systèmes optiques SDM nécessitent le développement de nouvelles fibres supportant la propagation de multiples trajets spatiaux, multiplexeurs spatiaux (MUX) et démultiplexeurs (DEMUX), amplificateurs optiques capables d'amplifier simultanément tous les trajets spatiaux. Actuellement, deux catégories de fibres optiques permettent la réalisation des systèmes SDM: Les fibres faiblement multimodes (Few-mode fibers: FMF) et les fibres multi-cœurs (Multicore fibers: MCF). Dans les deux cas, le couplage entre les trajets spatiaux est inévitable et la conception de fibres qui minimisent la diaphonie est importante. Pour les MCF, la conception de nouvelles fibres avec une grande séparation entre les cœurs peut réduire la diaphonie mais cette solution limite la densité spatiale des cœurs [12]. Dans un travail récent [14], les auteurs ont démontré qu'une fibre à 4 cœurs avec de grandes surfaces effectives présente une meilleure tolérance aux non-linéarités et fournit un facteur Q (Q-Factor) de 0.7 dB plus élevé qu'une fibre monomode ayant les mêmes propriétés de base. Pour les FMF, la conception de fibres supportant la propagation de modes ayant des constantes de propagation différentes est susceptible de réduire la diaphonie. Dans tous les cas, pour les MCF et les FMF, une diaphonie résiduelle subsistera, ce qui rend les techniques MIMO importantes pour que ces futurs systèmes pour séparer les trajectoires spatiales.

Lorsque le SDM est réalisé par les FMF, cette technique de multiplexage s'appelle multiplexage modale (Mode Division multiplexing MDM). Le MDM consiste à moduler chaque mode avec des données indépendantes, d'où la capacité du lien optique est augmentée par le nombre de modes. Dans les systèmes réels, la propagation à travers les FMF est également affectée par des dégradations nécessitant une compensation optique ou par traitement numérique du signal (digital signal processing: DSP). En plus des dégradations

physiques telles que la dispersion chromatique ou la dispersion en mode de polarisation également présentes dans les systèmes fibres optiques monomodes, les modes dans les FMF subissent des effets supplémentaires provoqués par la propagation simultanée de modes dans la même fibre. D'abord, les modes se propagent à des vitesses différentes, ce qui provoque un retard de groupe différentiel (Differential mode group delay: DMGD) qui doit être pris en compte dans la conception de la ligne. De plus, les modes sont également soumis à un couplage linéaire unitaire qui peut être compensé par un DSP approprié au niveau du récepteur. Le couplage modal peut également être non-unitaire, causant des pertes différents d'un mode à l'autre (Mode dependent loss: MDL), ce qui induit la réduction de la capacité et la limitation des performances des systèmes MDM. La MDL peut être soit distribué à travers la fibre (due aux imperfections de fabrication telles que des épissures ou des micro-courbures) ou local à l'insertion de composants optiques (tels que les amplificateurs ou multiplexeurs.

A.1.2 Motivations et contributions de la thèse

Dans cette thèse, nous présentons des techniques modernes de traitement numérique du signal pour combattre la MDL dans les FMF. Dans [6], les auteurs ont montré pour la première fois que le codage spatio-temporel (ST) conçu à l'origine pour les communications sans fil était très efficace pour atténuer la MDL dans les systèmes FMF. Des simulations numériques ont été effectuées sur des fibres à trois et six modes et des gains de codage ont été observés pour différents taux de couplage modal. Ces résultats intéressants ont initier ce projet de thèse pour approfondir l'étude de la capacité des systèmes FMF et d'étendre le travail sur les solutions de codage ST modernes pour compenser la MDL.

Cette thèse a débuté en octobre 2014 et a été menée au sein du laboratoire LTCI (Laboratoire de Traitement et de Communication de l'Information) de Télécom ParisTech. La première motivation de ce travail est d'étudier l'impact de la MDL sur la capacité des FMF. Les capacités moyennes et de coupures ont été analysées pour définir les capacités limites des systèmes FMF en présence de la MDL. Nous avons également proposé de nouvelles solutions optiques et DSP pour augmenter la capacité de ces systèmes.

Par la suite, nous avons analysé le codage ST pour les FMF de manière analytique en dérivant une borne supérieure pour la probabilité d'erreur. Cette analyse théorique a permis de comprendre le comportement du codage ST appliqué au canal optique. A partir de la borne supérieur trouvé, nous avons défini un critère de construction des codes ST spécifiques au canal FMF affecté par la MDL. De plus, pour améliorer les performances du codage, nous avons ajouté un code correcteur d'erreur (FEC) à notre système. Nous

avons observé une sommation des gains de codage apportés par les codes ST et FEC et expliqué ce comportement aussi par un calcul théorique.

Enfin, Nous avons conclu notre travail par une validation expérimentale du codage ST contre l'effet de la MDL pour les systèmes FMF. Cette expérience a nécessité un nombre considérable d'équipements et a été réalisée en collaboration avec le laboratoire IRCICA de l'Université de Lille. Nous avons montré pour la première fois expérimentalement l'efficacité des codes ST à combattre l'effet de la MDL dans une transmission à deux modes avec les deux polarisations.

A.2 Augmentation de la capacité des systèmes de transmission optiques à multiplexage modal

Dans cette section, nous nous intéressant à l'étude de la capacité des systèmes FMF affecté par la MDL. Après avoir présenté le modèle du canal optique, nous étudions les capacités moyennes et de coupures. Ensuite nous examinons l'apport de la connaissance du canal (Channel state information : CSI) à l'émetteur sur la capacité et nous proposons une connaissance moyenne du canal pour améliorer les performances. Dans la seconde partie, nous étudions la permutation de modes et son impact sur la capacité, nous proposons également une stratégie optimale pour permuter les modes. Enfin, nous présentons la sélection de mode comme une stratégie qui permet de déployer des fibres multimodes supportant la propagation d'un grand nombre de modes tout en utilisant seulement les modes les moins affectés par la MDL.

A.2.1 Modèle canal des systèmes optiques à multiplexage modal

Dans notre travail, nous considérons la MDL distribuée provenant des épissures et des micro courbures. Nous considérons les FMFs à gradient d'indice (GI-FMF) avec un rayon de coeur r_c et une ouverture numérique $NA = \sqrt{n_c^2 - n_{cl}^2} = 0.205$, avec n_c (respectivement n_{cl}) est l'indice de réfraction du coeur de la fibre (resp. de la gaine), la longueur d'onde est réglée sur $\lambda = 1.55\mu m$. Pour se concentrer sur l'impact de la MDL sur la capacité du système, une seule polarisation est considérée. Le choix des fibres GI-FMF plutôt que des fibres à saut d'indice a pour but de minimiser la DMGD entre les modes. Le nombre de modes se propageant dépend du rayon du cœur r_c, la longueur d'onde λ et l'ouverture numérique NA. Dans notre travail, nous fixons λ et NA et nous augmentons r_c pour permettre la propagation de plusieurs modes. Dans le tableau A.1, nous présentons les paramètres de nos GI-FMF utilisés. Le mode fondamental LP_{01} est toujours autorisé à se propager. Pour un rayon de coeur de $r_c = 6\ \mu m$, les deux modes dégénérés LP_{11a} et

LP_{11b} se propagent. Une augmentation du rayon du coeur à $r_c = 8.6\ \mu m$ donne lieu à trois autres modes qui sont les $LP_{21,a}$, $LP_{21,b}$ et le LP_{02}. Pour atteindre dix modes, le rayon du coeur est fixé à $r_c = 11\ \mu m$.

Table A.1: Paramètres des GI-FMFs pour 3, 6 et 10 modes avec $\lambda = 1.55\ \mu m$ et $NA = 0.205$

Nombre de modes	Rayon du coeur	Modes
3	6 μm	$LP_{01},\ LP_{11a,b}$
6	8.7 μm	$LP_{01},\ LP_{11a,b},\ LP_{21a,b},\ LP_{02}$
10	11 μm	$LP_{01},\ LP_{11a,b},\ LP_{21a,b},\ LP_{02},\ LP_{12a,b},\ LP_{31a,b}$

On considérant l'approximation d'un faible guidage dans les GI-FMFs donnée par $(n_c - n_{cl})/n_c \ll 1$, on peut exprimer la distribution du champs transverse des modes de propagation linéaires (Linearly-polarized: LP) par les polynômes de Laguerre-Gauss [68]:

$$E_{l,q}(r,\phi) = C_{l,q}\left(\frac{r}{w}\right)^{l} L_q^{(l)}\left(\frac{r^2}{w^2}\right)\exp\left(\frac{-r^2}{2w^2}\right)\begin{Bmatrix}\sin(l\phi)\\ \cos(l\phi)\end{Bmatrix} \tag{A.1}$$

L'équation précédente est donnée en coordonnées polaires r et ϕ. l. l est l'ordre ordre circonférentiel et q est l'ordre radial du mode LP_{lq}. $L_q^{(l)}(x)$ est le polynôme de Laguerre généralisé d'ordre l e de degré q et $w = \sqrt{r_c/(k_0.NA)}$ est la taille du point du mode fondamental LP_{01} avec $k_0 = 2\pi/\lambda$ représente le nombre de guidage en espace libre. $C_{l,q}$ est un facteur de normalisation pour satisfaire l'orthogonalité entre les modes tel que $\iint_A E_i.E_j dA = \delta_{i,j}$.

Dans notre analyse de la capacité, nous considérons une description physique de la propagation dans les fibres GI-FMF avec un couplage de mode non-unitaire réaliste généré par les épissures de fibres et des connecteurs. Cette modélisation est basée sur les distributions du champ électrique des modes spatiaux décrits précédemment plutôt que sur une modélisation mathématique basée sur des matrices aléatoires comme dans [34, 44]. Dans notre travail, nous ne considérons pas les effets non-linéaires, le canal MIMO linéaire résultant est donnée par:

$$Y_{M\times 1} = H_{M\times M}.X_{M\times 1} + N_{M\times 1} = \sqrt{L}\prod_{k=1}^{K}(T_k C_k)\,X_{M\times 1} + N_{M\times 1} \tag{A.2}$$

$X_{M\times 1}$ (resp. $Y_{M\times 1}$) est Le vecteur des symboles transmis (resp. reçus), $N_{M\times 1}$ est un vecteur de bruit additive blanc Gaussien de moyenne nulle et variance $2\sigma^2$ par mode.
La matrice $H_{M\times M}$ représente la FMF composé de K sections. T_k est une matrice diagonale avec des phases aléatoires $\exp(i\phi_m)$ et $\phi_m \in [0, 2\pi]$. Un couplage modal non-unitaire dû à des désalignements de fibres au point d'épissure est donné par une matrice de couplage

C_k, dont les entrées sont calculées en utilisant une intégrale de chevauchement des champs électriques des modes spatiaux aux sections de fibres comme dans [46]. L'effet cumulé de tous les désalignements se traduit par une MDL de bout en bout définie comme le rapport en décibels (dB) des valeurs propres maximum à minimum de $HH^{\dagger}$.

$$\mathrm{MDL}(dB) = 10.\log_{10}\left(\frac{\lambda_{max}}{\lambda_{min}}\right) \tag{A.3}$$

Dans nos simulations, nous considérons des fibres constitués de $K = 300$ concaténation de sections de fibres. Pour émuler différents niveaux de MDL, nous varions $\sigma_{x,y}$ en pourcentage du rayon du coeur de la fibre r_c.

A.2.2 Capacité des systèmes MDM affectés par la MDL

Un système MDM idéal multiplie la capacité disponible d'un lien donné par le nombre de modes M, dans ce cas tous les modes ont la même atténuation. A cause de la MDL, cette capacité est réduite et pour des niveaux élevés de MDL, la fibre supporte la propagation d'un seul mode spatial [44]. Cependant, la capacité des canaux des systèmes MDM affectés par la MDL peut être améliorée avec la disponibilité du CSI à l'émetteur.

Absence du CSI à l'émetteur : Dans le cas ou le CSI n'est pas disponible à l'émetteur, tous les modes spatiaux sont transmit avec la même puissance initiale [66, 67]. Dans ce cas la capacité est donnée par:

$$C_{ep} = \sum_{i=1}^{M} \log(1 + \frac{\rho_t}{M} \cdot \frac{\lambda_i}{2\sigma^2}) \tag{A.4}$$

avec $(\lambda_1, ..., \lambda_M)$ sont les valeurs propres de $HH^{\dagger}$ et $\sum_{i=1}^{M} \lambda_i = M$. Dans ce cas, chaque mode se voit attribué la puissance $P_i = \frac{\rho_t}{M}$. De plus, ceci une capacité linéaire qui augmente avec le SNR, si les non-linéarités sont prises en compte alors la capacité diminue après avoir atteindre son maximum à un niveau de puissance donné [69].

Présence du CSI à l'émetteur : Lorsque le CSI est disponible à l'émetteur, ce dernier envoie des symboles corrélés de puissances différentes sur chaque mode pour augmenter la capacité. Ceci est réalisé à travers un traitement MIMO à la réception. En effet, le récepteur estime le canal et calcul sa décomposition en valeur propre (SVD) $H = U\Lambda V^{\dagger}$, avec $\Lambda = \mathrm{diag}(\sqrt{\lambda_1}, ..., \sqrt{\lambda_M})$ et U, V sont des matrices unitaires, après cela, le récepteur envoie V et Λ à l'émetteur. La matrice diagonale Λ sera utilisé pour calculer les puissances optimales par mode et la matrice V servira à envoyer un vecteur de symboles corrélés. La

capacité en présence du CSI sera donné par C_{CSI}:

$$C_{CSI} = \sum_{i=1}^{N} \log(1 + p_i^* . \frac{\lambda_i}{2\sigma^2}) \tag{A.5}$$

Avec p_i^* la puissance optimale attribué au mode i. L'allocation de puissance avec le CSI est confronté à deux limitations majeurs pour une réelle implémentation. Premièrement, le CSI doit provenir à l'émetteur avant que le canal optique change. Deuxièmement, les puissance optimales doivent êtres mises à jour à chaque fois que le canal change. La satisfaction de ces deux contraintes pour les réseaux optique FMF est impossible pour le moment. Dans la partie suivante, nous proposons un CSI statistique pour une allocation de puissance indépendante de la variation du canal.

CSI statistique à l'émetteur : Dans les réseaux optiques, le CSI est disponible au récepteur à travers des séquences d'apprentissage du canal mais indisponible à l'émetteur à cause du trajet aller-retour très long. Nous proposons que le récepteur calcul une moyenne du canal optique qu'on notera: $\overline{H} = \overline{U}.\overline{\Lambda}.\overline{V}^{\dagger}$, avec $\overline{U}, \overline{V}$ des matrices unitaires, $\overline{\Lambda} = \text{diag}(\sqrt{\overline{\lambda}_1}, ..., \sqrt{\overline{\lambda}_M})$ contient les valeurs propres moyennes du canal. $\overline{V}$ et $\overline{\Lambda}$ représentent le CSI statistique. La matrice $\overline{\Lambda}$ sera utilisé pour calculer les puissances optimales par modes une seule fois seulement et la matrice $\overline{V}$ sera utilisé par l'émetteur pour envoyer des vecteurs de symboles corrélés indépendamment du changement du canal. Cette capacité sera donné par $C_{\overline{CSI}}$:

$$C_{\overline{CSI}} = \sum_{i=1}^{N} \log_2(1 + \overline{p_i^*} . \frac{\lambda_i}{2\sigma^2}) \tag{A.6}$$

avec $\overline{p_1^*}, ..., \overline{p_N^*}$ représentent les puissances moyennes allouées aux modes.

Nous avons simulés les capacités précédentes pour une fibre 6-mode et 10-mode. Les simulations ont été moyennés sur 10^5 réalisations du canal . La figure. E.4 montre la fonction de distribution cumulative complémentaire (CCDF) pour les trois capacités données par les équations A.4, A.5 et A.6 pour la fibre à 6-mode et pour une MDL = 15 dB. On constate que C_{CSI} et $C_{\overline{CSI}}$ dépassent C_{ep} et que plus le SNR augmente le gain apporté par le CSI diminue. Dans la figure E.5 nous avons tracé le gain en CSI définit par le rapport entre C_{CSI} (resp. $C_{\overline{CSI}}$) sur C_{ep} en fonction du SNR pour différentes valeurs de MDL. On remarque que le gain du CSI augmente avec la MDL et que pour des valeurs fortes de SNR le gain en CSI diminue. Dans ce qui suit, nous comparons les capacités moyennes sans CSI et avec le CSI moyen. La figure. E.6 montre ces capités C_{ep} et $C_{\overline{CSI}}$ pour les

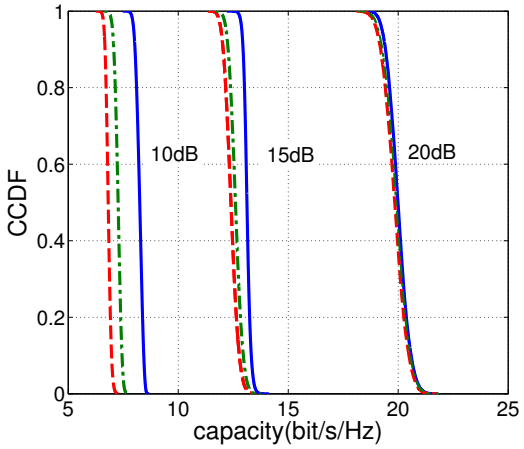

Figure E.4: Capacité CCDF avec CSI (solide), $\overline{CSI}$ (point-tiret) et *ep* (tiret) pour SNR=10,15,20 dB et MDL = 15dB

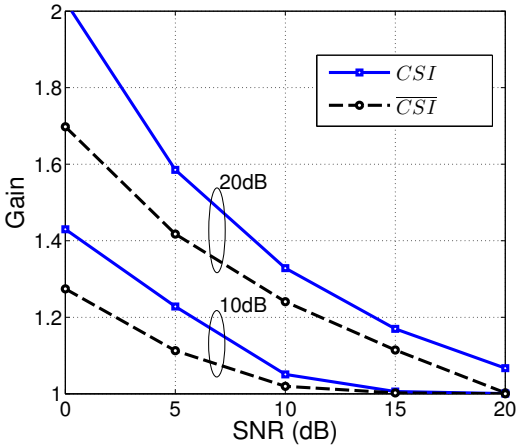

Figure E.5: Gain en C_{CSI} (solide), Gain en $\overline{CSI}$ (tiret) en fonction du SNR pour MDL = 10, 20 dB pour la fibre 6-mode.

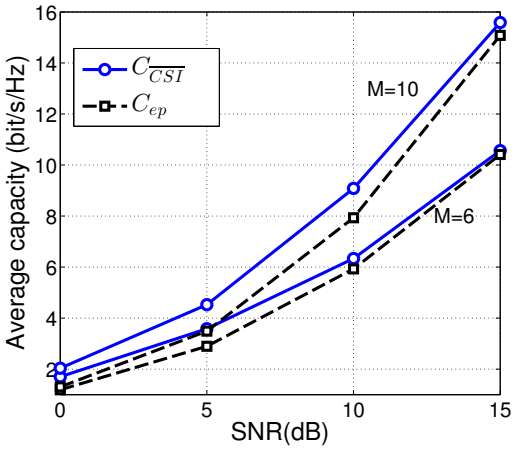

Figure E.6: Capacités moyennes vs SNR pour $M = 6, 10$ modes, MDL = 20dB.

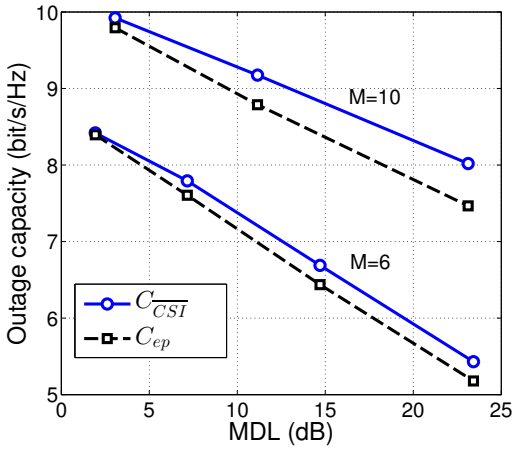

Figure E.7: Capacités de coupure vs MDL pour $M = 6, 10$ modes, SNR = 10dB.

fibres à 6-mode et 10-mode en fonction du SNR pour une MDL = 20 dB. On constate que le CSI moyen proposé augmente la capacité pour les deux fibres.

L'étude des capacités de coupures et très importante pour le design des systèmes optiques. En effet, puisque le canal change aléatoirement, les émetteurs sont configurés pour atteindre une capacité fixe qui est supérieure à la capacité de coupure du système. Dans la figure E.7 nous avons tracé les capacités de coupures pour une probabilité de coupure de 10^{-3} pour les fibres 6-mode et 10-mode en fonction de la MDL pour un SNR = 10 dB. Nous comparons les capacités avec des puissances d'émission des signaux égaux aux capacité utilisant le CSI moyen. D'après la figure, on remarque que les deux capacités décroit avec la MDL, toutefois, $C_{\overline{CSI}}$ reste nettement supérieur à C_{ep}. Pour une MDL = 20 dB

nous obtenons un gain de 0.3 bit/s pour la fibre 6-mode et 0.5 bit/s pour la fibre 10-mode. Par conséquent, puisque la disponibilité du CSI instantané donne les meilleurs performances mais reste malheureusement impossible à réaliser, le CSI statistique peut être une solution pour augmenter la capacité au lieu d'utiliser une allocation de puissances égales. La méthode proposé est à coût réduit car fonctionne indépendamment des variations du canal, donc peut être implémenté dans les applications réelles.

A.2.3 Augmentation de la Capacité des systèmes MDM par les brouilleurs de modes

Le brouillage de mode (Mode Scrambling : MS) a d'abord été utilisé pour surmonter la dépendance en fréquence des fibres multimodes et établir une distribution de puissance d'entrée uniforme pour tous les modes [70]. L'application du MS pour réduire la MDL et augmenter la capacité des systèmes MDM a d'abord été proposée dans [71], le principe consiste à introduire une permutation en mode aléatoire après K_{scr} épissures. Le canal MIMO résultant est donné par:

$$Y_{M\times 1} = \sqrt{L} \prod_{k=1}^{K} (T_k.C_k.P_k)\, X_{M\times 1} + N_{M\times 1} \tag{A.7}$$

La dernière équation est similaire à l'équation A.2, la seule différence est la présence de la matrice de brouillage de mode P_k correspondante à une matrice de permutation aléatoire si k est un multiple de la période de brouillage K_{scr}, ou une matrice d'identité dans le cas contraire. Après chaque MS, le signal modulé sur chaque mode est complètement transféré sur un autre mode. Par conséquent, tous les signaux modulés subissent les atténuations de tous les modes à l'extrémité de la fibre, ce qui réduit efficacement la MDL. Dans [71], les auteurs ont considéré des brouilleurs de mode idéals (matrices de permutation aléatoires parfaites) sans pertes modales. Ils ont montré que brouiller aléatoirement tous les modes après chaque épissure ($K_{scr} = 1$) conduit à un couplage modal complètement décorrélé. Cette stratégie peut réduire la MDL de la liaison, mais un grand nombre de brouilleurs est nécessaire.

A.2.3.1 Brouillage de mode Déterministe

Dans notre approche de brouillage, nous proposons d'utiliser un brouilleur de mode déterministe qui permute les modes ayant le plus de puissance reçue avec les modes ayant les puissances reçues les plus faibles. Pour avoir un aperçu de cette stratégie, nous considérons les fibres précédentes 6-mode et 10-mode. Au niveau de l'émetteur, nous lançons tous les modes avec une énergie unitaire $E_s = 1$ et nous calculons l'énergie reçue par mode au récepteur.

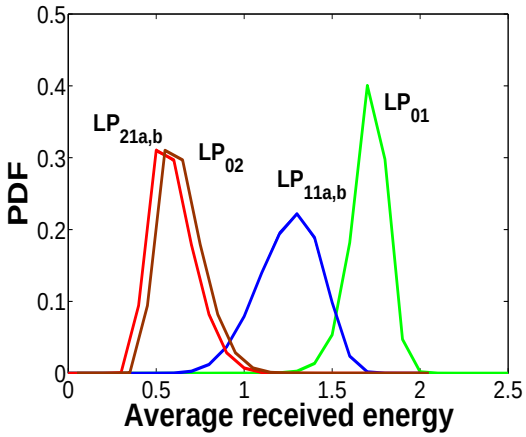

Figure E.8: Distribution de l'énergie reçue moyenne par mode pour la fibre 6-mode.

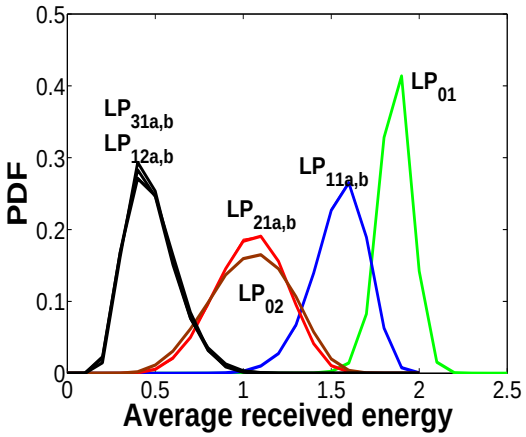

Figure E.9: Distribution de l'énergie reçue moyenne par mode pour la fibre 10-mode.

Les simulations sont moyennés sur 10^5 réalisations. Les deux fibres sont constituées de $K = 300$ sections avec des désalignements Gaussiens aléatoires indépendants de moyennes nulle et écart type (standart deviation: std) $\sigma_{x,y} = 0,26\mu m$. A partir des figures E.8 et E.9, nous constatons que certains modes arrives avec plus de puissances que d'autres. Pour la fibre 6-mode, les meilleurs modes sont le LP_{01} et les $LP_{11a,b}$ et les modes les plus faibles sont le LP_{02} et les $LP_{21a,b}$. Nous proposons donc de permuter le LP_{01} avec le LP_{02} et les $LP_{11a,b}$ avec les $LP_{21a,b}$. Pour la fibre 10-mode, les modes arrivant avec plus de puissances sont le LP_{01}, $LP_{11a,b}$ et les $LP_{21a,b}$, ces modes seront permuter avec les modes arrivant avec moins de puissance qui sont le LP_{02}, $LP_{31a,b}$ et les $LP_{12a,b}$.
Notre stratégie de brouillage évite les permutations entre modes arrivant avec des niveaux de puissances proches notamment entre les modes dégénérés qui arrivent avec la même puissance. Cependant, cette situation peut se produire si un brouillage de mode aléatoire est pris en compte, ce qui ne permet pas de moyenner les pertes efficacement entre tous les modes.

Pour avoir un aperçu de l'impact du MS, nous avons simuler les capacités moyennes et de coupures pour les mêmes fibres précédentes composés de $K = 300$ sections et contenant 6 brouilleurs de mode. Dans la figure E.10, nous traçons les capacités moyennes pour ces fibres pour différentes stratégies de brouillage. Nous remarquons que le MS augmente la capacité du système et que le MS déterministe surpasse le MS aléatoire. Pour les SNR faibles, les capacités moyennes sont presque les mêmes avec ou sans MS. Cependant, à mesure que le SNR augmente, le gain apporté par le MS devient plus important. Pour un SNR = 15 dB et un std $\sigma_{x,y} = 4\%$ Le gain de capacité apporté par l'utilisation du MS déterministe à une stratégie où aucun brouilleur de mode n'est utilisé est de 4.5 bit/s pour

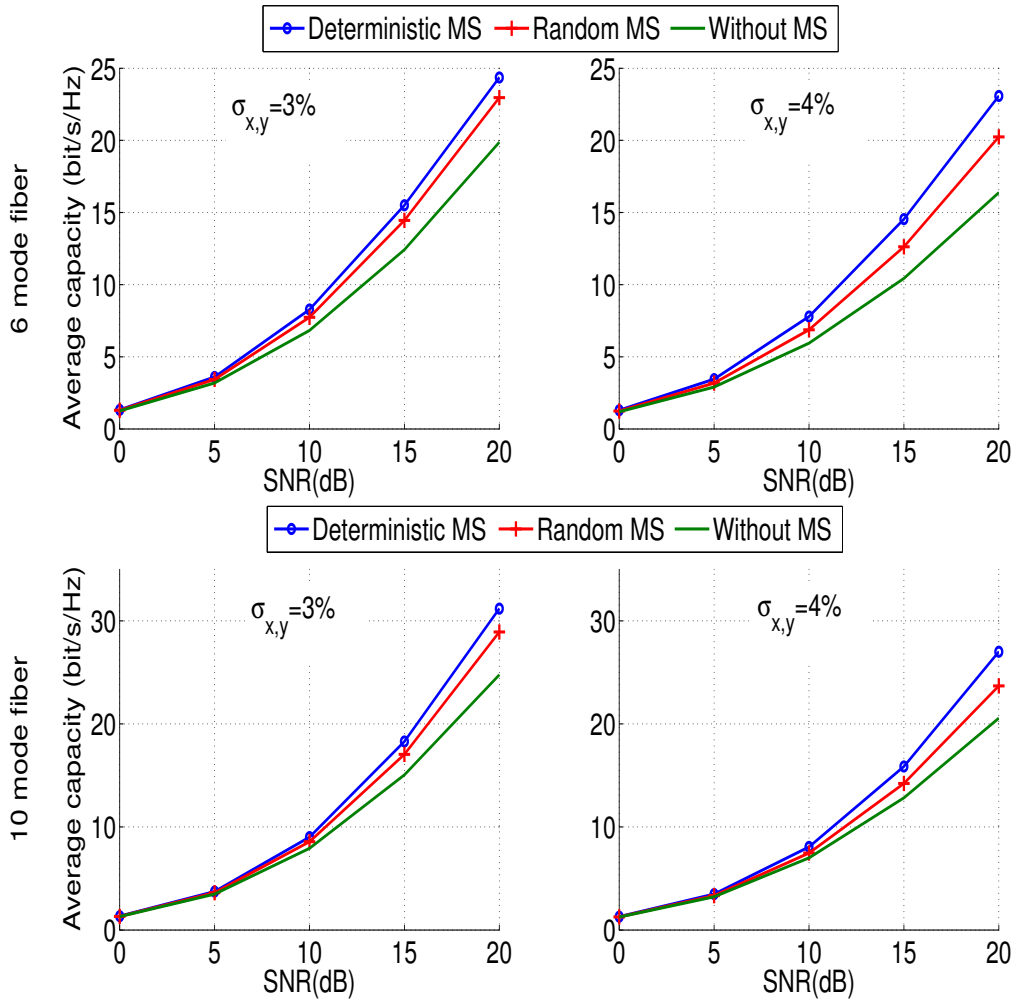

Figure E.10: Capacités moyennes pour les fibres 6- et 10-mode pour différentes stratégies de brouillages et un std $\sigma_{x,y} = 3\%,\ 4\%$.

la fibre 6-modes et 3.5 bit/s pour la fibre 10-modes. Par conséquent, le MS déterministe est plus efficace ce qui réduit considérablement la MDL et se traduit par une meilleure capacité moyenne.

Dans la figure E.11 et E.12, nous simulons la capacité de coupure en fonction du désalignement std $\sigma_{x,y}$ pour les différentes stratégies de brouillage et pour une probabilité de coupure de 10^{-3}. Nous remarquons que pour un std $\sigma_{x,y}$ qui augmente ce qui augmente aussi la MDL, les capacités de coupure diminuent. Cependant, l'utilisation du MS améliore considérablement ces capacités et le MS déterministe surpasse le MS aléatoire. Pour un std $\sigma_{x,y} = 4\%$. Le gain de capacité apporté par l'utilisation du MS déterministe à une stratégie où aucun brouilleur de mode n'est utilisé est de 7.8 bit/s pour la fibre 6-mode et de 5.2 bit/s pour la fibre 10-mode.

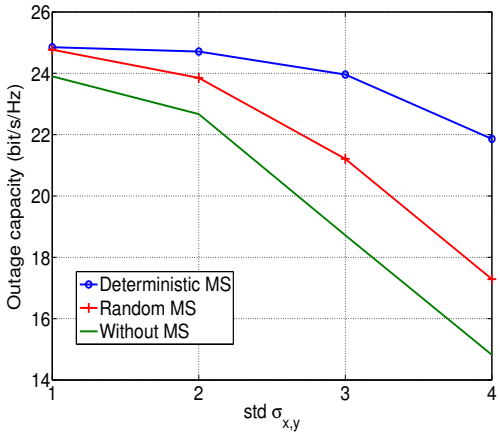

Figure E.11: Capacités de coupures en fonction du std pour la fibre 6-mode pour différentes stratégies de brouillage et un SNR = 20 dB

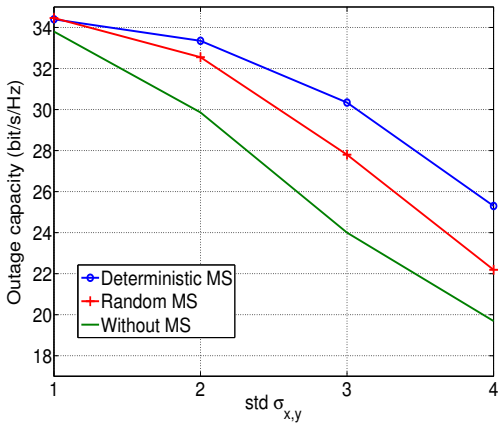

Figure E.12: Capacités de coupures en fonction du std pour la fibre 10-mode pour différentes stratégies de brouillage et un SNR = 20 dB

Dans nos simulations, nous avons considéré une période de brouillage de $K_{scr} = 50$ ce qui ne fait que 6 brouilleurs dans la ligne composée de $K = 300$ sections de fibres. Dans les systèmes de transmission réels, le nombre de brouilleurs à utiliser dans une ligne est un paramètre important dans la conception de l'architecture MDM. Les brouilleurs de mode peuvent être placés après les multiplexeurs ou les amplificateurs [52]. Dans la figure E.13 nous calculons la MDL moyenne en fonction du nombre de brouilleurs utilisés dans la ligne pour les deux stratégies de brouillage. D'après la figure, nous pouvons conclure que pour obtenir une MDL moyenne de 4 dB, seulement 8 brouilleurs de mode déterministes sont nécessaires au lieu de 60 brouilleurs de mode aléatoires. Par conséquent, le MS déterministe peut être considéré comme une solution émergente qui réduit très efficacement l'impact de la MDL et améliore la capacité des systèmes optiques à multiplexage modal.

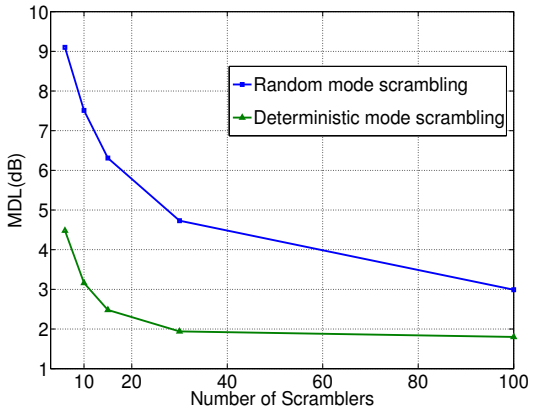

Figure E.13: MDL en fonction du nombre de brouilleurs de mode pour la fibre 6-mode.

A.2.4 Augmentation de la Capacité des systèmes MDM par la sélection de modes

Dans cette partie, nous étudions les performances d'un système optique MDM lorsqu'un ensemble approprié de modes est sélectionner pour le multiplexage selon un critère d'énergie. Nous considérons le modèle de canal précédent et nous sélectionnons un ensemble de modes $M_T < M$ pour multiplexer les données à l'émetteur et nous détectons $M_R \leq M$ modes au récepteur (avec $M_T \leq M_R$). Le canal MIMO résultant est donné par:

$$Y_{M_R \times 1} = H_{M_R \times M_T}.X_{M_T \times 1} + N_{M_R \times 1} \tag{A.8}$$

La matrice $H_{M_R \times M_T}$ couvre un sous espace de la matrice globale $H_{M \times M}$ donné par l'équation A.2. Le critère de sélection de modes consiste à choisir les modes qui arrivent avec plus de puissance au niveau du récepteur. En effet, à l'émetteur, on émet tous les modes avec une puissance unitaire $E_s = 1$, et on calcul les puissances moyenne reçues au niveau du récepteur. Les résultats ont déjà été montrés dans les figures E.8 et E.9.
Pour avoir un aperçu de l'avantage de la sélection de mode pour les systèmes MDM, nous comparons à la même efficacité spectrale (Spectral efficiency: SE) la capacité d'une fibre 3-mode à une fibre à 6-mode lorsque seuls les trois meilleurs modes sont utilisés. Nous comparons également la capacité d'une fibre 6-mode à celle d'une fibre à 10-mode lorsque seulement six modes sont utilisés. Puisque les fibres ont un rayon de cœur différent, il est plus commode de comparer les différents schémas à un désalignement std fixe $\sigma_{x,y}$ plutôt qu'à un std donné en pourcentage du rayon du cœur.

Dans la figure E.14, on compare une fibre 3-mode à une fibre 6-mode utilisant la sélection de trois modes à l'émission et réception ($M_T = M_R = 3$). On constate que la sélection des trois meilleurs modes dans la fibre à 6-mode donne de meilleurs capacités moyennes que la fibre à 3-mode. Pour un SNR de 20 dB, on a un gain de 0.4 bit/s pour un std $\sigma_{x,y} = 0.26\mu m$ et un gain de 2 bit/s pour un std $\sigma_{x,y} = 0.35\mu m$. Dans la figure E.15, on compare une fibre 6-mode à une fibre 10-mode utilisant la sélection de six modes à l'émission et réception ($M_T = M_R = 6$). On constate aussi que la sélection des six meilleurs modes dans la fibre à 10-mode donne de meilleurs capacités moyennes que la fibre à 6-mode. Pour un SNR de 20 dB, on a un gain de 1.1 bit/s pour un std $\sigma_{x,y} = 0.26\mu m$ et un gain de 3.6 bit/s pour un std $\sigma_{x,y} = 0.35\mu m$. Ces résultats montrent que la sélection de modes dans des fibres supportant un grand nombre de modes donne de meilleurs capacités que des fibres supportant ce même nombre de modes.

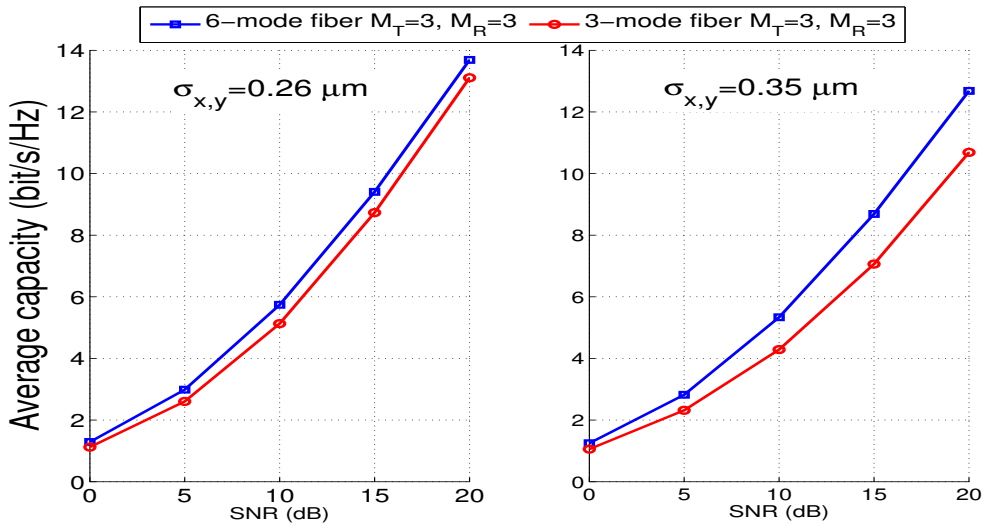

Figure E.14: Capacités moyennes pour la fibre 3-mode et la fibre 6-mode utilisant $M_T = M_R = 3$ modes à l'émission et la réception.

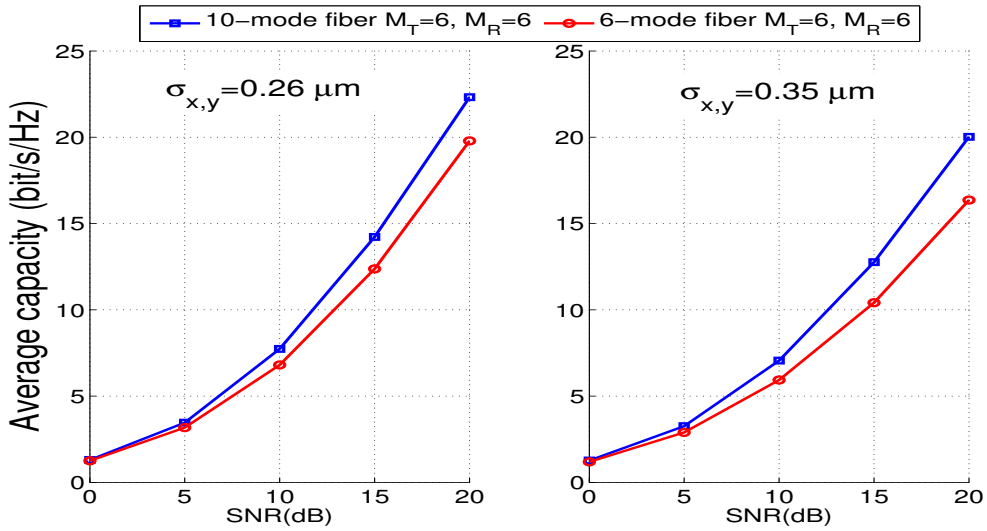

Figure E.15: Capacités moyennes pour la fibre 6-mode et la fibre 10-mode utilisant $M_T = M_R = 6$ modes à l'émission et la réception.

A.3 Codage Espace-Temps pour les systèmes optiques à multiplexage modal

Dans la section précédente, nous avons étudié les capacités moyennes et de coupures du canal FMF et proposé quelques techniques pour améliorer ces capacités. Une fois la capacité maximale d'un canal est déterminée, il est important de déterminer la fiabilité de la communication. Cela peut être fait en mesurant le taux d'erreur binaire (Bit-error rate: BER) de la transmission.

Dans cette partie, nous étudions l'efficacité des schémas de codage espace-temps (Space-

Time ST) pour les systèmes optiques MDM afin d'améliorer les performances du BER. Les codes ST étaient déjà appliqués dans une configuration MIMO 2×2 pour les systèmes à multiplexage de polarisations [28], des gains OSNR ont été observés à la fois dans les régimes linéaires et non linéaires de propagation. De plus, l'efficacité du codage ST dans l'atténuation de la MDL a été démontré par simulations numériques pour les systèmes FMF [6], les auteurs ont considéré le même modèle de canal que nous avons présenté dans la section précédente. Ce modèle de canal permet de simuler physiquement la FMF et de générer des MDL à partir d'effets non unitaires accumulés.

Dans cette section, nous souhaitons expliquer les gains de codage apportés par le codage ST aux systèmes optiques MDM affectés par la MDL à travers une analyse théorique de la probabilité d'erreur. Pour dériver une limite supérieure analytique de la probabilité d'erreur, un modèle de canal compact est requis. Par conséquent, nous considérons un modèle de canal mathématique qui décrit les effets de MDL et de couplage. Ensuite, nous calculons une limite supérieure pour la probabilité d'erreur qui fournira un critère de conception pour les codes ST pour absorber complètement MDL. Par la suite, nous étudions les performances de la concaténation des codes ST et des codes correcteurs d'erreur (FEC). Nous prouvons par des simulations numériques et aussi par une dérivation théorique de la probabilité d'erreur la somme des deux gains de codage.

A.3.1 Canal optique MDM en présence de la MDL

L'effet de la MDL sur la propagation a été le sujet de nombreuses études [34–36]. La MDL cumulée dépend du couplage modal et du nombre de tronçons de fibre concaténés. Afin d'étudier les avantages du codage indépendamment des statistiques de la liaison, nous considérons un modèle de canal simplifié constitué d'un seul élément de MDL localisé. Ce modèle a été utilisé dans [88] pour étudier les performances du canal optique affecté par la MDL pour différentes tailles de constellations, ainsi le même modèle a permis d'étudier la capacité secrète des systèmes MIMO MDM [89]. La transmission MIMO peut être décrite par:

$$Y_{M\times T} = H.X_{M\times T} + N_{M\times T} \tag{A.9}$$

$X_{M\times T}$ (resp. $Y_{M\times T}$) est le mot de code transmit (resp. reçu). $N_{M\times T}$ représente le bruit blanc additive Gaussien de moyenne nulle et de puissance $2\sigma^2$ par mode. La matrice canal est donnée par:

$$H = \sqrt{\alpha}\sqrt{D}U. \tag{A.10}$$

D est une matrice diagonale, ces éléments sont uniformément tirés entre $[\lambda_{min}, \lambda_{max}]$ et représentent les différentes atténuations modales de chaque mode. En l'absence de la

MDL, la matrice D est égale à la matrice identité ($D = I_M$). U est une matrice aléatoire unitaire qui représente le couplage entre les modes. La MDL est définit par le rapport en décibels (dB) entre le maximum et le minimum des valeurs propres de la matrice canal: $\text{MDL}_{(dB)} = 10.\log(\text{MDL}) = 10.\log(\frac{\lambda_{max}}{\lambda_{min}})$.

A.3.1.1 Dérivation de la borne de probabilité d'erreur

Pour dériver la borne supérieur de la probabilité d'erreur, on commence le calcul à partir de la probabilité d'erreur par paire 3.8. Soit $X_\Delta = \hat{X} - X$ la matrice différence de deux mots de codes, nous obtenons:

$$\Pr\left\{X \to \hat{X}\right\} \leqslant \mathbb{E}_H\left[\exp(-\frac{\left\|\sqrt{\frac{M}{\sum_{i=1}^{M}\lambda_i}}\sqrt{D}UX_\Delta\right\|^2}{8\sigma^2})\right] \tag{A.11}$$

$$\leqslant \mathbb{E}_H\left[\exp(-\frac{M}{\sum_{i=1}^{M}\lambda_i}\frac{\text{Tr}(DUX_\Delta X_\Delta^\dagger U^\dagger)}{8\sigma^2})\right] \tag{A.12}$$

Dans ce qui suit, nous dérivons la probabilité d'erreur pour les les codes orthogonaux, puis après, on s'interesse aux codes non-orthogonaux.

A. Codes ST Orthogonaux

La construction orthogonales des codes ST induit l'orthogonalité aux matrices différence de mots de codes X_Δ aussi [90], i.e. $X_\Delta X_\Delta^\dagger = \sum_k |x_{k,i} - x_{k,j}|^2 . I_M$ pour tous les mots de codes, avec $x_{k,i}$ (resp. $x_{k,j}$) les symboles transmit (resp. reçus). En appliquant cette propriété à l'équation A.12 on obtient:

$$\Pr\left\{X \to \hat{X}\right\} \leqslant \exp(-\frac{\|X_\Delta\|^2}{8\sigma^2}) \tag{A.13}$$

En remplaçant l'équation précédente dans 3.5, la probabilité d'erreur devient:

$$\text{Pr}_{error} \leq \sum_{X\in C}\frac{1}{\text{card}(C)}\sum_{X\neq\hat{X}}\exp(-\frac{\|X_\Delta\|^2}{8\sigma^2}) \tag{A.14}$$

La distance Euclidienne minimale d'un ST code ST est définie par: $d^2_{min,ST} = \underset{X\neq\hat{X},\ X,\hat{X}\in C}{min}\left\|X-\hat{X}\right\|^2$. par conséquent, le nombre de voisin minimal $N_{min,X}$ du mot de code X est définie par le nombre minimal de mot de code qui sont à la distance $d^2_{min,ST}$ de X. En utilisant le

nombre de voisin minimal $N_{min,X}$ of X on obtient:

$$\Pr_{error} \leq (\frac{1}{\text{card}(C)} \sum_{X \in C} N_{min,X}) \cdot \exp(-\frac{d^2_{min,ST}}{8\sigma^2}) \tag{A.15}$$

Notons $\overline{N}_{min} = \frac{1}{\text{card}(C)} \sum_{X \in C} N_{min,X}$ le nombre moyen de proche voisin de X, l'équation A.15 donne:

$$\Pr_{error} \leq \overline{N}_{min} \cdot \exp\left(-\frac{d^2_{min,ST}}{8\sigma^2}\right) \tag{A.16}$$

De l'équation précédente, on remarque que les codes ST orthogonaux donne une probabilité d'erreur qui est indépendante de la MDL. Donc, on conclut que les code ST orthogonaux absorbent complètement MDL.

B. Cas général des codes ST

DAns cette partie, on dérive la borne supérieur de la probabilité d'erreur dans le cad générale du codage espace-temps. On réécrit la probabilité d'erreur donné par l'équation 3.5 comme la sommation de deux termes. Le premier termes contient les mots de codes orthogonaux tandis que le second termes contient les mots de codes non-orthogonaux.

$$\Pr_{error} \leq \sum_{X \in C} \frac{1}{\text{card}(C)} \sum_{\substack{X \neq \hat{X} \\ X_\Delta \text{orthogonal}}} \Pr\left\{X \to \hat{X}\right\} + \sum_{X \in C} \frac{1}{\text{card}(C)} \sum_{\substack{X \neq \hat{X} \\ X_\Delta \text{ non orthogonal}}} \Pr\left\{X \to \hat{X}\right\} \tag{A.17}$$

Le premier terme de l'équation A.17 a été calculé dans la partie précédente et est égale à $\overline{N}_{min,1} \cdot \exp(-\frac{d^2_{min,ST}}{8\sigma^2})$, avec $\overline{N}_{min,1}$ le nombre de voisin moyen le plus proche de X avec X_Δ est orthogonal. Dans ce qui suit, on calcul le second terme en partant de l'équation A.12 et puisque $\sum_{i=1}^{M} \lambda_i \leqslant M\lambda_{max}$ on obtient:

$$\Pr\left\{X \to \hat{X}\right\} \leqslant \mathbb{E}_{D,U}\left[\exp(-\frac{\text{Tr}(DUX_\Delta X_\Delta^\dagger U^\dagger)}{8\sigma^2\lambda_{max}})\right] \tag{A.18}$$

Dans l'équation précédente, la moyenne est prise par rapport à la matrice diagonale D et la matrice unitaire U . $X_\Delta X_\Delta^\dagger$ est une matrice Hermitienne carré, donc peut être écrite sous la forme $\Sigma = \text{diag}(\sigma_1, ..., \sigma_M)$ avec: $X_\Delta X_\Delta^\dagger = V\Sigma V^\dagger$. On obtient:

$$\Pr\left\{X \to \hat{X}\right\} \leqslant \mathbb{E}_{D,U}\left[\exp(-\frac{\text{Tr}(DUV\Sigma V^\dagger U^\dagger)}{8\sigma^2\lambda_{max}})\right] \tag{A.19}$$

La matrice U is aléatoirement tiré de l'ensemble des matrice unitaires, donc le produit

UV suit la même loi de distribution que la matrice U [91], On obtient donc:

$$\Pr\left\{X \to \hat{X}\right\} \leqslant \mathbb{E}_{D,U}\left[\exp(-\frac{\mathrm{Tr}(DU\Sigma U^{\dagger})}{8\sigma^2\lambda_{max}})\right] \tag{A.20}$$

On développant le terme $DU\Sigma U^{\star}$ on arrive a:

$$\Pr\left\{X \to \hat{X}\right\} \leq \mathbb{E}_{D,U}\left[\exp(-\frac{\sum_{i,j=1}^{M}\lambda_i\sigma_j\left|u_{ij}\right|^2}{8\sigma^2\lambda_{max}})\right] \tag{A.21}$$

$$\leq \mathbb{E}_{D,U}\left[\prod_{i=1}^{M}\exp(-\lambda_i\frac{\sum_{j=1}^{M}\sigma_j\left|u_{ij}\right|^2}{8\sigma^2\lambda_{max}})\right] \tag{A.22}$$

Puisque les variables aléatoires λ_i's sont indépendantes, alors la moyenne du produit peut être remplacée par le prouit des moyennes:

$$\Pr\left\{X \to \hat{X}\right\} \leq \prod_{i=1}^{M}\mathbb{E}_{D,U}\left[\exp(-\lambda_i\frac{\sum_{j=1}^{M}\sigma_j\left|u_{ij}\right|^2}{8\sigma^2\lambda_{max}})\right] \tag{A.23}$$

maintenant, on moyenne sur les λ_i's qui sont uniformément tirés entre $[\lambda_{min},\lambda_{max}]$, on obtient:

$$\Pr\left\{X \to \hat{X}\right\} \leq \prod_{i=1}^{M}\mathbb{E}_{U}\left[\int_{\lambda_{min}}^{\lambda_{max}}\exp(-\lambda_i\frac{\sum_{j=1}^{M}\sigma_j\left|u_{ij}\right|^2}{8\sigma^2\lambda_{max}})\times P(\lambda_i)d\lambda_i\right] \tag{A.24}$$

$$= \prod_{i=1}^{M}\mathbb{E}_{U}\left[\frac{\exp(-\frac{\sum_{j=1}^{M}\sigma_j|u_{ij}|^2}{8\sigma^2}-\exp(-\frac{\lambda_{min}}{\lambda_{max}}\frac{\sum_{j=1}^{M}\sigma_j|u_{ij}|^2}{8\sigma^2})}{\frac{(\lambda_{max}-\lambda_{min})\sum_{j=1}^{M}\sigma_j|u_{ij}|^2}{8\sigma^2\lambda_{max}}}\right] \tag{A.25}$$

$$= \prod_{i=1}^{M}\mathbb{E}_{U}\left[\exp\left(-\frac{1}{2}(1+\frac{\lambda_{min}}{\lambda_{max}})\frac{\sum_{j=1}^{M}\sigma_j\left|u_{ij}\right|^2}{8\sigma^2}\right)\times 2\sinh\left(\frac{1}{2}(1-\frac{\lambda_{min}}{\lambda_{max}})\frac{\sum_{j=1}^{M}\sigma_j\left|u_{ij}\right|^2}{8\sigma^2}\right)\right] \tag{A.26}$$

Dans l'équation A.24 $P(\lambda_i)$ représente la distribution de λ_i et est donnée par:

$$P(\lambda_i) = \begin{cases} \frac{1}{\lambda_{max}-\lambda_{min}} & if\ \lambda_{min} \leqslant \lambda_i \leq \lambda_{max} \\ 0 & \text{elsewhere} \end{cases}$$

En utilisant l'approximation du Sinus hyperbolique à fort SNR: $\sinh(x) \underset{x\to\infty}{\to} \exp(x)/2$ on

obtient:

$$\Pr\left\{X \to \hat{X}\right\} \leq \prod_{i=1}^{M} \mathbb{E}_U \left[\exp(-(\frac{\lambda_{min}}{\lambda_{max}})\frac{\sum_{i=1}^{M}\sigma_j |u_{ij}|^2}{8\sigma^2})\right] \tag{A.27}$$

$$= \mathbb{E}_U \left[\exp(-\frac{\lambda_{min}}{\lambda_{max}}\frac{\sum_{j=1}^{M}\sum_{i=1}^{M}\sigma_j |u_{ij}|^2}{8\sigma^2})\right] \tag{A.28}$$

$$= \mathbb{E}_U \left[\exp(-\frac{\lambda_{min}}{\lambda_{max}}\frac{\sum_{j=1}^{M}\sigma_j}{8\sigma^2})\right] \tag{A.29}$$

$$= \mathbb{E}_U \left[\exp(-\frac{\|X_\Delta\|^2}{8\sigma^2 \mathrm{MDL}})\right] \tag{A.30}$$

l'équation A.30 est indépendante de la matrice unitaire U donc:

$$\Pr\left\{X \to \hat{X}\right\} \leq \exp\left(-\frac{\|X_\Delta\|^2}{8\sigma^2 \mathrm{MDL}}\right) \tag{A.31}$$

On remplaçant A.31 dans le second terme de A.17 on arrive à:

$$\mathrm{Pr}_{error} \leq \overline{N}_{min,1} \cdot \exp\left(-\frac{d^2_{min,ST}}{8\sigma^2}\right) + \sum_{X \in C} \frac{1}{\mathrm{card}(C)} \sum_{\substack{X \neq \hat{X} \\ X_\Delta \text{ non orthogonal}}} \exp\left(-\frac{\|X_\Delta\|^2}{8\sigma^2 \mathrm{MDL}}\right) \tag{A.32}$$

Soit $N_{min,2,X}$ le nombre de voisins minimales le plus proche de X tel que X_Δ est non-orthogonal, on obtient:

$$\mathrm{Pr}_{error} \leq \overline{N}_{min,1} \cdot \exp\left(-\frac{d^2_{min,ST}}{8\sigma^2}\right) + \sum_{X \in C} \frac{1}{\mathrm{card}(C)} N_{min,2,X} . \exp\left(-\frac{d^2_{min,ST}}{8\sigma^2 \mathrm{MDL}}\right) \tag{A.33}$$

On posons $\overline{N}_{min,2} = \sum_{X_i \in C} \frac{1}{\mathrm{card}(C)} N_{min,2,X}$ on arrive à:

$$\mathrm{Pr}_{error} \leq \overline{N}_{min,1} \cdot \exp\left(-\frac{d^2_{min,ST}}{8\sigma^2}\right) + \overline{N}_{min,2} \cdot \exp\left(-\frac{d^2_{min,ST}}{8\sigma^2 \mathrm{MDL}}\right) \tag{A.34}$$

A partir de l'équation précédente, on remarque que la borne supérieur de la probabilité d'erreur est composée de deux termes qui décroient exponentiellement en fonction du SNR. Ce comportement est différent du canal Rayleigh à évanouissement ou la probabilité d'erreur décroit en fonction de SNR^{-rn_r}. Par conséquent, le codage ST appliqué au canal optique ne ramène pas de gains de diversité mais seulement un gain de codage.

A.3.2 Critère de construction de codes ST pour le canal optique MDM

À partir de l'équation A.34, on remarque que la limite supérieure de la probabilité d'erreur est composée de deux termes. Le premier provient des différences de mots de code orthogonaux et est complètement indépendant de la MDL. Le second terme est affecté par MDL et provient des mots de code de différence non orthogonale. Par conséquent, afin de minimiser la borne supérieure de la probabilité d'erreur, le premier terme doit être le terme dominant de la limite supérieure.

Proposition: Pour minimiser la probabilité d'erreur, le nombre moyen de voisins les plus proches $\overline{N}_{min,1}$ d'un code ST tel que la matrice de différence de mots de code X_Δ est orthogonale doit être maximale.

Le critère de construction obtenu est directement lié à l'orthogonalité des différences de mot de code. Dans le Tableau A.2, nous avons calculé le nombre moyen de voisins orthogonaux et non-orthogonaux les plus proches d'un mot de code X pour différents codes ST de dimension 2×2 en utilisant une constellation 4-QAM.
Nous remarquons que le code Alamouti a $\overline{N}_{min,2} = 0$, ceci est dû à sa structure orthogonale. Les mots de code du code Silver ont plus de voisins orthogonaux (6.5 voisins) que les mots de code du code TAST (4 voisins). Les mots de code du code Golden n'ont pas de voisins orthogonaux les plus proches. Ces observations permettent de déduire que le code Silver donne les meilleures performances suivie du TAST puis du Golden code.

Table A.2: Nombre moyen de voisins orthogonaux et non orthogonaux d'un mot de code X pour différent codes ST de dimension 2×2.

	$\overline{N}_{min,1}$	$\overline{N}_{min,2}$	$\overline{N}_{min,Total}$
Silver Code	6.5	1.5	8
TAST Code	4	4	8
Golden Code	0	8	8
Alamouti Code	8	0	8

Pour valider les résultats théoriques obtenus, nous calculons par simulation numériques les performances de différents codes ST pour des systèmes optiques MIMO-MDM de dimension 2×2 et 3×3. Nous comparons les performances en termes de courbes BER par rapport au SNR. Au récepteur, un décodeur ML est implémenté.

A. Fibre optique à 2 modes

Pour étudier l'impact de l'orthogonalité des matrices de différence de mot de code sur la probabilité d'erreur, nous considérons quatre codes ST différents: le code Silver, Golden,

Alamouti et TAST. Afin de comparer les performances à la même efficacité spectrale, nous utilisons des symboles 4-QAM pour construire les mots de code du Silver, Golden et TAST qui sont des codes à plein débit avec 2 symboles par utilisation de canal. Nous utilisons des symboles 16-QAM pour construire les mots de code pour le code Alamouti qui est un code à moitié débit avec 1 symbole par utilisation de canal. Dans la figure E.16 nous reportons les performances du code Alamouti. Nous remarquons que ce code donne les mêmes performances pour différentes valeurs de MDL ce qui confirme la borne supérieure obtenue de l'équation A.34. On peut donc conclure que les codes ST orthogonaux permettent d'absorber complètement la MDL mais malheureusement ces codes sont pénalisés par leur débit de transmission réduit.

Dans la figure E.17 nous comparons les performances du code Silver, TAST et Golden pour MDL = 10dB. Nous remarquons que le code Silver surpasse les deux autres codes, ceci peut s'expliquer par le nombre plus élevé de différences orthogonales entre les mots de code codes du code Silver. Le code Golden est le moins performant en raison de l'absence de voisins orthogonaux à $d^2_{min,ST}$. Les performances du code TAST se situent entre le Golden et le TAST avec un nombre moyen de voisins orthogonaux égal à 4.

Ces résultats sont complètement différents du canal Rayleigh sans fil où le code Golden est le meilleur code. En fait, pour le canal Rayleigh, ces codes ont été construits afin de satisfaire aux critères de rang et de déterminant, mais ces critères ne sont pas pertinents pour le canal optique affecté par MDL.

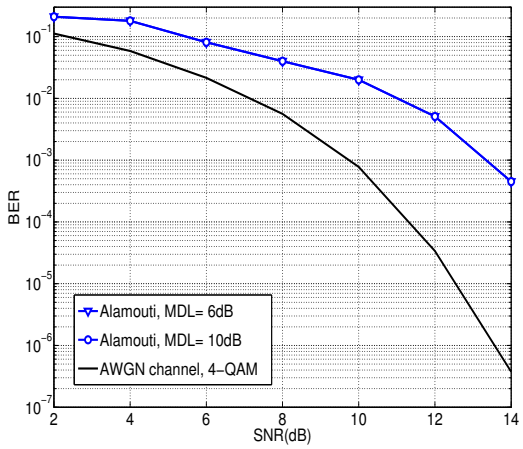

Figure E.16: BER vs SNR pour le code Alamouti, MDL = 6, 10 dB.

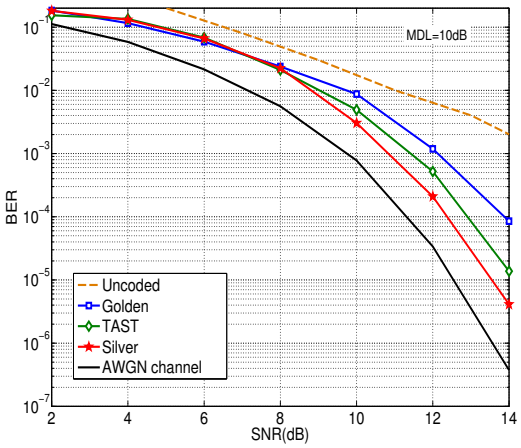

Figure E.17: BER vs SNR pour les codes {Silver, Golden, TAST}, MDL = 10 dB.

B. Fibre optique à 3 modes

Dans cette partie, nous considérons une fibre à 3 modes et étudions l'impact de MDL sur la probabilité d'erreur. Nous utilisons un code TAST de dimension 3×3 qui est un code

à débit plein. Dans la figure E.18 nous reportons les performances de ce code pour des MDL = 6 et 10 dB. On remarque que pour MDL = 6 dB, le code TAST permet d'atténuer complètement toute la MDL. Cependant, pour une MDL = 10 dB et à un BER = 10^{-4}, la pénalité en SNR du canal optique MDM par rapport au canal Gaussien est de 1.2 dB. Ce comportement peut aussi être expliqué par l'équation A.34. En effet, en augmentant la MDL, cela conduit à augmenter l'impact du second terme de la borne supérieure et donc induit une perte de performance.

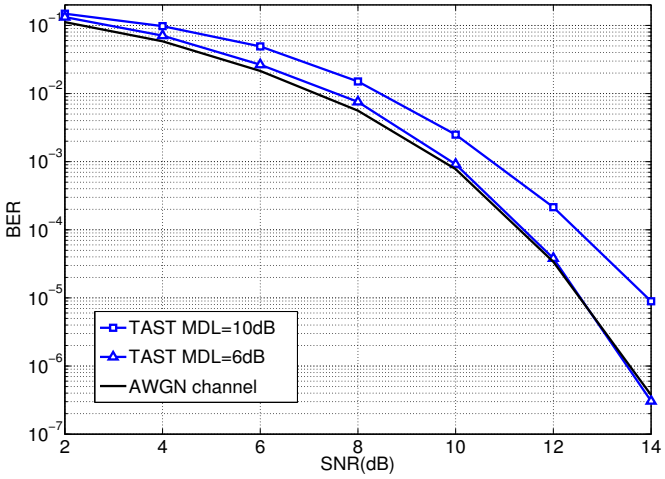

Figure E.18: BER vs SNR pour le code TAST, MDL = 6,10 dB.

A.3.3 Validation expérimentale du codage ST pour les systèmes MDM

Dans ce chapitre, nous démontrons expérimentalement pour la première fois l'atténuation de la MDL en utilisant un codage ST à débit plein. Nous menons une expérience de transmission MDM dans laquelle nous utilisons le format de modulation OFDM pour la gestion de la dispersion en appliquant un préfixe cyclique approprié. L'OFDM permet aussi de réduire la complexité de l'égalisation de canal à une simple inversion de la matrice canal. Le codage ST est utilisé pour combattre l'effet de la MDL. Pour une transmission MDM $M \times M$, M récepteurs cohérents à double polarisation sont nécessaires et chaque récepteur est couplé à la sortie du DEMUX. Le laboratoire de recherche fibre optique de Télécom ParisTech est orienté vers les transmissions fibre monomode, plus particulièrement l'étude des non-linéarités pour les systèmes longue distance. Pour surmonter le problème d'équipement, nous menons notre expérience en collaboration avec l'IRCICA (Institut de recherche sur les composants logiciels et matériel pour l'information et la communication avancée) de l'Université de Lille. L'IRCICA dispose d'une plate-forme de

transmission bien développée dédiée aux systèmes de multiplexage spatial. Nous avons prouvé pour la première fois l'efficacité du codage ST à débit plein pour atténuer la MDL.

A.3.3.1 Banc expérimental

Dans une transmission MDM, chaque mode nécessite un récepteur cohérent à double polarisation et un oscilloscope à quatre ports pour détecter les composantes en phase (réelle) et en quadrature (imaginaire) des constellations complexes transmises pour chacune des deux polarisations. De ce qui précède, la réalisation d'expériences de transmission multimodes impliquant plusieurs modes spatiaux devient très gourmande en termes d'équipement très coûteux. Notre démonstration expérimentale consiste en un système MIMO 4×4 basé sur la propagation de deux modes avec les deux polarisations. La MDL a été émulé à l'émetteur en ajustant différentes atténuations sur les modes.

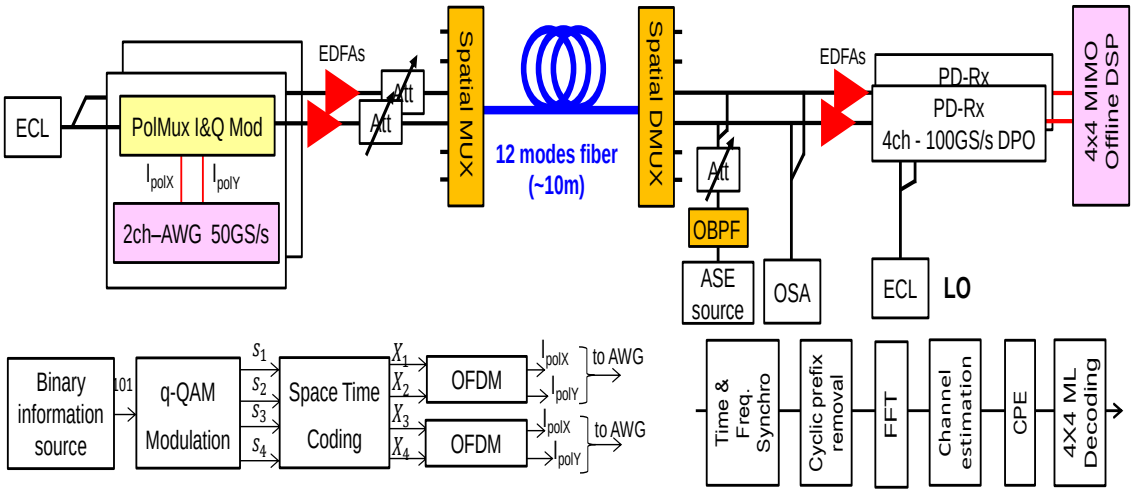

Figure E.19: Système de transmission MDM. MC: convertisseur de mode, ADC: convertisseur analogique-digital.

L'émetteur:

Deux émetteurs PDM-OFDM sont utilisés pour envoyer des signaux indépendants. En tant que source lumineuse, nous utilisons un laser à cavité externe (ECL) avec une largeur de ligne ∼100 kHz fonctionnant à 1531 nm. Pour réduire la sensibilité au bruit de phase des lasers, le signal OFDM est constitué de 90 sous-porteuses de données modulées en QPSK et 10 sous-porteuses pilotes pour l'estimation de la phase commune (CPE). Le préfixe cyclique de 18-échantillon est ajouté à chaque symbole OFDM pour absorber la DMGD et éviter les interférences entre symboles. Une séquence d'apprentissage de 22 symboles est inséré chaque 100 symboles OFDM pour la synchronisation temporelle, la compensation de décalage fréquentiel et l'estimation du canal. Deux générateurs de formes d'ondes arbitraires (AWG) Tektronix sont utilisés pour créer les symboles OFDM des polarisations `X`

et Y dont les spectres satisfont la propriété de symétrie hermitienne de sorte que le signal du domaine temporel est composé d'échantillons réels. Cette stratégie n'affecte pas notre analyse sachant que le complexe conjugué des sous-porteuses sont traités indépendamment des sous-porteuses originales au niveau du récepteur. Par ce moyen, nous n'utilisons que quatre AWG au lieu de huit pour générer les signaux complexes à double polarisation. Les signaux PDM ont une bande passante de 10 GHz, ce qui donne un débit binaire de 40 Gb/s.

Pour la transmission non codée, nous réalisons le multiplexage spatial en envoyant à chaque temps symbole i un vecteur $S_i = [s_1^i, s_2^i, s_3^i, s_4^i]^\intercal$ de symboles QPSK indépendants sur les deux polarisations. Pour la transmission codée en ST, nous utilisons un code TAST à débit plein de dimension 4×4. Nous envoyons différents mots de code par blocs de 4 temps symboles. La matrice mot de code est donnée par:

$$X_{4\times4} = \begin{bmatrix} f_1(S_1) & \phi^{\frac{3}{4}} f_2(S_4) & \phi^{\frac{2}{4}} f_3(S_3) & \phi^{\frac{1}{4}} f_4(S_2) \\ \phi^{\frac{1}{4}} f_1(S_2) & f_2(S_1) & \phi^{\frac{3}{4}} f_3(S_4) & \phi^{\frac{2}{4}} f_4(S_3) \\ \phi^{\frac{2}{4}} f_1(S_3) & \phi^{\frac{1}{4}} f_2(S_2) & f_3(S_1) & \phi^{\frac{3}{4}} f_4(S_4) \end{bmatrix} \tag{A.35}$$

avec $f_n(S_i) = \sum_{k=1:4} s_k^i (j^{n-1}\theta)^{k-1}$ une combinaison linéaire des symboles $\{s_1^i, s_2^i, s_3^i, s_4^i\}$, $\phi = \exp(\frac{i\pi}{6})$, $\theta = \exp(\frac{i\pi}{8})$. Dans un travail récent [113], Okonkwo a démontré que le codage à délaie et diversité ramène un gain considérable en OSNR dans une transmission sur fibre à 3 modes. Toutefois, à cause de la redondance temporelle des symboles transmit, la capacité du système est réduite et au meilleur cas la capacité d'une fibre monomode pouvait être atteinte. Dans notre codage ST, 16 différents symboles QPSK sont transmit durant 4 temps symbole sur chaque matrice de mot de code, ce qui permet d'avoir un débit plein de 4 symboles par utilisation du canal.

Ligne optique et récepteur:

La configuration utilisée est montrée dans la figure E.19. 10m de FMF à saut d'indice supportant la propagation de 12 modes spatiaux est utilisé. Deux modes LP non dégénérés $\{LP_{01}, LP_{02}\}$ et cinq dégénérés $\{LP_{11a,b}, LP_{21a,b}, LP_{31a,b}, LP_{12a,b}, LP_{41a,b}\}$. La différence d'indice effectif entre deux modes LP est supérieure à 9×10^{-4} pour minimiser le couplage entre modes, seulement les modes dégénérés du même mode LP sont fortement couplés [114]. Une telle fibre présente une larde DMGD ($\sim$ 14ps/m entre le LP_{01} et le LP_{02}). Par conséquent, le LP_{01} et LP_{02} peuvent être utilisés comme canaux de transmission indépendants. Pour injecter les signaux des fibres monomodes sur les modes spatiaux à l'entrée de la FMF et pour extraire les modes spatiaux de la FMF vers les fibres monomodes nous utilisons des MUX et DEMUX à 10 modes basés sur la conversion

de lumière multi-plans [59]. Pour caractériser les performances du MUX / DEMUX et la FMF, nous avons mesuré la perte d'insertion (IL) et la diaphonie (XT) entre les modes comme dans [59], les résultats sont moyennés par groupe de modes dégénérés et sont reportés dans le tableau A.3. le IL moyen (respectivement XT moyen) a été mesuré comme étant de -6,8 dB (resp. -19 dB).
Puisque nous sommes limités à seulement deux récepteurs cohérents, nous choisissons d'utiliser le LP_{01} et le LP_{02} pour multiplexer les données. Cet ensemble de modes nous permet de maintenir une quantité déterministe de MDL dans la transmission, plutôt que les modes fortement couplés dégénérés, où une étude statistique avec plus d'acquisitions de canaux est nécessaire. Pour émuler différents niveaux de MDL, deux atténuateurs variables sont insérés avant les ∼10m de la FMF pour ajuster le déséquilibre de puissance entre les modes spatiaux. Avec cette stratégie nous avons émulé différents niveaux de MDL. Après l'ajout du bruit au niveau du récepteur, les signaux sont détectés par des récepteurs

Table A.3: Insertion Loss (valeurs diagonales), crosstalk (valeurs non diagonales) pour le système formé de la FMF et des MUX/DEMUX.

Unit: dB	Output LP_{01}	Output $LP_{11a,b}$	Output $LP_{21a,b}$	Output LP_{02}	Output $LP_{12a,b}$	Output $LP_{31a,b}$
Input LP_{01}	-6.01	-16	-19	-17	-23	-30
Input $LP_{11a,b}$	-16	-6.80	-18	-22	-20	-22
Input $LP_{21a,b}$	-18	-19	-7.22	-15	-20	-20
Input LP_{02}	-17	-21	-17	-6.11	-19	-28
Input $LP_{12a,b}$	-23	-18	-19	-18	-7.96	-15
Input $LP_{31a,b}$	-25	-21	-18	-21	-14	-7.27

cohérents et ensuite échantillonnés à 100 GSymboles/s en utilisant des oscilloscopes Tektronix. Pour chaque valeur de MDL et OSNR, 5.10^6 échantillons sont enregistrés et un traitement hors ligne est effectué pour mesurer les BERs et les facteurs Q correspondants.

Tout d'abord, l'algorithme de Schmidl et Cox traite les signaux OFDM reçus pour une synchronisation temporelle et compense le décalage de fréquence des porteuses. Ensuite, la correction d'erreur de phase est effectuée en utilisant les 10 sous-porteuses pilotes. Après cela, le canal est estimé en utilisant la séquence d'apprentissage et l'estimateur LSE comme expliqué dans la sous-section 4.1.2.2. Enfin, un décodage à maximum de vraisemblance (ML) est effectué suivi d'une démodulation et d'un comptage d'erreur.

A.3.3.2 Résultats expérimentaux

Avant de transmettre des signaux OFDM codés en ST, nous effectuons des mesures préliminaires du BER en émettant des symboles QPSK indépendants non codés. Nous

évaluons les performances pour différents niveaux de MDL. Dans la figure E.20, nous traçons les performances du BER en fonction de l'OSNR. A partir de la figure, nous pouvons clairement remarquer la dégradation causée par MDL sur les performances du système. Pour un BER $= 10^{-3}$, lorsque la MDL est de 3 dB, la dégradation par rapport au canal sans MDL est de 2 dB et lorsque le niveau de MDL atteint 10 dB, la dégradation passe à 6 dB.

Après ces mesures préliminaires, nous procédons à une transmission OFDM codée en ST. Pour montrer les gains de codage ST obtenus, dans figure E.21, nous comparons les performances d'un système codé en ST par rapport à une transmission non codée. À partir de la figure, nous remarquons un gain important obtenu par le codage ST par rapport au schéma non codé. Pour un BER $= 10^{-3}$, un gain de 1.4 dB (resp. 2 dB) est observé pour MDL = 6 dB (resp. MDL = 10 dB).

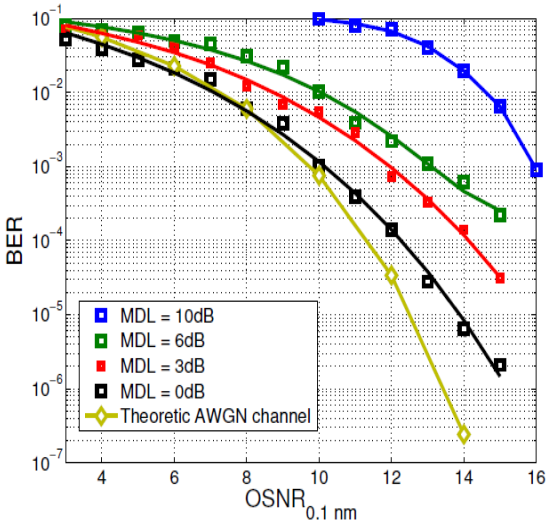

Figure E.20: BER vs OSNR pour différentes MDL, système non codé.

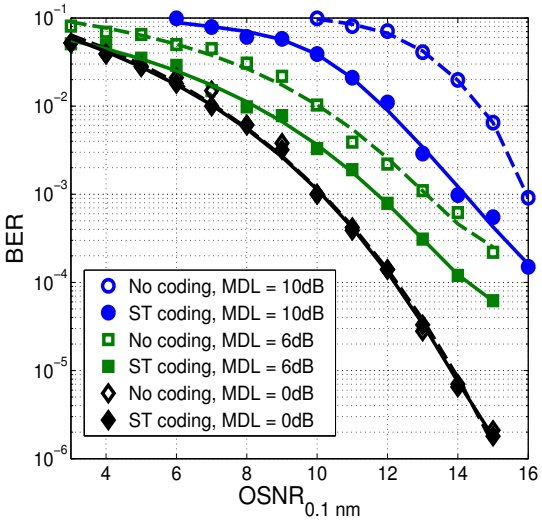

Figure E.21: BER vs OSNR avec et sans codage ST, MDL= 0, 6, 10 dB

Les gains apportés par le codage ST s'expliquent par le fait que le même signal est transmis sur les deux modes affectés par différentes atténuations. Cela permet au signal d'expérimenter différentes conditions du canal. Au niveau du récepteur, le détecteur ML estime les données à partir de différentes copies atténuées différemment et donne donc une meilleure estimation.

De plus, nous avons calculé pour une MDL allant de 0 à 10 dB les pénalités en facteur Q obtenues pour les schémas non codés et codé en ST par rapport à un système sans MDL à un OSNR de 14 dB. Les résultats sont reportés sur la figure E.22. À partir de

la figure, nous remarquons que la transmission codée en ST surpasse la transmission non codée. La pénalité en facteur Q est réduite de 1.1 dB lorsque la MDL est de 6 dB et de 3.4 dB lorsque la MDL atteint 10 dB.

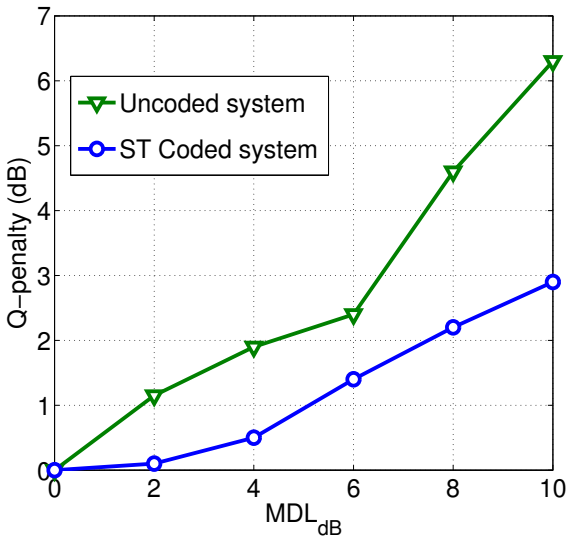

Figure E.22: Q-penalty vs MDL pour un OSNR = 14 dB

A.4 Conclusions

La croissance continue de la demande pour plus de capacité optique entraînera probablement un changement majeur dans l'architecture du réseau optique. Au cours de la dernière décennie, des systèmes PDM cohérents commerciaux fonctionnant à 100 Gb/s étaient suffisants pour acheminer le trafic de données dans le réseau optique. Cependant, avec la croissance exponentielle du trafic générée par le développement d'Internet et le nombre croissant d'utilisateurs et de machines connectés, la situation est sur le point de changer. L'augmentation de l'efficacité spectrale par des formats de modulation plus élevés et la réduction de l'espacement traditionnel entre canaux WDM par des techniques comme le Nyquist-WDM où la largeur de bande de la porteuse est rectangulaire et égale au débit symbole ont permis de démontrer des systèmes fonctionnant autour de 100 Tb/s. De plus, le multiplexage spatial est le dernier degré qui permettra d'aller au-delà de la capacité de 100 Tb/s.

Dans cette thèse, nous nous sommes intéressés aux fibres faiblement multimode en tant que réalisation possible du multiplexage spatial. La meilleure mise en œuvre du MDM n'est pas encore un point d'accord de tous les laboratoires de recherche. En effet, alors que certaines équipes de recherche considèrent que les transmissions de modes à faible

couplage ayant une DMGD élevé sont très simples sur le plan logistique, d'autres proposent des modes à fort couplage avec une faible DMGD comme solution attractive avec des fonctionnalités prometteuses. Dans les deux cas, la MDL, un effet non-unitaire, a un impact négatif sur la capacité et la qualité de la transmission des systèmes optiques MDM. En conséquence, pour réduire l'impact de la MDL, les principales contributions consistent à améliorer les composants fabriqués pour introduire une faible MDL. Cependant, même avec des composants optiques sophistiqués pour le MDM, la MDL accumulé sur toute la ligne peut atteindre des niveaux importants.
Dans notre travail, nous proposons des techniques de codage DSP modernes pour améliorer la capacité et la fiabilité des systèmes MDM. Ces solutions DSP peuvent être complémentaires à l'avancement des composants optiques pour réduire la MDL. De plus, les techniques DSP mises en œuvre peuvent être évolutives lorsque le nombre de modes augmente, ce qui en fait une solution à fort potentiel pour les systèmes optiques actuels et futurs.
Les systèmes MDM permettent d'augmenter la capacité des systèmes optiques par le nombre de modes. Cependant, en présence de la MDL, cette capacité est réduite. Dans ce travail, nous avons étudié les capacités moyennes et de coupures des systèmes optiques MDM et nous avons proposé trois techniques pour les améliorer. Premièrement, nous avons montré que l'information sur l'état du canal (CSI) donne des informations pertinentes sur le canal optique et peut être utilisée au niveau de l'émetteur pour augmenter la capacité. De plus, nous avons proposé un CSI statistique pour l'amélioration de la capacité avec une complexité de mise en œuvre réduite. Deuxièmement, nous avons proposé une stratégie de brouillage déterministe pour permuter les modes ayant plus de puissance avec ceux ayant moins. Cette stratégie de brouillage permet de réduire l'effet de la MDL en moyennant la puissance plus efficacement entre les modes augmentant ainsi les capacités moyennes et de coupure. Enfin, nous avons montré que la sélection de mode qui consiste à utiliser des fibres à large cœur au lieu de fibres à petit cœur est une solution à haut potentiel pour commencer à déployer des fibres supportant un nombre élevé de modes tout en obtenant de meilleures performances. Pour une amélioration supplémentaire des performances, les trois techniques précédentes peuvent être combinées pour avoir une grande infrastructure MIMO où seuls des schémas MIMO de faible complexité sont utilisés avec le brouillage de mode et CSI pour augmenter la capacité.

Par la suite, nous avons étudié les avantages du codage ST pour atténuer la MDL dans les systèmes optiques MDM. Nous avons mené une étude complète, théorique, par simulations et expérimentale pour valider l'efficacité du codage ST. Nous avons commencé par une dérivation de la borne supérieure de probabilité d'erreur du canal MDM affecté

par la MDL. Cette borne supérieure nous a permis d'expliquer le gain de codage obtenu par le codage ST et nous avons pu définir un critère de conception pour la construction des codes ST afin d'atténuer complètement la MDL. Nous avons montré que l'orthogonalité des différences de mot de code est le paramètre important qui permet d'absorber la MDL. Pour compléter notre étude, nous avons validé les résultats obtenus précédemment en effectuant une démonstration expérimentale de la transmission optique MDM codée en ST. Dans cette étude, nous avons utilisé le format OFDM pour gérer la DMGD de la fibre et réduire la complexité de décodage ML. Nous avons considéré un système MIMO de dimension 4×4 en transmettant sur deux modes avec les deux polarisations. Les résultats expérimentaux obtenus montrent que le codage ST apporte une amélioration significative du BER en présence de la MDL.

Bibliography

[1] "Cisco Visual Networking Index" Forecast and methodology 2015-2020. *Cisco Systems, Inc*, 2015. Cited pages xi, xiv, 7, 8, 119, and 120

[2] D.J. Richardson, J.M. Fini, and L.E. Nelson. "Space-division multiplexing in optical fibres". *Nature Photonics*, (7):354–362, 2013. Cited pages xi, xiv, 2, 10, and 122

[3] P.J. Winzer. "Spatial multiplexing in fiber optics: The 10x scaling of metro/core capacities". *Bell Labs Technical Journal*, (19):22–30, 2014. Cited pages xi and 28

[4] Tingye Li. "Optical Fiber Communication-The State of the Art". *IEEE Transactions on Communications*, (26):946–955, 1978. Cited pages 1, 10, and 121

[5] L. Gruner-Nielsen et al. "Few Mode Transmission Fiber With Low DGD, Low Mode Coupling, and Low Loss". *Journal of Lightwave Technology*. Cited page 2

[6] Elie Awwad, Ghaya Rekaya-Ben Othman, and Yves Jaouën. "Space-Time Coding Schemes for MDL-Impaired Mode-Multiplexed Fiber Transmission Systems". *Journal of Lightwave Technology*, (33):5084–5094, 2015. Cited pages 3, 63, 77, 124, and 136

[7] M. P. Yankov, D. Zibar, K. J. Larsen, L. P. B. Christensen, and S. Forchhammer. "Constellation Shaping for Fiber-Optic Channels With QAM and High Spectral Efficiency". *IEEE Photonics Technology Letters*, (26):2407–2410, 2014. Cited pages 9 and 120

[8] S. Fujita, M. Kitamura, T. Torikai, N. Henmi, H. Yamada, T. Suzaki, I. Takano, K. Komatsu, and M. Shikada. "A 10-Gb/s 100-km optical fiber transmission experiment using a high-speed MQWDFB-LD and a back-illuminated InGaAs-APD". *in Proc. Picosecond Electronics Optoelectronics Conf*, Postdeadline paper-3. 1989. Cited pages 10 and 122

[9] Tingye Li. "The impact of optical amplifiers on long-distance lightwave telecommunications". *in Proceedings of the IEEE*, (82):1568–1579, 1993. Cited pages 10 and 122

[10] H. Kogelnik. "High-capacity optical communications: personal recollections". *in IEEE Journal of Selected Topics in Quantum Electronics*, (6):1279–1286, 2000. Cited pages 10 and 122

[11] D. Qian, M. Huang, E. Ip, Y. Huang, Y. Shao, J. Hu, and T. Wang. "101.7-Tb/s (370×294-Gb/s) PDM-128QAM-OFDM Transmission over 3×55-km SSMF using Pilot-based Phase Noise Mitigation". *Optical Fiber Communication Conference*, paper PDPB5, 2011. Cited pages 11 and 122

[12] R. J. Essiambre, R. Ryf, N. K. Fontaine, and S. Randel. "Breakthroughs in Photonics 2012: Space-Division Multiplexing in Multimode and Multicore Fibers for High-Capacity Optical Communication". *in IEEE Photonics Journal*, (5):pp. 0701307, 2013. Cited pages 11 and 123

[13] Nicolas K. Fontaine. "Components For Space-Division Multiplexing". *European Conference on Optical Communication*, paper W3F1, 2017. Cited pages 11 and 123

[14] Roland Ryf, Nicolas K. Fontaine, Sun Hyok Chang, Juan Carlos Alvarado, Bin Huang, José Antonio-Lopez, Haoshuo Chen, René-Jean Essiambre, Ellsworth Burrows, Robert W. Tkach, Rodrigo Amezcua-Correa, Tetsuya Hayashi, Yoshiaki Tamura, Takemi Hasegawa, and Toshiki Taru. "Long-Haul Transmission over Multi-Core Fibers with Coupled Cores". *European Conference on Optical Communication*, paper M2E1, 2017. Cited pages 11 and 123

[15] H. Shalom, A. Zadok, M. Tur, P. J. Legg, W. D. Cornwell, and I. Andonovic. "On the various time constants of wavelength changes of a DFB laser under direct modulation". *in IEEE Journal of Quantum Electronics*, 34:1816–1822, 1998. Cited page 13

[16] K. Nosu. "Advanced coherent lightwave technologies". *in IEEE Communications Magazine*, (26):15–21, 1988. Cited page 17

[17] Govind P. Agrawal. "Fiber-Optic Communication Systems". *Wiley Series in Microwave and Optical Engineering*, Third edition, 2002. Cited pages 18, 19, 22, and 25

[18] R. M. Jopson, L. E. Nelson, G. J. Pendock, and A. H. Gnauck. "Polarization-mode dispersion impairment in return-to-zero and nonreturn-to-zero systems". *Optical Fiber Communication Conference*, WE3-1, 1999. Cited page 23

[19] H. Jiang, R. Saunders, and S. Colaco. "SiGe equalizer IC for PMD mitigation and signal optimization of 40 Gbits/s transmission". *Optical Fiber Communication Conference*, paper OWO2, 2005. Cited page 23

[20] Seb J. Savory. "Digital filters for coherent optical receivers". *Opt. Express*, (16):804–817, 2008. Cited page 23

[21] Sander L. Jansen, Itsuro Morita, Tim C. W. Schenk, and Hideaki Tanaka. "Long-haul transmission of 16x52.5 Gbits/s polarization-division multiplexed OFDM enabled by MIMO processing". *Journal of optical networking*, (7):173–182, 2008. Cited pages 23 and 99

[22] M. A. Bhatti and A. S. Siddiqui. "Measurement of polarization dependent loss in optical fiber and bulk optical devices". *Optical Fiber Measurement Conference*, pp.25–26, 1995. Cited page 24

[23] L. Ducos, R. Clin, P. Blanchard, and F. Gautier. "Polarization dependent loss of passive optical components". *Optical Fiber Measurement Conference*, pp.25–26, 1995. Cited page 24

[24] N Gisin. "Statistics of polarization dependent losses". *Optics Communications*, (114):399–405, 1995. Cited page 24

[25] Antonio Mecozzi and Mark Shtaif. "The Statistics of Polarization-Dependent Loss in Optical Communication Systems". *IEEE Photonics technology letters*, (14):313–315, 2002. Cited page 24

[26] T. Duthel, C. R. S. Fludger, J. Geyer, and C. Schulien. "Impact of Polarisation Dependent Loss on Coherent POLMUX-NRZ-DQPSK". *Conference on Optical Fiber Communication*, OThU5, 2008. Cited pages 25 and 104

[27] C. Zhu, Binhuang Song, Leimeng Zhuang, B. Corcoran, and A. J. Lowery. "Pairwise coding to mitigate polarization dependent loss". *Optical Fiber Communications Conference*, W4K.4, 2015. Cited page 25

[28] Elie Awwad, Yves Jaouën, and Ghaya Rekaya-Ben Othman. "Polarization-time coding for PDL mitigation in long-haul PolMux OFDM systems". *Opt. Express*, (21):22773–22790, 2013. Cited pages 25, 63, and 136

[29] A. D. Ellis, M. E. McCarthy, M. A. Z. Al Khateeb, M. Sorokina, and N. J. Doran. "Performance limits in optical communications due to fiber nonlinearity". *Adv. Opt. Photon.*, (9):429–503, 2017. Cited page 27

[30] E. Desurvire, J. R. Simpson, and P. C. Becker. "High-gain erbium-doped traveling-wave fiber amplifier". *Opt. Lett*, (12):888–890, 1987. Cited page 27

[31] R. J. Mears, L. Reekie, I.M. Jauncey, and D.N. Payne. "Low-noise erbium-doped fibre amplifier operating at 1.54 um". *Electronics Letters*, (23):1026–1028, 1987. Cited page 27

[32] P. M. Becker, A. Olsson, and J. R. Simpson. "Erbium-Doped Fiber Amplifiers : Fundamentals and Technology". *Academinc press*, 1999. Cited page 27

[33] René-Jean Essiambre, Gerhard Kramer, Peter J. Winzer, Gerard J. Foschini, and Bernhard Goebel. "Capacity Limits of Optical Fiber Networks". *Journal of Lightwave Technology*, (28):662–701, 2010. Cited page 28

[34] Peter J. Winzer and Gerard J. Foschini. "MIMO capacities and outage probabilities in spatially multiplexed optical transport systems". *Opt. Express*, (19):16680–16696, 2011. Cited pages 28, 32, 33, 47, 58, 77, 100, 126, and 136

[35] R. Ryf et al. "Mode-Division Multiplexing Over 96 km of Few-Mode Fiber Using Coherent 6x6 MIMO Processing". *Journal of Lightwave Technology*, (30):521–531, 2012. Cited pages 30 and 101

[36] Adriana Lobato, Filipe Ferreira, Maxim Kuschnerov, Dirk van den Borne, Sander L. Jansen, Antonio Napoli, Bernhard Spinnler, and Berthold Lankl. "Impact of mode coupling on the mode-dependent loss tolerance in few-mode fiber transmission". *Optics Express*, (20):29776–29783, 2012. Cited pages 30, 33, 77, and 136

[37] S. Ö. Arik, D. Askarov, and J. M. Kahn. "Effect of Mode Coupling on Signal Processing Complexity in Mode-Division Multiplexing". *Journal of Lightwave Technology*, (31):423–431, 2013. Cited pages 30 and 32

[38] Clemens Koebele, Massimiliano Salsi, Laurent Milord, Roland Ryf, Cristian Bolle, Pierre Sillard, Sébastien Bigo, and Gabriel Charlet. "40km Transmission of Five Mode Division Multiplexed Data Streams at 100Gb/s with low MIMO-DSP Complexity". *37th European Conference and Exposition on Optical Communications*, Th.13.C.3.4, 2011. Cited page 30

[39] P. Sillard, M. Bigot-Astruc, and D. Molin. "Few-Mode Fibers for Mode-Division-Multiplexed Systems". *Journal of Lightwave Technology*, (32):2824–2829, 2014. Cited page 31

[40] Keang-Po Ho and Joseph M. Kahn. "Statistics of Group Delays in Multimode Fiber With Strong Mode Coupling". *Journal of Lightwave Technology*, (29):3119–3128, 2011. Cited page 31

[41] Luca Palmieri. "Modal Dispersion Properties of Few-Mode Spun Fibers". *Optical Fiber Communications Conference*, Tu2D.4, 2015. Cited page 31

[42] F. Ferreira, S. Sygletos, and A. D. Ellis. "Impact of linear mode coupling on the group delay spread in Few-mode fibers". *Optical Fiber Communications Conference*, Tu2D.1, 2015. Cited page 31

[43] Filipe M. Ferreira, Naoise Mac Suibhne, Stylianos Sygletos, and Andrew D. Ellis. "Few-Mode Fibre Group-Delays with Intermediate Coupling". *European Conference on Optical Communication*, pp 0201, 2015. Cited page 31

[44] Keang-Po Ho and Joseph M. Kahn. "Mode-dependent loss and gain: statistics and effect on mode-division multiplexing". *Opt. Express*, (19):16612–16635, 2011. Cited pages 32, 33, 39, 47, 48, 100, 126, and 127

[45] A. Lobato et al. "Maximum-Likelihood Detection in Few-Mode Fiber Transmission With Mode-Dependent Loss". *in IEEE Photonics Technology Letters*, (25):1095–1098, 2013. Cited page 32

[46] Stefan Warm and Klaus Petermann. "Splice loss requirements in multi-mode fiber mode-division-multiplex transmission links". *Opt. Express*, (19):519–532, 2013. Cited pages 32, 48, 100, and 127

[47] Sun Hyok Chang, Sang-Rok Moon, Haoshuo Chen, Roland Ryf, Nicolas K. Fontaine, Kyung Jun Park, Kwangjoon Kim nad, and Joon Ki Lee. "All-fiber 6-mode multiplexers based on fiber mode selective couplers". *Opt. Express*, (25):5734–5741, 2017. Cited page 32

[48] A. Li, J. Ye, X. Chen, and W. Shieh. "Fabrication of a Low-Loss Fused Fiber Spatial-Mode Coupler for Few-Mode Transmission". *in IEEE Photonics Technology Letters*, (25):1985–1988, 2013. Cited pages 32, 33, 34, 100, 101, and 102

[49] Guillaume Le Cocq, Yves Quiquempois, Antoine Le Rouge, Géraud Bouwmans, Hicham El Hamzaoui, Karen Delplace, Mohamed Bouazaoui, and Laurent Bigot. "Few mode Er3+ doped fiber with micro-structured core for mode division multiplexing in the C-band". *in Workshop on Specialty Optical Fibers and their Applications,*, (21):31646–31659, 2013. Cited page 32

[50] E. Ip et al. "146 x 6 x 19-Gbaud Wavelength-and Mode-Division Multiplexed Transmission Over 10 x 50-km Spans of Few-Mode Fiber With a Gain-Equalized Few-Mode EDFA". *in Journal of Lightwave Technology*, (32):790–797, 2014. Cited page 32

[51] P. J. Winzer, H. Chen, R. Ryf, K. Guan, and S. Randel. "Mode-dependent loss, gain, and noise in MIMO-SDM systems'. *European Conference on Optical Communication*, Mo.3.3.2, 2014. Cited page 33

[52] A. Lobato, F. Ferreira, J. Rabe, M. Kuschnerov, B. Spinnler, and B. Lankl. "Mode scramblers and reduced-search maximum-likelihood detection for mode-dependent-loss-impaired transmission". *European Conference on Optical Communication*, pages pp. 1–3, 2014. Cited pages 33, 57, and 133

[53] Yunhe Zhao, Yunqi Liu, Liang Zhang, Chenyi Zhang, Jianxiang Wen, and Tingyun Wang. "Mode converter based on the long-period fiber gratings written in the two-mode fiber". *Opt. Express*, (24):6186–6195, 2016. Cited pages 33, 34, 100, and 102

[54] R. Ryf, C. Bolle, and J. von Hoyningen-Huene. "Optical coupling components for spatial multiplexing in multi-mode fibers". *European Conference on Optical Communication*, page Th.12.B.1, 2011. Cited page 34

[55] M. Salsi et al. "Mode-Division Multiplexing of 2 x 100 Gb/s Channels Using an LCOS-Based Spatial Modulator". *in Journal of Lightwave Technology*, (30):618–623, 2012. Cited page 34

[56] A. Li, A. A. Amin, X. Chen, S. Chen, G. Gao, and W. Shieh. "Reception of Dual-Spatial-Mode CO-OFDM Signal Over a Two-Mode Fiber". *Journal of Lightwave Technology*, (30):634–640, 2012. Cited page 34

[57] A. Li, X. Chen, A. Amin, and W. Shieh. "Fused Fiber Mode Couplers for Few-Mode Transmission". *in IEEE Photonics Technology Letters*, (24):1953–1956, 2012. Cited page 34

[58] N. Hanzawa, K. Saitoh, T. Sakamoto, T. Matsui, S. Tomita, and M. Koshiba. "Demonstration of mode-division multiplexing transmission over 10 km two-mode fiber with mode coupler". *Optical Fiber Communications Conference*, WA4.4, 2011. Cited page 34

[59] G. Labroille, P. Jian, N. Barre, B. Denolle, and J. F. Morizur. "Mode selective 10-mode multiplexer based on multi-plane light conversion". *Optical Fiber Communication Conference*, Th3E.5, 2015. Cited pages 34, 109, and 146

[60] Sebastian Randel, Roland Ryf, Alberto Sierra, Peter J. Winzer, Alan H. Gnauck, Cristian A. Bolle, René-Jean Essiambre, David W. Peckham, Alan McCurdy, and Robert Lingle. "6x56-Gb/s mode-division multiplexed transmission over 33-km few-mode fiber enabled by 6x6 MIMO equalization". *Opt. Express*, (19):16697–16707, 2011. Cited page 35

[61] A. Viterbi. "Nonlinear estimation of PSK-modulated carrier phase with application to burst digital transmission". *IEEE Transaction on Information Theory*, (29):543–551, 1982. Cited page 35

[62] C. Shannon. "A mathematical theory of communication". *Bell Sys. Tech. Journal*, (24):379–423, 1948. Cited page 40

[63] C.E. Shannon. "Communication in the Presence of Noise". *Proceedings of the IRE*, (37):10–21, 1949. Cited page 41

[64] E. Telatar. "Capacity of multi-antenna Gaussian channels". *European Transaction. on Telecommunication*, (6):585–596, 1999. Cited pages 42 and 43

[65] Yang Wen Liang. "Ergodic and outage capacity of narrowband MIMO Gaussian channels". *Department of Electrical and Computer Engineering, University of British Columbia*, 2005. Cited pages 43 and 44

[66] A. Tulino, A. Lozano, and S. Verdu. "MIMO capacity with channel state information at the transmitter". *Eighth IEEE International Symposium on Spread Spectrum Techniques and Applications*, pages 22–26, 2005. Cited pages 43, 49, and 127

[67] G. Caire and S. Shamai. "On the capacity of some channels with channel state information". *in IEEE Transactions on Information Theory*, (45):2007–2019, 1999. Cited pages 43, 49, and 127

[68] H.-G. Unger. "Planar Optical Waveguides and Fibers". *Oxford University Press*, 1977. Cited pages 47 and 126

[69] C. Koebele, M. Salsi, G. Charlet, and S. Bigo. "Nonlinear Effects in Mode-Division-Multiplexed Transmission Over Few-Mode Optical Fiber". *Photonics Technology Letters*, (23):1316–1318, 2011. Cited pages 49 and 127

[70] W. F. Love. "Novel mode scrambler for use in optical-fiber bandwidth measurements". *Optical Fiber Communications Conference*, ThG2, 1979. Cited pages 52 and 130

[71] S. Warm and K. Petermann. "Capacity increase in spliced mode-multiplexed transmission systems by using mode mixers". *IEEE Photonics Society Summer Topical Meeting Series*, pages pp. 201–202, 2012. Cited pages 52 and 130

[72] Andreas F. Molisch, Moe Z. Win, Yang-Seok Choi, and Jack H. Winters. "Capacity of MIMO systems with antenna selection". *IEEE Transaction on Wireless Communications*, (3):1759–1771, 2005. Cited page 58

[73] Sang Wu Kim and Eun Yong Kim. "Optimum receive antenna selection minimizing error probability". *IEEE Wireless Communications and Networking*, (1):441–447, 2003. Cited page 58

[74] Xi Chen, Jia Ye, Yue Xiao, An Li, and Jiayuan He. "Equalization of two-mode fiber based MIMO signals with larger receiver sets". *IEEE Wireless Communications and Networking*, (20):B413–B418, 2012. Cited page 58

[75] John G. Proakis. "Digital Communications". Fifth edition- Hill Internationnal edition, 2008. Cited pages 65, 66, 87, and 88

[76] V. Tarokh, N. Seshadri, and AR. Calderbank. "Space-time codes for high data rate wireless communication: performance criteria and code construction". *IEEE Transactions on Information Theory*, (49):744–765, 1998. Cited page 66

[77] David Tse and Pramod Viswanath. "Fundamentals of Wireless communications". *Cambridge university press*, 2005. Cited page 67

[78] Babak Hassibi and Bertrand M. Hochwald. "High rate codes that are linear in space and time". *IEEE Transactions on Information Theory*, (48):1804–1824, 2002. Cited page 67

[79] S. Alamouti. "A simple transmit diversity technique for wireless communications". *IEEE Journal on selected areas in communications*, (16):1451–1458, 1998. Cited page 69

[80] T. Vahid, H. Jafarkhani, and A.R. Calderbank. "Space-time block codes from orthogonal designs". *IEEE Transactions on Information Theory*, (45):1456–1467, 1999. Cited pages 69 and 70

[81] J.C Belfiore, G. Rekaya, and E. Viterbo. "The golden code: a 2x2 full rate space time code with nonvanishing determinant". *IEEE Transactions on Information Theory*, (51):1432–1436, 2005. Cited page 70

[82] Ezio Biglieri, Yi Hong, and Emanuele Viterbo. "On fast decodable space time block codes". *IEEE Transactions on Information Theory*, (55):542–530, 2009. Cited page 70

[83] H. El-Gamal and M. O. Damen. "Universal space-time coding". *IEEE Transactions on Information Theory*, (49):1097–1119, 2003. Cited pages 71 and 89

[84] Emanuele Viterbo and Joseph Boutros. "A universal lattice code decoder for fading channels". *IEEE Transactions on Information Theory*, (55):1639–1642, 1999. Cited page 73

[85] Oussama Damen, Ammar Chkeif, and Jean-Claude Belfiore. "Lattice Code Decoder for Space-Time Codes". *IEEE Communications Letters*, (4):161–163, 2000. Cited page 74

[86] M. Biguesh and A. B. Gershman. "Training-based MIMO channel estimation: a study of estimator tradeoffs and optimal training signals". *IEEE Transactions on Signal Processing*, (54):884–893, 2006. Cited page 75

[87] G. J. Foschini, G. D. Golden, R. A. Valenzuela, and P. W. Wolniansky. "Simplified processing for high spectral efficiency wireless communication employing multi-element arrays". *IEEE Journal on Selected Areas in Communications*, (17):1841–1852, 1999. Cited page 76

[88] K. Guan, P. J. Winzer, and M. Shtaif. "BER Performance of MDL-Impaired MIMO-SDM Systems With Finite Constellation Inputs". *IEEE Photonics Technology Letters*, (12):1223–1226, 2014. Cited pages 77 and 136

[89] Kyle Guan, Antonia M. Tulino, Peter J. Winzer, and Emina Soljanin. "Secrecy Capacities in Space-Division Multiplexed Fiber Optic Communication Systems". *IEEE Transactions on Information Forensics and Security*, (7):1235–1335, 2015. Cited pages 78 and 136

[90] O. Tirkkonen and A. Hottinen. "Square-matrix embeddable space-time block codes for complex signal constellations". *IEEE Transactions on Information Theory*, (48):384–395, 2002. Cited pages 78 and 137

[91] F. Mezzadri. "How to generate random matrices from the classic compact groups". *Notices of the American Mathematical Society*, (54):592–604, 2007. Cited pages 80 and 139

[92] Alex Alvarado, Erik Agrell, Domanic Lavery, and Polina Bayvel. "LDPC Codes for Optical Channels: Is the "FEC Limit" a Good Predictor of Post-FEC BER?". *Optical Fiber Communication Conference*, Th3E.5, 2015. Cited page 84

[93] R. G. Gallager. "Low-density parity-check codes". *IRE Transactions on Information Theory*, (48):21–28, 1962. Cited page 85

[94] S. Mumtaz, J. Li, S. Koenig, Y. Jaouën, R. Schmogrow, G. Rekaya-Ben Othman, and J. Leuthold. "Experimental Demonstration of PDL Mitigation using Polarization-Time Coding in PDM-OFDM Systems". *Signal Processing in Photonics Communications Conference*, SPWB6, 2011. Cited page 93

[95] E. Awwad, G. R. B. Othman, and Y. Jaouën. "Design criterion of polarization-time codes for optical fiber channels". *IEEE International Conference on Communications ICC*, pages 3428–3432, 2013. Cited page 93

[96] E. Awwad, G. Rekaya-Ben Othman, Y. Jaouën, and Y. Frignac. "Space-Time Codes for Mode-Multiplexed Optical Fiber Transmission Systems". *Advanced Photonics for Communications*, SM2D.4, 2014. Cited pages 93, 100, 104, and 106

[97] "Part 11: Wireless LAN Medium Access Control (MAC) and Physical Layer (PHY) Specifications: High-Speed Physical Layer in the 5 GHz Band". *IEEE Standard 802.11a*, 1999. Cited page 94

[98] Q. Pan and R. J. Green. "Bit-error-rate performance of lightwave hybrid AM/OFDM systems with comparison with AM/QAM systems in the presence of clipping impulse noise". *Electron. Lett.*, (8):278–280, 1996. Cited page 94

[99] A. J. Lowery, L. Du, and J. Armstrong. "Orthogonal frequency division multiplexing for adaptive dispersion compensation in long haul WDM systems". *Optical fiber communication conference*, PDP, 2006. Cited page 94

[100] W. Shieh and C. Athaudage. "Coherent optical orthogonal frequency division multiplexing". *Electron. Lett.*, (42):587–589, 2006. Cited page 94

[101] Y. Lu et al. "Experimental comparison of 32-Gbaud Electrical-OFDM and Nyquist-WDM transmission with 64GSa/s DAC". *European Conference on Optical Communication*, We.1.C.3, 2013. Cited page 94

[102] W. Shieh. "PMD-supported coherent optical OFDM systems". *IEEE Photonics Technology Letters*, (19):134–136, 2007. Cited page 94

[103] W. Shieh, X. Yi, , and Y. Tang. "Transmission experiment of multi-gigabit coherent optical OFDM systems over 1000 km SSMF fiber". *Electron. Lett.*, (43):183–185, 2007. Cited page 95

[104] S. L. Jansen, I. Morita, N. Takeda, and H. Tanaka. "20-Gb/s OFDM transmission over 4160-km SSMF enabled by RF-Pilot tone phase noise compensation". *Optical Fiber Communication Conference*, PDP15, 2007. Cited page 95

[105] V. Sleiffer et al. "73.7 Tb/s (96 x 3 x 256-Gb/s) mode-division-multiplexed DP-16QAM transmission with inline MM-EDFA". *European Conference on Optical Communication*, Th.3.C.4, 2012. Cited page 95

[106] R. Ryf et al. "10-Mode Mode-Multiplexed Transmission with Inline Amplification". *European Conference on Optical Communication*, pp. 1-3, 2016. Cited page 95

[107] Beril Inan et al. "DSP complexity of mode-division multiplexed receivers". *Optics Express*, (20):10859–10869, 2012. Cited pages 95 and 96

[108] W. Shieh, X. Yi, Y. Ma, and Y. Tang. "Theoretical and experimental study on PMD-supported transmission using polarization diversity in coherent optical OFDM systems". *Optics Express*, (15):9936–9947, 2007. Cited page 95

[109] X. Yi, W. Shieh, and Y. Ma. "Phase Noise Effects on High Spectral Efficiency Coherent Optical OFDM Transmission". *Journal of Lightwave Technology*, (26):1309–1316, 2008. Cited page 98

[110] T. M. Schmidl and D. C. Cox. "Robust frequency and timing synchronization for OFDM". *IEEE Transactions on Communications*, (45):1613–1621, 1997. Cited page 99

[111] Mahdieh B. Shemirani, Wei Mao, Rahul Alex Panicker, and Joseph M. Kahn. "Principal Modes in Graded-Index Multimode Fiber in Presence of Spatial- and Polarization-Mode Coupling ". *Journal of Lightwave Technology*, (27):1248–1261, 2009. Cited page 101

[112] B. Inan et al. "Low computational complexity mode division multiplexed ofdm transmission over 130 km of few mode fiber". *Optical fiber communication conference*, OW4F.4, 2013. Cited page 107

[113] Chigo Okonkwo, Roy van Uden, Haoshuo Chen, Huug de Waardt, and Ton Koonen. "Advanced coding techniques for few mode transmission systems". *Journal of Lightwave Technology*, (23):1411–1420, 2015. Cited pages 108 and 145

[114] M. Bigot-Astruc, D. Boivin, and P. Sillard. "Design and fabrication of weakly-coupled few-modes fibers". *IEEE Photonics Society Summer Topical Meeting Series*, pages 189–190, 2012. Cited pages 109 and 145

Publications

Journal paper

- **El-Mehdi Amhoud**, Ghaya Rekaya Ben-Othman, Yves Jaouën. "Concatenation of Space-Time Coding and FEC for Optical MIMO Systems" IEEE Phot. Technol. Letters, vol. 29, pp. 603-606, 2017

International Conference Proceedings

- **El-Mehdi Amhoud**, Ghaya Rekaya-Ben Othman, Laurent Bigot, Mengdi Song Esben Ravn Andresen, Guillaume Labroille, Marianne Bigot-Astruc, Yves Jaouën. "Experimental Demonstration of Space-Time Coding for MDL Mitigation in Few-Mode Fiber Transmission Systems" paper M1D2, ECOC, 2017
- **El-Mehdi Amhoud**, Yves Jaouën, Ghaya Rekaya Ben-Othman. "Combined Polarization- and Mode-Dependent Loss Effects on Few-Mode Fibers systems" paper. SpM4F.3 SppCom, 2017
- **El-Mehdi Amhoud**, Yves Jaouën, Ghaya Rekaya Ben-Othman. "Non-Unitary Effects Mitigation for Few-Mode Fiber Transmission Systems" In the Proceedings of the EMN Optical Communications Meeting, November 2016. **(*Invited*)**
- Yves Jaouën, **El-Mehdi Amhoud**, Ghaya Rekaya Ben-Othman. "Optical MIMO Techniques for MDL Mitigation in Few-Mode Fiber Transmission Systems" paper ATh2C.3 ACP, 2016. **(*Invited*)**
- **El-Mehdi Amhoud**, Yves Jaouën, Ghaya Rekaya Ben-Othman. "Optimal Mode Scrambling for Mode-Multiplexed Optical Fiber Transmission Systems" paper SpTu3F.2 SppCom, 2016.
- **El-Mehdi Amhoud**, Yves Jaouën, Ghaya Rekaya Ben-Othman. "Joint Space-Time Coding and FEC for MDL Mitigation in Few-Mode Fiber Systems" paper JTu4A.35 SppCom, 2016

- **El-Mehdi Amhoud**, Ghaya Rekaya Ben-Othman, Yves Jaouën. "Design Criterion of Space-Time Codes for SDM Optical Fiber Systems" In the Proceedings of the International Conference on Telecommunications, Greece, May 2016.
- **El-Mehdi Amhoud**, Yves Jaouën, Ghaya Rekaya Ben-Othman. "Capacity Enhancement of Space Division Multiplexed Systems by Using Statistical Channel State Information" paper AS4E.2, ACP 2015.
- **El-Mehdi Amhoud**, Elie Awwad, Ghaya Rekaya-Ben Othman,Yves Jaouën. "Mode Selection and Larger Set Equalization for Mode Division Multiplexed Fiber Transmission Systems" paper Th1D.3, OFC, 2015.

Patents

- **El-Mehdi Amhoud**, Ghaya Rekaya Ben-Othman, Yves Jaouën "Joint Space-Time Coding and FEC Coding for MDL Mitigation in Multi-mode Fiber Optical Transmission Systems" Filed as a European Patent application by Institut Mines-Telecom, patent No 16305926.4, October 2016.
- **El-Mehdi Amhoud**, Ghaya Rekaya Ben-Othman, Yves Jaouën "Scrambler for a multimode optical fiber and optical transmission system using such scrambler " Filed as a European Patent application by Institut Mines-Telecom, patent No 16305925.6, October 2016.
- **El-Mehdi Amhoud**, Ghaya Rekaya Ben-Othman, Yves Jaouën. "Space-Time Coding Methods and Devices for Optical MIMO Systems" Filed as a European Patent application by Institut Mines-Telecom, patent No 16305565.0, July 2016.

Coding Techniques for Space-Division Multiplexed Optical Fiber Systems

El-Mehdi AMHOUD

RÉSUMÉ : Les deux dernières décennies ont connu une croissance exponentielle de la demande pour plus de capacité dans les réseaux optiques. Cette croissance a été principalement causée par le développement d'Internet et le trafic croissant généré par le nombre croissant des utilisateurs. La fibre optique offre plusieurs degrés de liberté pour augmenter la capacité. La fréquence, le temps, la phase, la polarisation ont déjà été utilisés pour satisfaire la demande de bande passante, ainsi le multiplexage spatial (SDM) reste le seul degré de liberté disponible pouvant être utilisé dans les systèmes optiques afin d'augmenter la capacité. Cependant, les interactions entre les différents canaux spatiaux dans le même milieu de propagation est inévitable. Ces interactions, si elles ne sont pas compensées, entraînent des dégradations qui détériorent les performances du système. À cette fin, des recherches intensives sont menées récemment afin de développer un traitement de signal avancé capable de traiter ces détériorations dans les systèmes à multiplexage spatial. Motivés par le rôle potentiel des fibres optiques multimodes (MMF) dans les futurs systèmes SDM, dans cette thèse, nous présentons des solutions de codage modernes pour réduire la diaphonie non-unitaire qui affecte les modes spatiaux dans les fibres multimodes entraînant une dégradation des performances.

MOTS-CLEFS : Communications Optiques, Multiplexage Spatial, Fibres Optiques Multimodes (MMFs), Codage Espace-Temps, Systèmes à Entrées et Sorties Multiples (MIMO), Modulation OFDM.

ABSTRACT : In a very fast pace, the last two decades have known an exponential growth in the demand for more optical network capacity, this growth was mainly caused by the built-out of the Internet and the growing traffic generated by an increasing number of users. Since frequency, time, phase, polarization have already been used to satisfy the demand for bandwidth, space-division multiplexing (SDM) remains the only available degree of freedom that can be used in optical transmission systems in order to increase the capacity. However, interactions between spatial channels in the same propagation medium is inevitable. These interactions, if not compensated, result in impairments that deteriorate the system performance. For this purpose, intensive research is being carried out in recent years in order to provide advanced signal processing capable to deal with these impairments in spatial multiplexing systems. Motivated by the potential role of multi-mode fibers (MMFs) in future SDM systems, in this thesis, we present modern coding solutions to mitigate the non-unitary crosstalk known as mode-dependent loss (MDL) that affects spatial modes of MMFs resulting in degraded system performance.

KEY-WORDS : Optical Communications, Spatial Division Multiplexing, Multi-mode Fibers (MMFs), Space-Time Coding, Multiple-Input-Multiple-Output (MIMO), Orthogonal Frequency Division Multiplexing (OFDM).

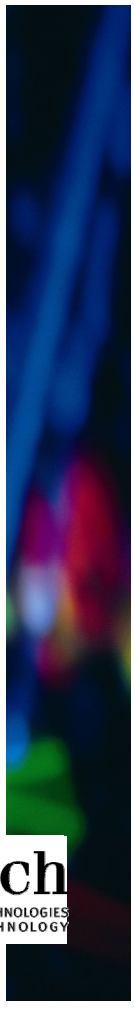

TELECOM ParisTech

EDiTE

ParisTech
INSTITUT DES SCIENCES ET TECHNOLOGIES
PARIS INSTITUTE OF TECHNOLOGY